Development of Spectroscopic Assays for Rapid Monitoring of Estrogen Biodegradation

Celeste Marie Felion

Submitted in fulfilment of the requirements for the
Degree of Doctor of Philosophy

James Watt School of Engineering
College of Science and Engineering
University of Glasgow

November 2023

Abstract

Estrogen hormones are well-established environmental micropollutants which have been linked to endocrine disruption in aquatic organisms in wastewater discharge sites. Biological degradation is the primary wastewater treatment mechanism for estrogen removal. However, treatment efficacy is highly variable and difficult to engineer due to the "black box" nature of biological treatment. Microbial strain selection is a critical impediment towards engineering estrogen biodegradation, since isolating endogenous strains with specific metabolic traits requires lengthy enrichment cultures and is limited to culturable organisms. Furthermore, the highly sensitive and selective chemical trace analysis techniques used to measure estrogen removal are relatively expensive and inefficient.

In this thesis, we developed rapid, high-throughput spectroscopic methods designed to monitor estrogen biodegradation. The spectroscopic methods include a fluorometric assay based on the uptake of a fluorescently-labelled estrogen and a colorimetric biosensor using gold nanoparticles (AuNPs) and an aptamer bioreceptor. A synthetic microbial community comprised of characterised estrogen-degrading reference strains was used to evaluate the fitness for purpose of the developed methods.

A trace analysis method using conventional chromatography was developed to validate the use of the fluorescent probes with the synthetic microbial community. The biochemical fate and distribution of the BODIPY-estrogen in the estrogen-degrading bacteria – specifically, the biotransformation of BODIPY-estradiol to BODIPY-estrone by *Caenibius tardaugens* – was used to inform the design of the fluorometric assay. The fluorometric assay utilises a cell impermeable halide quencher to suppress the extracellular fluorescence, and thus, the obtained fluorescence response was attributed to the selective internalisation of BODIPY-estrogen by *C. tardaugens*.

While the fluorometric assay was developed to screen for estrogen-degrading bacteria, the colorimetric aptasensor, which was adapted from published AuNP biosensors and aptamers for this application, was developed to quantify 17β-estradiol (E2) in buffered culture media. The developed aptasensor was evaluated against industry guidelines for ligand-binding assays. While the analytical performance of the aptasensor satisfied the majority of the guidelines' acceptance criteria, the method suffered from biological interferences by the estrogen-degrading bacteria.

The work in this thesis contributes towards expanding the available bioanalytical methods in environmental biotechnology.

Contents

List of Tables

List of Figures

Acknowledgements

I would like to first express my deepest gratitude to my supervisors, Prof Caroline Gauchotte-Lindsay, Dr William Peveler and Dr Zhugen Yang, for their invaluable guidance and continuous support. I sincerely appreciate their patience and dedication in helping me complete this PhD. Their mentorship made this experience a rewarding journey of professional and personal development. I would also like to acknowledge and thank the University of Glasgow College of Science and Engineering for the scholarship which allowed me to pursue this degree.

I express my sincere thanks to Dr Marta Vignola, Dr Eri Tsagkari, Dr Lucille Chatellard, Dr Rungroch Sungthong, Dr James Minto, and Laura Cossu for sharing their time and expertise to help with this project. I would also like to thank our collaborators from University of Christchurch – Prof Rudi Marquez, Dr Alan Sewell and Dr Ricardo Lopez-Gonzalez – for their expertise and help in synthesising the fluorescent estrogens used in this thesis and for their significant contributions to our journal publication. I would also like to thank Prof Phil Whitfield and Dr Clement Regnault from the University of Glasgow Polyomics facility for their help in the non-targeted LC-MS analysis. In addition, I would like to thank all the technicians for their generous support in the lab and technical knowledge – Julie Russell, Anne McGarrity, Elizabeth Palmer, Alysha Hunter, and Marie-Claire Toukum.

To my fellow researchers – Dr Kate Fell, Dr Anca Amariei, Dr Melissa Moore, Dr Kelly Stewart, and Franziska Tuerk – thank you for your unwavering support and encouragement. This PhD experience would not have been the same without you. To the many researchers in the hiRACE and Water & Environment group, thank you for allowing me to share this experience with you; it was a privilege to work alongside such talented scientists and wonderful humans.

Lastly, I would like to express my sincerest gratitude to my friends and family for their unconditional love, support, patience, and encouragement which helped me navigate this experience. To Ankush, thank you, for everything.

Declaration

Statement of Originality to Accompany Thesis Submission

Name: Celeste Marie Felion
Registration Number:

I certify that the thesis presented here for examination for a PhD degree of the University of Glasgow is solely my own work other than where I have clearly indicated that it is the work of others (in which case the extent of any work carried out jointly by me and any other person is clearly identified in it) and that the thesis has not been edited by a third party beyond what is permitted by the University's PGR Code of Practice.

The copyright of this thesis rests with the author. No quotation from it is permitted without full acknowledgement.

I declare that the thesis does not include work forming part of a thesis presented successfully for another degree.

I declare that this thesis has been produced in accordance with the University of Glasgow's Code of Good Practice in Research.

I acknowledge that if any issues are raised regarding good research practice based on review of the thesis, the examination may be postponed pending the outcome of any investigation of the issues.

Signature: [redacted]

Date: 27 November 2023

Abbreviations

General Terms

AA-QS	Annual Average - Quality Standards
AFO	Animal feeding operations
ANN	Artificial neural network
AS	Activated sludge
BNR	Biological nutrient Removal
EDC	Endocrine disrupting chemicals
EEQ	Estradiol-equivalent (ng E2 L^{-1})
GA	Genetic algorithm
GMM	Genetically modified microorganisms
HRT	Hydraulic retention time
L	Lagoon
MBR	Membrane bioreactor
SRT	Sludge or solids retention time
TF	Trickling filter
WWTF	Wastewater treatment facility
WWTP	Wastewater treatment plant

Enzymes

17β-HSD	17β-Hydroxysteroid dehydrogenase
AMO	Ammonia monooxygenase
ER	Estrogen receptors
HAO	Hydroxylamine oxidoreductase

Chemicals

ACN	Acetonitrile
BODIPY, BDP	4,4-difluoro-4-bora-3a,4a-diaza-s-indacene
BODIPY-E1, BDP-E1	BODIPY-Estrone
BODIPY-E2, BDP-E2	BODIPY-Estradiol
BODIPY-E3, BDP-E3	BODIPY-Estriol
BODIPY-N3, BDP-N3	BODIPY-Azide
BSTFA	N,O-bis(trimethylsilyl)trifluoroacetamide
E1	Estrone
E2	17β-Estradiol
E3	Estriol
EE2	17α-Ethinylestradiol
HPβ-CDX	2-Hydroxypropyl-β-cyclodextrin
MeOH	Methanol
MMB	Minimal medium B
TMS	Trimethylsilyl

Trace Analysis Terms

ANOVA	Analysis of variance
AuNP	Gold nanoparticle
BP-n, XTI-5, HP-n, DB-n	GC stationary phases
C18	Octadecylsilyl
D	Derivatisation
DLVO	Derjaguin-Landau-Verwey-Overbeek (Theory)
ECD	Electrochemical detection
EDL	Electric double layer
EI	Electron (impact) ionisation
EM	Electromagnetic (spectrum)
ESI	Electrospray ionisation
FID	Flame ionisation detector
FLD	Fluorescence detector
FS	Full scan
GC	Gas chromatography
HOMO	Highest occupied molecular orbital
HPLC	High performance liquid chromatography
IC	Internal conversion
IR	Infrared
ISC	Intersystem crossing
IT	Ion trap
LC	Liquid chromatography
LLE	Liquid-liquid extraction
LOD	Limit of detection
LOQ	Limit of quantitation
LUMO	Lowest unoccupied molecular orbital
MIP	Molecularly imprinted polymer
MS	Mass spectrometry
MS/MS	Tandem mass spectrometry
PDA	Photodiode array detection
Q	Quadrupole mass filter
QC	Quality control
QqQ	Triple quadrupole
RSD	Relative standard deviation
SAE	Spiked after extraction
SBE	Spiked before extraction
SELEX	Systematic evolution of ligands by exponential enrichment
SIM	Selected ion monitoring
SPE	Solid phase extraction
SRM	Selected reaction monitoring
ssDNA	Single-stranded DNA
TIC	Total ion chromatogram
TOF	Time of flight
UV	Ultraviolet

Variables (units where appropriate)

α	Selectivity factor
ΔG	Energy potential (kT)
ε	Molar extinction coefficient ($M^{-1}cm^{-1}$)
λ	Wavelength (nm)
λ_{Em}	Emission wavelength (nm)
λ_{Ex}	Excitation wavelength (nm)
λ_{max}	Wavelength of maximum absorbance (nm)
μ	Mean
ν	Frequency (Hz)
$\overline{\nu}$	Wavenumber (cm^{-1})
Φ_f	Quantum efficiency
σ	Standard deviation
A	Absorbance (a.u.)
c	Speed of light (m/s)
c	Concentration (M or µg/L)
E	Energy (J)
F	Fluorescence intensity (i.u.)
h	Planck's constant (J Hz^{-1})
I	Irradiance (W m^{-2})
K	Partition coefficient
k	Capacity factor
k	Spectrofluorometer proportionality constant
K_d	Partition equilibrium constant
l	Optical path length (cm)
m/z	Mass to charge ratio
N	Number of theoretical plates
PA	Peak area
r	Pearson's correlation coefficient
R^2	Coefficient of determination
Rs	Resolution
S, S_0	Singlet state, ground
S^*, S_1^*	Singlet state, excited
T	Transmittance (i.u.)
T^*	Excited triplet state
t_m	Retention time of the mobile phase
t_R	Retention time (min)
$'t_R$	Adjusted retention time (min)
W	Peak width (min)
$W_0.5$	Peak width at half maximum (min)
x	Concentration (M or µg/L)
x_c	Calculated concentration (M or µg/L)
x_i	True concentration (M or µg/L)
y	Response
log$P$	Partition coefficient between octanol and water

Chapter 1

Introduction

Despite the first evidence of water treatment dating back to 4000 BC, widespread access to safe drinking water remains a global challenge today [1]. Recently, UNESCO included the "availability and sustainable management of water and sanitation" as Goal No. 6 of the Sustainable Development Goals in the 2030 Agenda for Sustainable Development [2]. One of the challenges in meeting this goal is the release of hazardous chemicals into the environment. Estrogen hormones are a class of chemical pollutants which have been detected in environmental waters and sediments at levels causing adverse effects [3]. Despite their natural origins, the elevated levels of estrogen in the environment are directly linked to human activity, particularly intensive animal husbandry practices [3].

There are many approaches for the treatment and removal of estrogen micropollutants (i.e., pollutants present at trace-level concentrations), such as physical sequestration and chemical treatment [4]. However, biological treatment – i.e., the use of microbes to enzymatically transform or metabolise contaminants – is the most cost-effective approach towards removing micropollutants which can be readily incorporated into a range of existing treatment systems [5]. Despite these advantages, engineering a biological treatment system for enhanced estrogen removal has significant challenges. One approach for enhancing pollutant removal is bioaugmentation, which is the addition of microbes with desirable metabolic traits to a biological treatment system [5]. Yet, isolating microbes with the ability to degrade micropollutants is a challenge in itself. In addition, identifying the specific treatment facility operating parameters and conditions which enhance removal requires multiple varied experiments.

Chemical trace analysis plays an instrumental role in biotechnology. Analytical methods provide the tools to characterise and quantify biomolecules (DNA, proteins, lipids, and metabolites). However, many bioanalytical methods are optimised and designed for biomedical applications, where the cells, tissues, and compounds of interest are relatively consistent between sources. Thus, bioanalytical methods must be optimised and developed specifically for environ-

mental samples. Currently, the trace analysis techniques used in research concerning estrogen micropollutant biodegradation are based on the chromatography and mass spectrometry methods used for environmental monitoring [6]. In this thesis, the role trace analysis plays in engineering biodegradation was revisited.

As previously mentioned, there are a number of challenges in engineering biodegradation of estrogens. We have identified the detection of estrogen-degrading bacteria within a community as well as estrogen quantification as the main tasks which would benefit from the availability of high-throughput – i.e., rapid and scalable – analytical techniques. While the current trace analysis methods used for these tasks are effective, instrumental chromatography is a relatively expensive and low-throughput technique. Conversely, spectroscopic techniques – such as absorbance and fluorescence – are simpler, inexpensive, and potentially high-throughput. However, spectroscopic methods for monitoring micropollutant biodegradation via microbial activity and quantitative chemical analysis had not yet been explored, due to the limited selectivity and sensitivity of standalone techniques. Development and validation of spectroscopic methods which are fit for the purpose of measuring estrogens in microbial cultures is a necessary step towards their application in service of engineering enhanced biological removal of estrogen micropollutants. The spectroscopic methods developed in this thesis – which were evaluated against established guidelines for suitability – contribute towards advancing the role of bioanalytical methods in environmental science.

1.1 Thesis Aim and Objectives

The aim of this thesis was to develop high-throughput fluorometric and colorimetric trace analysis methods for monitoring biodegradation of estrogens in microbial communities. To achieve the aim of this thesis, the following objectives were set:

Objective 1 Develop an analytical method based on gold standard chromatographic methods to be used as the benchmark to compare the spectroscopic methods against for characterising estrogen biodegradation.

Objective 2 Characterise the degradation and fate of natural estrogen compared to a fluorescently-labelled estrogen by a synthetic community of estrogen-degrading bacteria.

Objective 3 Develop and evaluate a fluorometric method based on the fluorescently-labelled estrogen which can be used to monitor biodegradation.

Objective 4 Develop and evaluate a colorimetric method based on available colorimetric biosensors for environmental samples which has been adapted for measuring estrogen in bacteria cultures.

1.2 Thesis Outline

The thesis consists of 7 chapters which detail the rationale and approach towards the development of the fluorometric and colorimetric methods for monitoring biodegradation of estrogens.

- Chapter 2 presents a comprehensive review of the literature concerning biological degradation and trace analysis of estrogen micropollutants. The specific methodological gaps in engineering biological treatment for enhanced estrogen removal are identified. This chapter also establishes the rationale – i.e., the advantages in method simplicity and throughput – behind the spectroscopic techniques selected to address the methodological gaps.

- Chapter 3 presents the development and validation of a traditional analytical workflow based on liquid-liquid extraction and chromatographic analysis of natural estrogens and fluorescently labelled estrogen derivatives.

- Chapter 4 presents the characterisation of the biochemical fate and distribution of natural and fluorescently labelled estradiol by reference strains of estrogen-degrading bacteria, both individually and as a consortium.

- Chapter 5 presents the development and evaluation of a fluorometric assay based on the fluorescently labelled estradiol which detects estrogen-degrading bacteria.

- Chapter 6 presents the development and evaluation of a colorimetric gold nanoparticle-based biosensor for detecting estrogen in cultures with estrogen-degrading bacteria. The colorimetric method was adapted for bacteria cultures from available methods in the literature which were originally designed for environmental matrices.

- Chapter 7 summarises the key results of the research herein in relation to the individual objectives and overall aim of the thesis. This chapter concludes by highlighting recommendations for future work.

Chapter 2

Literature Review

2.1 Introduction

Estrogens are a chemical class of hormones, which are the signalling molecules that regulate biological functions of multicellular organisms [7]. 17β-Estradiol (E2) is the predominant and most potent estrogen produced in premenopausal women [7]. Estrone (E1) and estriol (E3), which have less biological activity compared to E2, are produced primarily in postmenopausal and pregnant women, respectively [7]. Synthetic estrogens, such as estrogen-analogue contraceptive 17α-ethinylestradiol (EE2), are manufactured as therapeutics to manage female hormonal activity and dysregulation [7].

Endogenous estrogens are produced through the steroid biosynthesis pathway from cholesterol and several androgenic precursors [8]. Steroid molecules are characterised by a tetracyclic carbon backbone which vary in their substituents, configuration, and bond order. Estrogens are 18-carbon steroid derivatives with a methyl group at C13 and an aromatised A-ring (Figure 2.1). Estrogen production is a terminal point in steroid biosynthesis, following the creation of an aromatic system at the A-ring and a ketone reduction at C17 (Figure 2.2) [7, 8]. From this stage, 17β-estradiol may be converted into a less potent form by transformation back to estrone or oxidation at C2, C4, or C16 [9]. The hydroxylated estrogen metabolites can then be conjugated with sulphate or glucuronide for further inactivity and greater hydrosolubility [9, 10].

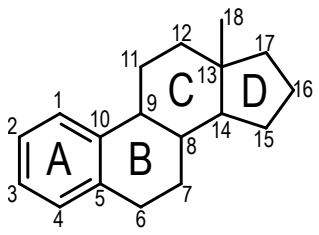

Figure 2.1: Estrogen carbon backbone with enumerated carbons and rings.

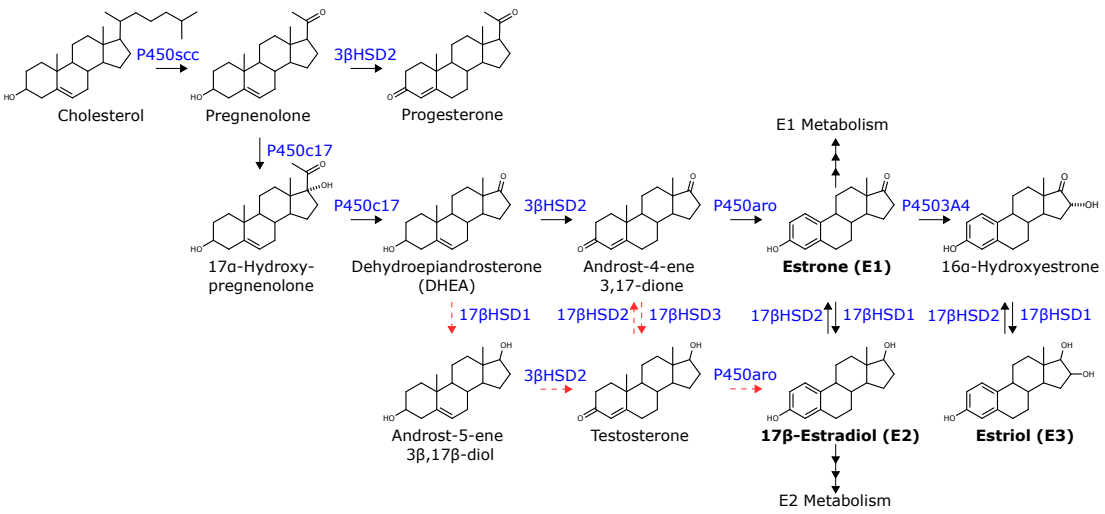

Figure 2.2: Estrogen biosynthesis pathway. The major synthesis steps are indicated with black solid arrows, and the minor synthesis steps are indicated with red dashed arrows. Figure adapted from [8] and [9].

Despite their natural origin, estrogen hormones are widely recognised as environmental micropollutants by environmental regulatory authorities, including in the UK [11–13]. Micropollutants are defined as compounds which are present at or below parts-per-billion (ppb)-levels in the environment and are capable of causing adverse effects at these low concentrations [14]. Estrogens have been detected at concentrations above their toxicity limits in environmental waters around the world [6]. The elevated levels of estrogens in surface waters and groundwater have been directly attributed to human activity – specifically, the inadequate removal of estrogens from the collected sewage from municipalities and agricultural practices prior to release into the environment [3, 15]. The excess estrogen in the receiving waters has been further linked to ecological disturbances by disrupting normal endocrine functions in aquatic organisms [3].

Estrogen micropollutants originate from human and animal excretions. It has been previously estimated that the global human population discharges 30,000 kg of endogenous estrogen per year, plus an additional 700 kg yr^{-1} of synthetic estrogens used in contraceptives [3]. However, a more recent estimate predicted this amount to be ten times greater (300 tonnes in 2015) [16]. In addition, livestock waste discharges an even greater amount of hormones [3, 16]. In the UK, it has been estimated that up to 83% of estrogens discharged (2,145 kg yr^{-1}) comes from farm animals [17]. Globally, it was estimated that livestock contributed 98% of the estrogens excreted in 2015, with most steroid emissions coming from Asia (34.5% animal origin, 39.6% total) [16].

Exposure to exogenous estrogens, which are inherently bioactive compounds, can have serious effects on aquatic organisms, especially fish and amphibians [18]. The primary effect is reproductive disruption in male organisms, such as decreased sperm abundance, decreased gona-

dosomatic index, and increased vitellogenin – a protein associated with egg production in female organisms [19–21]. Female aquatic organisms exposed to exogenous estrogens may have impaired ovary development [19, 21]. In addition, population distributions may be disrupted, with higher rates of intersex organisms and female-biased sex ratios [19].

Studies have confirmed these endocrine-disrupting effects by exposing aquatic species to estrogens and estrogen-contaminated effluents *in vitro* [20]. However, there are many real-world examples of ecological disruption by estrogen micropollutants, where the biota of estrogen-contaminated field sites were compared against control sites (Figure 2.3). Since WWTPs release a wide variety of organic micropollutants, including other EDCs such as alkylphenols and phthalates, the estrogenicity of the effluent or receiving water is commonly reported as the E2-equivalent value (EEQ, ng E2 L^{-1}) [22]. The EEQ measures the combined activity of a chemical mixture on ER proteins relative to a given amount of E2, which has the highest activity of natural estrogens for ER. The long-term effects of estrogen micropollutants on the environment remain uncertain, however, there is evidence that the adverse effects on affected fish in receiving waters may be reversed by upgrading WWTP treatment processes [20, 23].

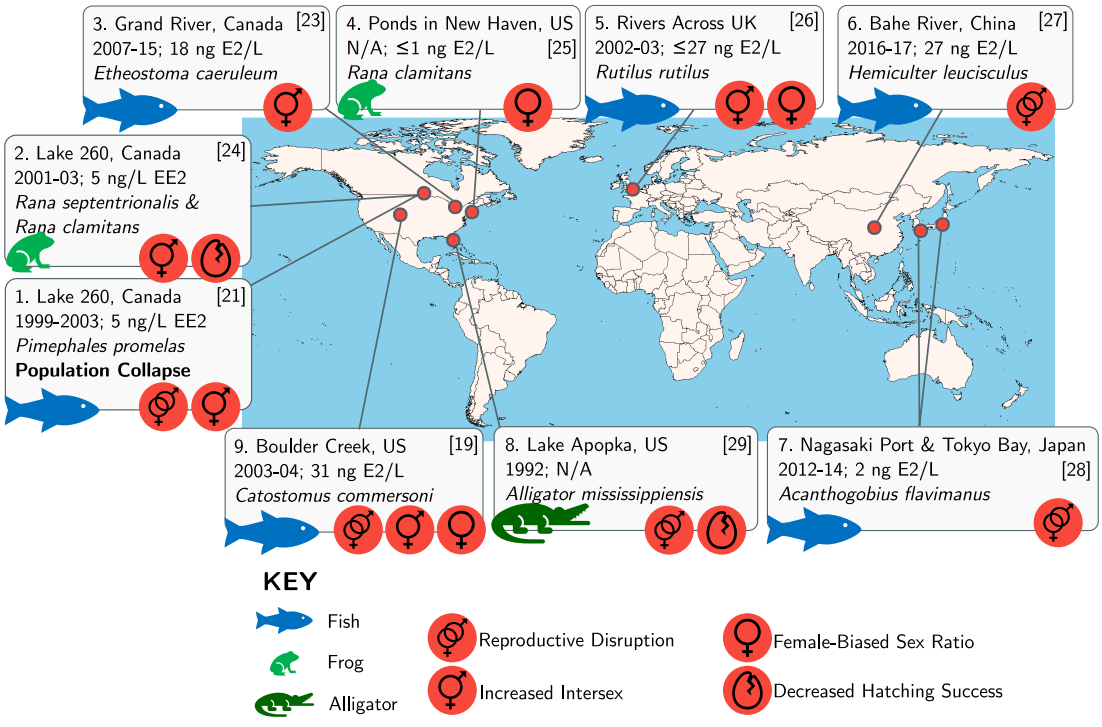

Figure 2.3: Ecological disturbances linked to estrogen pollution reported in the literature. The following are noted for each study: sampling location and time, observed adverse effects, affected species, and EEQ measured in the surface water (except for 1 and 2, which contained specifically 5 ng L^{-1} EE2) [19, 21, 23–29].

2.2 Biological Degradation of Estrogens

2.2.1 Emission Routes and Occurrence

The routes for estrogen hormones from human and animal excreta to enter the environment originate from both point and nonpoint sources (Figure 2.4) [16]. Point sources of estrogen pollution – i.e., specific, identifiable points of pollutant discharge, such as a pipe or ditch – include municipal and livestock wastewater treatment facility or plant (WWTF or WWTP) discharges, as well as domestic septic system discharges [15, 30]. Animal feeding operations (AFOs) which release raw, untreated sewage are particularly deleterious point sources of estrogen pollution [31]. Surface runoff from applied biosolids – sewage sludge which has been digested, dehydrated, and treated primarily for pathogen removal – is recognised as a nonpoint (i.e., non-specific, diffuse) source of estrogen pollution [30].

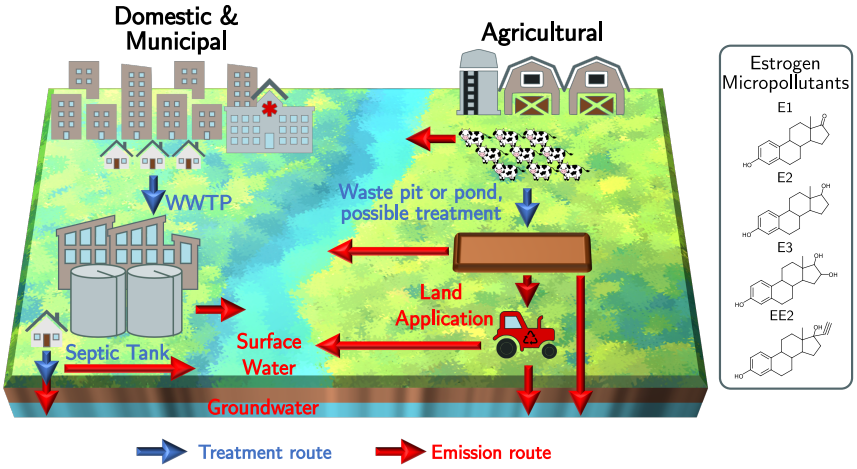

Figure 2.4: Pathways for estrogens to enter the environment. Estrogens in domestic and municipal wastewater are discharged following incomplete removal during treatment at a centralised WWTP or decentralised septic tank system. Estrogens in agricultural waste may be discharged directly without treatment or collected in a manure pit or holding pond. The collected livestock waste may then be discharged or undergo treatment prior to being discharged into surface waters or recycled onto land for soil enrichment.

Wastewater treatment facilities are designed to decontaminate wastewater to established quality standards before returning the final effluent to the local water system [32]. Current wastewater treatment quality standards require the removal of nutrients (e.g., organic matter, nitrogen species, and phosphates), suspended solids, dissolved gases, pathogenic microorganisms, and some heavy metals [32]. Wastewater treatment processes are categorised by three treatment stages: primary, secondary, and tertiary (Figure 2.5). Before primary treatment, larger debris ($>$1 mm) is physically screened out of the raw influent, and dense grit is removed by sedimen-

tation [33]. In primary treatment, suspended solids, which are less dense than grit and have more organic content, sediment slowly in large settling tanks and are removed from the liquid as primary sludge.

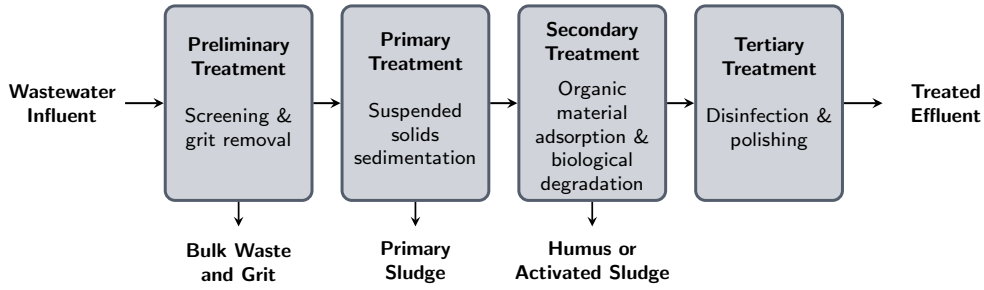

Figure 2.5: Wastewater treatment facility generalised flowsheet.

Secondary treatment is the principal wastewater treatment stage and primarily relies on biological processes. A wide variety of processes are used as secondary treatment, such as trickling filters, sand filters, activated sludge, sequencing batch reactors, membrane bioreactors, constructed wetlands, and aerated lagoons [33]. Secondary treatment is commonly aerobic since biological treatment occurs much faster in oxic environments, however, anaerobic processes are also employed [33]. Treatment is mediated by the microorganisms present in the sewage which form biofilms on suspended flocks or fixed surfaces, depending on the process used. The microbes degrade up to 95% of the organic matter from the primary treatment effluent and produce humus (i.e., the biomass which accumulates on filters) or excess activated sludge (i.e., the suspended solids which contain a high proportion of microorganisms) as waste products [33]. The humus and sludge can then be removed from the liquid for disposal or, in activated sludge systems, recycled back through the treatment process to maintain the microbial density. The treated secondary effluent is clarified in settling tanks prior to being discharged to receiving waters, if no further treatment is required to meet the quality standards [33].

Tertiary treatment is, broadly, any additional treatment applied after secondary treatment. Additional treatment is less common, since it is mainly utilised when the wastewater contaminant load is high or when the treated effluent is being discharged into ecologically sensitive receiving waters [34]. Tertiary treatment may be chemical (e.g., advanced oxidation, chlorination, UV radiation), physical (e.g., micro- or nanofiltration, activated carbon adsorption), or biological (e.g., constructed wetlands) in nature [33].

The incomplete removal of estrogen by WWTPs prior to effluent discharge into receiving surface waters has been extensively documented (Table 2.1). An in-depth review by Liu *et al.* (2015) on the fate of estrogens in WWTPs noted that estrogen removal rates are influenced by operational parameters and, therefore, are highly variable [35]. Indeed, there are examples of good removal of estrogens by WWTPs. Studies by Braga *et al.* (2005) and Andersen *et al.*

(2003) reported that municipal WWTPs with advanced treatment processes successfully reduced E1, E2, and EE2 in the effluent below detection limits of 0.1 ng L^{-1} or 1 ng L^{-1}, respectively [36, 37]. However, Braga *et al.* also reported negligible estrogen removal from the influent (7% of 58 ng L^{-1} E1 and 0% of 14 ng L^{-1} E2) at a facility without advanced treatment [36]. Moreover, a study by Gabet-Giraud *et al.* (2010) reported large variations in estrogen effluent levels across 14 different WWTPs (0.1–58 ng L^{-1} E1 and 0.5–11.9 ng L^{-1} E2), and Baronti *et al.* (2000) observed temporal variations in effluent estrogens over 5 months in 6 different WWTPs [38, 39].

Table 2.1: Estrogen concentrations in wastewater treatment effluents reported in the literature.

					Effluent Concentration (ng L^{-1})			
Ref	Location	Type	No. WWTP	No. Samples	E1	E2	E3	EE2
[39]	Italy	Municipal	6	30	9.3[a]	0.9[a]	-	0.45[a]
[40]	UK	Municipal	7	21	9.4[a]	6.3[a]	-	<0.2[a]
[38]	France	Municipal	14	31	6.8[b]	3.9[b]	24.6[b]	2.6[b]
[41]	Korea	Municipal	5	10	6[b]	<2.7[b]	<6[b]	-
[42]	Argentina	Municipal	3	6	<16[b]	308[b]	-	111[b]
[43]	New Zealand	Municipal	3	-	<3–84.7[c]	<3–14.8[c]	<6[b]	<10[b]
[43]	New Zealand	Livestock	8	-	796[b]	96[b]	<6[b]	<10[b]
[44]	US	Livestock	1	5	11[b]	1.6[b]	3.8[b]	-

[a]Concentration reported as median of the total number of samples. [b]Concentration is the mean of the total number of samples. [c]Concentration range (minimum – maximum) measured, where overall mean or median could not be estimated due to values below detection limit.

During specific treatment processes, estrogens may become sequestered to the sludge component in the sewage. A study by Muller *et al.* (2008) measured an average of 5 ng g^{-1} E1, 3 ng g^{-1} E2, and 5.5 ng g^{-1} EE2 in the excess sludge of a domestic wastewater treatment facility [22]. In comparison to the treated effluent, which contained 3.5 ng L^{-1} E1 and 2 ng L^{-1} E2, the estrogen mass fraction (i.e., ppb) was 1000 times greater in the sludge, and the overall estrogen mass flux from the influent was twice as high in the sludge compared to the treated effluent (4% versus 2%) [22]. Estrogens are moderately hydrophobic – with log$P$ values between 2.5 and 4.0 – and, thus, favour adsorbing to the richly organic sludge [3]. In livestock facilities, the dry waste (excreta and bedding) has been reported to have very high estrogen content. In two swine farrowing (i.e., birthing) facilities in the US, the dry waste contained an average 54 ng g^{-1} E1 and 41 ng g^{-1} E2 [45]. In another study from the US, a dairy farm measured an average 697 ng g^{-1} E1 and 37 ng g^{-1} E2 in the collected dry waste [46]. In both of these studies, the farms reportedly used the livestock dry waste as soil amendment [45, 46].

As a result of their inconsistent removal by treatment processes, estrogens have been de-

tected in surface waters, sediments, and groundwater above their recommended limits (Table 2.2). Currently, EU regulators advise the following average annual quality standards (AA-QS): 0.18 ng L^{-1} E2 and 0.0032 ng L^{-1} EE2 for fresh water; and 0.009 ng L^{-1} E2 and 0.0016 ng L^{-1} EE2 for saltwater [47]. Baronti *et al.* (2000) noted that while environmental estrogen levels were not detectable downstream of a WWTP discharge site, all three major natural estrogens and EE2 were detected downstream of untreated municipal sewage discharge sites [39]. In this study, only EE2 was present at concentrations above the AA-QS [39]. However, Cargouët *et al.* (2004) measured high estrogen concentrations – exceeding the AA-QS for E2 and EE2 –downstream of four WWTPs in France [48]. A recent review by Ciślak *et al.* (2023) compiled the concentrations of estrogens in the environment across Europe reported in the literature [15]. Ciślak *et al.* found that most cases reported estrogen levels in surface and groundwater above European quality standards and highlighted high-density populations and animal husbandry practices as major risk factors [15]. In summary, the environmentally relevant concentrations of estrogens are approximately 0.001–30 ng L^{-1}, based on the EU AA-QS and the detected concentrations in WWTP effluents and discharge sites.

Table 2.2: Estrogen concentrations in the environment reported in the literature.

					Environmental Concentration (ng L^{-1} or ng g^{-1})			
Ref	Location	Discharge Type	Discharge Site	Sampling Site	E1	E2	E3	EE2
[39]	Italy	Municipal WWTP Effluent	River	River, Downstream	<0.008	<0.02	<0.02	<0.03
		Municipal Untreated Effluent	River	River, Downstream	1.5	0.11	0.33	0.04
[48]	France	Municipal WWTP Effluent	River	River, Downstream	2.7	3	2.5	1.8
		Domestic WWTP Effluent	River	River, Downstream	1.4	1.7	2.2	1.3
		Municipal WWTP Effluent	River	River, Downstream	2.2	3.2	2.1	2.3
		Domestic WWTP Effluent	River	River, Downstream	3	3	2.5	2.9
[19]	US	Municipal WWTP Effluent	River	River, Discharge Site	36	1.6	-	0.7
[49]	UK	Domestic WWTP Effluent	River	Sediment, Downstream	0.4–3.3[a]	<0.03–1.2[a]	-	<0.04
[50]	Switzerland	Livestock Slurry Runoff	Land Applied	River, Downstream	0.37	0.03	0.18	-
		Livestock Slurry Runoff	Land Applied	River, Downstream	0.55	0.06	0.26	-
		Livestock Slurry Runoff	Land Applied	River, Downstream	0.27	0.06	0.27	-
		Livestock Slurry Runoff	Land Applied	River, Downstream	0.28	0.02	0.21	-
		Livestock Slurry Runoff	Land Applied	River, Downstream	0.18	0.03	0.13	-
[51]	Israel	Livestock Lagoon Leachate	Lagoon	Groundwater, Discharge Site	-	<0.5–2.5[b]	-	-
		Livestock Lagoon Leachate	Lagoon	Sediment, Discharge Site	-	<0.05–0.2[b]	-	-
[52]	China	Municipal Runoff	River + Coast	River, Downstream	0.3–3.6[a]	<0.2	-	0.7
		Municipal Runoff	River + Coast	Coast, Downstream	0.2–1.0[a]	<0.2	-	0.4–0.6[a]

Concentrations are the mean value, except where noted otherwise. [a]Concentration range (minimum – maximum) measured, where the mean could not be estimated due to values below detection limit or only the range was reported. [b]Concentrations were conservatively estimated from graphical data.

2.2.2 Estrogen Removal in WWTPs

The incomplete removal of estrogens by wastewater treatment facilities and the associated environmental impacts have led researchers to further investigate removal mechanisms. WWTPs use several sequential processes to treat wastewater before returning the treated effluent back into the environment [53]. In conventional treatment facilities, the processes associated with biological treatment are the primary mechanisms for removing estrogen from the waste stream [53]. While physical adsorption is partly responsible for their removal, enzymatic degradation of estrogens (and other organic micropollutants) by endogenous microorganisms fully eliminates the hazardous compounds from wastewater.

A selection of publications from the literature reporting the fractional removal of estrogens from the influent in each treatment stage are provided in Table 2.3, and the fractional removal rates are presented graphically in Figure 2.6. Estrogens are primarily removed from wastewater during secondary treatment (Figure 2.6a) [53]. In studies investigating estrogen removal during secondary treatment in WWTPs, activated sludge (AS) was the most commonly used process and had better removal of natural estrogens E1 and E2 than the pharmaceutical EE2 (Figure 2.6b). During AS treatment, estrogens are initially removed by adsorbing to the sludge before biodegradation. The solids or sludge retention time (SRT) is a key parameter in AS treatment, where longer SRTs (e.g., 10–15 days) increase estrogen removal [54]. Enhanced removal is particularly evident in nitrification treatment (i.e., the biological oxidation of ammonia), which generally requires longer SRTs due to the slow growth of nitrifying bacteria [54, 55].

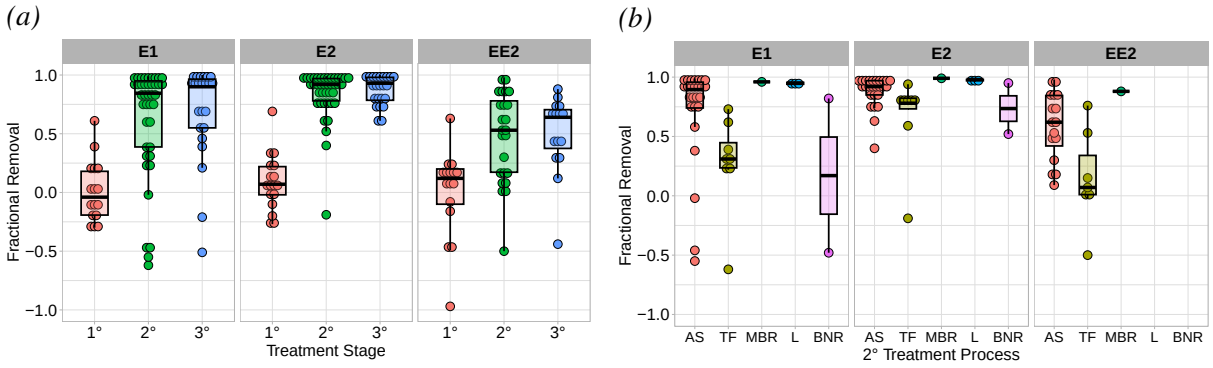

Figure 2.6: Fractional removal of estrogens from WWTP reported in the literature by (a) treatment stage or (b) secondary treatment process. Points are the values in Table 2.3; boxes represent the 25%, 50% and 75% quartiles; whiskers are 1.5 times the interquartile range (IQR). Treatment processes: AS - activated sludge; TF - trickling filter; MBR - membrane bioreactor; L - lagoon; BNR - biological nutrient removal.

Trickling filters (TF) were the next most frequently used treatment process but had the poorest removal rates – a characteristic which has been repeatedly noted in the literature [53, 61, 62].

Table 2.3: Fractional removal of estrogens from wastewater treatment reported in the literature.

			Primary Treatment				*Secondary Treatment*						*Tertiary Treatment*				
			Fractional Removal						*Fractional Removal*					*Fractional Removal*			
Ref.	Location	WWTP ID	E1	E2	E3	EE2	Process	Nitrification	E1	E2	E3	EE2	Process	E1	E2	E3	EE2
[56]	UK	1	0.61	0.07	-	-0.44	TF	Yes	0.24	0.78	-	0.07	FST	-0.51	0.76	-	-0.44
		2	0.23	0.24	-	0.1	TF	No	0.31	0.78	-	-0.02	GP & L	0.97	0.99	-	0.81
		3	-0.13	-0.2	-	0.05	TF	Yes	0.62	0.94	-	0.04	Clarifiers	0.39	0.88	-	0.12
		4	0.39	0.36	-	0.2	TF	Yes	0.31	0.83	-	-0.5	FST	0.95	0.98	-	0.44
		5	0	-0.02	-	-0.97	TF	No	0.73	0.82	-	0.76	FST	0.53	0.77	-	0.7
		6	-0.3	0.07	-	0.14	TF	Yes	0.39	0.78	-	0.15	FST	0.21	0.8	-	0.27
		7	-0.2	0.05	-	0.2	TF	Yes	0.22	0.59	-	0.53	BAFF	0.57	0.88	-	0.64
		8	0.01	0.05	-	-0.16	AS	Yes	0.91	0.97	-	0.51	FST	0.91	0.97	-	0.43
		9	0.18	0.13	-	-0.08	AS	Yes	0.97	0.98	-	0.6	SF	0.99	0.99	-	0.71
		10	-0.1	0.22	-	0.08	AS	-	0.94	0.98	-	0.74	FST	0.94	0.98	-	0.76
		11	0.06	0.31	-	0.25	AS	Yes	0.9	0.91	-	0.53	FST	0.9	0.94	-	0.64
		12	-0.19	-0.1	-	-0.49	AS	Yes	0.38	0.63	-	0.46	UV	0.97	0.98	-	0.32
		13	-0.08	-0.27	-	0.19	AS	-	0.73	0.95	-	0.3	FST	0.71	0.93	-	0.43
		14	-0.28	-0.25	-	0.16	AS	No	-0.02	0.82	-	0.73	FST	-0.21	0.7	-	0.7
		15	-	-	-	-	MBR	-	0.96	0.99	-	0.88	FST	0.96	0.99	-	0.88
		16	-	-	-	-	BNR	-	-0.48	0.52	-	-2.62	UV	0.7	0.76	-	-2.03
[37]	Germany	1	1.14	0.69	-	0.63	AS	Yes	0.98	0.98	-	0.98	-	-	-	-	-
[39]	Italy	1	-	-	-	-	AS	-	0.94	0.89	0.79	0.86	-	-	-	-	-
		2	-	-	-	-	AS	-	0.98	0.88	0.80	0.94	-	-	-	-	-
		3	-	-	-	-	AS	-	0.99	0.84	0.75	0.18	-	-	-	-	-
		4	-	-	-	-	AS	-	0.84	0.76	0.79	0.09	-	-	-	-	-
		5	-	-	-	-	AS	-	0.99	0.92	0.82	0.84	-	-	-	-	-
		6	-	-	-	-	AS	-	0.97	0.92	0.84	0.64	-	-	-	-	-
[36]	Australia	1	-	-	-	-	AS	-	0.85	0.96	-	-	MF & RO	1.00	1.00	-	-
[57]	New Zealand	1	-	-	-	-	AS	Yes	0.89	0.74	-	-	-	-	-	-	-
[22]	France	1	0.18	0.14	-0.04	0.23	AS	-	0.96	0.92	-	0.86	-	-	-	-	-
[58]	Canada	1	-	-	-	-	SF	Yes	-	-	-	-	SF	0.667	0.829	-	-
		2	-	-	-	-	AS	Partial	0.73	0.97	-	-	-	-	-	-	-
		3	-	-	-	-	AS	No	-0.55	0.40	-	-	-	-	-	-	-
		4	-	-	-	-	AS	Partial	0.77	0.93	-	-	-	-	-	-	-
		5	-	-	-	-	AS	Partial	0.85	0.98	-	-	-	-	-	-	-
		6	-	-	-	-	AS	Partial	-0.46	0.76	-	-	-	-	-	-	-
		7	-	-	-	-	SF	Yes	-	-	-	-	SF	0.965	0.933	-	-
		8	-	-	-	-	GF	Yes	-	-	-	-	GF	0.978	0.988	-	-
		9	-	-	-	-	AS	Yes	0.95	0.98	-	-	-	-	-	-	-
		10	-	-	-	-	L	No	0.93	0.98	-	-	-	-	-	-	-
		11	-	-	-	-	SF	No	-	-	-	-	SF	0.464	0.805	-	-
		12	-	-	-	-	L	No	0.95	0.96	-	-	-	-	-	-	-
		13	-	-	-	-	L	No	0.96	0.98	-	-	-	-	-	-	-
		14	-	-	-	-	BNR	Yes	0.82	0.95	-	-	-	-	-	-	-
		15	-	-	-	-	AS	No	0.81	0.96	-	-	-	-	-	-	-
		16	-	-	-	-	AS	No	0.95	0.97	-	-	-	-	-	-	-
		17	-	-	-	-	TF	No	-0.62	-0.19	-	-	-	-	-	-	-
		18	-0.29	-0.01	-	-	-	-	-	-	-	-	-	-	-	-	-
[59]	Germany	1	-	-	-	-	-	-	-	-	-	-	Clarifiers	-	0.68	-	-
	Brazil	2	-	-	-	-	TF	-	0.67	0.92	-	0.64	-	-	-	-	-
[60]	Switzerland	1	-	-	-	-	AS & MBR	-	0.58	0.91	0.75	0.18	Clarifiers	-	0.68	-	-
		2	-	-	-	-	-	-	-	-	-	-	Ozone	0.9	0.61	-	-
		3	-	-	-	-	-	-	-	-	-	-	PAC & UF	0.92	0.61	-	-

Treatment processes: TF - trickling filter; AS - activated sludge; MBR - membrane bioreactor; BNR - biological nutrient removal; SF - sand filtration; GF - granular anthracite filtration; L - lagoon; FST - final settlement tank; GP - grass plots; BAFF - biological aerated flood filter; UV - ultraviolet radiation; MF - microfiltration; RO - reverse osmosis; PAC - powdered activated carbon; UF - ultrafiltration.

The lower removal by trickling filters has been attributed to lower hydraulic retention times (HRT) compared to activated sludge treatment (4–14 h in AS versus $<$1 h in TF), allowing less time for the wastewater to interact with the microbiota [53]. In comparison, the studies which investigated estrogen removal by membrane bioreactors, biological nutrient removal, and lagoons showed high rates of removal [56, 58, 60].

The importance of secondary treatment in estrogen removal has also been demonstrated by studies within the UK. Desbrow *et al.* (1998) measured estrogens in effluents from 7 municipal wastewater treatment facilities at ranges from 1–76 ng L^{-1} E1 and 3–48 ng L^{-1} E2, where the facility which utilised only primary settlement had higher estrogen effluent levels than five other WWTPs [40]. The only treatment facility with higher estrogen levels used biological filtration but had a remarkably low daily flow per capita: 0.05 m^3 compared to 0.22 ($\pm$ 0.03) m^3 for the other six facilities [40]. A more recent study of 16 UK wastewater treatment facilities by Gardner *et al.* (2013) found that E2 was well removed during secondary ($\sim$80%) and tertiary treatments ($\sim$90%) [56], while E1 and EE2 were only removed approximately 60% and 50% after tertiary treatment, respectively [56].

Similar to municipal WWTPs, the removal of estrogens by wastewater treatment in AFOs improves with sequential treatment processes. The manure pits or holding ponds where bovine and swine waste is first collected often contains the highest concentration of estrogens [44, 45]. A study by Shappell *et al.* (2007) evaluated the estrogen loads across a swine farrowing facility which included anaerobic lagoons and constructed wetlands [44]. The manure pit was determined to have 0.2 µg L^{-1} E2, 2 µg L^{-1} E1, and 0.4 µg L^{-1} E3 (original values in pM), and the first lagoon reduced the combined estrogen load by 96% [44].

2.2.3 Microorganisms Associated with Biodegradation

Aerobic bacteria are the primary agents of estrogen biodegradation [63]. Over the past 20 years, a number of bacteria strains capable of utilising estrogens as a carbon or energy source (i.e., catabolic metabolism or catabolism) have been independently isolated by researchers from activated sludge or sediments (Table 2.4) [63]. Estrogen-catabolising bacteria strains are isolated from samples of the built and natural environment by enrichment culture – i.e., the use of chemically-defined culture medium which contains a specific carbon and energy source (such as estrogen) to selectively favour the growth of specific bacteria from the microbial community [64]. Isolated estrogen-catabolising bacteria have been primarily of the genera *Rhodococcus*, *Sphingomonas*, and *Pseudomonas*. In recent years, however, many more new estrogen-degrading bacteria have been isolated, including *Ochrobactrum* sp., *Lysinibacillus sphaericus*, and *Stenotrophomonas maltophilia* [65–67].

Furthermore, numerous studies have shown that bacteria associated with nitrification – the

process of oxidising ammonia (NH_3) to nitrite (NO_2^-) and nitrate (NO_3^-) – are able to degrade a variety of organic micropollutants, including estrogens [68–70]. A study by Vader *et al.* (2000) was among the first to report oxidation of EE2 by nitrifying microorganisms in activated sludge [71]. The findings by Vader *et al.* were followed by further studies linking nitrifying bacteria and, specifically, ammonia monooxygenase enzyme to the oxidation of EE2 and natural estrogens E1, E2 and E3 [69, 72, 73]. An investigation by Shi *et al.* (2004) confirmed that nitrifying bacteria *Nitrosomonas europaea* was capable of degrading all three natural estrogens and EE2 [72].

Most nitrifying bacteria, including *Nitrosomonas*, are chemolithoautotrophic – i.e., they utilise inorganic nitrogen (NH_3, NO_2^-) as an electron source and assimilate inorganic carbon (CO_2) by the Calvin-Benson-Bassham cycle [74]. Thus, contrary to catabolic metabolism, the organic estrogen molecule provides no apparent growth advantage to the bacteria and is simply transformed by non-selective enzymes. This form of non-growth-related biodegradation is referred to as "cometabolism" [63]. While cometabolism is readily discernible by chemolithoautotrophic bacteria, very few heterotrophic organisms which require an organic growth substrate to cometabolise estrogens have been identified. One notable example is a study by Pauwels *et al.* (2008) which isolated six heterotrophic bacteria (two *Pseudomonas* sp., two *Acinetobacter* sp., *Ralstonia pickettii*, and *Phyllobacterium myrsinacearum*) which could catabolise E1, E2, and E3 and yet only cometabolise EE2 [75].

Over the past two decades, there has been significant progress in understanding bacterial degradation of estrogens, particularly through studying the many estrogen-degrading isolates. However, current cultivation techniques are incapable of culturing the vast majority of the $\sim 10^{12}$ microbial species across the biosphere [76]. Thus, there are likely many more bacteria involved in estrogen biodegradation which have yet to be discovered due to the limitations of culture-dependent methods. A recent study by Zhang *et al.* (2021) investigated E2 biodegradation in Taihu Lake sediments and surface waters using stable isotope probing – a culture-independent technique to study incorporation of ^{13}C from isotope-labelled estrogen by bacteria [77]. Zhang *et al.* found that genera relating to many known isolates (including *Novosphingobium*, *Ralstonia*, *Pseudomonas*, *Sphingomonas*, *Nitrosomonas*, and *Alcaligenes*) had assimilated the labelled estrogen, as well as taxa not yet known to be associated with estrogen biodegradation, such as Desulfurellaceae [77].

Table 2.4: Estrogen degrading bacteria reported in the literature, including their source and enrichment procedure.

Ref	Source	Enrichment Procedure	Class	Species	Strain	Degradation Type
[78]	Activated sludge	Bioreactors, 3 mg/L E1, E2, Ambient, 6 months	Alphaproteobacteria	*Aminobacter* sp.	KC6	Partial E1, E2 degradation
				Aminobacter aminovorans	KC7	Partial E1, E2 degradation
				Sphingomonas sp.	KC8	E1, E2 catabolism
[79]	Activated sludge	Not specified	Alphaproteobacteria	*Novosphingobium* sp.	JEM-1	E1, E2, EE2 degradation
[80]	Activated sludge	Batch culture, 1000 mg/L E2	Alphaproteobacteria	*Novosphingobium tardaugens*	ARI-1	E1, E2, E3 catabolism
[75]	Compost	Batch culture, 50 mg/L EE2, 28°C, 1 month	Alphaproteobacteria	*Phyllobacterium myrsinacearum*	BP1	E1, E2, E3 catabolism; EE2 cometabolism
			Betaproteobacteria	*Ralstonia pickettii*	BP2	E1, E2, E3 catabolism; EE2 cometabolism
			Gammaproteobacteria	*Acinetobacter* sp.	BP8, BP10	E1, E2, E3 catabolism; EE2 cometabolism
				Pseudomonas aeruginosa	BP3	E1, E2, E3 catabolism; EE2 cometabolism
				Pseudomonas sp.	BP7	E1, E2, E3 catabolism; EE2 cometabolism
[81]	Artificial sandy aquifer	Batch culture, 1 mg/L E1, E2, E3, EE2, 30°C	Actinobacteria	*Agromyces* sp.	LHJ3	E3 degradation
			Alphaproteobacteria	*Sphingomonas* sp.	CYH	E1, E2 degradation
[82]	Agricultural soil	Batch culture, 200 mg/L E2, 25°C	Actinobacteria	*Rhodococcus* sp.	ED6, ED7, ED10	E1, E2 catabolism
			Alphaproteobacteria	*Sphingomonas* sp.	ED8, ED9	E1, E2 catabolism
[83]	Activated membrane sludge	Batch culture, 0.1–5.5 mg/L E2, 20°C	Betaproteobacteria	*Achromobacter* sp.	NA	E1, E2, E3 degradation
				Ralstonia sp.	NA	E1, E2, E3 degradation
[84]	Soil	Batch culture, 1000 mg/L E2, 30°C	Betaproteobacteria	*Alcaligenes* sp.	NA	E2 catabolism
[72]	Reference strain	Reference strain	Betaproteobacteria	*Nitrosomonas europaea*	NCIMB11850	E1, E2, E3, EE2 cometabolism
[85]	Reference strain	Reference strain	Betaproteobacteria	*Nitrosomonas europaea*	ATCC19718	E2, EE2 cometabolism
[86]	Seawater	Agar plates, 1 mM testosterone, 27°C	Gammaproteobacteria	*Buttiauxella* sp.	S19-1	E2 catabolism
[87]	Activated sludge	Batch culture, 20 mg/L E2, 30°C, 7 days	Gammaproteobacteria	*Pseudomonas aeruginosa*	TJ1	E2 catabolism
[88]	Reference strain	Reference strain	Betaproteobacteria	*Leptotrhix discophora*	LMG8142	EE2 cometabolism
			Gammaproteobacteria	*Pseudomonas putida*	LMG2321, -2322, -2323	EE2 cometabolism
[89]	Seawater	Agar plates, 1 mM testosterone, 27°C	Gammaproteobacteria	*Vibrio* sp.	H5	E2 catabolism
[90]	Activated sludge	Bioreactor, 1 mg/L E2, 10 weeks	Actinobacteria	*Rhodococcus equi*	Y50155, Y50156, Y50157	E1, E2, E3, EE3 degradation
			Actinobacteria	*Rhodococcus zopfii*	Y50158	E1, E2, E3, EE3 degradation
[91]	Reference strain	Reference strain	Actinobacteria	*Rhodococcus equi*	ATCC12557	EE2 cometabolism
				Rhodococcus erythropolis	ATCC4277	EE2 cometabolism
[92]	Activated sludge	Batch culture, 10 mg/L EE2, 30°C, 1 week	Bacteroidetes	*Sphingobacterium* sp.	JCR5	E1, E2, E3, EE2 catabolism
[93]	Activated sludge	Batch culture, 0.1–1mg/L E2, 28°C, 5 months	Firmicutes	*Bacillus* sp.	E2Y1, E2Y4	E1, E2 degradation
[65]	Activated sludge	Batch culture, 10 mg/L E2, 200 rpm, 30°C, 1 month	Alphaproteobacteria	*Ochrobactrum* sp.	FJ1	E2 catabolism
[94, 95]	Soil	Batch culture, 5–100 mg/L E2, 120 rpm, 30°C, 1 week	Actinobacteria	*Rhodococcus equi*	DSSKP-R-001	E1, E2, E3 catabolism
			Gammaproteobacteria	*Acinetobacter* sp.	DSSKY-A-001	E1, E2, EE2 catabolism
[96]	Activated sludge	Batch culture, 10mg/L E2, 180 rpm, 30°C, 1 month	Gammaproteobacteria	*Pseudomonas putida*	STJE-1	E1, E2, E3 catabolism

2.2.4 Estrogen Biodegradation Pathways

Presently, the aerobic biodegradation pathways of estrogen have been only partially elucidated [63, 97]. Biodegradation of E2 often begins with conversion to E1 by 3β,17β-hydroxysteroid dehydrogenase enzyme; the gene for this enzyme (*oecA*) has been identified in estrogen-degrading bacteria *Spingomonas* sp. KC8 and *Caenibius tardaugens* 16702 (formerly *Novosophingobium tardaugens* ARI-1) [98, 99]. The most well-characterised biodegradation pathway is the 4,5-*seco* pathway (I. in Figure 2.7), which begins with estrone 4-hydroxylase (*oecB*) introducing a hydroxyl group at C4 [100]. Next, 4-hydroxyestrone 4,5-dioxygenase (*oecC*) mediates *meta*-cleavage of the A-ring, after which a few different transformations may occur [100]. The ring-cleavage product may form pyridinestrone (a terminal product) abiotically or form a thioester with coenzyme A (CoA) and undergo subsequent degradation [99, 100].

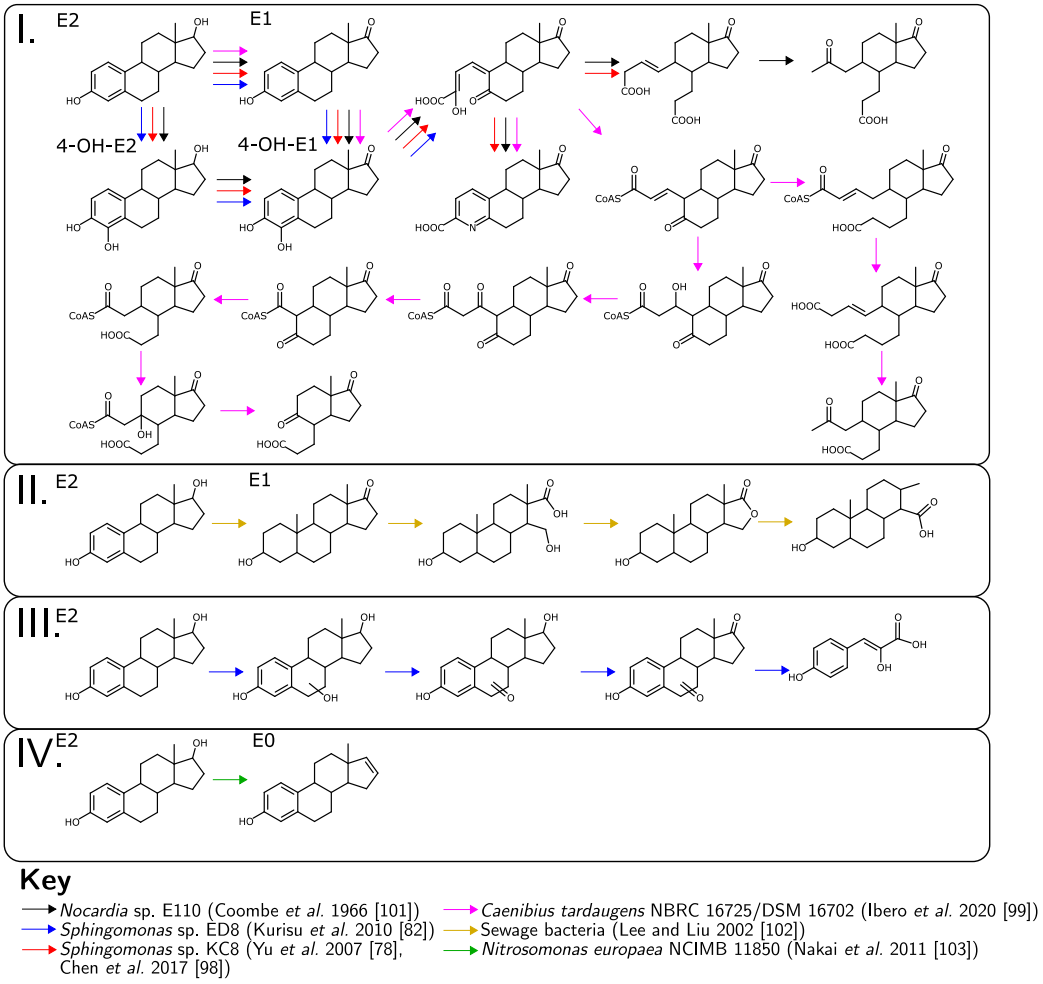

Figure 2.7: Estrogen biodegradation pathways published in the literature grouped into four initiation mechanisms, adapted from [97]. I. Hydroxylation at C4 on the A-ring and formation of 4-hydroxyestrone (4-OH-E1); II. lactone formation on the D-ring; III. hydroxylation on the B-, C-, or D-rings; and IV. dehydration of C17 on the D-ring [78, 82, 98, 99, 101–103].

Several other biodegradation pathways of natural estrogens have been observed, however, the structures of most of the proposed metabolites have not yet been confirmed [97]. A study by Lee and Liu (2002) on the aerobic biodegradation of E2 by a sample of activated sludge found degradation began with the formation of lactone on the D-ring (II. in Figure 2.7) [102]. Interestingly, Kurisu *et al.* (2010) found that *Sphingomonas* sp. ED8 utilised two separate pathways to degrade E2: the 4,5-*seco* pathway, which occurs primarily via the A-ring, and another pathway that hydroxylates one of the other saturated rings (III. in Figure 2.7) [82]. Very little is known about the cometabolic biotransformation of natural estrogen by *N. europaea* (IV. in Figure 2.7). Currently, only the transformation to estratetraenol (E0) has been confirmed, however, this dehydration does not fit the expected action of ammonia monooxygenase enzyme [103]. Although the biochemical characterisation of estrogen biodegradation is currently incomplete, it is clear that environmental bacteria are highly diverse in their approach towards metabolising estrogen micropollutants.

2.3 Engineering Biodegradation of Estrogens

The majority of biological treatment facilities in the UK are based on trickling filters, which have been shown to be one of the least effective secondary treatment processes for removing estrogens and other organic micropollutants [102]. However, the WWTP operational parameters which enhance estrogen biodegradation, such as longer SRT and HRT, are not always feasible to implement. Thus, engineering the microbial communities in wastewater treatment has become an attractive strategy for improving biodegradation of organic micropollutants, including estrogens. Current approaches towards engineering microbial communities for enhanced estrogen removal include bioaugmentation and biostimulation [79, 104, 105]. In addition, *in silico* methods, including those based on machine learning, are currently being applied towards enhancing biodegradation of environmental contaminants [106]. Through the perspectives of synthetic design and practical implementation, we identify the specific methodological gaps in engineering biodegradation which can be improved through trace analysis.

2.3.1 Bioaugmentation Process

Bioaugmentation is the addition of selected microorganisms to enhance remediation of a contaminated ecosystem (e.g., wastewater, environmental waters, and sediments) [107, 108]. Bioaugmentation typically involves the selection and cultivation of bacteria or fungi that possess desirable traits, such as the capability to metabolise or transform specific micropollutants. These microorganisms can be naturally occurring or genetically modified to possess the desired metabolic capabilities.

A review by Herrero and Stuckey (2015) outlined the following key factors for successful bioaugmentation [109]:

- Basic knowledge of the microbial ecology common to the target treatment system;
- Selection of suitable microbial strains or consortium;
- Continuous and repeated application of bioaugmentation to the treatment system;
- Monitoring techniques which supervise the survival and activity of the inoculum;
- Immobilisation techniques, particularly with membrane bioreactors;
- Horizontal gene transfer techniques which introduce catabolic genes to indigenous microbial community instead of introducing selected strains.

Microbial ecology characterisation is important for understanding the important metabolic processes in a given treatment setting [109]. Dejonghe *et al.* (2001) suggested that microbial diversity can be viewed under the framework of the Pareto principle, where 20% of the microbial species are responsible for 80% of the total energy flux [109, 110]. Therefore, the organisms introduced to a given treatment system should be able to participate in the main catabolic processes to ensure viability and activity [110].

Microbial strain selection is one of the most widely reviewed aspects of bioaugmentation [108, 111]. A single strain or a consortium of organisms with desirable metabolic capabilities may be applied to the contaminated environment. The selected microbes are usually enriched directly from the target contaminated ecosystem ("autochthonous") or an environment with similar conditions ("allochthonous") [112, 113]. While pure and mixed cultures for bioremediation are commercially available, microbes endogenous to the contaminated environment are more likely to thrive post-inoculation [113]. However, this is not always practicable, as the enrichment of metabolically competent organisms requires weeks to months of culturing (Table 2.4). Furthermore, the enrichment conditions are usually very different to the realities of treatment system. Therefore, the cultivation bias for metabolic competence in the laboratory does not always translate to the target ecosystem.

Various strategies have been proposed for improving microbial strain selection. Singer *et al.* (2005) proposed three strategies as alternatives to traditional enrichment cultures [111]. The first method makes use of "heirloom" strains – highly competent microorganisms previously isolated and maintained in culture collections. The second method cultivates degrading microorganisms on plant roots and is primarily applicable for soil bioremediation. The third method involves "priming" a sample of the microbial community with repeated exposure to the target contaminant. Priming is a form of biostimulation, i.e., altering physical conditions to encourage the

indigenous microbial community to increase specific metabolic activities [111]. Bioaugmentation with primed microorganisms has the distinct advantage of including microorganisms which are otherwise unculturable [111]. Genetically modified microorganisms (GMMs) and horizontal gene transfer techniques have also been explored in bioaugmentation, however, most examples are confined to lab-scale experiments due to the general concern around the fate of GMMs in the environment [109].

The introduction of the selected microorganisms into the target environment is the main process of bioaugmentation. It is well understood that the augmented microorganisms decline in abundance after inoculation, and therefore, significant attention has been devoted to understanding how to ensure the viability and activity of the bacteria post-inoculation [109, 112]. In particular, the effects of inoculum dosing size and frequency have been evaluated. A study by Schwartz and Scow (2001) evaluated both of these parameters in *Arthrobacter* mineralisation of the polyaromatic hydrocarbon (PAH) phenanthrene in contaminated soil [114]. Schwartz and Scow reported greater mineralisation (i.e., oxidation of an organic substrate to inorganic CO_2) of phenanthrene with increasingly higher inoculum doses. However, over several months, there was a loss of bio-mineralisation activity following the initial application compared to uninoculated soil, and the bio-mineralisation activity recovered upon re-inoculation of the soil [114]. In addition to continuous or repeated inoculation, cell immobilisation has been noted as a useful inoculation strategy, since it generates protective barriers around the microbes and increases their metabolic activity [109, 115].

This emerging biotechnology has been successfully implemented in the field to remediate recalcitrant industrial pollutants. Examples of such applications include remediation of chlorinated ethenes in sandy aquifers augmented with *Dehalococcoides* [116], methyl *tert*-butyl ether in groundwater aquifers augmented with *Methylibium petroleiphilum* [117], and partial remediation of petroleum hydrocarbons in soil augmented with microbial consortia containing *Rhodococcus*, *Acinetobacter*, and *Pseudomonas* [118]. More recently, there has been growing interest in applying bioaugmentation for the targeted removal of non-industrial micropollutants [119].

2.3.2 Bioaugmentation for Estrogen Removal

Bioaugmentation has been applied towards enhanced estrogen removal in lab-scale treatment systems with moderate success. One example of successful bioaugmentation is a study by Peng *et al.* (2023), which applied *Pseudomonas citronellolis* SJTE-3 to pig manure spiked with 1 mg L^{-1} EE2 and achieved 70% removal compared to 15% removal in un-augmented manure [105]. In another example, primary effluent in bench-scale batch reactors augmented with *Novosphingobium* sp. JEM-1 only partially removed estrogens – 60% E1 and 65% E2 compared

to the un-augmented control systems [79]. Partial removal of estrogen was also achieved in bioaugmented wetland gravel biofilms [104]. In addition, Haig *et al.* (2016) showed that the bioaugmentation of estrogen-degrading bacteria to lab-scale slow sand filters not only enhanced estrogen removal from the influent (79% E1 and 35% E2, compared to 2% E1 and -67% E2 in the control systems), but the decreased estrogenic potency of the treated water changed the microbial community in the filter and improved coliform removal [120].

A study by Roh *et al.* (2011) is one example where bioaugmentation was shown to be only a minor contributor to estrogen biodegradation. The authors spiked *Sphingomonas* sp. KC8 into sequencing batch reactors containing nitrifying activated sludge with different SRTs (5, 10, and 20 days) [121]. The applied estrogen (1 mg L^{-1} E2) was fully removed in the two longer SRTs while complete removal was inconsistent in the 5-d SRT. However, the abundance of the augmenting organism KC8 had decreased and stabilised after three mixed liquor exchanges corresponding with the SRTs, and the authors suggest that "unknown slow-growing" degraders are responsible for biodegradation of estrogens [121].

Notably, in each of the estrogen bioaugmentation studies presented here, the inoculating organisms were isolated *de novo* by the research groups. As previously indicated, strain selection is an important design parameter in successful bioaugmentation, and endogenous or allochthonous bacteria have a greater potential to thrive post-inoculation. However, the enrichment and isolation process to cultivate metabolically competent bacteria is extremely slow (Table 2.4), with enrichment cultures ranging from a minimum of a week up to several months [87, 92, 120]. Furthermore, studies often screen multiple environments – e.g., sludge and wastewater from WWTPs, soils, sediments, surface water, compost, and faeces – to isolate estrogen-degrading strains [75, 80, 90, 122]. In one notable example, Shi *et al.* (2002) screened "hundreds" of soil and manure samples to isolate *Fusarium proliferatum* HNS-1 [122]. Thus, the literature around bioaugmentation for estrogen removal is limited. Potential gaps in understanding estrogen removal by bioaugmentation include the application of consortium communities, directly comparing bioaugmentation with different strains, the use of more environmentally relevant estrogen concentrations, the use of immobilisation techniques, and performing bioaugmentation in large-scale systems or field sites.

2.3.3 *In silico* Methods in Biodegradation

Computational methods have the potential to be particularly useful for environmental microbiology due to the practical limitations around culturing environmental organisms *in vitro* [123]. Following advances in computational methods, novel *in silico* approaches are being explored to engineer microbial communities for enhanced biodegradation of micropollutants [106]. Through computational techniques, like machine learning algorithms, the operational treatment parame-

ters which enhance micropollutant removal rates and efficiencies can be identified [124–126].

Some of the machine learning techniques employed in enhancing biodegradation include evolutionary or genetic algorithms (GA), which treat biodegradation as a parameter optimisation problem, and artificial neural networks (ANN), which identify variable patterns that correlate with enhanced biodegradation [123, 127]. GA can be employed for optimising parameters (e.g., temperature, pump rates, contaminant concentration, etc.) for a single objective (e.g., "maximise contaminant removal") or multiple objectives (e.g., "maximise contaminant removal and minimise operational costs") [128]. GA may also be used in conjunction with other optimisation techniques, such as gradient-based methodology [129, 130]. For example, an investigation by Zafar *et al.* (2010) combined GA and response surface methodology to identify media components which enhance bioremediation of naphthalene by *Pseudomonas putida* in batch cultures [129].

Alternatively, ANN is used to predict how the variables of different input parameters will affect different output variables. One study which utilised ANN for understanding operational parameters on biodegradation was conducted by Nourouzi *et al.* (2012), where ANN was used to show that pH and contaminant concentration affected glyphosate degradation efficiency in batch cultures, while the inoculum size affected degradation rate [124]. However, an important limitation of ANN is the large quantity of data required to train the model. In some cases, the model is trained by GA or other algorithms, but where experimental data is used, usually hundreds of data points are required [124–126]. While GA does not require training data, the fitness values must be informed by calculation, simulation, or experimental results [106]. A recent study by Mohammadi *et al.* (2023) collected a total of 90 samples over 17 experiments for using ANN to model the optimal conditions for efficient removal of estrogens in a lab-scale moving-bed biofilm bioreactor containing synthetic wastewater [131]. The estrogen concentrations were determined by a gas chromatography-mass spectrometry method with an analysis time of 29 min per sample [131].

Thus, while *in silico* methods have significant benefits over physical experiments, including scalability and being unaffected by the limitations of available laboratory techniques, some experimental data is still required to inform, train, and validate the models. Currently, the literature around modelling estrogen biodegradation is limited. Mohammadi *et al.* (2023) proposed testing additional treatment technologies from WWTPs (e.g., AS and TF) and longer monitoring periods to enhance the applicability of their model and to evaluate the model's robustness [131]. Since advanced computational methods may require large quantities of data – specifically, the contaminant removal rates and efficiency (i.e., fractional removal) – there is a crucial need for chemical analysis methods which can efficiently measure estrogen concentrations in biodegradation experiments at scale.

2.3.4 Methodological Gaps

Here, we identify two significant bottleneck points in engineering biodegradation for enhanced removal of estrogen micropollutants: 1) strain selection for bioaugmentation and 2) trace analysis of estrogens to determine removal rates and efficiency.

1. Currently, individual strain selection relies heavily on lengthy enrichment cultures. Furthermore, the enrichment culture process is biased towards catabolising organisms which grow well under the enrichment culture conditions that do not accurately reflect the conditions where bioremediation will occur.

2. The current methodologies used to measure estrogen concentrations (which are explored in detail in the next chapter) are highly effective but low-throughput. This presents a conflict for using computational methods to optimise or predict the parameters which enhance biodegradation, as they require significant quantities of data – specifically, micropollutant removal efficiencies and rates – to generate the models.

There have been major advances in understanding microbial ecology in biodegradation, particularly due to the availability of advanced and high-throughput molecular biology techniques, such as gene abundance, transcript abundance, and metagenomics [109]. However, the processes of strain selection and estrogen trace analysis currently rely on inefficient and, in the case of the former, inelegant solutions.

Therefore, we propose that these two methodological gaps may be addressed with new chemical trace analysis methods. In strain selection, we propose that the ability to selectively measure the uptake of estrogen by bacteria in a mixed community can be used to screen for metabolically competent organisms. In chemical trace analysis, we propose the use of estrogen-targeted biological sensors, a relatively new but scalable technology which does not rely on traditional analytical workflows. Since time- and cost-efficiency are the parameters we aim to improve, we propose the use of spectroscopic analytical techniques. Spectroscopic detection is rapid and, with the use of multi-well microplates, scalable (i.e., high-throughput). In addition, the instrumentation for spectroscopy is relatively simple and widely available in most microbiological laboratories.

2.4 Trace Analysis of Estrogens

Analysing estrogen micropollutants in the environment is a critical step towards determining their impact. In order to establish how their presence may affect the local ecosystem, it is necessary to know the concentrations of estrogens and the characteristics of their degradation

products. However, detection of estrogens at environmentally relevant concentrations in complex matrices requires highly sensitive and selective analytical methods. Chemical trace analysis – the selective detection or quantification of the chemical constituents in a sample in very small quantities, i.e., 100 parts-per-million (ppm) or less – is performed using advanced sample preparation procedures and sensitive instruments which use a variety of modalities to detect compounds of interest [132]. The most common analytical workflows for trace analysis of estrogen micropollutants combined an extraction method with a chromatographic method (Table 2.5).

Table 2.5: Analytical methods for environmental estrogens reported in the literature.

Ref	Sample Type (Volume)	Analytical Workflow	SPE	Column	Detection	Method Quant. Limit (ng L^{-1})
[39]	Influent (0.15 L) Effluent (0.4 L) River water (4 L)	SPE - LC - ESI - MS/MS	GCB	C18	QqQ - SRM	E1 = 0.008–0.2 E2 = 0.02–0.6 E3 = 0.02–0.6 EE2 = 0.03–0.9
[133]	Influent (0.1 L) Effluent (0.25 L) River water (0.25 L)	SPE - LC - ESI - MS/MS	HLB	C18	QqQ - SRM	E1 = 0.4–1.0 E2 = 0.6–1.4 E3 = 0.8–2.6 EE2 = 1.2–3.0
[42]	Effluent (0.4 L) Surface water (0.4 L)	SPE - LC - ESI - MS/MS	C18	PFP	QqQ - SRM	E1 = 48 E2 = 66 EE2 = 45
[134]	Pure water (0.01 L) Tap water (0.1 L) Surface water (0.1 L)	SPE - LC - UV	MIP	C18	280 nm	E1 = 9.3[a]
[135]	Surface water (0.5 L)	SPE - LC - ESI -MS/MS	HLB	C18	QqQ - SRM	E2 = 0.06 EE2 = 0.02
[136]	Pure water (2 L) Influent (1 L) Effluent (1 L) River water (2 L)	SPE - D - GC - MS/MS	HLB	BP-1 or BP-5	IT - SRM	E1 = 0.5–1 E2 = 1–2 E3 = 1.5–3 EE2 = 1.5–3
[40]	Tap water (20 L) Effluent (20 L)	SPE - LC - UV - LLE - GC - MS	C18	C18 [GC-?]	210 nm IT - SIM	E1 = 0.2 E2 = 0.2 E3 = 0.2 EE2 = 0.2
[59]	Groundwater (1 L) Influent (1 L) Effluent (1 L)	SPE - D - GC - MS/MS	C18	XTI-5	IT - SRM	E1 = 1 E2 = 1 EE2 = 1

[a] - Method detection limit (ng L^{-1}). SPE - solid phase extraction; LLE - liquid-liquid extraction; D - derivatisation; LC - liquid chromatography; GC - gas chromatography; ESI - electrospray ionisation; UV - ultraviolet detector; MS - mass spectrometry; MS/MS - tandem MS. GCB - graphitised carbon black; HLB - hydrophobic-lipophilic balance; MIP - molecularly imprinted polymer; C18 - octadecylsilyl; PFP - pentafluorophenyl. QqQ - triple quadrupole MS; IT - ion trap MS; SIM - selected ion monitoring; SRM - selected reaction monitoring.

As previously noted, the environmentally relevant concentrations for estrogens in water were found to be around 0.001–30 ng L^{-1}. In addition, the EU maximum acceptable method detection limit (i.e., the lowest detectable concentration by an analytical method) is 0.4 ng L^{-1} for E1 and E2 and 0.035 ng L^{-1} for EE2 [12]. Therefore, highly sensitive analytical methods are required to detect these concentrations. This is primarily achieved by concentrating large sample volumes (e.g., >100 mL) into a smaller extract volume. Most workflows include solid phase extraction (SPE), which can process large sample volumes and concentrate the analytes by orders of magnitude. For example, the SPE method used by Quintana *et al.* (2004) extracted estrogens from 2 L of river water into 100 µL of ethyl acetate [136]. The most common SPE sorbent materials were hydrophobic-lipophilic balance (HLB) and octadecylsilyl (C18) which are suited to extract to non-polar estrogens [3]. Other SPE sorbent materials, including graphitised carbon black (GCB) and molecularly imprinted polymers (MIP), have also been employed to extract estrogens [39, 134].

The estrogens extracted from environmental samples were then analysed using liquid chromatography (LC) or gas chromatography (GC). When GC analysis was used, the estrogens were usually derivatised prior to analysis with a silylation reagent, such as *N*-trimethylsilyl-*N*-methyl trifluoroacetamide (MSTFA) [59, 136]. Chromatographic separation was often coupled with mass spectrometry (MS) or tandem mass spectrometry (MS/MS). Tandem MS/MS, in particular, was performed with triple quadrupole (QqQ) or ion trap (IT) mass spectrometers. Detection with UV is less common for environmental samples since it has less selectivity and sensitivity than MS. For example, Wang *et al.* (2008) analysed tap water, river water, and lake water spiked with 10 µg L^{-1} E1 using LC-UV [134]. In contrast, Miège *et al.* (2009) developed an analytical method using LC coupled with a triple quadrupole mass spectrometer which achieved method quantitation limits as low as 1 ng L^{-1} E1 and 1.4 ng L^{-1} E2 in an identical volume (100 mL) of WWTP influent – a much dirtier sample matrix [133].

Trace analysis is also used to quantify and characterise estrogen micropollutants in controlled biodegradation experiments (Table 2.6). Analysis of estrogen biodegradation in laboratory cultures or lab-scale treatment systems was often done with much higher working concentrations than those observed in the environment – up to five orders of magnitude (mg L^{-1}). Therefore, while laboratory biodegradation studies also used chromatographic methods, there was more diversity in the extraction and detection methods used. The sample volumes are much smaller, and therefore, liquid-liquid extraction (LLE) or simple filtration was more commonly used in sample preparation. When filtration was used, the sample was injected directly into the LC or mixed with an organic solvent, such as methanol, to solubilise the hydrophobic estrogens [75, 82, 83].

Since the working concentrations were much higher, detectors which are less sensitive or selective than MS were used, including UV, photodiode array (PDA), fluorescence (FLD), elec-

Table 2.6: Analytical methods for laboratory estrogen biodegradation reported in the literature.

Ref	Sample Type	Analytical Workflow	Column	Detection	Working Conc. ($\mu g\ L^{-1}$)
[79]	Bench-scale AS system	SPE - LC - ESI - MS/MS	C18	QqQ - SRM	E1 = 0.045 E2 = 0.02
[97]	Batch cultures	LLE or SPE - LC - ESI - MS/MS	C18	Q - TOF - FS	E1 = 2.7×10^5
[97]	Batch cultures	SPE - LC - PDA	C18	200-450 nm	E1 = 2.7×10^5
[92]	Batch cultures	LLE - LC - UV	C18	280 nm	EE2 = 30×10^3
[99]	Batch cultures	LC - PDA - ESI - MS	C18	240 nm IT - SRM	E2 = 5×10^5 E3 = 5×10^5
[83]	Batch cultures with AS	Filt - LC - PDA or FLD	C18	210 nm 220 nm/315 nm	E2 = 1.5×10^5 EE2 = 3×10^5
[72]	Batch cultures with AS	Filt - LC - ECD	C18	-	E1 = 1×10^3 E2 = 1×10^3 E3 = 1×10^3 EE2 = 1×10^3
[75]	Batch cultures with AS, compost, or faeces	Filt - LC - UV or FLD	C18	205 nm 230 nm/290 nm	E1 = 5×10^3 E2 = 5×10^3 E3 = 5×10^3 EE2 = 1×10^3
[120]	Lab-scale SSF system	SPE - D - GC - MS	HP-5MS	Q - SIM	E1 = 0.05 E2 = 0.012 E3 = 0.039
[82]	Batch cultures	Filt - GC - FID	HP-1	-	E1 = 2×10^5 E2 = 2×10^5
[82]	Batch cultures	LLE - D - GC - MS	DB-5H	Q - FS	E1 = 2×10^5 E2 = 2×10^5
[78]	Batch cultures	LLE - D - GC - MS	DB-5MS	Q - SIM	E1 = 3×10^3 E2 = 3×10^3

AS – activated sludge; SSF – slow sand filtration. SPE - solid phase extraction; LLE - liquid-liquid extraction; Filt - filtration; D - derivatisation; LC - liquid chromatography; GC - gas chromatography; PDA - photodiode array detector; UV - ultraviolet detector; FLD - fluorescence detector; MS - mass spectrometry; MS/MS - tandem MS; ECD - electrochemical detector; FID - flame ionisation detector. Q - quadrupole MS; QqQ - triple quadrupole MS; TOF - time-of-flight MS; IT - ion trap MS; SIM - selected ion monitoring; SRM - selected reaction monitoring; FS - full scan.

trochemical (ECD) and flame ionisation detectors (FID). These detectors were used for quantitative analysis to establish removal rates or efficiencies [72, 75, 82, 92, 97]. However, MS and MS/MS was be used for quantifying *in vitro* estrogen biodegradation at more environmentally relevant concentrations [78, 79, 120]. In addition, mass spectrometry was used for qualitative analysis of degradation products [97, 99]. A study by Chen *et al.* (2018) used high-resolution MS/MS with a quadrupole-time-of-flight (Q-TOF) tandem mass spectrometer to evaluate the

metabolites generated from biodegradation of estrone [97].

Chromatography with MS detection has been described as the "gold standard" technique for organic micropollutant trace analysis [137]. Since LC does not require derivatisation, LC-MS/MS is the preferred platform for estrogen micropollutant detection [137, 138]. Although these methods are fit for purpose in analysing trace chemicals in a complex mixture, chromatographic techniques are low-throughput, capable of analysing only one sample at a time. Analysis times vary from 15 to 30 minutes by LC and 30 to 45 minutes by GC [39, 82, 133, 136]. In addition, sample preparation and derivatisation further prolong the turnaround time. The methodological gaps identified previously demonstrated there was a need for more efficient, high-throughput methods to measure estrogen concentrations and to detect estrogen-degrading bacteria. The remainder of this chapter will discuss the theory behind trace analysis methods in detail, beginning with gold standard chromatographic techniques. This will be followed by the proposed methods to address the methodological gaps, which includes fundamental spectroscopic techniques and colorimetric biosensors.

2.5 Analytical Figures of Merit

Both qualitative and quantitative analytical methods are described by the following performance characteristics: throughput, selectivity, specificity, and sensitivity. Method throughput is the number of samples which can be analysed over a period of time, and it is improved by increasing the method speed or the number of samples analysed (e.g., parallel versus sequential processing) [139]. Selectivity and specificity are both used to describe the extent to which other substances interfere with analyte detection [140]. According to the International Council for Harmonisation of Technical Requirements for Pharmaceuticals for Human Use (ICH), selectivity is "the ability of an analytical method to differentiate and measure the analyte in the presence of potential interfering substances" [140]. Selectivity is commonly described in relation to matrix interference, where other components within a sample can interfere with detecting the target analyte of interest by increasing or decreasing the response [140]. Additionally, selectivity describes the ability of a method to detect multiple target analytes independently and concurrently [141]. Specificity is the ability to "detect and differentiate the analyte from other substances, including its related substances" according to the ICH [140]. While selectivity should be demonstrated with experimental validation, specificity can be ensured through the technical parameters of certain instruments, such as isotope resolution in mass spectrometry [140]. Sensitivity (Equation 2.1) is the rate of change of the instrument response (y) over the difference in analyte concentration (x):

$$\text{Sensitivity} = \frac{\Delta y}{\Delta x}. \tag{2.1}$$

Quantitative trace analysis is achieved by comparing the measured response of a sample to a calibration equation (Figure 2.8) [140]. The response of the instrument is first calibrated using a set of calibration standards (i.e., reference materials which contain a known quantity of the target analytes across the range of concentrations which elicit a response from the instrument). The calibration equation is then obtained by performing regression analysis on the concentration of the calibration standards (the dependent variable, x) and the respective instrument response (the independent variable, y). Thus, the slope of the calibration curve at a given point is equivalent to the method sensitivity (Equation 2.1). Linear equations are the most common models used to describe the relationship between analyte concentration and instrument response and are usually fit by least-squares linear regression (Equations 2.2–2.4) [142, 143]:

$$\text{slope} = a = \frac{\sum_i [(x_i - \bar{x})(y_i - \bar{y})]}{\sum_i (x_i - \bar{x})^2} \tag{2.2}$$

$$\text{y-intercept} = b = \bar{y} - a\bar{x} \tag{2.3}$$

$$y = ax + b \tag{2.4}$$

where y_i is the measured response for each individual measurement i, x_i is each concentration of each calibration standard, and $\bar{x}$ and $\bar{y}$ are the mean of calibration standard concentrations and responses, respectively. Other nonlinear equations (exponential, polynomial, and logarithmic transformations) and weighted least-squares regression are also sometimes used if the linear equation does not accurately describe the data [143].

2.5.1 Analytical Method Validation

Analytical method validation is one of the core tenets of trace analysis, particularly for quantitative analysis [144]. In method validation, the performance characteristics of the method are systematically tested to establish that it is fit for its intended purpose. The performance characteristics which are evaluated include selectivity and specificity, linearity, range, limits of detection and quantitation, precision, accuracy, and robustness [140, 144].

- **Selectivity and specificity** are evaluated by analysing the target compound(s) in the presence of anticipated interferences. This can be achieved comparing the response of the reference standard to chemically related compounds or by spiking the reference standard into target-free sample matrix [140].

- **Linearity** is evaluated by how well the linear regression model fits the data and is usually

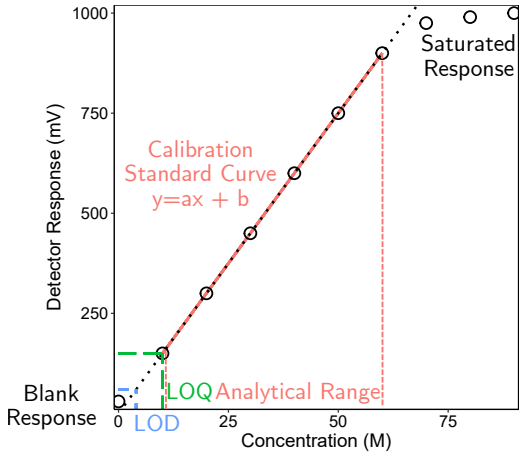

Figure 2.8: Example calibration standard curve with linear regression (dashed black line). The analytical range is noted in the graph, as well as the response of concentrations outside the analytical range, including the blank. The limits of detection and quantitation (LOD, LOQ) are included for illustrative purposes, as their true values depend on the response signal-to-noise, standard deviation of the blank, or error of the regression curve y-intercept.

described by the coefficient of determination (R^2, Equation 2.5):

$$R^2 = 1 - \frac{RSS}{TSS} = \frac{\sum_i (\hat{y}_i - \bar{y})^2}{\sum_i (y_i - \bar{y})^2} \tag{2.5}$$

where RSS and TSS are the sum of square residuals and total square residuals, respectively, and $\hat{y}_i$ is the predicted response for the known concentration (x_i) as calculated by the linear regression equation (Equation 2.4) [142].

- The **analytical range** is the interval of concentrations measured by the method, bounded by the upper and lower calibration standard [140].
- The **limits of detection and quantitation** (LOD, LOQ) are the lowest concentration the method can reliably detect or quantify to a degree of statistical certainty [144]. There are several accepted methods to determine LOD and LOQ, including the signal-to-noise of the response, standard deviation of the blank response, and error of the intercept from the regression curve. In each case, a factor of 3 or 3.3 is used to estimate LOD, and a factor of 10 is used to estimate LOQ [140, 142].
- **Precision and accuracy** are usually determined by repeated measurements of quality control (QC) samples – i.e., samples with a known quantity of analyte that are distinct from the calibration standards and are used to monitor the performance of the method.

  - **Precision** measures the degree of scatter of the response or measured concentration and is reported as percentage relative standard deviation (% RSD, Equation 2.6):

$$\% \text{ RSD} = 100\% \times \frac{\sigma}{\mu} \tag{2.6}$$

    where σ is standard deviation and μ is mean of either the response (y) or measured concentration (x) of the QC [140, 142]. Precision is described in at least two levels: "repeatability", which measures the short-term precision; and "intermediate precision", which measures the precision across a longer period, such as a lengthy batched run or across different days.

  - **Accuracy** measures the trueness of the measured concentration and is reported as percentage recovery (Equation 2.7) or error (Equation 2.8):

$$\% \text{ Recovery} = 100\% \times \frac{x_c}{x_i} \tag{2.7}$$

$$\% \text{ Error} = 100\% \times \frac{x_c - x_i}{x_i}. \tag{2.8}$$

    Here, x_c represents the concentration as calculated from the response (y) of the QC using the calibration equation, and x_i represents the true concentration of the quality control [140, 142].

- **Robustness** describes how resilient the method is to variations in the method parameters. Robustness is usually determined by deliberately modifying method parameters (e.g., mobile phase conditions) and evaluating how the figures of merit are affected [144].

Laboratories which perform testing services are regulated by government or industry authorities and must adhere to the published guidelines for analytical method validation [140, 144, 145]. These guidelines specify the assessment methodology and acceptance criteria for each figure of merit. While there are small variations in rigour and detail, the performance characteristics outlined in the guidelines are largely identical across sectors. Research facilities are not held to such standards in analytical method validation, however, the published guidelines serve as a useful reference tool for evaluating independently developed methods. This systematic assessment process not only ensures the method is fit for purpose, but it also allows researchers to compare method performance across laboratories, as well as within a laboratory (e.g., across time, consumable batches, and operators).

2.6 Chromatographic Techniques

Chromatography is a powerful tool used to physically separate individual compounds in a mixture for analysis [146, 147]. In chromatography, the sample or mixture is dissolved in a liquid or gas, called the "mobile phase". The mobile phase determines the technique as gas chromatography (GC) or liquid chromatography (LC). The mobile phase continuously flows through a system which contains an immobile material called the "stationary phase". In column chromatography, the stationary phase is made of chemical moieties bonded to viscous liquid lining a capillary tube or silica particles packed into a column. Separation occurs by the different affinities of the chemical components for the mobile phase versus the stationary phase. Those analytes which adsorb or partition to the stationary phase with greater affinity will pass through the column slower. As the analytes elute from the column, a detector measures an electronic signal in real-time which is proportionate to the amount of analyte. The results are presented as a chromatogram: a graph of the detector signal versus time (Figure 2.9). The time of elution, indicated by a peak in the chromatogram, is known as the "retention time" (t_R) and is ideally selective for each individual compound.

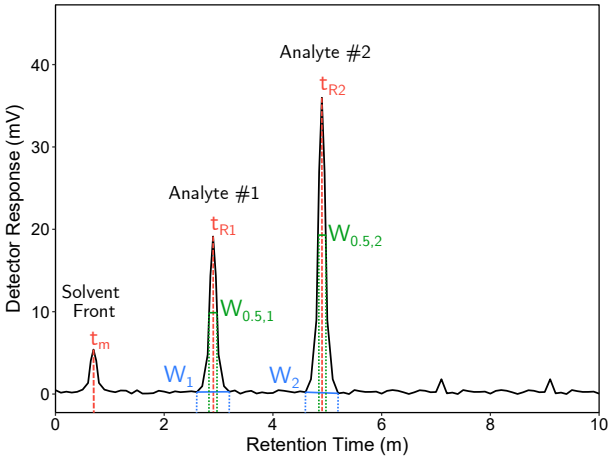

Figure 2.9: Example chromatogram with solvent front or analyte peak retention times (t_m and t_R, respectively) indicated in red, peak widths (W) indicated in blue, and peak widths at half maximum ($W_{0.5}$) indicated in green.

2.6.1 Theory

The basis of chromatography separation is the continuous partitioning of compounds between the mobile and stationary phases as the mobile phase flows through the system [146]. There are two main approaches to describe how analytes (A) with different affinities for the mobile and stationary phase are separated by chromatography. The first approach is "Plate Theory", which

assumes the analytes are in equilibrium between the two phases (Scheme R2.1). According to Plate Theory, the partition coefficient (K, Equation 2.9) is the ratio of the concentration of the analyte ([A]) in stationary (s) to mobile phase (m) [146]:

$$[\mathrm{A}]_{\mathrm{mobile}} \rightleftharpoons [\mathrm{A}]_{\mathrm{stationary}} \tag{R2.1}$$

$$K = \frac{[\mathrm{A}]_s}{[\mathrm{A}]_m}. \tag{2.9}$$

The partition coefficient is directly related to the adjusted retention time (t'_R). The adjusted retention time (Equation 2.10) is the total time the analyte takes to reach the detector (t_R) minus the time needed for the mobile phase and any nonretained compounds to pass straight through the system (i.e., the injection port, tubing, and column) to the detector (t_m) [146]:

$$t'_R = t_R - t_m. \tag{2.10}$$

Fundamentally, the adjusted retention time is the time the analyte spends interacting with the stationary phase. The capacity factor (k, Equation 2.11) is the proportion of the amount of time the analyte spends interacting with the stationary phase compared to the mobile phase [146, 147]:

$$k = \frac{\text{time of A in stationary phase}}{\text{time of A in mobile phase}} = \frac{t'_R}{t_m}. \tag{2.11}$$

The relative amount of time an analyte spends in a given phase is directly proportional to the relative amount of moles of analyte in that phase, thus [146]:

$$k = \frac{\text{moles of A in stationary phase}}{\text{moles of A in mobile phase}} = \frac{[\mathrm{A}]_s V_s}{[\mathrm{A}]_m V_m} = K\frac{V_s}{V_m}. \tag{2.12}$$

Therefore, the capacity factor is a measure of how well a compound is retained by the system. An optimal k value is be between 2–10, where k<2 indicates the compound is not being sufficiently retained by the stationary phase, and k>10 indicates the compound affinity for the stationary phase is too high.

The above terms describe how an individual analyte is retained by the chromatography system. Building upon these terms, we can describe how well the compounds in a mixture are separated from each other. One example is the selectivity factor (α, Equation 2.13) which is the ratio of capacity factors of two compounds (the compounds being 1 and 2, where $t_{R2} > t_{R1}$) [146]:

$$\alpha = \frac{t'_{R2}}{t'_{R1}} = \frac{k_2}{k_1}. \tag{2.13}$$

A selectivity factor of at least 1.1 indicates there is good chromatographic separation between

the compounds. Resolution (*Rs*, Equations 2.14 and 2.15) differs from the selectivity factor by taking into account the width of the peaks at the base (W) or at half of the maximum response ($W_{0.5}$) [147]:

$$Rs = \frac{t_{R2} - t_{R1}}{0.5(W_1 + W_2)} \tag{2.14}$$

$$Rs = 1.18 \times \left(\frac{t_{R2} - t_{R1}}{W_{0.5,1} + W_{0.5,2}} \right). \tag{2.15}$$

The peak width is the interval of time which an analyte elutes from the column, where a narrower peak is preferred for good resolution and signal intensity. Two peaks with good resolution have an *Rs* greater than 1.5 [147].

Chromatographic efficiency is the overall ability of a chromatography system to separate compounds. According to Plate Theory, the number of "theoretical plates" (N) within a column represents the number of theoretical equilibration points between the stationary and mobile phase, where a greater number of theoretical plates yields greater chromatographic separation. The number of theoretical plates (Equations 2.16 and 2.17) can be calculated from retention time and peak widths [146, 147]:

$$N = 16 \left(\frac{t_R}{W} \right)^2 \tag{2.16}$$

$$N = 5.54 \left(\frac{t_R}{W_{0.5}} \right)^2. \tag{2.17}$$

The height equivalent of the theoretical plates ($HETP$) is another measure of efficiency and is calculated by L/N, where L is the length of the column [146]. As with resolution, good efficiency is achieved with longer retention times and narrower peaks. Resolution between two compounds is related to the chromatographic efficiency by the following equation [146]:

$$Rs = \left(\frac{\sqrt{N}}{4} \right) \left(\frac{\alpha - 1}{\alpha} \right) \left(\frac{k_2}{k_2 + 1} \right). \tag{2.18}$$

The second approach to describe chromatography is "Rate Theory", which assumes there are non-equilibrium effects in the system [146, 147]. Plate Theory does not account for the effects of the chromatography operating parameters, such as particle size, flow rate, and temperature, which are known to influence peak broadening. The van Deemter equation (Equation 2.19) concisely accounts for the such effects on chromatographic efficiency [147]:

$$HETP = \boldsymbol{A} + \frac{\boldsymbol{B}}{v} + \boldsymbol{C}v \tag{2.19}$$

where $\boldsymbol{A}$ represents eddy diffusion, $\boldsymbol{B}$ represents longitudinal diffusion, $\boldsymbol{C}$ represents resistance to mass transfer, and v is flow rate. Eddy diffusion accounts for the "multiple paths" effect in

packed columns, where the mobile phase meanders around the particles. ***A*** is determined by the particle shape and size as well as the uniformity of the particle packing within the column. Longitudinal diffusion is the broadening of the analyte peak as it travels along the column in accordance with Fick's Law of Diffusion. The resistance to mass transfer accounts for the time the analytes require to diffuse between the stationary and mobile phases depending on their affinity and proximity to a given phase. ***C*** is a complex term which is related to the capacity factor of the analyte. The diffusivity coefficient of the analyte in mobile phase – a temperature-dependent term – is directly proportional to ***B*** and inversely proportional to ***C***. According to Rate Theory, for a given chromatography system, there is an optimal flow rate for optimal chromatographic efficiency [147].

2.6.2 Gas Chromatography

Gas chromatography is a common technique used in environmental analyses to separate volatile components in a sample or extract (Figure 2.10) [148]. In GC analysis, the mobile phase is referred to as the carrier gas and is usually He, however N_2 and H_2 may also be used in certain applications. GC separation occurs by injecting a small volume (e.g., 1 µL) of liquid or gaseous sample into a heated port, instantly volatilising the sample. The evaporated sample is picked up by the carrier gas and flows through a heated column to the detector.

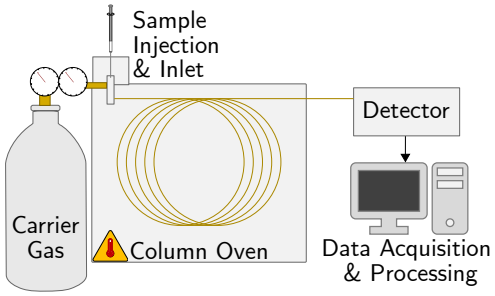

Figure 2.10: Diagram of gas chromatography system.

The columns used in GC trace analysis are open tubular capillaries made of fused silica coated with polyimide to provide mechanical support [148]. Since open tubular columns used in GC are not packed, there is no multi-path effect – i.e., $A = 0$ in Equation 2.19. Therefore, GC has much greater chromatographic efficiency compared to LC. Capillary columns have a narrow internal diameter (0.1–0.5 µm) and are very long (usually 30–60 m) [148]. The inner surface of the capillary is coated in a thin film of liquid which serves as the stationary phase. The stationary phase is a chemically inert, thermally stable polymer covalently bonded to the silica surface and cross-linked to itself. The chemical functional groups of the stationary phase are selected based on the polarity of the target analytes. Since estrogens and many organic micropollutants are non-polar to moderately polar (i.e., log$P$ values ~0.5–4.0), (diphenyl)$_x$-(dimethyl)$_{1-x}$polysiloxane is

the most common polymer used for stationary phase for separating such compounds, where x is the fraction of diphenyl in the polymer (up to 0.65, increasing in polarity) [41, 56].

The primary mechanism for GC separation is the boiling point of the analytes, while interaction with the stationary phase serves as a secondary mechanism for separation [148]. Compounds with lower boiling points flow through the column faster and elute first. The retention of the analytes can be controlled by programming the temperature of the column oven. When the column is maintained at a constant temperature, it is referred to "isocratic elution" [148]. During isocratic elution, the analytes with boiling points lower than the column oven temperature may elute rapidly and very close together, while the analytes with higher boiling points may not elute at all. Increasing the temperature during separation in a controlled, steady manner allows for efficient separation of a wider range of boiling points within a single analysis; this is referred to as "gradient elution".

Since gas chromatography is only feasible with volatile and thermally stable analytes, non-volatile compounds, such as estrogens, must be chemically derivatised prior to analysis. The aim of derivatisation for GC analysis is to impart thermal stability to thermolabile functional groups (OH, COOH, SH, NH, and CONH) and to increase volatility of the compound of interest [149]. This is achieved with three types of reactions which replace the active (polar) hydrogens: acylation (Scheme R2.2), alkylation (Scheme R2.3), and silylation (Scheme R2.4) [149].

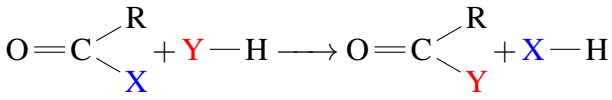

(R2.2)

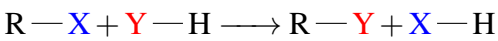

(R2.3)

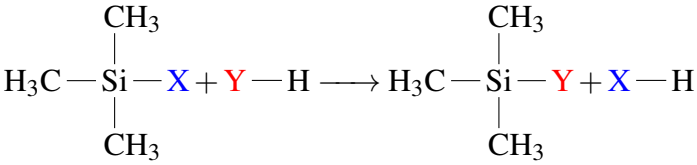

(R2.4)

These derivatisation reactions are nucleophilic substitutions, where the heteroatom on the analyte of interest serves as the nucleophile (Y) and the derivatisation reagent contains the leaving group (X).

2.6.3 High-Performance Liquid Chromatography

High-performance liquid chromatography (HPLC) is a form of liquid chromatography commonly used in trace analysis of environmental samples (Figure 2.11) [150]. In HPLC analysis, the liquid mobile phase is pumped through a column uniformly packed with particles, generating a high back-pressure. The liquid sample is first injected into a 6-port injection valve which

loads the sample into a loop of tubing at atmospheric pressure and then injects the loaded sample onto the column along with mobile phase at high pressure [150]. The sample dissolved in the mobile phase is pumped through the column to the detector, after which the eluate is collected as solvent waste if the detection method was non-destructive. In certain applications, such as preparative HPLC, the fraction of eluate containing the purified compound may be collected for further analysis.

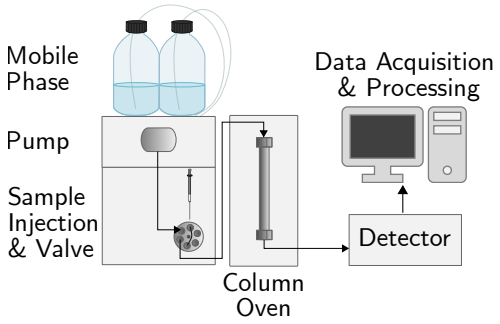

Figure 2.11: Diagram of high-performance liquid chromatography system.

The HPLC column is much shorter than the GC column (5–30 cm) and has a larger internal diameter (1–5 mm). The column is constructed of steel and is packed with tiny microporous (10–50 Å pore size) particles usually made of silica [150]. Standard HPLC uses particles of around 3–5 µm in diameter, while ultra high-performance liquid chromatography (UHPLC) uses particles $\leq$2 µm. The smaller particles in UHPLC yield greater resolution and chromatographic efficiency compared to standard HPLC by creating a more uniform flow path for the mobile phase and requiring less distance for the analyte to diffuse into the particle (i.e., decreased A and C terms in Equation 2.19) [151]. However, the smaller particles in UHPLC generate much greater back-pressure than standard HPLC ($\leq$15,000 psi versus $\leq$6,000 psi); therefore, UHPLC requires a special pump and valves [151].

The stationary phase for HPLC is covalently bonded to the particles and is available in a wide range of chemistries for various applications. As with GC, a non-polar stationary phase is used for separating estrogens and other non-polar to moderately polar organic micropollutants. Octadecylsilyl (C18) is the most commonly used non-polar stationary phase, followed by octylsilyl (C8) and phenylsilyl. When a non-polar stationary phase is utilised, it is paired with an organic polar mobile phase, such as methanol or acetonitrile [150]. This type of separation (i.e., non-polar stationary phase with polar mobile phase) is referred to as "reverse phase" chromatography (RPLC). When a polar stationary phase (e.g., bare silica or bonded with amino, cyano, or diol groups) is paired with non-polar mobile phase (e.g., hexane), this is referred to as "normal phase" chromatography (NPLC) and is used to separate polar analytes [151]. Hydrophilic interaction chromatography (HILIC) is a variation of NPLC that is compatible with the more environmentally-friendly polar organic solvents used in RPLC [151].

In contrast to GC separation, RPLC separation occurs primarily via the differential hydrophobic interactions between the analytes and stationary phase [151]. The analytes which are more non-polar (i.e., higher log$P$ values) will adsorb to the stationary phase with greater affinity and elute later than the more polar analytes. The mobile phase competes with analytes for adsorption sites on the stationary phase. The adsorption energy for a particular solvent on the stationary phase is referred to as the "elution (or eluotropic) strength" and is a measure of how easily the solvent displaces analytes from the stationary phase [151]. The elution strength of the mobile phase in RPLC can be optimised by mixing miscible solvents with different strengths, such as methanol and water. In HPLC, isocratic elution is when the mobile phase maintains a constant eluotropic strength, and gradient elution is when the eluotropic strength increases during separation. In gradient elution, the eluotropic strength is controlled by the pump, which can be programmed to mix solvents at different ratios throughout the chromatographic run.

2.6.4 Detectors

While the mobile and stationary phases are important considerations for separating the compounds in a chemical mixture, the detector captures that separation in real-time and generates a measurable output that analysts can interpret. Two important characteristics in chromatographic detectors are low noise and high sensitivity [151]. Noise – i.e., the rapid, random variations in the detector output – is a consequence of the electrical fluctuations in the detector circuitry and the background chemicals which enter the detector, such as contaminants in the mobile phase, leached plasticisers from sample handling, and the chemical milieu of the laboratory atmosphere [151]. The noise is calculated automatically by chromatography software by a variety of algorithms, such as peak-to-peak envelope and root mean square of the baseline [151]. Sensitivity represents the responsiveness of the detector per unit change in the amount of analyte. Detectors with low background noise and high sensitivity are thus able to observe lower concentrations of analytes (i.e., they have a lower detection limit) [151].

The detectors for chromatographic trace analysis can be grouped into two categories based on their detection mechanism – universal (non-selective) and selective [151]. Under these two categories, there are a variety of detection modalities which are suited to different chemical classes. The different modalities are related to the transducer mechanism, or how the detector converts a physical stimulus into an electrical response. Here, the detectors associated with analysis of small organic molecules are discussed.

2.6.4.1 Universal (Non-Selective) Detectors

Universal detectors respond (to a degree) to all of the substances that pass through the detector [151]. They are sometimes referred to as "bulk property detectors", since they monitor a

particular physicochemical property of the eluate which changes in the presence of a chemical compound other than the mobile phase. As bulk property detectors, they are not tunable or selective for sub-classes of analytes beyond those compatible with the associated chromatography system. As such, there are universal detectors for both GC and LC (Table 2.7).

The universal detectors used for GC analysis include thermal conductivity detection (TCD) and electron capture detection (ECD). Detection with ECD is much more sensitive than the TCD, however, the mechanism of ECD is biased towards more electronegative compounds [148, 151]. There are more universal detectors available for reverse phase HPLC analysis of small organic molecules, including refractive index detection (RID), electrochemical detection (ED), electrical light scattering detection (ELSD), and charged aerosol detection (CAD) [150, 151]. RID detection has relatively poor sensitivity, which results in a higher detection limit, and therefore, it is not commonly used for trace analysis. Furthermore, RID and ED need to operate with isocratic elution, as the mobile phase composition must be consistent.

In TCD, ECD, ED, and CAD detectors, the electrical signal is generated by the analytes directly affecting electronics in the detector (e.g., voltage, current, or charge), while optical RID and ELSD detectors use a photodiode or photomultipler tube (PMT) as a transducer. Photodiodes and photomultiplier tubes convert light (i.e., photons) into an electric current via the photoelectric effect using a *p*-*n* junction semiconductor or a photocathode coupled with electron-propagating dynodes, respectively [151, 152]. The amplification process endows PMTs with detection limits significantly lower than the photodiode (30 photons$\cdot$s^{-1} versus 6000 photons$\cdot$s^{-1}).

2.6.4.2 Selective Detectors

Selective chromatographic detectors respond to a particular trait of the chemical compounds in the eluate [151]. As with universal detectors, there are selective detectors specific for GC and HPLC systems (Table 2.8). Flame ionisation detetion (FID) is the most common detector for GC systems, as it detects all volatile hydrocarbon analytes [148]. Other selective GC detectors include flame photometric detection (FPD) and photoionisation detection (PID), which are further selective for sulphur- or phosphorus-containing compounds and aromatic or unsaturated compounds, respectively [148]. Ultraviolet (UV) absorbance detection is the most common detector for HPLC [150, 151]. Absorbance detection across multiple wavelengths can be achieved with photodiode array detection (PDA). Fluorescence detection (FLD) is another common detector used with HPLC and achieves the lowest detection limit. Detection by UV-Vis absorbance and fluorescence is selective for compounds which are chromophoric (i.e., absorb light at a particular wavelength) and fluorophoric (i.e., absorb light and re-emit the light at a lower energy); these spectroscopic concepts are discussed in greater detail in Section 2.7 [151].

Table 2.7: Universal detectors for GC and HPLC analysis [148, 150].

Separation	Detector	Mobile Phase	Transducer Mechanism	Measured Electronic Signal	Detection Limits
GC	TCD	He	Thermal conductivity of the eluate affects temperature and resistance of a filament	Applied voltage to maintain constant current or temp.	10 ng
	ECD	H_2 or 5% CH_4 in Ar	Eluate attracts β particles (e^-) emitted by radioactive ^{63}Ni which affects standing current generated by the particles	Applied voltage pulse rate to maintain constant current	0.1 pg
HPLC	RID	Isocratic Only	Refractive index of the eluate affects the path of the source light to photodiode array	Irradiated photodiode array	100–1000 ng
	ELSD	Volatile Only	Solid compound particles in nebulised eluate scatter source light path to an offset photodiode or photomultiplier	Irradiated photodiode or photomultiplier	0.1–1 ng
	ED	Isocratic Only	Eluate is reduced or oxidised on an electrode which affects the flow of electrons with a counter electrode	Current flow	0.01–1 ng
	CAD	Volatile Only	Ionised, solid compound particles in charged and nebulised eluate flow into an electrometer filter.	Electrical charge	0.1–10 ng

Table 2.8: Selective detectors for GC and HPLC analysis [148, 150].

Separation	Detector	Selectivity	Transducer Mechanism	Measured Electronic Signal	Detection Limits
GC	FID	Hydrocarbons	Ions produced by combusted eluate generate a current between electrostatic electrodes	Current flow	2 pg
	FPD	Compounds with P, S	Ions produced by combusted eluate emit light at specific wavelengths which is captured by photomultiplier	Irradiated photomultiplier	<1 pg (P) <10 pg (S)
	PID	Unsaturated compounds	Eluate irradiated by high-energy UV is ionised and emits electrons which generate a current	Current flow	25 pg
HPLC	UV-Vis/ PDA	Chromophoric compounds	Absorbance of eluate at specific wavelength(s) captured by photodiode or photodiode array	Irradiated photodiode or photodiode array	0.1 ng
	FLD	Fluorophoric compounds	Fluorescence of eluate at a specific wavelength captured by photomultiplier	Irradiated photomultiplier	0.001 ng

2.6.5 Mass Spectrometers

Mass spectrometers (MS) are highly sensitive and specific instruments which give information about the molecular weight of a compound and its relative abundance [153]. Mass spectrometry can be used as both a universal and a selective detector, making it a powerful tool in trace analysis. Briefly, MS detection is achieved by ionising the compounds in the eluate [153]. The ions are then accelerated in an electric field under high vacuum which separates the ions according to their mass-to-charge ratio (m/z). The current of ions is captured by a detector, and the readout is the "mass spectrum" – i.e., a graph of ion abundance versus m/z. When the ion carries a single charge (e.g., $M^{\bullet+}$, $[M+H]^+$, or $[M-H]^-$), the m/z value is equivalent to the molecular weight of the observed ion, corrected for any mass difference from the adduct.

2.6.5.1 Ion Source

There are three main components to a mass spectrometer: the ion source, the mass analyser, and the detector [153]. The ion source is where the eluate is ionised before separation in the mass analyser [154]. In GC- and LC-MS, the chromatography column is connected to the MS system at the ion source; this connection point is the sample inlet or interface. In GC-MS systems, the GC eluate flows directly from the column into the ion source via a heated segment of capillary tubing. Electron ionisation (EI) is the most common ion source for GC-MS (Figure 2.12a); it uses a heated tungsten or rhenium filament to emit electrons, which are then accelerated towards an anode (or electron trap) at 70 eV under vacuum [153, 154]. These accelerating electrons bombard molecules (M in Scheme R2.5) in the eluate as it flows into the source. These high energy electrons generate radical molecular cations ($M^{\bullet+}$ in Schemes R2.5 and R2.6), which are unstable and break into fragment ions with neutral losses (F and N in Scheme R2.6, respectively) [154]:

$$M + e^-(70\,eV) \longrightarrow M^{\bullet+} + 2e^- \tag{R2.5}$$

$$M^{\bullet+} \longrightarrow ({F_1}^+ + N^{\bullet}) + ({F_2}^{\bullet+} + N_2) + ... \tag{R2.6}$$

The ions are then guided and accelerated into the mass analyser by a charged repeller and lenses. The intramolecular fragmentation reactions induced by EI are highly reproducible and unique for different compounds; thus, the EI fragmentation pattern detected by the MS can be used for compound identification by comparing against reference libraries [153]. However, the unstable nature of the molecular ion means its abundance is very low, and therefore, "softer" ionisation techniques which result in less fragmentation are sometimes used to preserve the original molecule. One example of soft ionisation in GC-MS is chemical ionisation (CI), which uses a reagent gas (e.g., CH_4) to form ion adducts (e.g., $[M+H]^+$) [154].

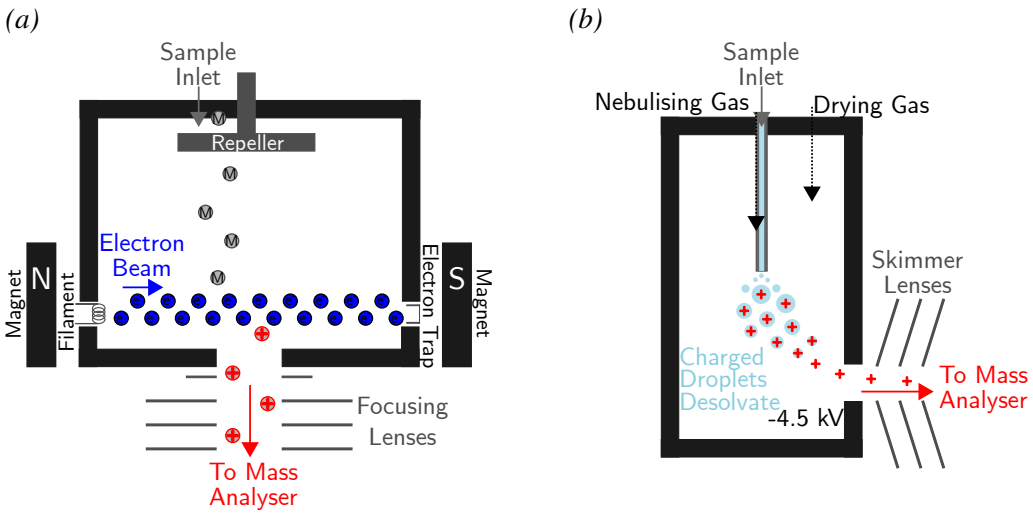

Figure 2.12: Diagrams of (a) electron ionisation and (b) electrospray ionisation sources.

Electrospray ionisation (ESI) is a soft ionisation technique which is commonly used with LC-MS analysis (Figure 2.12b) [153, 154]. Prior to MS analysis, the compounds must be in the gas phase; therefore, the HPLC eluate must be transformed from liquid solvent into a vapour. ESI achieves this by passing the HPLC eluate through a steel capillary along a coaxial flow of a sheath gas (N_2) which nebuilises the eluate. The eluate is charged by a potential difference applied to the steel capillary relative to the counter electrode. The charged spray particles form a Taylor cone, and the repulsive forces between the charged particles break them into increasingly smaller droplets until the solvent has evaporated and only the ions remain [153]. In contrast to EI, the ESI source operates at atmospheric pressure, and the pressure is only reduced after the ions pass through counter electrode and skimmer lenses [154]. However, ESI suffers from matrix effects, where co-eluting mobile phase constituents enhance or suppress ionisation of the analyte. While ESI is the most commonly used technique, other soft ionisation methods used in LC-MS include atmospheric pressure ionisation (APCI), which combines CI with a nebuliser, and atmospheric pressure photoionisation (APPI), which uses UV radiation [154].

2.6.5.2 Mass Analyser & Detector

There is a wide variety of mass analysers – i.e., the component of the MS where ion separation occurs under an electrical or magnetic field [155]. One of the most broadly applied techniques is the use of radio frequency (RF) and/or direct current (DC) voltages to filter or trap ions; this is the basis for quadrupole mass filters, ion traps, and Orbitraps (Figure 2.13) [155]. Quadrupole mass filters are one of the most common mass analysers and are compatible with both EI and ESI sources. Separation in quadrupole mass analysers occurs by applying both a constant DC voltage

(U) and alternating RF voltage ($V\cos(\omega t)$), where V is amplitude, ω is angular frequency, and t is time) to four parallel metal rods with alternating polarity under vacuum (10^{-6}–10^{-5} Torr) [155]. After exiting the source, ions are focussed into the space between the rods and oscillate within this electric field; this oscillation motion is described by the Mathieu equation:

$$\frac{\partial^2 \varphi}{\partial \tau^2} = -\varphi[a_\varphi - 2q_\varphi \cdot \cos(2\tau)] \tag{2.20}$$

where φ is the direction, τ is $0.5\omega t$, a is a parameter linked to DC voltage ($a \propto U \cdot (m/z)^{-1}$), and q is a parameter linked to RF voltage ($q \propto V \cdot (m/z)^{-1}$) [155]. The quadrupole varies the voltage intensities by $+2U/V$, and when a particular m/z is in resonance with the applied DC and RF potentials, that ion becomes stable and is transmitted through to detector. As the quadrupole scans from low to high voltages, ions of increasing m/z are transmitted. The chromatogram of the full scan (FS) acquisition – i.e., the cumulative abundance of all the ions in the defined mass spectrum range – is the total ion chromatogram (TIC). In addition, the instrument software can be instructed to apply the voltages which transmit only a specific, user-defined m/z, for example, that of an analyte of interest. This form of data acquisition is referred to as "selected ion monitoring" (SIM) [155].

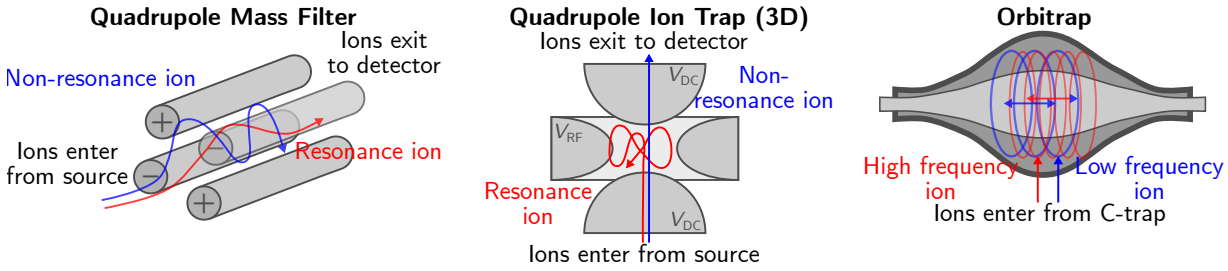

Figure 2.13: Diagrams of quadrupole mass filter, ion trap, and Orbitrap mass analysers.

Quadrupole ion traps operate in a different fashion to quadrupole mass filters. Linear ion traps are constructed from four parallel rods with end-cap electrodes at a fixed repelling potential, and 3D ion traps are constructed from a ring electrode with two end-cap electrodes at ground potential [155]. The same general scanning principles apply, where increasing the voltage magnitude of the rod or ring electrodes releases ions of increasing m/z, except the ions eject from the trap when they are unstable rather than stable. One notable distinction between quadrupole mass filters and ion traps is their abilities to perform tandem mass spectrometry (MS/MS). Tandem mass spectrometry selectively fragments a precursor ion of a specific m/z to smaller fragment ions ("product ions"), providing some information about the molecular structure based on the mass of the neutral loss [155]. MS/MS can be performed by arranging three quadrupole mass filters in series, called a "triple quadrupole". The first and last quadrupoles are used as m/z filters, and the RF-only middle quadrupole is used as a collision cell with inert gas to fragment

the precursor ion transmitted from the first quadrupole. The last quadrupole receives all of the fragment ions generated in the collision cell and either scans all of the fragments ("product ion scan") or filters for a specific fragment ion ("selected reaction monitoring", SRM). Conversely, ion traps are not only capable of selecting and fragmenting a precursor ion within a single trap, but this process can be iterated multiple times (MS^n) [155].

Quadurpole mass filters and ion traps have low resolving power ($<$1000 $m/\Delta m$, where m is the mass measured and Δm is the minimum distance between two well-resolved mass peaks), such that only the nominal (unit) mass can be obtained from the m/z [155]. The Orbitrap is a type of ion trap which has very high resolving power ($>$100,000), allowing separation of m/z values to the 4th or 5th decimal [155]. In Orbitrap mass analysis, the ions are first accumulated in an RF-only "C-trap" ion trap and then pulse-injected into the Orbitrap. The Orbitrap traps accelerating ions in orbit around an inner spindle electrode, while simultaneously oscillating along their orbital axis. The harmonic axial oscillations of the ions are detected by an outer barrel electrode as an image current (i.e., the increase in attractive charges on the electrode surface), where the period of the oscillations is proportional to $(m/z)^{1/2}$ [155]. The image current is Fourier transformed from the time-domain to the frequency-domain and then converted to a mass spectrum. Orbitraps may be coupled with either a quadrupole and collision cell or an ion trap for MS/MS capabilities.

After ion separation in a quadrupole mass filter or ion trap, the ions are directed to a detector which generates an electronic signal that can be converted to a digital output [156]. Electron multipliers are a type of detector commonly used in mass spectrometers. Electron multipliers, like photomultipliers, use a series of cascading dynodes that propagate electrons to amplify the signal, except a conversion dynode is used instead of a photocathode.

Comparing the sensitivity and instrument detection limits between mass spectrometer systems is complicated due to the fact each individual component – the ion source, mass analyser, detector, and data acquisition settings – has an effect on how efficiently an analyte is detected. While both EI and ESI sources are capable of detecting picomoles of analyte, nano-ESI (i.e., ESI performed with ultra-low flow rates $<$1 µL min^{-1}) is even more efficient and is capable of detecting femtomoles [151]. In mass analysers, greater sensitivity can be achieved through increased selectivity – for example, by high mass resolving power as well as SIM or SRM scanning in lieu of full spectral acquisition [154]. Generally, triple quadrupoles (particularly when using SRM) are best-suited for sensitive quantitative analysis as they can achieve very low limits of detection, while high-resolution Orbitraps are more appropriate for non-targeted analysis (i.e., where analytes of interest are not pre-defined) [154]. However, ion traps are more sensitive than triple quadrupoles for full spectral acquisition since the trap accumulates more ions [154].

In summary, mass spectrometers used in combination with chromatography provide multi-dimensional data:

- the total ion chromatogram, which contains the chromatographic retention time versus the total ion abundance,
- the mass spectrum for each measurement of total ion abundance, which contains the relative intensities of each individual m/z,
- and any additional user-defined data acquisition (e.g., SIM, SRM, and product ion scan).

Thus, mass spectrometry coupled with chromatography is an exceptionally effective tool for selective trace analysis of multiple chemical components.

2.6.6 Sample Preparation

One of the most effective ways to enhance the selectivity and sensitivity of chromatographic analyses is to separate the analyte of interest from the sample matrix components [146, 147]. Extraction has several advantages, including selective isolation of the target analyte from chemically different compounds; co-extraction of analytes which are chemically similar, such as degradation products and metabolites; and concentration of the analyte to enhance sensitivity. Two common forms of sample extraction – liquid-liquid extraction (LLE) and solid phase extraction (SPE) – are based on partitioning the analyte between different chemical phases.

In liquid-liquid extraction, the analyte partitions between two immiscible solvents (Figure 2.14a) [147]. Aqueous samples (e.g., environmental waters or liquid culture media) are thus extracted using an immiscible organic solvent. The sample and extraction solvent are agitated together, and the two liquid phases separate according to their density. During agitation, the analyte moves out of the aqueous sample and into the organic solvent, which can be collected, evaporated, and redissolved in a smaller volume for higher concentration of analyte [147].

The extractability of the analyte in LLE is characterised by two terms: the partition equilibrium constant (K_d, Equation 2.21) which is the proportion of analyte concentration in the organic phase versus the aqueous phase, and the partition coefficient (log$P$, Equation 2.22) which is the logarithm of the proportion of analyte concentration in octanol versus water [147]:

$$K_d = \frac{[\mathrm{A}]_{\mathrm{Organic}}}{[\mathrm{A}]_{\mathrm{Aqueous}}} \tag{2.21}$$

$$\log P = \log\left(\frac{[\mathrm{A}]_{\mathrm{Octanol}}}{[\mathrm{A}]_{\mathrm{Water}}}\right). \tag{2.22}$$

The log$P$ is a measure of analyte polarity, where a larger log$P$ is less polar and more hydrophobic; it is intrinsic to the analyte. The K_d, however, can be influenced by the extraction parameters, such as choice of organic solvent, charge state of the analyte (e.g., ionic or neutral), and

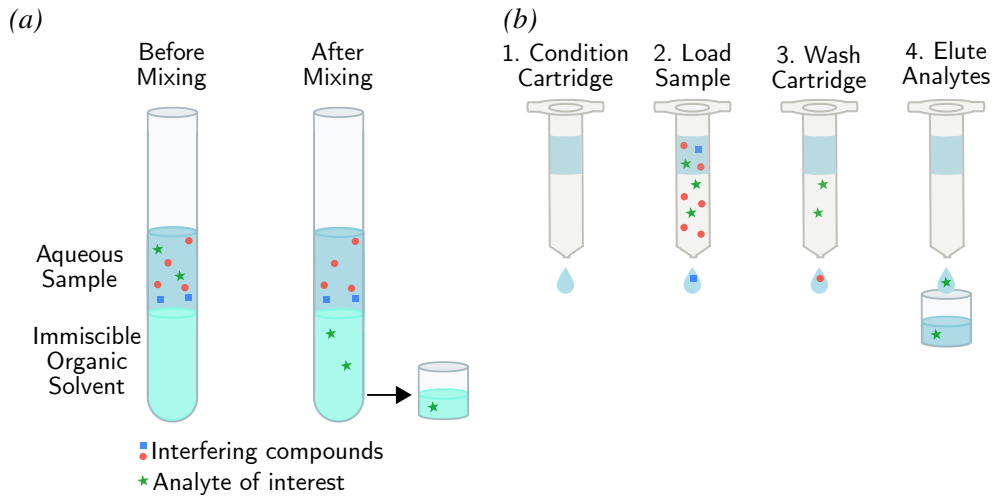

Figure 2.14: Generalised workflow of (a) liquid-liquid extraction and (b) solid phase extraction.

ionic strength of the aqueous phase [147]. In addition to optimising these parameters, LLE recovery can be improved with larger extraction volumes or by performing sequential extractions.

Solid phase extraction uses a solid resin- or silica-based matrix packed within a cartridge with a specific chemical property, such as bonded ionic, polar, or non-polar moieties (Figure 2.14b) [146]. Liquid sample is added to the pre-conditioned solid phase, where analytes and chemically similar impurities retain by ion exchange or polar/non-polar interactions, while the rest of the sample (including unretained compounds and liquid media) is removed as a filtrate. The solid phase is then washed in a low elution-strength solution to remove weakly retaining compounds. Finally, an elution solvent that disrupts the chemical interaction with the solid phase is used to elute the retained compounds, which can then be concentrated by evaporation. SPE has a number of advantages over LLE, including extraction manifolds which process multiple samples at a time, the ability to extract large sample volumes relatively easily, and less solvent consumption per sample.

The chosen extraction method should be evaluated for recovery and matrix effects, which can influence the analytical measurement of the compound [140]. Recovery is determined by comparing a known quantity of analyte in pre-extracted sample with the same quantity spiked into a sample post-extraction, and matrix effects are evaluated by comparing the post-extraction spike sample with an un-extracted reference standard of the same concentration [157].

2.7 Spectroscopic Techniques

Spectroscopic techniques were amongst the earliest trace analysis methods to be developed and are fundamentally very simple in concept and design [132]. Spectroscopy is simply the study of

how electromagnetic radiation (light) interacts with matter [158]. While there are spectroscopic techniques for every part of the electromagnetic (EM) spectrum, trace analysis of micropollutants (i.e., small organic molecules) is primarily associated with near infrared (IR), visible, and UV light regions.

The instrumentation associated with analysis of these regions – spectrophotometers – consist of: a light source which emits radiation at the energy of the associated EM region; a dispersive element (e.g., grating or prism) which separates the source light into a spectrum of its constituent radiation energies; a monochromator which selects for a narrow window of radiation energy from the dispersed light; an optically transparent cell which contains the sample; and a photon detector (e.g., photodiode or photomultipler, see Section 2.6.4.1) [152, 159]. Spectrophotometers (Figure 2.15) can be used to detect light-matter interactions such as absorption and emission, and the intensity of the measured response is proportional to the analyte concentration [159]. The general theory behind these interactions and the specific responses are described below.

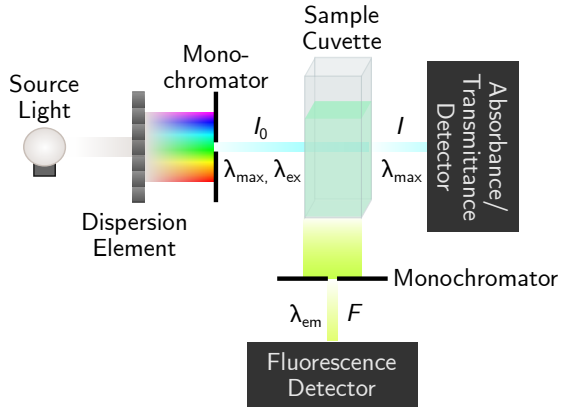

Figure 2.15: Diagram of a spectrophotometer.

2.7.1 Theory

Electromagnetic radiation is described in terms of its photonic energy (E) [J], which is directly proportional to its frequency (ν) [s^{-1} or Hz] and inversely proportional to its wavelength (λ) [m, usually expressed as nm or µm] [158]. Wavenumber ($\overline{\nu}$) – which is the inverse wavelength (λ^{-1}) and is usually expressed in units cm^{-1} – is also sometimes used to describe the energy of light. This relationship is summarised in Equation 2.23:

$$E = h\nu = \frac{hc}{\lambda} = hc\overline{\nu} \tag{2.23}$$

where h is Planck's constant (6.639×10^{-34} J s) and c is the velocity of light (3.0×10^{8} m s^{-1} in vacuum) [158]. The electromagnetic spectrum is the range of these photonic energies, and

the EM regions are associated with the type of intramolecular effect that energy level induces (Table 2.9).

Table 2.9: Regions of the EM spectrum and associated intramolecular processes [159].

Region	Wavelength (λ)	Wavenumber ($\overline{\nu}$, cm^{-1})	Frequency (ν, Hz)	Intramolecular Processes
Far UV	10–200 nm	–	10^{16}–10^{15}	Inner shell electron transitions
Near UV	200–400 nm	–	10^{15}–7.5×10^{14}	Valence electron transitions
Visible	400–750 nm	25000–13000	7.5×10^{14}–4.0×10^{14}	Valence electron transitions
Near IR	0.75–2.25 μm	13000–4000	4.0×10^{14}–1.2×10^{14}	Molecular vibrations
Mid IR	2.5–50 μm	4000–200	1.2×10^{14}–6.0×10^{12}	Molecular vibrations
Far IR	50–1000 μm	200–10	6.0×10^{12}–10^{11}	Low lying vibrations and rotations

The intramolecular effects of EM radiation associated with spectrophotometry are primarily electron energy state transitions and molecular vibrations (Figure 2.16) [158]. Electrons in a molecule can transition between their lowest energy state (i.e., ground-state, S_0) to a higher energy state (i.e., excited-state, S_1^*) by absorbing photonic energy that is equivalent to the energy difference between the ground and excited states:

$$\Delta E = E_{S_1^*} - E_{S_0}. \tag{2.24}$$

The transition with the smallest energy difference (ΔE) is between highest occupied molecular orbital (HOMO) to the lowest unoccupied molecular orbital (LUMO) [158]. If the electron promoted to the LUMO has a quantum spin opposite to the other unpaired electron, the molecule is in a singlet excited-state (S^*). Conversely, if the quantum spin is parallel with the unpaired electron, it is in a triplet excited-state (T^*). The transition from ground-state (S_0) to excited-state is always via S^*, while T^* – which has lower energy than S^* – occurs via intersystem crossing (ISC, i.e., the slow, non-radiative relaxation of the singlet excited-state to the triplet excited-state). If the EM radiation energy is not equal to the ΔE of the HOMO-LUMO gap, the photonic energy absorbed by the molecule alters the vibrational state within its energy state [158].

A molecule in the excited-state will return to its ground-state by radiative or non-radiative relaxation processes – i.e., processes where the energy state transition occurs with or without the re-emission of a photon, respectively [158]. The first step in the relaxation process is vibrational relaxation – a non-radiative process where the molecule transfers excess energy kinetically via intra- or intermolecular interactions. In vibrational relaxation, the molecule decreases in energy to the lowest vibrational state for a given energy state. Since there are vibrational states for each energy state, this can occur for a molecule in the excited-state or ground-state.

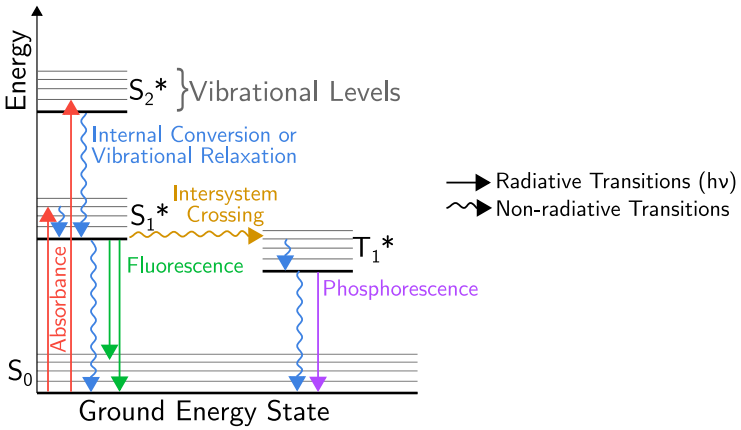

Figure 2.16: Jablonski diagram of energy state and vibrational level transitions for radiative and non-radiative energy.

Once an excited-state molecule is in its lowest vibrational state, there are three possible outcomes. First, the molecule can undergo non-radiative internal conversion (IC) to S_0, where the lowest vibrational state of S_1^* is of similar energy to the highest vibrational states of S_0; this is then followed by vibrational relaxation [158]. Second, the molecule can undergo non-radiative intersystem crossing to T_1^*; this can then be followed by another ISC to S_0. As with IC, ISC is more likely to occur if the energy of the vibrational states of T_1^* overlap with the lowest vibrational state of S_1^*. Third, the molecule will release the excess energy in the form of a photon. When this radiative relaxation process occurs from S_1^*, it is referred to as "fluorescence", while radiative relaxation from T_1^* is referred to as "phosphorescence".

Absorption and re-emission of EM radiation by organic molecules are observed by absorbance and fluorescence spectroscopic techniques, respectively [158]. These methods are primarily associated with UV-Vis spectroscopy, and thus, detect electron energy state transitions. These spectroscopic methods are discussed in the following sections.

2.7.2 Absorbance & Transmittance

When light is absorbed by a molecule, the irradiance of that light (i.e., the power of the light per unit of area of the light beam) decreases. This decrease is measured as transmittance (T),

$$T = \frac{I}{I_0} \tag{2.25}$$

which is the proportion of irradiance of the source light passed through the sample (I) relative to the irradiance of the source light passing through a reference (I_0) [158]. The reference includes the material of the optical cell which holds the sample and the analyte-free solvent. Absorbance

(A) is the negative logarithm of transmittance [158]:

$$A = -\log T = \log\left(\frac{I_0}{I}\right). \tag{2.26}$$

While irradiance has units of W m^{-2}, absorbance and transmittance are dimensionless. The absorbance spectrum for a compound can be obtained by measuring A across a range of wavelengths of source light. The wavelength of light with the greatest absorbance (λ_{max}) is related to the ΔE energy state transition and, therefore, is related to the molecular structure.

Absorbance is directly proportional to the concentration of the absorbing molecule (c) in the sample. The concentration can be determined via Beer-Lambert's Law, which is summarised as:

$$A = \varepsilon l c \tag{2.27}$$

where l is the optical path length (1 cm in standard cuvette spectrophotometers) and ε is the molar extinction coefficient in units M^{-1} cm^{-1} [158]. The molar extinction coefficient is a measure of how much light a compound absorbs and depends on the wavelength of light and solvent. Thus, there is a linear relationship between A and c as the independent and dependent variables, respectively, and εl as the coefficient. For quantitative analysis, A measured at λ_{max} will generally give the best analytical sensitivity.

2.7.3 Fluorescence & Emission

When light is absorbed by a fluorescent molecule (or fluorophore), it is re-emitted as the fluorophore transitions from excited-state to ground-state [158]. Unlike absorbance, which measures the logarithmic proportion of un-attenuated to attenuated light, fluorescence simply measures the intensity of light emitted. Furthermore, the emitted light – which is lower in energy than the absorbed source light – is measured orthogonal or anti-parallel to the source light beam path [158]. Thus, because fluorescence is not comparing small differences between two responses and the emission light is distinct from the source light, fluorescence is a much more sensitive technique than absorbance [158]. The intensity of fluorescence emission (F) [arbitrary intensity units] is proportional to the fluorophore molecule's concentration (c), and this relationship is summarised as:

$$F = (kI_0\Phi_f\varepsilon l)c \tag{2.28}$$

where k is a proportionality constant specific to the instrument and Φ_f is the quantum yield (i.e., fluorescence efficiency, or photons emitted per photon absorbed) [158]. There is a linear relationship between F and c, as the rest of the terms are intrinsic to the instrument and compound of interest [158].

In fluorescence spectroscopy, the excitation wavelength (λ_{ex}) is the energy of the source light used induce the $S_0 \rightarrow S_1^*$ transition, and the emission wavelength (λ_{em}) is the energy of the light emitted as fluorescence. The optimum λ_{em} is determined by the maximum F in the fluorescence emission spectra, which is obtained by measuring F across a range of wavelengths with a fixed λ_{ex}. The optimum λ_{ex} is closely related, if not identical, to a molecule's λ_{max} and can be used for obtaining the emission spectra [158]. The optimum λ_{ex} is determined by the maximum F in the fluorescence excitation spectra, which is obtained by measuring F at a fixed λ_{em} across a range of source light wavelengths. The fluorescence excitation and emission spectra usually mirror each other [158]. Since energy is lost during vibrational relaxation, λ_{ex} is smaller (i.e., higher energy) than the λ_{em}, and the gap between these wavelengths is referred to as the "Stokes shift" [158].

2.7.4 Spectroscopy of Small Organic Molecules

While absorbance and fluorescence detectors are commonly used with chromatography separation (see Section 2.6.4.2), the previously discussed spectroscopic techniques are also employed as standalone methods. Here, the merits and limitations of using spectroscopic methods for trace analysis of estrogens and other organic micropollutants are discussed.

2.7.4.1 Direct Analysis

UV-Vis absorbance spectroscopy can be performed on organic micropollutants which are chromophoric – i.e., molecules with a λ_{max} in the UV-Vis region [160]. As previously mentioned, the λ_{max} is related to the structure of the molecule. In organic molecules, sigma (σ) and pi (π) bonds are types of covalent bonds which determine molecular structure and reactivity [158]. A sigma bond forms when two atomic orbitals overlap head-on, allowing electrons to be shared along the internuclear axis. Pi bonds form when two parallel p-orbitals overlap, creating a region of electron density above and below the internuclear axis. While σ bonds provide rigidity and strength to the molecular structure, π bonds contribute to the de-localisation of electron density, facilitating phenomena such as resonance and the formation of double and triple bonds [158].

The energy gap for $\sigma \rightarrow \sigma^*$ (i.e., the transition of sigma bond electrons from ground to excited state) corresponds with the far UV region, which is out of range of most spectrophotometers. Molecules which can undergo $\pi \rightarrow \pi^*$ are detectable by UV-Vis spectroscopy. Conjugated π-systems – where two double bonds are separated by one single bond between C, O, or N atoms – create a zone of de-localised electrons, which provides both resonance and stability to molecule [160]. These extended π-systems decrease the HOMO-LUMO gap, and the λ_{max} generally shifts to lower energies in the near UV-visible region. Organic molecules which are capable of intense fluorescence (fluorophores) have even larger conjugated π-systems. Ex-

tended π-systems which impart rigidity to the molecule have higher fluorescence intensity, since less energy is lost as vibrations [160]. Organic structures may have their fluorescence intensity quenched by certain functional groups, for example heavy atoms (e.g., halogens) and electron-withdrawing carbonyl or nitro groups [160].

Natural estrogens contain a phenol group which acts as the chromophore (Figure 2.17). However, the overall system of de-localised electrons is fairly limited, and thus, the molar extinction and quantum yield of estrogen are relatively low (Table 2.10). In comparison, the photosynthetic pigment chlorophyll *a* has an ε of 89,800 M^{-1} cm^{-1} and a Φ_f of 0.32 [161]. As per Equations 2.27 and 2.28, both terms are directly related to analytical sensitivity. In addition, the absorbance maximum for natural estrogens, as well as other organic micropollutants, is very similar to the wavelength signature used to detect proteins (280 nm), which makes detecting most micropollutants in biological samples by absorbance virtually impossible due to non-selectivity [158].

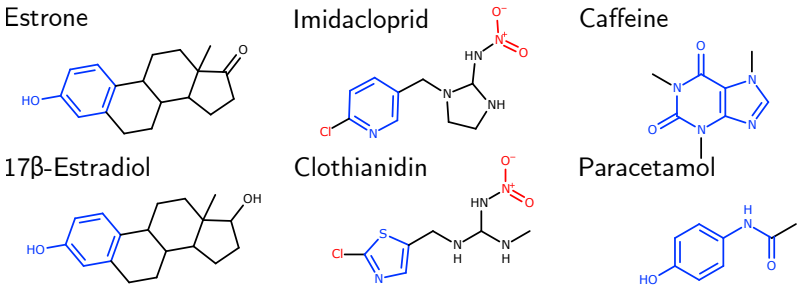

Figure 2.17: Chemical structures of estrogens E1 and E2 and other organic micropollutants. The resonant structures are marked blue and the quenching structures are marked red.

Table 2.10: UV-Vis spectral properties of estrogens and other organic micropollutants.

Ref	Compound	Use	Solvent	λ_{max} (nm)	λ_{em} (nm)	ε ($M^{-1}cm^{-1}$)	Φ_f
[162, 163]	17β-Estradiol	Hormone	Water	279	304	~1750[a]	0.103 ± 0.005
			Acetonitrile	281	302	2020 ± 50	0.14 ± 0.02
			Methanol	282	304	2040 ± 50	0.127 ± 0.006
[162, 163]	Estrone	Hormone	Water	279	304; 402	~1100[a]	0.009 ± 0.002
			Acetonitrile	281	302; 411	2170 ± 60	0.011 ± 0.002
			Methanol	282	303; 407	2120 ± 50	0.012 ± 0.004
[164]	Imidacloprid	Pesticide	Not specified	270	–	22054	–
[165]	Clothianidin	Pesticide	Not specified	265.5	–	Not specified	–
[166]	Caffeine	Pharmaceutical	Ethanol	274	–	20000	–
[167]	Paracetamol	Pharmaceutical	Ethanol	250	–	13800	–

[a]Visual estimate from graphical data.

The separation of chemical mixtures in chromatography provides inimitable selectivity compared to direct spectrophotometric analysis of the estrogens and other organic micropollutants. A relatively small proportion of molecules possess unique chromophores which absorb outside the UV region, and an even smaller proportion of molecules are capable of intense fluorescence. Therefore, direct analysis of most organic micropollutants in either field or laboratory samples by independent spectroscopic techniques is not practical.

2.7.4.2 Indirect Analysis

The intrinsic properties of estrogen and many other small organic molecules are not amenable to spectroscopic analysis at trace concentrations in complex matrices. Therefore, spectrophotometric methods for small organic compounds in a complex sample often employ alternative strategies which don't rely on direct detection of the analyte. In biological samples, indirect spectroscopic analysis is achieved with biochemical probes, biochemical assays, and optical sensing techniques (Figure 2.18) [168–170].

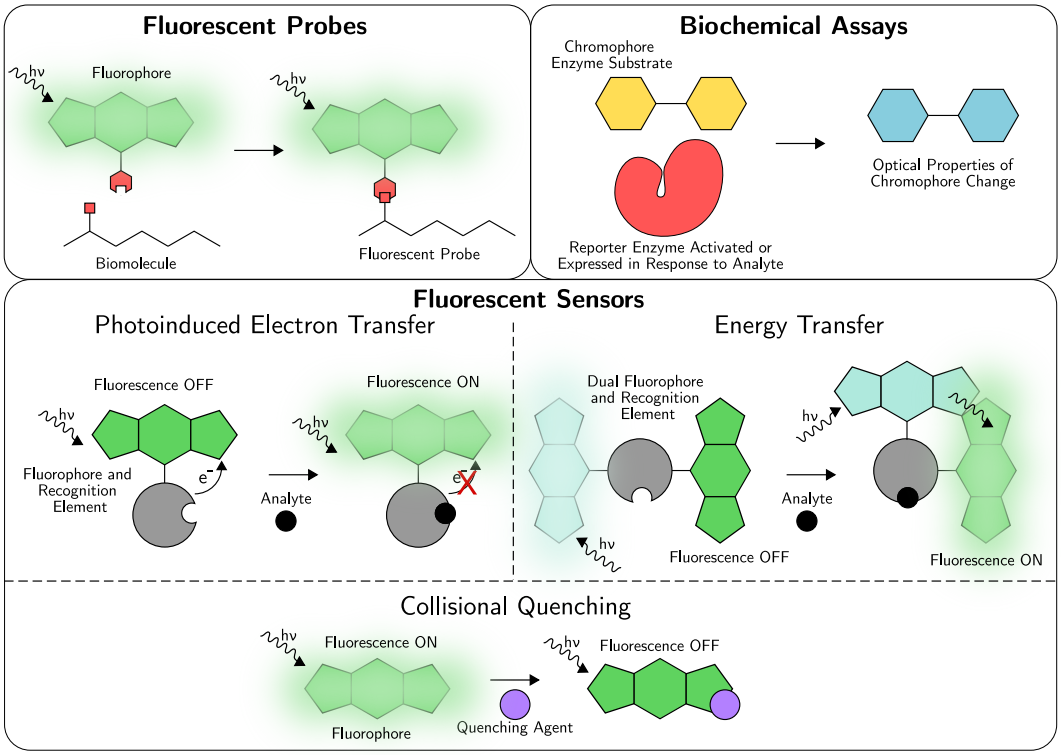

Figure 2.18: Diagrams of indirect spectroscopic analysis of organic molecules using chromophores and fluorophores in probes, biochemical assays, and fluorescent sensors [169, 171].

Biochemical probes are biomolecules (e.g., DNA, peptides, lipids) or substrates which have been modified for selectively observing biological processes [170]. Biochemical probes are usually labelled with stable isotope substitutions (e.g., ^{13}C, ^{2}H, ^{18}O) or conjugated with a

fluorophore [170]. Derivatisation with a fluorophore is used to enhance spectroscopic detection of non- or weakly fluorescent compounds [168]. There is a wide variety of commercially available organic fluorophores which absorb and emit across the visible spectrum (Figure 2.19) [168]. These fluorophores contain reactive groups (R groups in Figure 2.19) that can form covalent bonds with the active hydrogens of organic analytes. Some common reactive groups include: isothiocyanate, sulfochloride, and triazinylchloride which react with amines; *N*-hydroxysuccinimide which reacts with carboxylic acids; and isocyanate which reacts with alcohols [168, 172].

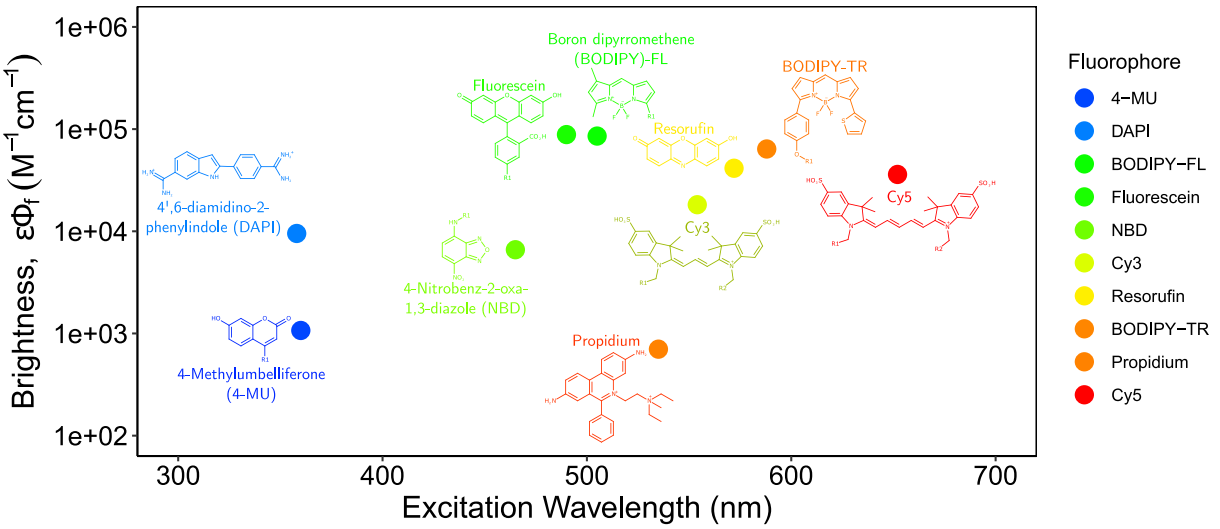

Figure 2.19: Examples of commercially available fluorophores, including derivatisation reagents and common fluorescent dyes (DAPI, resarufin, propidium). The potential sites for derivatisation reactive groups are indicated with R. Brightness and wavelength values are from [171].

Fluorescently labelled oligonucleotides which hybridise with complementary DNA or RNA sequences are one of the most widely used probes [168]. Fluorescent oligonucleotides are used in fluorometric techniques such as fluorescence *in situ* hybridisation (FISH), which uses fluorescence microscopy to obtain the spatial distribution of the fluorescent probe, and flow cytometry, which uses microfluidics coupled with fluorescence detector to count individual cells in a sample population based on their fluorescence intensity [169, 173]. Fluorescently labelled substrates may also be used with microscopy and flow cytometry, as well as standard fluorometry to measure substrate uptake [168, 169, 174].

Another approach of indirect spectrophotometry is generating an optical response to the analyte of interest using a chromogenic or fluorogenic reagent. Certain types of biochemical assays use the activity of biological molecules (e.g., DNA, enzymes) or whole cells to mediate the optical response. Many common biochemical assays, such as MTT assay and enzyme-linked immunosorbent assay (ELISA), generate an optical response with chromogenic or fluorogenic

substrates for oxidoreductase enzymes [175]. Yeast estrogen screen (YES) is a biochemical assay which measures estrogenicity (i.e., EEQ) [176]. The YES assay uses recombinant *Saccharomyces cerevisiae* with genes for estrogen receptor (ER) protein and reporter enzyme β-galactosidase [176]; the β-galactosidase cleaves a colorimetric galactoside substrate proportional to the amount ER-estrogen binding [176].

Fluorescent sensors use a fluorophore whose emission properties – i.e., the intensity, spectrum, lifetime, or polarisation of the emitted light – are altered in response to a change in its environment [169]. Here, the term "fluorescent sensor" is used to describe an analyte-responsive compound which indicates the presence of the target, rather than an optical sensor device. Fluorescent sensors have several advantages over other indirect detection mechanisms. Since biochemical assays generally rely on an enzyme – which is either intrinsic to the organism or supplied as an assay reagent – to mediate an optical response, the target analytes are limited to biomolecules. Conversely, fluorescent probes can be synthesised from virtually any organic analyte of interest [168]. However, the bulk fluorescence intensity only provides information about the distribution of the probe, and the fluorescent signal of the distributed fluorophore is usually distinguished by physically removing, washing, or filtering away the undistributed probes.

There are several mechanisms for fluorescent sensing, including electron transfer, energy transfer, and collisional quenching [169]. The first two mechanisms generally utilise a fluorophore conjugated to a target-recognition element. The recognition element may be supramolecular structures capable of host-guest interactions (e.g., chelators, macrocycles, and cyclodextrins), metal-organic frameworks (MOFs), or molecularly imprinted polymers (MIPs) [169]. In photoinduced electron transfer (PET), an electron is transferred either from an electron donor to an excited fluorophore or from an excited fluorophore to an electron acceptor. This electron transfer process inhibits fluorescence emission and is contingent on analyte binding to the recognition element. Energy transfer processes, including Förster resonance energy transfer (FRET), involve the transfer of energy between two chromophores in close proximity, where the donor chromophore's emission spectra overlaps with the acceptor chromophore's excitation spectra [177]. Collisional quenching is a form of dynamic quenching – i.e., where the radiative emission from the excited state is prevented – that uses a separate molecule or atom in solution to deactivate the fluorophore (i.e., a quenching agent). Collisional quenching occurs via a variety of mechanisms, including Dexter energy transfer process (which occurs at much smaller intermolecular distances than FRET) and intersystem crossing [169].

2.8 Gold Nanoparticle-Based Colorimetric Biosensors

Gold nanoparticle (AuNP)-based biosensors are one of the most simple nanomaterials-based analytical sensor devices [178]. While the unique optical properties of colloidal gold (i.e., a liquid

suspension of gold nanoparticles) have been observed since the 4th-century AD, possibly the earliest example of an AuNP-based biosensor was a colorimetric test published in 1913 to detect syphilis in cerebrospinal fluid [178]. AuNP-based colorimetric biosensors have since been developed extensively for biomedical applications [178]. However, their simple design, low cost, and portability have found wide appeal in environmental applications, including for micropollutant trace analysis [179]. Although AuNP-based colorimetric biosensors are convenient and easy to use, the underlying mechanisms are the combination of multiple intricate physical processes, including colloidal particle interactions, the spectroscopic phenomenon of localised surface plasmon resonance, and biochemical ligand binding.

2.8.1 Nanobiosensors

Biosensors are analytical devices which measure chemical or biological targets using a biological recognition element (i.e., "bioreceptor") [180]. Biosensor devices have three main components: the bioreceptor, the transducer, and the signal processor (Figure 2.20) [180]. The bioreceptor is a biological material – e.g., complementary DNA, enzyme, antibody, aptamer, or cell – which serves as the analyte recognition element. The transducer in a biosensor generates a measurable electronic output in response to the analyte-bioreceptor binding event. Common biosensor transducers include photon detectors, electrodes, and microbalances for optical, electrochemical, or piezoelectric responses, respectively [179]. A signal processing system then amplifies and digitises the signal generated by the transducer before generating an output of values.

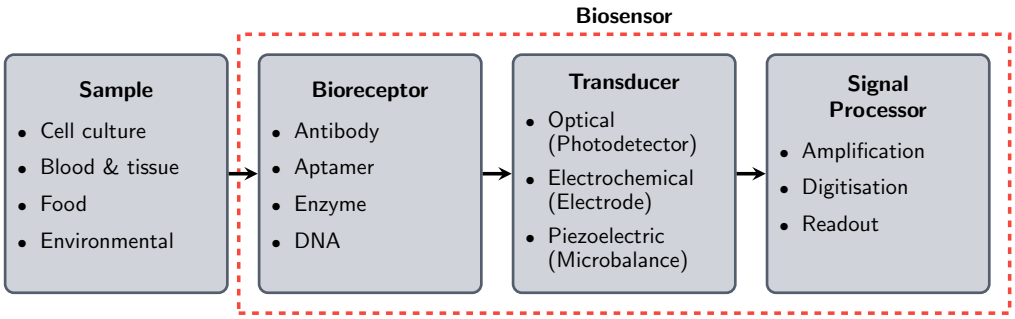

Figure 2.20: Generalised biosensor workflow.

Nanomaterials (i.e., structures $<$100 nm in at least one dimension) are widely used in biosensors due to their unique physicochemical properties [181]. At this scale, most of the constituent atoms are at or near the surface and, therefore, have low coordination numbers (i.e., number of bonds) [181]. As a result, nanomaterials possess a very high surface energy which makes them unstable and highly responsive to changes in their environment. In addition, nanomaterials possess very high surface area-to-volume ratio, which provides ample surface to functionalise with

bioreceptors. The high degree of surface reactivity and large surface area available for bioreceptor modification make nanomaterials particularly suitable as transducer materials in biosensors. The specific size, geometry, and material composition of nanomaterials are defined and generally optimised for the sensor transduction mechanism [181]. In AuNP-based colorimetric biosensors, the particles are spherical in shape, and the diameter (13–300 nm) size distribution should be as narrow as possible [178].

2.8.2 Colloidal Gold Nanoparticles

Colloidal gold nanoparticles are one of the most widely used materials for nanobiosensors [178]. The optical properties of colloidal AuNPs are tunable to the particle size, which is determined during synthesis or by destabilising the colloid suspension. AuNPs are synthesised by reducing $HAuCl_4$ (Au^{3+}) to Au^0 with sodium citrate or sodium borohydride under reflux [182]. The nanoparticles form from the gold atoms clustering together in a process of nucleation and growth. Seminal work by Turkevich *et al.* (1951) and Frens (1973) showed that AuNP size could be controlled by the amount of sodium citrate used in the reaction, where increasing the amount of citrate leads to smaller particle diameters, down to approximately 10 nm [183, 184].

In addition, Turkevich *et al.* (1951) demonstrated that citrate serves as a passivating agent which moderately stabilises the gold nanoparticles against aggregation [183]. Stabilisation of the AuNPs is a particularly important parameter in colorimetric biosensors, since the high surface energy of the particles and attractive van der Waals forces compel the particles to aggregate in order to decrease their energy. The stability of nanoparticles is explained by Derjaguin-Landau-Verwey-Overbeek (DLVO) Theory (Figure 2.21), which states the energy potential between colloidal particles (ΔG_{Total}) is the combination of van der Waals attraction (ΔG_{att}) and electrostatic repulsion (ΔG_{rep}) [178, 185]:

$$\Delta G_{\text{Total}} = \Delta G_{\text{att}} + \Delta G_{\text{rep}}. \tag{2.29}$$

The electrostatic repulsion is due to the electric double layer (EDL) between the AuNP surface and bulk solution [185]. The EDL is the composed of two layers of counter-ions (e.g., citrate anions) – an inner layer strongly bound at the surface (i.e., the Stern layer) and an outer diffuse layer. As the interparticle distance decreases, the electrostatic repulsion increases, and the energy required to overcome the repulsive forces is the "energy barrier" [186]. The magnitude of the energy barrier represents the stability of the colloidal system, where a high energy barrier indicates the particles will remain stable and dispersed.The energy barrier is measured by the energy potential at the interface of the EDL and bulk solution, also known as the ζ-potential [186]. The energy barrier is affected by a number of parameters, including particle size, electrolyte concentration and valency, and temperature [185, 186]. When the energy barrier is surpassed, the attractive forces dominate, and the particles destabilise and irreversibly aggregate. When

nanoparticles aggregate, their effective size increases which causes their optical properties to change. Modulation of the colloidal AuNPs between stable/dispersed and unstable/aggregated is the basis for AuNP-based colorimetric sensing.

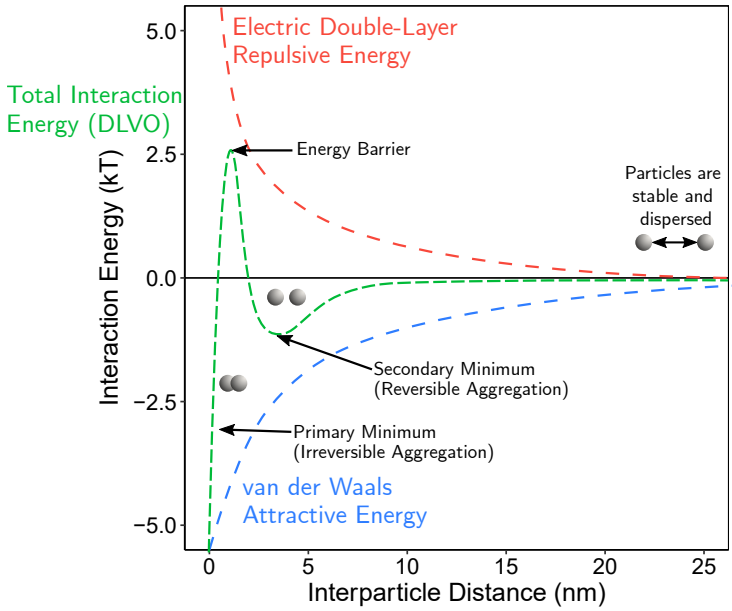

Figure 2.21: Example DLVO graph of the attractive, repulsive, and combined interaction energies for colloidal nanoparticles in relation to their interparticle distance.

2.8.3 Localised Surface Plasmon Resonance

The optical properties of AuNPs are the result of localised surface plasmon resonance (LSPR) [178]. Localised surface plasmon resonance is the collective oscillation of de-localised electrons at the surface of conductive nanoparticles, where the oscillation frequency corresponds with a particular wavelength of incident light (Figure 2.22) [178]. In noble metal nanoparticles (e.g., AgNPs and AuNPs), the resonant incident light is in the visible light region [187]. The relationship between the LSPR wavelength and the particle size is described mathematically by Mie Theory [187].

Mie theory uses Maxwell's equations for electromagnetic fields to describe the elastic scattering of light by homogeneous, spherical dielectric particles [187, 188]. According to Mie theory, the associated colour of the colloid suspension of a given refractive index and particle diameter can be determined by calculating the optical cross-sections ($\boldsymbol{\sigma}$, i.e., the rates of energy divided by the light intensity in units of area) of the incident light absorption, scatter, and extinction, where

$$\boldsymbol{\sigma}_{\text{extinction}} = \boldsymbol{\sigma}_{\text{absorption}} + \boldsymbol{\sigma}_{\text{scatter}}. \tag{2.30}$$

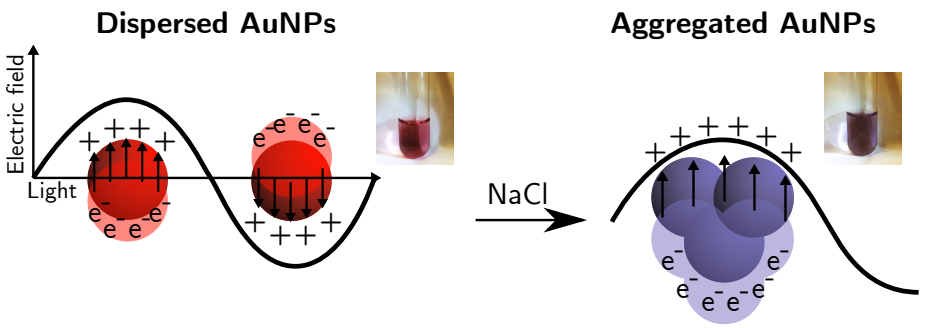

Figure 2.22: Diagram of LSPR in gold nanoparticles. The inset photos show AuNPs (25 nm) dispersed and aggregated with NaCl.

The optical cross-sections are expressions of infinite series of electrical and magnetic multipoles and are proportional to λ^2. The absolute maximum λ for absorption or extinction can be determined from the simulated optical cross-section spectra [188]. The maximum absorption or extinction wavelength from the simulated spectra can then be used to predict the colour of the colloidal nanoparticles. The optical efficiency coefficients are calculated as the optical cross-section divided by the particle's surface area [189]. Colloidal noble metal nanoparticles have particularly high absorption and extinction coefficients and, thus, produce intense colours [189].

2.8.4 Aptamer Bioreceptors

Aptamers are single-stranded oligonucleotides (usually ssDNA) whose sequence-dependent three-dimensional conformation of loops and pins selectively binds to a specific chemical or biological target via non-covalent interactions with high affinity (Figure 2.23) [190]. As a recognition element in biosensors, aptamers are an attractive alternative to antibodies – immunological proteins which bind to target analytes with high affinity and specificity – since they are easier to manufacture, have a longer shelf life, and are stable under a wide range of conditions [190].

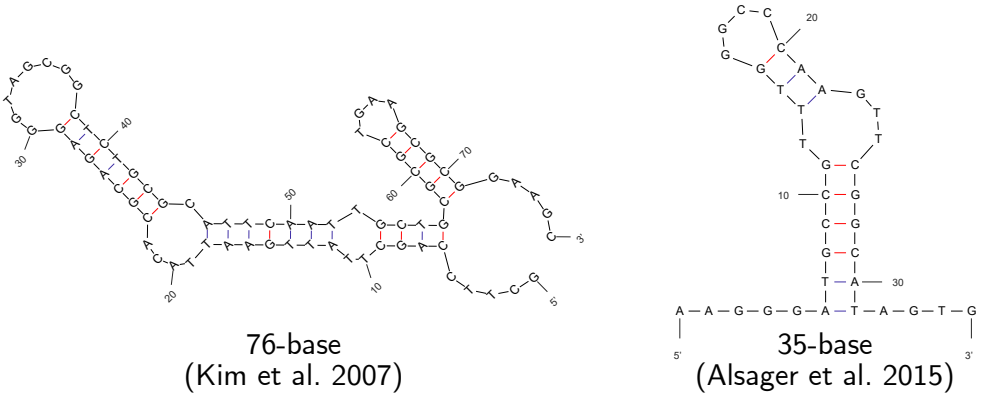

Figure 2.23: Secondary loop-and-pin structures for 17β-estradiol aptamers by Kim et al. (2007) [191] and Alsager et al. (2015) [192]. The structures were generated using mFold software.

Aptamers are synthesised by a process called Systematic Evolution of Ligands by EXponential enrichment (SELEX), which uses three stages – selection, partitioning, and amplification [190, 193]. The selection process begins with incubating the target analyte with a very large library (10^{16}) of random oligonucleotide sequences which are flanked on either end with short defined sequences. A selection of the library will bind to the target analyte, and the non-binding sequences are removed in the partitioning stage. Partitioning is performed by size-exclusion filtration (which assumes the target-bound sequences will be larger) or by immobilising the target and washing away the unbound sequences. After removing the non-binding oligonucleotides, the selected bound sequences are dissociated from the target. The selected oligonucleotides are then copied and amplified by polymerase chain reaction, using the sequence-defined portion as primer binding sites. The process is then repeated several times to obtain the sequence with the greatest binding affinity, determined as having the lowest dissociation constant [190].

In AuNP-based biosensors which use aptamers (i.e., aptasensors), ssDNA aptamers can be immobilised onto the gold surface via covalent Au-SH bonds using thiolated oligonucleotides [194]. Alternatively, the nucleotide bases of ssDNA non-covalently interact with the gold surface, and an ssDNA aptamer will spontaneously adsorb to the AuNP [195]. Several mechanisms have been proposed to explain the adsorption of ssDNA to gold surfaces, including chemical bonding and hydrophobic interactions, however, van der Waals interactions between the bases and gold seems to be the most accepted [195, 196].

Gold nanoparticles functionalised with aptamers possess a higher energy barrier than simple citrate-capped AuNPs and, therefore, are sterically stabilised against conditions which may induce aggregation (for example, increasing the electrolyte concentration) [195, 196]. While thiolated aptamers are immobilised on the surface, adsorbed ssDNA aptamers become desorbed when the target is present, lowering the energy barrier [196]. Kim *et al.* (2011) described sensing with adsorbed aptamer as an "affinity ratio" between the competitive binding of AuNPs–aptamer and aptamer–target, and a suitable colorimetric AuNP sensor will have a balance between these two interactions [197]. Target sensing by immobilised aptamers is achieved by different mechanisms, such as the use of ssDNA complementary to the aptamer to cross-link the AuNPs or polydiallyl dimethyl ammonium chloride (PDDA) polymer which can hybridise with ssDNA and induce AuNP aggregation [198].

2.9 Rationale of the Thesis Aim and Objectives

The gold standard methods used to analyse estrogen micropollutants have been optimised for sensitivity and selectivity. The methods combine extraction procedures, which selectively isolate and enrich estrogens from sample matrices, with chromatography, which separates the chemical constituents in the extract. In analysing estrogen micropollutants, chromatographic separation

is captured in real-time by selective detectors (e.g., FID and UV/PDA) or mass spectrometers (Tables 2.5 and 2.6). Chromatographic workflows are particularly useful for selectively detecting multiple target analytes. In environmental samples, estrogens are often analysed as part of a suite of organic micropollutants [56]. Furthermore, high-resolution MS analysis with Orbitrap or Q-TOF is particularly suited to characterise degradation products [97, 98]. However, in bench-scale estrogen biodegradation studies, estrogen may be the only target analyte for quantitative analysis [79, 85]. While chromatography is highly effective at measuring estrogen concentrations, this technique is neither rapid nor scalable. In addition, this approach for single-target analysis is inefficient data collection. The chromatograms (compound abundance versus time) and mass spectra (ion abundance vs *m/z*) contain large quantities of data, most of which is not used for targeted quantitative analysis.

We propose the use of simple, high-throughput spectroscopic techniques based on absorbance and emission to quantify estrogen biodegradation and screen microbial communities for metabolically competent bacteria to address the methodological gaps. **Therefore, the aim of this thesis was to develop fluorometric and colorimetric trace analysis methods for monitoring biodegradation of estrogens in microbial communities with the potential for high-throughput analysis.** However, the intrinsic optical properties of estrogen are not favourable for direct analysis, since the chromophoric phenol group absorbs and emits light in the same wavelengths as many other organic molecules and with low molar efficiency (i.e., ε and Φ_f). Thus, the chosen spectroscopic methods must demonstrate adequate selectivity for the target analyte.

Gold nanoparticle-based colorimetric biosensors combine selective detection via a biological recognition element with the spectroscopic phenomenon of localised surface plasmon resonance to detect a variety of analytes, including small organic molecules. In addition, there are a multitude of colorimetric aptasensor methods available in the literature, including published estrogen-specific aptamer sequences [192, 197, 199]. However, the colorimetric aptasensors for estrogen analysis in the literature, which were developed for environmental water samples, have not yet been tested in microbiological cultures [192, 199, 200].

The ICH Guideline M10 on bioanalytical method validation outlines the procedures for validating ligand-binding assays, which applies to most aptasensors [140]. The ICH Guideline specifically notes that selectivity should be assessed for non-specific matrix components, such as degrading enzymes, which may interfere with analyte detection. The U.S. Department of Health Bioanalytical Method Validation Guidance for Industry further recommends testing the matrix effects from different biological sources to establish selectivity in ligand-binding assays [145]. Since the selectivity of AuNP-based E2 aptasensors for biological applications had not yet been explored, we decided to develop a colorimetric aptasensor for measuring estrogen concentrations in cultures with estrogen-degrading bacteria and evaluate the method according to

the relevant bioanalytical method validation guidelines (**Objective 4**). The colorimetric aptasensor was developed to address the methodological gap of measuring estrogen concentrations more efficiently for treatment optimisation by *in silico* methods.

Fluorescent probes – i.e., molecules of interest conjugated with a fluorophore – have been used extensively in understanding biological processes in near-real-time. Fluorescent probes of organic substrates have been applied in a wide variety of fluorometric techniques, including fluorescence microscopy, flow cytometry, and spectrofluorometry [201, 202]. The use of indirect spectroscopic analysis for micropollutants (i.e., biochemical probes, biochemical assays, and optical sensing techniques), particularly in the context of microbiological interactions, has not been widely implemented. While fluorescent probes have been utilised in environmental microbiology for studying distribution of heavy metals in biofilms [203] and measuring coliform load [204, 205], the use of fluorescently labelled organic micropollutants to study biodegradation has not yet (to our knowledge) been explored in detail.

Previously, Dr Sarah-Jane Haig, a former PhD researcher at the University of Glasgow, utilised BODIPY-labelled estrogens to visualise estrogen-degrading bacteria isolated *de novo* by fluorescence microscopy [206]. BODIPY is an intense fluorophore based on boron dipyrromethene framework and is commonly used in biochemical probes [207]. Therefore, we investigated the use of BODIPY-estrogens previously used by Haig (2014) in a fluorometric assay to address the methodological gap of screening mixed microbial communities for estrogen-degrading organisms (**Objective 3**) [206].

The role of enrichment cultures in screening microbial communities for estrogen catabolising bacteria was described previously in Section 2.2.3. While many estrogen-degrading bacteria have been isolated by enrichment (Table 2.4), the procedure is lengthy (at least one week) and biased towards catabolising organisms that thrive in unitrophic (i.e., single carbon substrate), non-competitive conditions. In addition, chemical trace analysis with chromatography is required to investigate estrogen cometabolism, since it is not directly observable by enrichment cultures [72, 75]. An assay based on fluorescently-labelled estrogens would address key limitations of enrichment cultures which use natural estrogen as the sole carbon source. Specifically, a fluorescent estrogen probe would enable mixotrophic growth conditions (i.e., multiple carbon substrates), which would support the growth of competitor bacteria as well as cometabolising organisms. Therefore, the assay culture conditions would be more comparable to the conditions of the target environment for bioremediation.

A fit-for-purpose fluorometric assay should detect a selective response by the BODIPY-estrogens in the presence of estrogen-degrading bacteria. However, the fate of the fluorescently-labelled estrogen – for example, de-conjugation, transformation, uptake, quenching, or spectral changes – had to be established first, as it would inform the basis of the fluorometric response. Before developing a fluorometric assay, we first characterised the fate – i.e., transformation,

removal, and spatial distribution – of the BODIPY-estrogens by estrogen-degrading reference bacteria (**Objective 2**). We selected two strains from Table 2.4 which are publicly available in culture collections – *N. tardaugens* ARI-1 (now identified as *Caenibius tardaugens* DSM 16702) and *N. europaea* NCIMB 11850 – to create a synthetic community of degrading organisms. While the reference strains were used to characterise the fate of the BODIPY-labelled estrogen, the bacteria also served as the biological system to test both spectroscopic methods' fitness for purpose. As noted previously, bacteria use a variety of metabolic pathways to degrade estrogen micropollutants. Thus, the use of an autotrophic nitrifying bacteria and a heterotrophic estrogen-catabolising bacteria allowed us to evaluate the spectroscopic methods' ability to monitor biodegradation by two different pathways.

We characterised the biochemical fate of the natural and fluorescent estrogen by developing a traditional chromatographic workflow to accurately measure the natural and fluorescent estrogens. The chromatographic method was developed to measure the change in concentration and detect potential metabolites of the fluorescent estrogen probe. In addition, the "gold standard" chromatographic method served as the benchmark to compare the analytical figures of merit of the spectroscopic assays (**Objective 1**). A summary of the three analytical methods developed in this thesis is provided in Table 2.11.

Table 2.11: Summary of the spectroscopic assays that will be developed to address the methodological gaps compared against a gold standard method for trace analysis of estrogens.

	Gold Standard	**Spectroscopic Assays**	
Method	LLE with HPLC-PDA or GC-MS	BODIPY-Estrogen Probes	AuNP Colorimetric Aptasensor
Detection	Chromatography + Absorbance or Mass Spectrum	Fluorescence	Absorbance (Extinction)
Overview	Estrogens are semi-selectively extracted from a liquid bacteria culture by liquid partitioning. Compounds in the extract are then separated by their individual physical or chemical properties in a continuous flow of solvent through a column packed with sorbent. Eluted analytes are detected in real-time by absorbance or ion abundance. The output is a two-dimensional plot of the response versus time, and the area under each compound's response peak is directly proportional to concentration.	Estrogens are tagged with a BODIPY fluorophore and added to bacteria medium as a surrogate to natural estrogen. In theory, as the BODIPY-estrogen probe is metabolised by bacteria, the fluorescence intensity – which is proportional to the concentration of BODIPY – will be affected. Additionally, the BODIPY-estrogen probe may be used to visualise bacterial uptake by fluorescence microscopy or flow cytometry. Ultimately, we aim to use BODIPY-estrogens to identify contaminant-degrading bacteria within a mixed culture.	Estrogen biodegradation bacterial culture samples are mixed with AuNPs which have been reversibly modified with aptamers. The aptamers dissociate from the AuNPs and selectively bind to the target. The addition of electrolytes via the culture medium causes AuNPs which are not coated by aptamers to aggregate. When aggregated, the LSPR of the AuNPs changes, causing a visible colour change from red to blue which is proportional to the concentration of estrogen.
Pros	Extensively Used Method Good Sensitivity Good Selectivity	Rapid Inexpensive Good Sensitivity Good Selectivity No Sample Prep High-throughput on Microplate	Rapid Inexpensive Moderate Selectivity with Aptamer No Sample Prep High-throughput on Microplate Methods Available in Literature
Cons	Low-throughput Expensive Lengthy Sample Prep	Potential Metabolite Interference Modified Estrogen	Sensitivity & Selectivity Uncertain Vulnerable to Matrix Interference

62

Chapter 3

Development of an Analytical Workflow for Natural and Fluorescent Estrogens

3.1 Introduction

There has been increasing interest in utilising fluorescently labelled substrates to study biochemical processes in near real-time. Fluorescent probes are widely used in fluorescence microscopy for spatial in situ analysis and as sensors for biochemical assays [208, 209]. A recent publication by Leivers *et al.* (2022) demonstrated the use of 2-aminobenzamide fluorophore in a multi-technique approach to study substrate-specific biodegradation of glycans by gut microbiome, highlighting the breadth of information that can be gleaned using fluorescent probes [202]. Although most applications have been in biomedical research, fluorescent probes have also been used in environmental science, for example to study the distributions of Giardia cysts [210] and heavy metals in microbial communities [203].

Advances in organic fluorophores and conjugation techniques have expanded the possibilities for research using fluorescent probes [211]. In particular, 4,4-difluoro-4-bora-3a,4a-diaza-*s*-indacene (BODIPY) dyes are used extensively in bioconjugation due to their excellent photophysical properties, such as intense fluorescence, high degree of photostability, and a scaffold that is readily tunable to different excitation and emission wavelengths [212–214]. Previously, BODIPY-labelled estrogens have been used to visualise estrogen-degrading bacteria isolated from slow sand filters [206].

Part of the work in this chapter has been published in "BODIPY-Labeled Estrogens for Fluorescence Analysis of Environmental Microbial Degradation", Felion, C., Lopez-Gonzalez, R., Sewell, A.L., Marquez, R. and Gauchotte-Lindsay, C. *ACS Omega* 2022 7 (45), 41284-41295 DOI: 10.1021/acsomega.2c05002.

Although BODIPY fluorophores possess several advantages, there are some practical challenges in using them in biological research. BODIPY dyes are widely known to form dimers and aggregates in polar solutions which affect their solubility, bioavailability, and fluorescence intensity [215, 216]. Traditionally, water solubility has been improved by derivatising the BODIPY core with hydrophilic groups, including galactose [217], sulfonate, phosphonate, and carboxylate groups [218]; however, these groups increase the steric hindrance and reduce the chemical stability of the fluorophore. Furthermore, for small molecules, the fluorophore drastically increases the molecular weight and changes the chemical nature of the parent substrate. This presents a twofold challenge in using BODIPY probes in biological systems: the poor aqueous solubility and the impact of conjugated fluorophore on metabolism. Thus, before BODIPY conjugates of micropollutants can be confidently used to investigate biodegrading microorganisms, it is important to understand the impact of BODIPY conjugation on the solubility of the substrate and on its biological activity using well-characterised reference strains. Chromatographic analyses of the substrate products are crucial for validating fluorescently tagged substrates as viable surrogates [202, 219]. However, presently, there is limited information about the analytical methods used to extract and analyse BODIPY conjugated molecules compared to their native structure.

As discussed in Chapter 2, chromatography is the most widely used technique used for trace analysis of estrogens. These semi-polar compounds are particularly amenable to reversed-phase high performance liquid chromatography (HPLC) separation and are readily detectable by ultraviolet (UV), fluorescence, and electrochemical detectors [72, 75, 92]. Estrogens have also been separated by gas chromatography (GC) following silylation of the thermolabile hydroxyl groups [136]. Mass spectrometry (MS), however, remains the gold standard detection method for both GC and HPLC separation of estrogens. Thus, in addition to validating the suitability of fluorescent substrates in biodegradation, chromatography combined with mass selective detection is the most logical standard to compare against novel analytical methods.

The aim of this work was to develop and validate an analytical workflow based on liquid-liquid extraction and chromatographic analysis which will be used for measuring natural and BODIPY-labelled estrogens (Figure 3.1) in bacteria cultures. The workflow will also serve as the benchmark to compare the spectroscopic methods against.

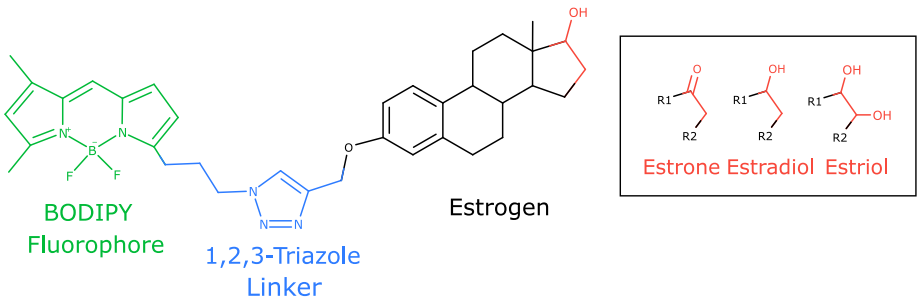

Figure 3.1: Structure of the BODIPY-conjugated estrogens used in this work. The BODIPY fluorophore was conjugated to estrone, 17β-estradiol, and estriol via an aromatic triazole linker ligated to the oxygen at C3 of the aromatic A-ring of estrogen.

3.2 Materials & Methods

3.2.1 Reagents

Estrogens estrone (≥99%), 17β-estradiol (≥98%), and estriol (≥97%), derivatisation reagent *N,O*-bis(trimethylsilyl)trifluoroacetamide (BSTFA), and HPLC-grade solvents were purchased from Sigma Aldrich UK. Ultrapure water (18.2 MΩ·cm) was procured from a Milli-Q water system (Millipore UK) or a PURELAB water system (ELGA LabWater UK).

BODIPY-labelled estrogens (Figure 3.1) were synthesised by Dr Alan Sewell from the Department of Chemistry at the University of Glasgow for Dr Sarah-Jane Haig. Briefly, BODIPY estrogens were synthesised by a copper-catalysed click reaction between azido-BODIPY and estrogen-propargyl ether [220]. Individual stock solutions of each estrogen (native or BODIPY-tagged) were prepared in methanol at 1 mg/mL and stored in the dark at -20°C.

The minimal salts medium, Modified Medium B (MMB; 10 mM $(NH_4)_2SO_4$, 3 mM KH_2PO_4, 0.75 mM $MgSO_4{\cdot}7H_2O$, 0.2 mM $CaCl_2{\cdot}2H_2O$, 10 µM $FeSO_4{\cdot}7H_2O$, 16 µM $Na_2EDTA{\cdot}2H_2O$, 1 µM $CuSO_4{\cdot}5H_2O$, 43 mM $NaH_2PO_4{\cdot}2H_2O$, 4 mM K_2HPO_4, 0.04% Na_2CO_3), was prepared by dissolving salts in deionised water and adjusting to pH 8.0. The media was filter-sterilised and stored at room temperature. 2-Hydroxypropyl-β-cyclodextrin (average molecular weight 1460 Da, HPβ-CDX) was prepared as a filter-sterilised stock solution of 40% (w/v) in deionised water and diluted to the working concentration in MMB media.

3.2.2 GC-MS Analysis

Analysis was carried out by Agilent GC/MSD System (Agilent Technologies), which consisted of autosampler (7693), gas chromatograph (7890A) and single-quadrupole mass spectrometer (5975C) with electron ionisation (70eV, pos.). The capillary column was J&W DB-5 (30 m × 0.25 mm × 0.25 µm) and mobile phase was helium gas. Samples (1 µL) were injected into a

splitless inlet liner at 250°C. Separation was carried out by an initial hold at 50°C, followed by an increase to 220°C at +10°C per minute, then another increase to 280°C at +5°C per minute where it was held at for 10 minutes (40 min. total run-time). Derivatised estrogens were detected using the following selected ion monitoring (SIM) values: TMS-estrone at 342 *m/z*, 2TMS-estradiol at 416 *m/z*, and 3TMS-estriol at 504 *m/z*. Peak detection and integration were carried out using OpenChrom (v1.3.0 Dalton) software.

3.2.3 HPLC Analysis

Analysis was carried out by the Prominence HPLC-PDA system (Shimadzu Corp.), which consisted of inline degasser (DGU-10A SR), quaternary pump (LC-20AT), autosampler (SIL-20A HT), column oven (CTO-10AS VP), and photodiode array detector (SPD-M20A). The analytical column was a Purospher RP-18 (150×4.6 mm^2, 5-µm pore) from Millipore and was maintained at 35°C during analysis. Mobile phase consisted of ultrapure water (A) and acetonitrile (B) at a flow rate of 0.5 mL/min. The injected volume was 10 µL. Elution was carried out by an initial hold of 60%A:40%B for 3 minutes, followed by an increase to 100% B at +5% B per minute, then a purge at 100% B for 3 minutes before reconditioning at 60%A:40%B for 10 minutes (28 min. total run-time). Non-derivatised estrogens were measured at 230 nm, and BODIPY-tagged estrogens were measured at 503 nm. Peak detection and integration were carried out using Shimadzu LabSolutions software.

3.2.4 Standards Preparation

Six calibration standards and three quality control (QC) samples were prepared by diluting stock solutions in acetonitrile. A separate standard of the same concentrations as the top standard was used for determining system suitability and precision. Prior to GC-MS analysis, calibration standards and QCs (50 µL) were derivatised with 50 µL BSTFA in crimp-sealed vial inserts for 100 minutes at 85°C. In GC-MS analysis, each standard and QC (Table 3.1) contained E3 as a surrogate standard which also underwent derivatisation. Each HPLC standard and QC (Table 3.2) contained E3 and BODIPY-E3 as internal standards (IS) for detection at 230 nm and 503 nm, respectively.

3.2.5 Liquid-Liquid Extraction

The extraction method was developed using MMB as the sample matrix. LLE was conducted in 15-mL glass test tubes by gently vortexing 0.25 mL of MMB spiked with estrogen mixture (1 mg/L each of E1, E2, E3, BODIPY-E1, BODIPY-E2, and BODIPY-E3 and 0.5 mg/L BODIPY-N3) with 1 mL of dichloromethane for 30 s. Exactly 0.8 mL of organic phase was

Table 3.1: Standards and quality controls used for GC-MS method evaluation.

	Before Derivatisation						*After Derivatisation*					
	E1		E2		E3[a]		TMS-E1		2TMS-E2		3TMS-E3[a]	
	µg/L	µM	µg/L	µM	µg/L	µM	µg/L[c]	µM	µg/L[c]	µM	µg/L[c]	µM
s1	40	0.15	40	0.15			20	0.07	20	0.07		
s2	80	0.29	80	0.29			40	0.15	40	0.15		
s3	160	0.59	160	0.59			80	0.29	80	0.29		
s4	240	0.88	240	0.88			120	0.44	120	0.44		
s5	320	1.18	320	1.18	200	0.69	160	0.59	160	0.59	100	0.35
s6[b]	400	1.47	400	1.47			200	0.74	200	0.74		
QC H	360	1.32	360	1.32			180	0.66	180	0.66		
QC M	200	0.74	200	0.74			100	0.37	100	0.37		
QC L	60	0.22	60	0.22			30	0.11	30	0.11		

[a]3TMS-E3 is a surrogate internal standard used for quantifying derivatised estrogens. [b]The concentrations of s6 were used for the precision and system suitability standard. [c]The µg/L values shown for TMS derivatives is the equivalent amount of underivatised estrogen for the given molarity.

Table 3.2: Standards and quality controls used for HPLC-PDA method evaluation.

	E1		E2		E3[a]		BODIPY-E1		BODIPY-E2		BODIPY-E3[a]	
	µg/L	µM	µg/L	µM	µg/L	µM	µg/L	µM	µg/L	µM	µg/L	µM
s1	60	0.22	60	0.22			45	0.07	45	0.07		
s2	80	0.29	80	0.29			90	0.15	90	0.15		
s3	120	0.44	120	0.44			180	0.29	180	0.29		
s4	160	0.59	160	0.59			270	0.44	270	0.44		
s5	200	0.74	200	0.74	200	0.69	360	0.59	360	0.59	225	0.37
s6[b]	240	0.88	240	0.88			450	0.74	450	0.74		
QC H	220	0.81	220	0.81			405	0.66	405	0.66		
QC M	140	0.52	140	0.52			225	0.37	225	0.37		
QC L	70	0.26	70	0.26			67.5	0.11	67.5	0.11		

[a]E3 and BODIPY-E3 are internal standards used for quantifying non-tagged and tagged-estrogens, respectively. [b]The concentrations of s6 were used for the precision and system suitability standard.

recovered and evaporated to dryness at 37°C before resuspending in 0.2 mL of acetonitrile. The analysis was conducted as described in Section 3.2.3.

When the spiked MMB was diluted 50:50 with acetonitrile prior to extraction, LLE was conducted by gently vortexing 0.5 mL of diluted sample with 1 mL of dichloromethane for 30 s. Filtered samples were prepared using 0.45-µm hydrophilic PTFE syringe filter.

3.2.6 System Suitability

The analytical methods were first evaluated for system suitability for each analyte. Six replicate measurements were used to determine theoretical plates and resolution. Resolution (Rs) was calculated for a given analyte using the retention time (t_R) and peak width (W) or width at half-maximum ($W_{0.5}$) and against the analyte preceding in order of elution, i.e. where $t_{R2} > t_{R1}$. Because different values were available on each data processing software, Equation 3.1 was used for GC-MS and Equation 3.2 was used for HPLC-PDA:

$$Rs = \frac{t_{R2} - t_{R1}}{0.5(W_1 + W_2)} \tag{3.1}$$

$$Rs = 1.18 \times \left(\frac{t_{R2} - t_{R1}}{W_{0.5,1} + W_{0.5,2}} \right). \tag{3.2}$$

The theoretical plate number (N) was also calculated using the retention time and width or width at half-maximum for each analyte. Equation 3.3 was used for GC-MS and Equation 3.4 was used for HPLC-PDA:

$$N = 16 \left(\frac{t_R}{W} \right)^2 \tag{3.3}$$

$$N = 5.54 \left(\frac{t_R}{W_{0.5}} \right)^2. \tag{3.4}$$

The HPLC-PDA values for t_R and $W_{0.5}$ were reported by Lab Solutions software. The GC-MS values for t_R and W were reported by OpenChrom software.

3.2.7 Chromatographic Method Evaluation

The chromatographic methods were evaluated according to the International Conference on Harmonization (ICH) Guidelines Q2 (R1) for method validation in terms of specificity, precision, linearity, range, accuracy and instrumental limits of detection and quantitation. Method evaluation was carried out by running a batch of six calibration standards and duplicate measurements of three QC samples on three separate days. In one batch, six replicate injections of a precision standard were also measured at the start and end of the batch. In a separate batch on a different day, six replicate injections of a precision standard were measured at the start of the batch for

inter-assay reproducibility. The calculations for each figure of merit are described below.

3.2.7.1 Linearity

Linearity for each batch was determined using unweighted linear regression of the concentration (x) versus the response (i.e. peak area) ratio of analyte to internal or surrogate standard (y). The coefficient of determination (R^2) of the calculated linear regression equation ($y = ax + b$, where a is the slope and b is the intercept) was used to evaluate the linearity of the method. Additionally, the percent error (Equation 3.5) was used to verify the accuracy of the regression equation in accordance with the FDA Bioanalytical Method Validation Guidance for Industry:

$$\% \text{ Error} = 100\% \times \frac{x_c - x_i}{x_i} \tag{3.5}$$

Here, x_c represents the concentration as calculated from the standard's response ratio (y) using the regression equation and x_i represents the true concentration of the standard.

3.2.7.2 Precision

Precision was determined by the percent relative standard deviation (%RSD) of a set of replicate injections. Repeatability was evaluated by the %RSD for the initial six repeat injections at the start of the first batch (Injections #1-6). Intra-assay precision was evaluated by the %RSD of the initial six repeat injections and final six repeat injections at the end of the first batch (Injections #1-12). Inter-assay precision was evaluated by the %RSD of the repeat injections from the first batch and another six injections at the start of the third, final batch (Injections #1-18).

3.2.7.3 Accuracy

Accuracy was determined by the percent error (Equation 3.5) of the three QCs measured in duplicate over three separate batches, as recommended by the Bioanalytical Method Validation Guidance for Industry. Additionally, the percent recovery (Equation 3.6) was used as an additional measure of trueness as recommended by the ICH Guidelines and Eurachem Guide to Method Validation:

$$\% \text{ Recovery} = 100\% \times \frac{x_c}{x_i}. \tag{3.6}$$

3.2.7.4 Instrument Limits of Detection and Quantitation

The instrument limits of detection (LOD) and quantitation (LOQ) were calculated for each calibration curve using Equation 3.7,

$$\text{Instrument Limit} = k\frac{s_b}{S}, \tag{3.7}$$

where k is 3.3 for LOD and 10 for LOQ, s_b is the standard error of the intercept, and S is the regression slope. This model is based on the ICH Guidelines for determining limits of detection and quantitation, which states that the standard deviation of the y-intercept may be used as representation for standard deviation of the response. Because the estimates of the instrumental limits of detection and quantitation are based on the regression curves, these values were also determined for each individual batch.

3.2.8 Extraction Method Evaluation

The extraction method was evaluated by relative recovery and efficiency. The relative recovery (Equation 3.8) was determined from the ratio of the analyte peak area (PA) in the sample spiked before extraction (SBE) versus the analyte peak area in the sample spiked after extraction (SAE) and before evaporating:

$$\%\ \text{Recovery} = 100\% \times \frac{PA_{SBE}}{PA_{SAE}}. \tag{3.8}$$

The extraction efficiency (Equation 3.9) was determined from the ratio of the analyte peak area in the sample spiked before extraction versus the analyte peak area of a standard of the expected concentration.

$$\%\ \text{Efficiency} = 100\% \times \frac{PA_{SBE}}{PA_{Std}}. \tag{3.9}$$

3.2.9 Statistical Analysis

Analytical figures of merit were calculated using MS Excel. Plots of the figures of merit were produced using the ggplot2 package in R [221].

3.3 Results & Discussion

Before evaluating the synthesised BODIPY-estrogen conjugates as fluorescent proxies in environmental bacteria, we first needed to establish reliable and robust analytical methods for quantitative analysis of both natural and fluorescent estrogens in culture media. First, the suitability of each chromatography system and method were evaluated to ensure analyses of native and BODIPY-tagged estrogens were fairly compared. After selecting the optimal chromatographic platform and conducting a method validation, the impact of the BODIPY fluorophore on the sample extraction method from minimal salts culture media was evaluated. The chemical structures of the estrogen compounds and fluorophores evaluated in this method development are provided in Figure 3.2, and the relevant physical properties of each compound are provided in Table 3.3.

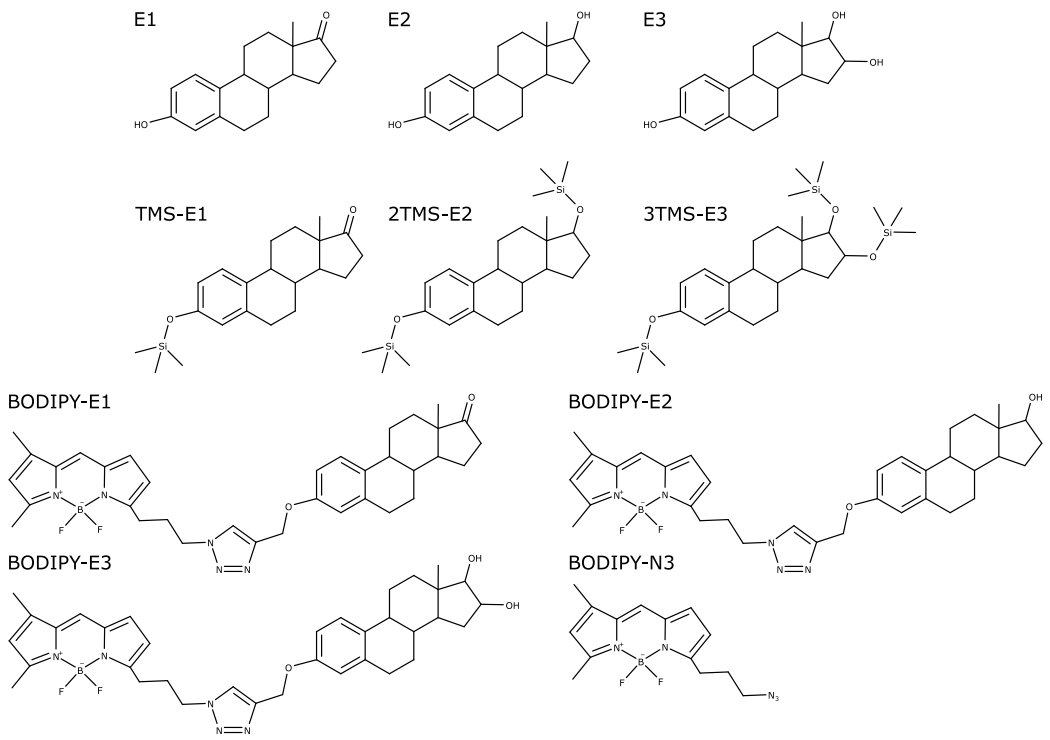

Figure 3.2: Chemical structures of the estrogen compounds and fluorophore used in method development.

Table 3.3: Relevant physical properties of the estrogen compounds used in method development.

Analyte	ID	Analysis	λ_{max} (nm)	Formula	Molecular Weight (Da)
Estrone	E1	HPLC@230 nm	280	$C_{18}H_{22}O_2$	270.37
17β-Estradiol	E2	HPLC@230 nm	280	$C_{18}H_{24}O_2$	272.38
Estriol	E3	HPLC@230 nm	280	$C_{18}H_{24}O_3$	288.39
TMS-Estrone	TMS-E1	GC-MS@342 m/z	-	$C_{21}H_{30}O_2Si$	342.55
2TMS-Estradiol	2TMS-E2	GC-MS@416 m/z	-	$C_{24}H_{40}O_2Si_2$	416.74
3TMS-Estriol	3TMS-E3	GC-MS@504 m/z	-	$C_{27}H_{48}O_3Si_3$	504.92
BODIPY-Estrone	BDP-E1	HPLC@503 nm	503	$C_{35}H_{40}O_2N_5BF_2$	611.53
BODIPY-Estradiol	BDP-E2	HPLC@503 nm	503	$C_{35}H_{42}O_2N_5BF_2$	613.55
BODIPY-Estriol	BDP-E3	HPLC@503 nm	503	$C_{35}H_{42}O_3N_5BF_2$	629.55
BODIPY-Azide	BDP-N3	HPLC@503 nm	503	$C_{14}H_{16}BF_2N_5$	303.12

3.3.1 GC-MS Analysis

3.3.1.1 System Suitability

The derivatised forms of the natural estrogens–TMS-E1, 2TMS-E2, and 3TMS-E3–were readily detected by the GC-MS (Figures 3.3a, 3.3c, 3.3e). The identity of the resulting peaks were confirmed by matching the molecular ion m/z with the derivatives' expected molecular weights and matching the EI mass spectra against NIST Mass Spectra Library 11. The BODIPY-estrogens were not detected by the GC-MS (Figures 3.3b, 3.3d, 3.3f). The BODIPY fluorophore and 1,2,3-triazole linker do not contain active hydrogens for derivatisation with BSTFA, and the C3 hydroxyl group in the natural estrogens was transformed into a propargyl ether for BODIPY conjugation. The BODIPY-estrogens, which are nearly twice the molecular weight of the non-volatile native form, naturally also require modification for increased volatility. However, due to their high molecular weight and lack of sites for chemical derivatisation, the BODIPY-estrogens were unsuited for GC-MS analysis.

Selected ion monitoring of the molecular ions was used to detect and quantify the derivatised estrogens with greater sensitivity and selectivity than afforded by extracted ion analysis of the full scan (Figures 3.4a, 3.4c, 3.4e). When applied to the BODIPY-estrogens, SIM scan did not show even trace evidence of BODIPY-estrogens' decomposition into native estrogens for silylation. The peak observed at approximately 21 minutes in the three BODIPY-estrogen SIM scans was putatively identified by the NIST Library as trimethyl(1-methylethoxy)silane (Figures 3.4b, 3.4d, 3.4f). The same peak was also observed in the derivatised natural estrogens' SIM chromatograms and appears to be a non-interfering contamination from the GC-MS system.

In order to compare chromatographic performance across systems, the analytical range tested on both the GC-MS and HPLC was selected to be comparable. The analytes generated well-resolved ($Rs > 1.5$) Gaussian peaks with a very high degree of efficiency (N) (Table 3.4). Thus, the developed GC-MS system and method were deemed suitable for evaluating the analytical performance.

Table 3.4: GC-MS system suitability parameters–theoretical plate count N and resolution Rs–for derivatised estrogens detected by SIM.

	N	*Rs*
TMS-E1	7.43E+06	[a]
2TMS-E2	8.80E+06	75
3TMS-E3	9.55E+06	18

[a] Analyte was the first compound eluted.

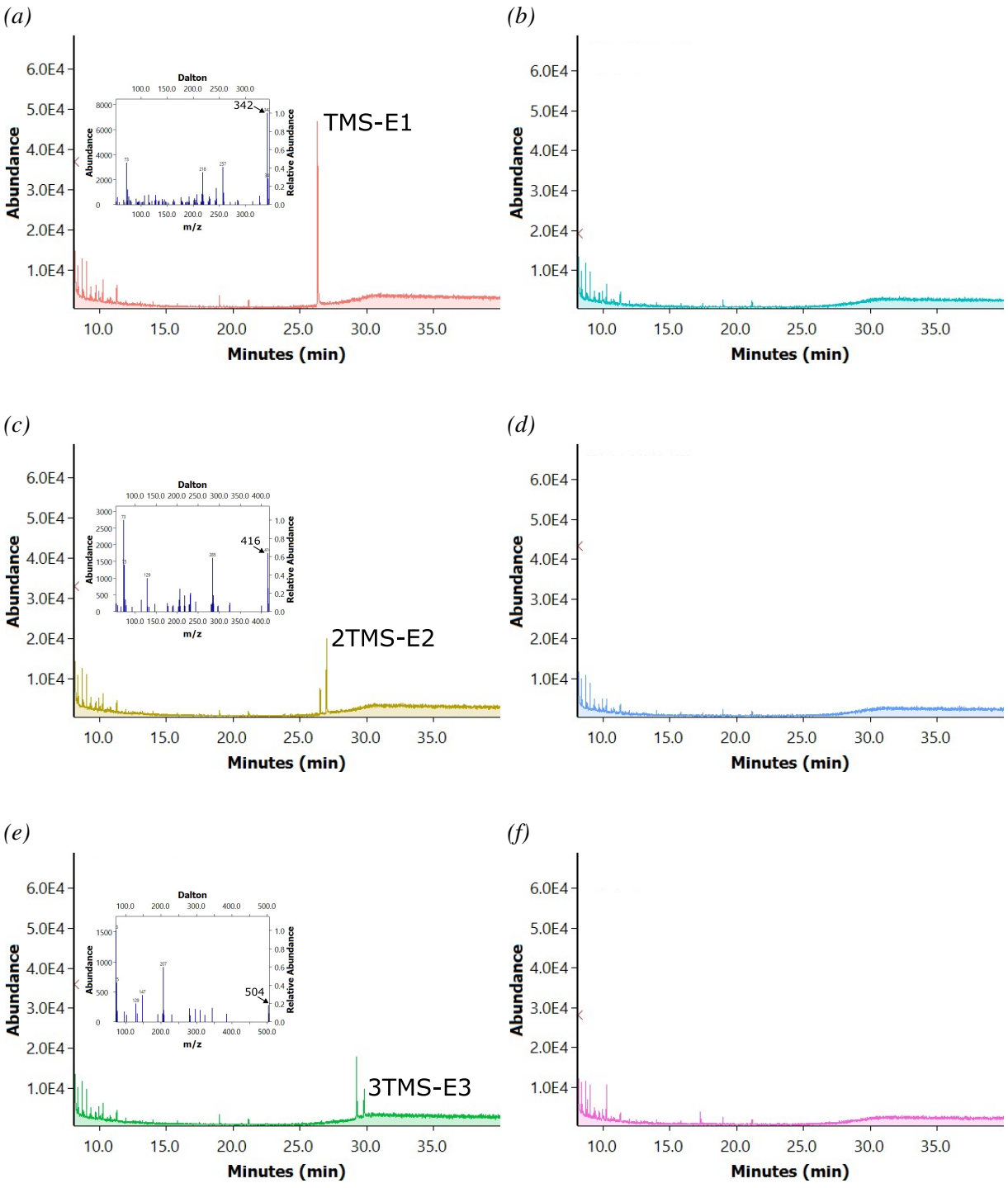

Figure 3.3: Representative total ion chromatograms for derivatised 10 mg/L (a) E1, (c) E2, and (e) E3, and 22 mg/L (b) BODIPY-E1, (d) BODIPY-E2, and (f) BODIPY-E3. Inset plots are the mass spectra for the analyte peak; the molecular ion is noted with an arrow. No analyte peaks were detected for the BODIPY-estrogens.

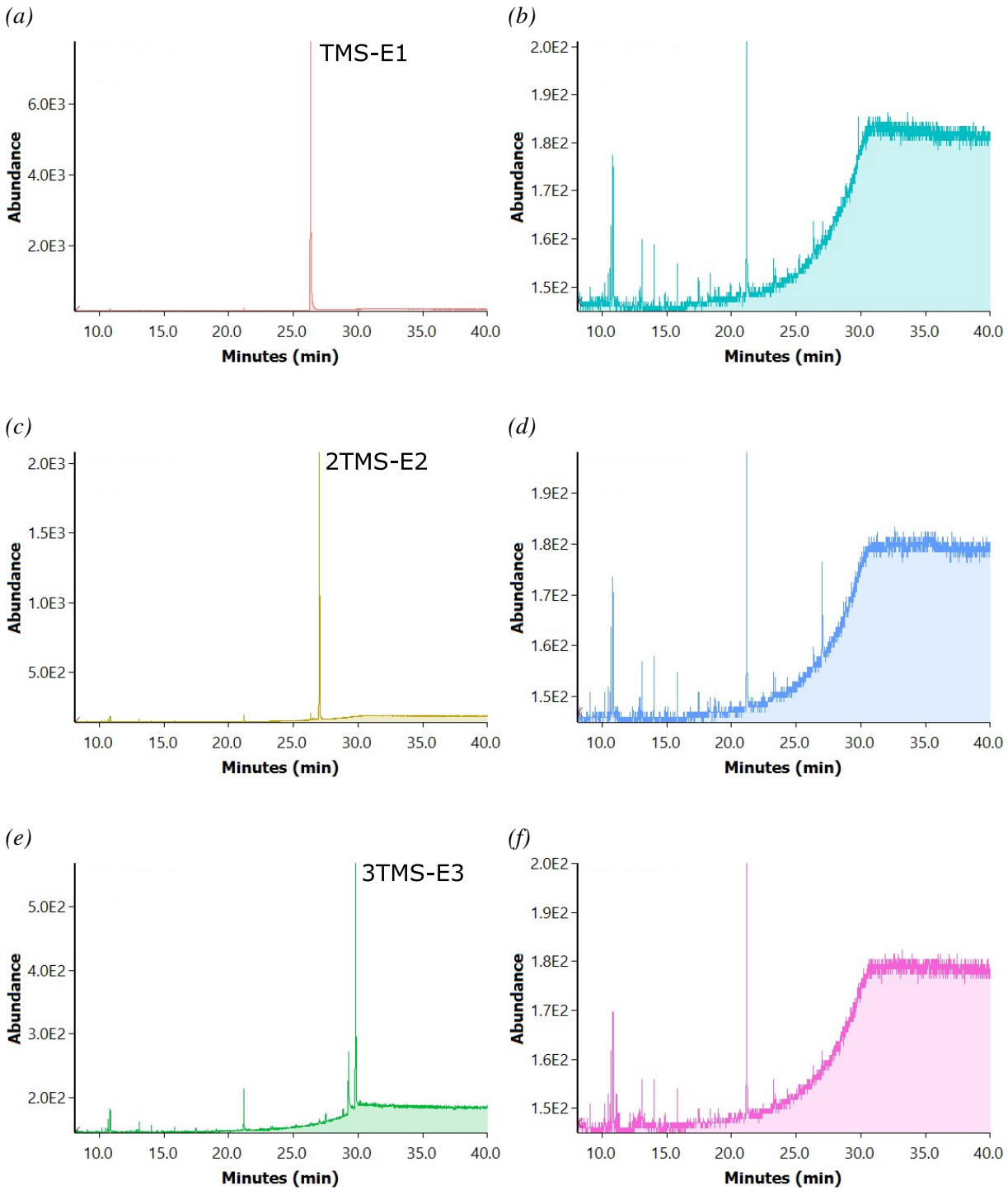

Figure 3.4: Representative SIM chromatograms (m/z 342, 416, 504) for derivatised 10 mg/L (a) E1, (c) E2, and (e) E3, and 22 mg/L (b) BODIPY-E1, (d) BODIPY-E2, and (f) BODIPY-E3. No analyte peaks were detected for the BODIPY-estrogens.

3.3.1.2 Method Evaluation

The chromatography method was then evaluated following the ICH Guidelines Q2 (R1) for analytical method validation and using the acceptance criteria set by the FDA Bioanalytical Method Validation Guidance [145, 222]. The ICH Guidelines describe "intermediate precision" as an expression of intra-laboratory variations, and this was investigated by comparing the response of a standard over a lengthy (>12 h) batch and between the first and final batches [222]. Since the BODIPY-estrogens were not detectable, only natural estrogens E1 and E2 were evaluated; E3 was used as a surrogate standard for derivatisation and for calculating the peak area ratio.

Table 3.5: Results of GC-MS method evaluation.

	Precision			*Accuracy*		*Calibration Statistics*		
Analyte	Repeat.	Intra-Assay	Inter-Assay	% Recovery	% Error	LOD	LOQ	Linearity (R^2)
TMS-E1	4	5	10	100	8.9	**0.07 ± 0.01**	**0.20 ± 0.02**	0.992 ± 0.001
						17 ± 7	50 ± 20	
2TMS-E2	4	6	11	93	9.0	**0.06 ± 0.03**	**0.19 ± 0.08**	0.992 ± 0.005
						18 ± 1	55 ± 4	

Precision values are percent relative standard deviation. Limits of detection (LOD) and quantitation (LOQ) are reported in micromolar (**bold**, top values) and µg/L (bottom values). Linearity and limit values are the means of the three different batches (n=3) and include standard deviation (± value).

The precision and accuracy satisfied the acceptance criteria recommended by the FDA method validation guidelines (<15% RSD for precision and ±15% for error) (Table 3.5) [145]. Unweighted linear regression showed a high degree of linearity for both E1 and E2 (R^2 0.992 ± 0.001 E1, 0.992 ± 0.005 E2, $n = 3$). The limits of detection (17 ± 7 µg/L E1, 18 ± 1 µg/L E2, $n = 3$) and quantitation (50 ± 20 µg/L E1, 55 ± 4 µg/L E2, $n = 3$) were slightly greater than the instrumental LOQ (10 µg/L E1 and E2) obtained in the study by Quintana *et al.* (2004), from whom this GC-MS method was adapted [136].

3.3.2 HPLC Analysis

3.3.2.1 System Suitability

All estrogenic analytes were analysed on the same run method at two different wavelengths. Non-derivatised estrogens were measured at 230 nm, which yielded a signal-to-noise ratio greater than 280 nm, the maximum absorbance wavelength (λ_{max}) determined by the detector (Table 3.3 and Figures 3.5a, 3.5c, 3.5e). BODIPY-tagged estrogens, as well as the BODIPY-

azide tag, were measured at the λ_{max}, 503 nm (Figures 3.5b, 3.5d, 3.5f, 3.5g). Simultaneous analysis of native and fluorescent substrates allows for efficient sample processing and direct comparison of the overall chromatogram between samples.

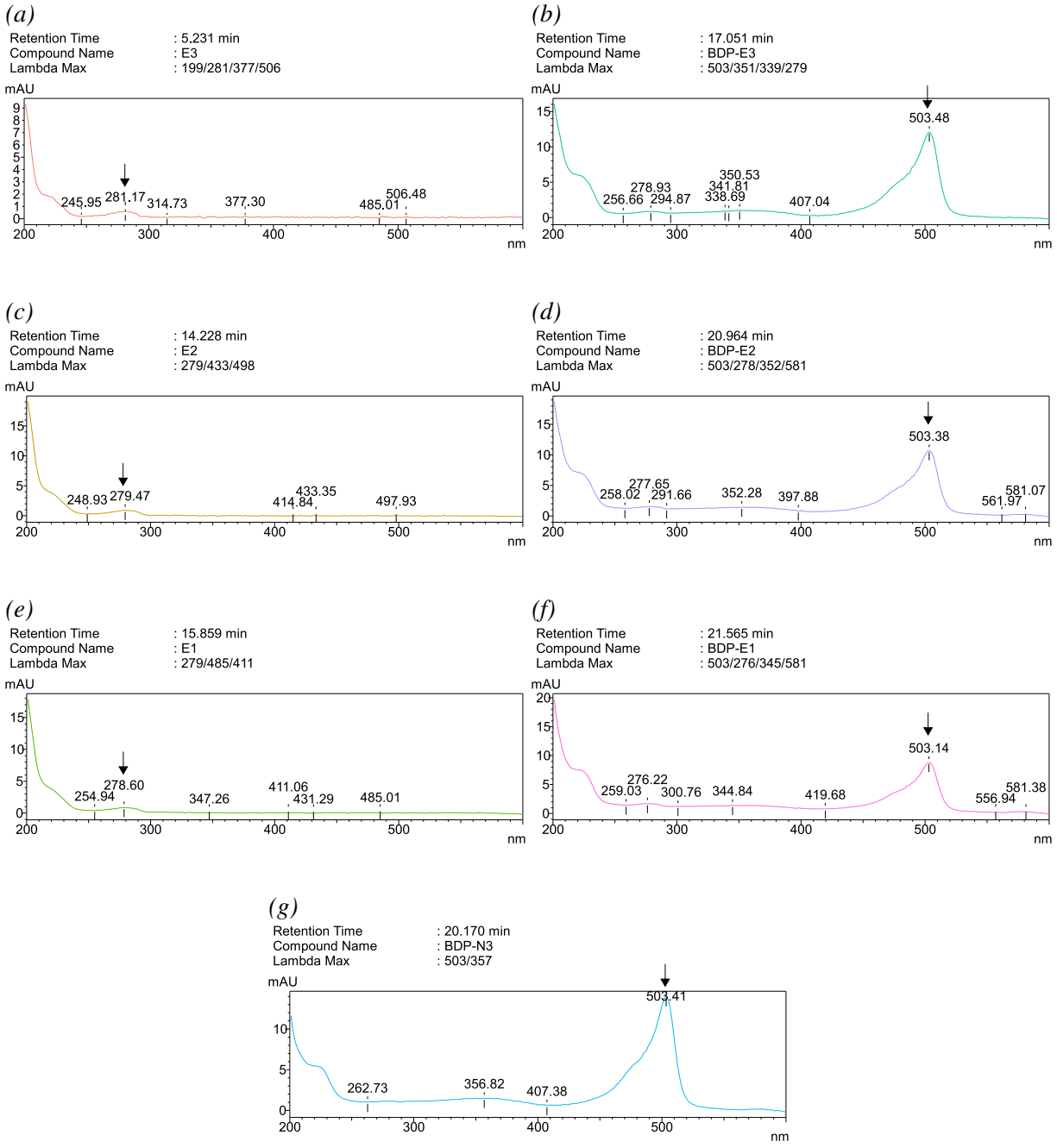

Figure 3.5: Representative PDA absorbance spectra for native (a, c, e) and BODIPY-tagged (b, d, f; 1 mg/L) estrogens and the BODIPY-azide tag (g; 0.5 mg/L). The λ_{max} is indicated with an arrow.

The analytes generated well-resolved Gaussian peaks (Figure 3.6). In fact, the chromato-

graphic efficiency (N) was an order of magnitude greater for BODIPY-E1 and -E2 ($p < 0.0025$) than E1 and E2, respectively (Table 3.6). Thus, the developed method for concurrent analysis of natural and BODIPY-estrogens was deemed suitable for assessing analytical performance.

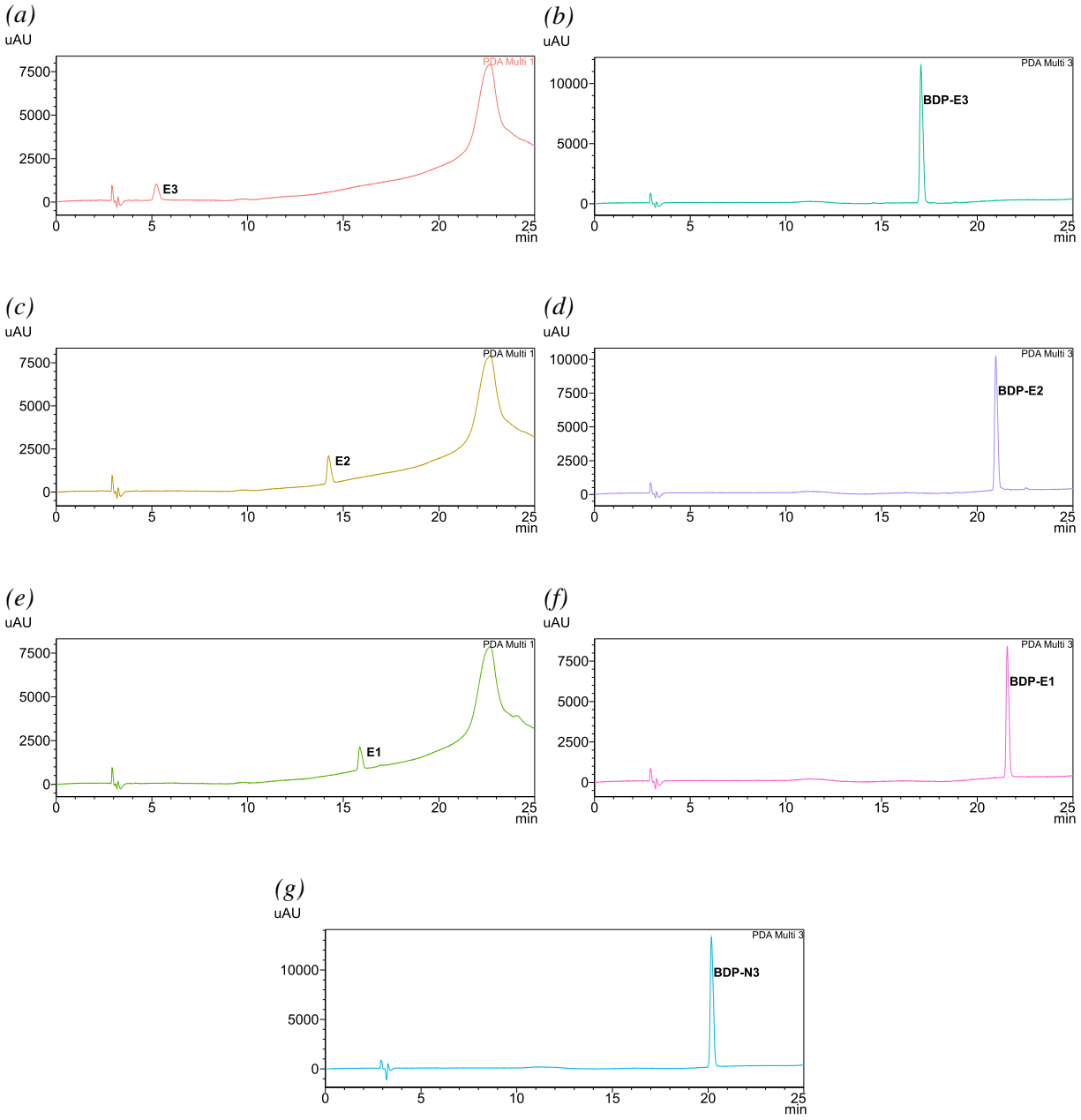

Figure 3.6: Representative HPLC-PDA chromatograms for native (a, c, e; 1 mg/L) and BODIPY-tagged (b, d, f; 1 mg/L) estrogens and the BODIPY-azide tag (g; 0.5 mg/L).

Table 3.6: HPLC-PDA system suitability parameters–theoretical plate count N and resolution Rs–for estrogens with and without BODIPY.

	N		*Rs*	
	Untagged	BODIPY-tagged	Untagged	BODIPY-tagged
E1	9.06E+04	2.07E+05	7	3
E2	5.95E+04	1.78E+05	28	20
E3	2.63E+03	1.30E+05	[a]	6

[a] Analyte was the first compound eluted.

3.3.2.2 Method Evaluation

The HPLC method was evaluated following the same standards as the GC-MS method, using E3 and BODIPY-E3 as the internal standards for native and BODIPY-estrogens, respectively. The intermediate precision for all analytes not only satisfied the recommended acceptance criteria recommended by the FDA method validation guidelines (<15% RSD), but the non-derivatised estrogens had much higher variability compared to the BODIPY-estrogens (Table 3.7) [145].

Table 3.7: Results of HPLC-PDA method evaluation.

		Precision		*Accuracy*		*Calibration Statistics*		
Analyte	Repeat.	Intra-Assay	Inter-Assay	% Recovery	% Error	LOD	LOQ	Linearity (R^2)
E1	10	10	10	100	8.5	**0.09 ± 0.03** 24 ± 8	**0.27 ± 0.09** 72 ± 24	0.991 ± 0.005
E2	10	10	9	100	7.1	**0.10 ± 0.04** 27 ± 12	**0.3 ± 0.1** 82 ± 36	0.988 ± 0.009
BODIPY-E1	1	1	1	97	4.3	**0.02 ± 0.01** 14 ± 7	**0.07 ± 0.03** 42 ± 21	0.999 ± 0.001
BODIPY-E2	1	1	1	96	4.8	**0.02 ± 0.01** 13 ± 6	**0.07 ± 0.03** 40 ± 19	0.999 ± 0.001

Precision values are percent relative standard deviation. Limits of detection (LOD) and quantitation (LOQ) are reported in micromolar (**bold**, top values) and µg/L (bottom values). Linearity and limit values are the means of the three different batches (n=3) and include standard deviation (± value).

The BODIPY-estrogens showed good quantitative accuracy compared to native estrogen

HPLC analysis (Table 3.7). The percent recovery and percent error were generally within the recommended acceptance criteria: ±15% for the middle and high QC and ±20% for the lowest QC [145]. In particular, the percent error for the BODIPY-estrogens was significantly less than those of the natural estrogens. Unweighted linear regression of the calibration standards consistently showed a high degree of linearity across all platforms (from 0.988 ± 0.009 to 0.999 ± 0.001, n=3). Additionally, the percent error for each calibration standard was within ±15 % (except for lowest standard which was within ±20%) both with and without BODIPY. Lastly, the instrument limits of detection and quantitation were calculated from the calibration curve linear regression of each batch. The calculated LOD and LOQ (Table 3.7) were lower for estrogens tagged with BODIPY (0.02 μM and 0.07 μM) than the non-tagged estrogens (0.09-0.10 μM and 0.27-0.30 μM).

Interestingly, the addition of BODIPY not only did not impede chromatographic analysis, but it improved each analytical figure of merit compared to the untagged analytes. The conjugated fluorophore greatly increased the theoretical plate count for better efficiency, which in turn had beneficial effects on the signal-to-noise and the relevant performance criteria. The precision, accuracy, linearity, and limits of detection of the BODIPY-estrogens are further improved due to the increased signal-to-noise of the fluorophore, which has a greater molar absorptivity at 503 nm (nearly 10^5 $M^{-1}cm^{-1}$) compared to natural estrogens detected by UV (2000 $M^{-1}cm^{-1}$) [162, 207]. Indeed, BODIPY has previously been used to derivatise biomolecules such as thiols [223], fatty acids [224], and aliphatic aldehydes [225] to enhance their chromatographic analysis. Thus, in addition to demonstrating that we have a reliable analytical method to measure the biodegradation of native and BODIPY-tagged estrogens, these results notably support the use of BODIPY derivatives for enhanced HPLC detection.

3.3.3 Validation of the Selected HPLC Method

Since the HPLC was able to measure both natural and fluorescent estrogens with a detection limit comparable to the GC-MS, the HPLC was selected as the chromatographic system for analysis. The analytical ranges used in determining the optimal chromatography platform were chosen to detect as low as possible with good accuracy. However, this is impractical for measuring biodegradation, and a more fit-for-purpose analytical range across one order of magnitude (100–1000 μg/L) was validated (Table 3.8). The precision for the untagged estrogens improved with the wider analytical range, however, the calculated limits of detection and quantitation increased. The LOD and LOQ are calculated from the standard error of the intercept, and the variance in the calibration curve regression errors gave very imprecise estimates for the instrumental limits. The signal-to-noise ratio at 3 and 10 is also commonly used to estimate instrumental limits of detection and quantitation, respectively. The mean S/N ratio for the lowest standard is 4.9 ± 0.6

for E1, 5 ± 1 for E2, 37 ± 3 for BODIPY-E1, and 42 ± 3 for BODIPY-E2. Therefore, the lowest concentration measured by the calibration curve will be used as the limit for quantitation.

Table 3.8: Results of selected HPLC-PDA method evaluation.

	Precision			*Accuracy*		*Calibration Statistics*		
Analyte	Repeat.	Intra-Assay	Inter-Assay	% Recovery	% Error	LOD	LOQ	Linearity (R^2)
E1	2	2	2	98	5.1	**0.3 ± 0.2** 77 ± 60	**0.9 ± 0.7** 235 ± 181	0.992 ± 0.01
E2	2	2	1	98	4.9	**0.3 ± 0.2** 83 ± 53	**0.9 ± 0.6** 251 ± 162	0.992 ± 0.01
BODIPY-E1	0.4	0.4	0.4	100	6.4	**0.09 ± 0.1** 59 ± 60	**0.3 ± 0.3** 176 ± 181	0.994 ± 0.008
BODIPY-E2	0.4	0.3	0.3	97	4.9	**0.11 ± 0.08** 68 ± 50	**0.3 ± 0.2** 208 ± 152	0.994 ± 0.008

Precision values are percent relative standard deviation. Limits of detection (LOD) and quantitation (LOQ) are reported in micromolar (**bold**, top values) and µg/L (bottom values). Linearity and limit values are the means of the three different batches (n=3) and include standard deviation (± value).

3.3.4 Effects of Filtration on Liquid-Liquid Extraction

BODIPY-estrogens present unique complications that can affect extraction, including low solubility and intermolecular interactions. Preliminary work with SPE using hydrophobic-lipophilic balance (HLB) sorbent in extracting BODIPY-estrogens by standard protocols for native estrogens showed inadequate recovery. Liquid-liquid extraction (LLE) was thus selected for sample preparation due to the simple process of chemical partitioning between two immiscible phases. In addition, because ionic strength can influence extraction, the LLE method was developed and optimised for minimal salts media Modified Medium B (MMB).

Filtration of biological samples is an important measure to preserve the integrity of the HPLC system and column, irrespective of the extraction method. However, syringe filtration appeared to remove the BODIPY compounds from solution. In aqueous solution, the BODIPY-estrogens produce an orange hue (Figure 3.7a), in contrast to the vibrant green color observed in organic solvent such as acetonitrile or methanol. The orange color of BODIPY in aqueous solutions is understood to be the result of insoluble aggregates [226]. The chromophoric BODIPY compounds were visually confirmed to have been filtered out of the media (Figure 3.7b) and retained

in the filter material (Figure 3.7c). Therefore, to prevent the loss from filtration, the MMB media was diluted 50% (v/v) with acetonitrile, as it enabled solubilization of the BODIPY compounds.

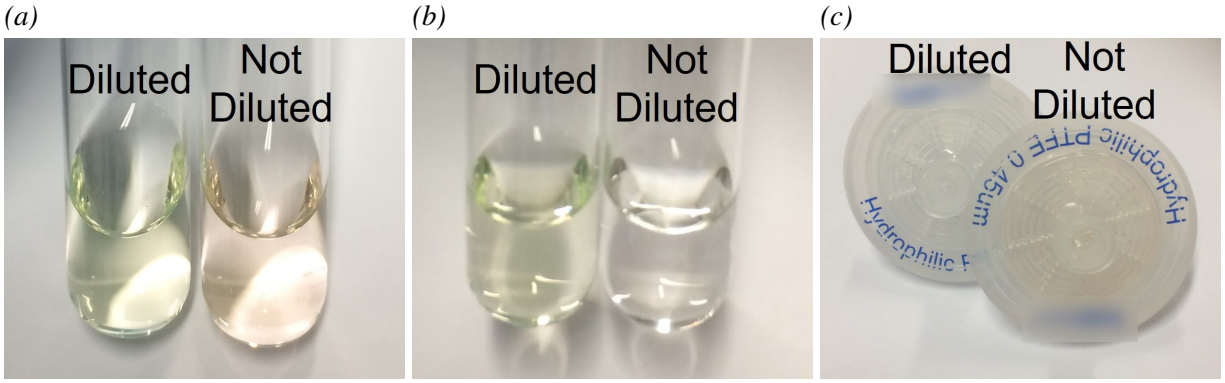

Figure 3.7: Photographs of estrogen and BODIPY-estrogen mixtures before (a) and after (b) filtration, showing the retention of green hue in the diluted mixture and loss of the orange hue in the undiluted mixture. (c) The syringe filters after filtration, showing an orange hue retained in the filter used on the undiluted mixture. The "Diluted" mixture was combined with 50% (v/v) acetonitrile, and the "Not Diluted" mixture is in neat MMB media.

The effects of dilution and filtration on the extraction recovery of natural and BODIPY-estrogens were quantitatively investigated (Figure 3.8a). BODIPY-azide was included in the recovery evaluation to assess the extraction performance on the fluorophore independently. The results of this work demonstrated both processes have a significant impact on the extraction recovery of BODIPY compounds (Figure 3.8b). The samples filtered without dilution recovered only the natural estrogens. BODIPY-estrogens were not detected following extraction, and BODIPY-azide was only minimally recovered. Furthermore, the recovery of natural estrogens was poorer after filtering, indicating that filtration impedes extraction of natural estrogens as well. When the samples were diluted with acetonitrile prior to filtration, however, there was no difference in recovery between filtered and unfiltered samples for all compounds tested.

The extraction recovery for diluted and filtered samples across three concentrations (0.1, 0.5, and 1.0 mg/L each for natural and BODIPY-estrogens and 0.05, 0.25, and 0.5 mg/L for BODIPY-azide) was also determined to assess any concentration-dependent effects (Figure 3.8c and Table 3.9). The extraction recovery was highly reproducible across concentrations of natural estrogens, except for the low concentration of E3. The high variability and difference from other estrogens may be explained by the lower response factor of E3, which has been reported previously in the literature [227, 228]. The extraction recovery performance was also highly reproducible across BODIPY compounds, including BODIPY-azide (average overall recovery 66.4% to 67.9%). The extraction recovery was slightly greater at the high concentration for BODIPY-estrogens and -azide, but within 7.3% difference of the middle and low concentrations.

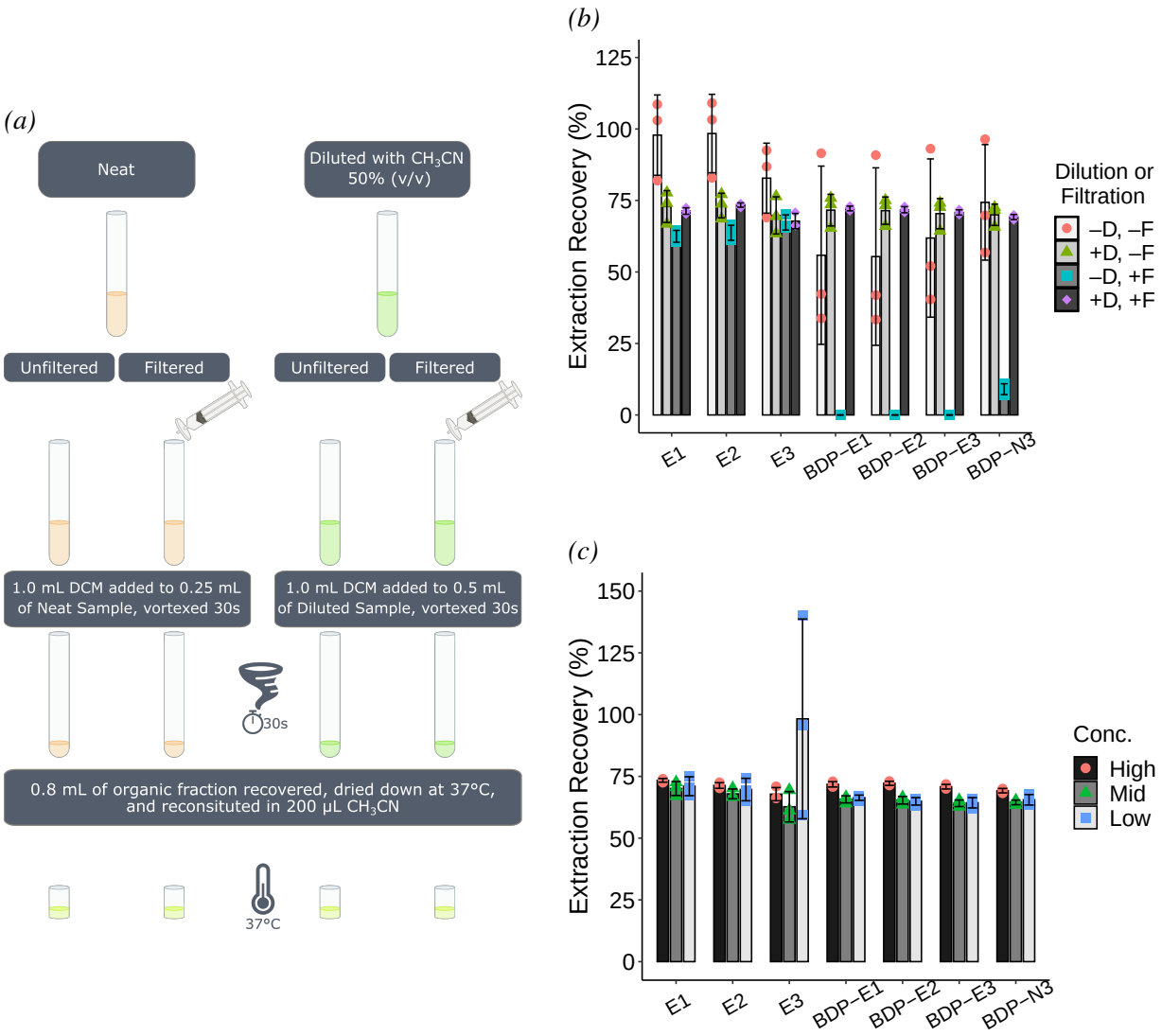

Figure 3.8: (a) Workflow of LLE method development. (b) Extraction recovery percentage of 1 mg/L estrogens and 0.5 mg/L BODIPY-azide by liquid-liquid extraction with (+D) and without dilution (−D) with acetonitrile and with (+F) and without (−F) filtration. (c) Extraction recovery percentage of estrogens and BODIPY azide with dilution and filtration. Low, Mid, and High concentrations are 0.1, 0.5, and 1.0 mg/L for estrogens and 0.05, 0.25, and 0.5 mg/L for BODIPY-azide. Columns are the mean and error bars are standard deviation of replicate samples extracted (n=3, individual extractions shown as points).

Lastly, the extraction recovery for natural and BODIPY-estrogens were comparable (average overall recovery 66.4% to 71.5%).

The BODIPY fluorophore had a significant impact on both filtration and phase partitioning. By evaluating BODIPY-azide along with the BODIPY-estrogens, it was clear that it was not the conjugation with steroids, but the fluorophore itself that primarily affected extraction recovery. We believe this is directly related to the aggregative properties and low aqueous solubility

Table 3.9: Percent recovery values for the different LLE methods assessed.

		% Recovery						
Version	Conc.	E1	E2	E3	BODIPY-E1	BODIPY-E2	BODIPY-E3	BODIPY-N3
Diluted + Filtered	Low	71 ± 4	70 ± 5	98 ± 40	66 ± 1	65 ± 2	64 ± 2	66 ± 2
	Mid	70 ± 3	68 ± 2	63 ± 6	66 ± 1	65 ± 2	64 ± 1	65 ± 1
	High	73 ± 1	71 ± 1	68 ± 3	72 ± 1	72 ± 1	71 ± 1	69 ± 1
	Mean	72 ± 3	70 ± 3	80 ± 30	68 ± 3	68 ± 4	66 ± 4	66 ± 3
HPβ-CDX + Filtered	Mid	90 ± 4	100 ± 20	N.D.	43 ± 4	67 ± 3	82 ± 2	66 ± 2
	High	80 ± 10	60 ± 10	N.D.	27 ± 7	40 ± 10	70 ± 10	50 ± 10
	Mean	80 ± 10	80 ± 30	N.D.	30 ± 10	60 ± 10	70 ± 10	60 ± 10
HPβ-CDX + Diluted + Filtered	Low	72 ± 5	81 ± 6	N.D.	68 ± 3	70 ± 3	71 ± 3	71 ± 3
	Mid	70 ± 1	66 ± 1	16 ± 1	66 ± 1	66 ± 1	67 ± 1	68 ± 1
	High	65 ± 1	64 ± 2	34 ± 2	62 ± 3	62 ± 3	63 ± 3	63 ± 3
	Mean	69 ± 4	70 ± 9	20 ± 10	65 ± 3	66 ± 4	67 ± 4	68 ± 4

Recovery values are the mean (± standard deviation) of 3 replicate samples extracted (n=3) at different concentrations. The "Mean" concentration is the average recovery across all concentrations assessed. N.D. - Not detected.

of BODIPY. While there are extraction protocols for BODIPY-labelled lipids in the literature, these methods were not used for co-extracting the natural molecule [229, 230]. The extraction recoveries for the developed method were not as high as many published methods for natural estrogens. However, the method was reproducible across multiple estrogen species and a range of concentrations, both with and without the BODIPY tag. Thus, the measured concentrations, obtained by simultaneous extraction and analysis of natural and fluorescent estrogens, can be directly compared.

3.3.5 Effects of Cyclodextrin on Liquid-Liquid Extraction

The low solubility of BODIPY-estrogens still presented a challenge for assessing biodegradation in aqueous biological samples. When prepared at 1 mg/L in MMB media, BODIPY-estrogens slowly (within 24 hours) precipitate. Biodegradation experiments with high concentration of natural estrogens (0.5 g/L) were previously carried out by including methylated β-cyclodextrin [99]. To ensure the concentration in solution remains consistent for the duration of experiments, HPβ-CDX (Figure 3.9) was added to the minimal media to solubilise the BODIPY-estrogens.

First, the recovery of natural and BODIPY-estrogens and BODIPY-azide was assessed in MMB media supplemented with 2% HPβ-CDX with filtration but without dilution, as it was expected cyclodextrin might replace the requirement for dilution (Figure 3.10a and Table 3.9). The results show that cyclodextrin has a notable effect on the extraction performance of all com-

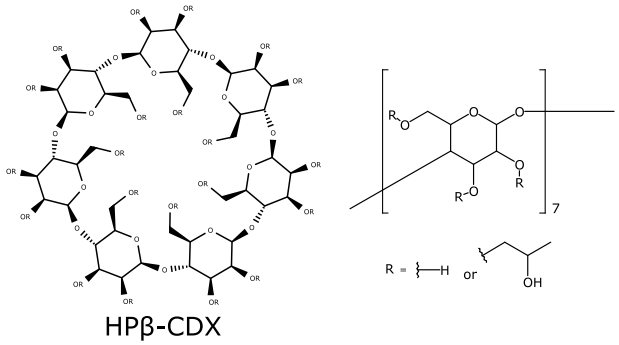

Figure 3.9: Chemical structure of 2-hydroxypropyl-β-cyclodextrin (HPβ-CDX).

pounds. Most notably, the BODIPY-estrogens and BODIPY-azide were recovered (overall average recovery 34.9% to 73.4%), whereas these were not recoverable without HPβ-CDX (Figure 3.8b). Estriol, however, was not recovered in the presence of cyclodextrin following filtration. In addition, the extraction recovery was influenced by the analyte concentration and chemistry. Of the two concentrations investigated, the lower concentration consistently showed better extraction recovery. Additionally, extraction recovery correlated negatively with hydrophobicity for the BODIPY compounds (BODIPY-E3 > BODIPY-azide > BODIPY-E2 > BODIPY-E1).

Next, the recovery was assessed including both cyclodextrin and 1:2 dilution with acetonitrile before filtration (Figure 3.10b and Table 3.9). The pre-dilution of the media supplemented with 2% HPβ-CDX with acetonitrile significantly diminished the combined effects of cyclodextrin and filtration as reported in Figure 3.10a. The extraction recovery was highly consistent across the natural estrogens and BODIPY compounds, again, with the exception of E3. Aside from estriol, there was a slight increase in extraction recovery at lower concentrations for all analytes tested, particularly for E2 (63.5% at 1.0 mg/L versus 80.6% at 0.1 mg/L). However, the overall average recovery for all estrogens (except E3) and BODIPY compounds fell between 65.2% to 70%.

Lastly, the influence of HPβ-CDX on the LLE process was investigated without dilution and filtration. Increasing concentrations of cyclodextrin minimally improved the extraction efficiency for all compounds investigated, except for E3 (Figure 3.10c). Increasing concentrations of cyclodextrin significantly reduced the extraction efficiency of E3. The markedly different extraction performance may be a consequence of the greater hydrophilicity of E3 com-pared to the other analytes investigated. However, the inverse effect was not observed, as the strongly hydrophobic BODIPY-estrogens and BODIPY-azide showed a similar extraction efficiency as E1 and E2. Since there was no significant difference in extraction performance for most of the analytes tested at the concentrations of HPβ-CDX evaluated, the highest concentration of 2% (w/v) was selected to ensure solubility of BODIPY-estrogens and potential metabolites.

Although cyclodextrin introduced some concentration-dependent effects and sacrificed E3,

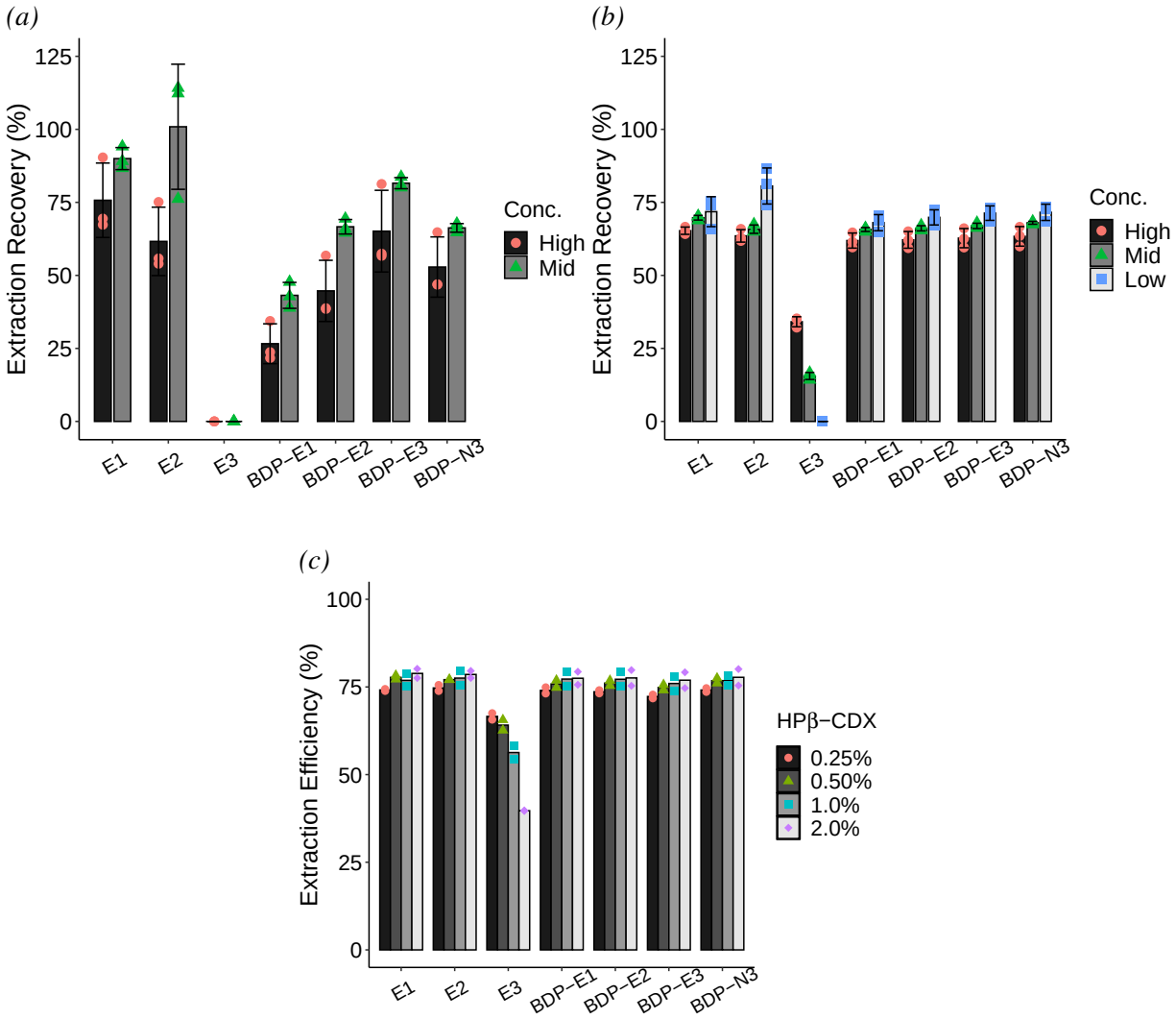

Figure 3.10: (a) Extraction recovery percentage of estrogens and BODIPY-azide in MMB media with 2% HPβ-CDX by LLE with filtration but without dilution. (b) Extraction recovery percentage of estrogens and BODIPY-azide in MMB media with 2% HPβ-CDX by LLE with dilution with acetonitrile and filtration. Low, Mid, and High concentrations are 0.1, 0.5, and 1.0 mg/L for estrogens and 0.05, 0.25, and 0.5 mg/L for BODIPY-azide. Columns are the mean and error bars are standard deviation of replicate samples extracted (n=3, individual extractions shown as points). (c) Extraction efficiency percentage of 1 mg/L estrogens and 0.5 mg/L BODIPY-azide in MMB media with four different concentrations of HPβ-CDX by LLE without filtration or dilution. Columns are the mean of replicate samples extracted (n=2, individual extractions shown as points).

the developed LLE method reliably and simultaneously extracted most natural and all BODIPY-tagged estrogens from minimal media without concern for solubility. Since the analyte concentration had a small effect on extraction recovery, it is not appropriate to apply a recovery factor to correct the analytical results, as the recovery factor varies slightly by concentration [231]. Furthermore, E3 cannot be used as a surrogate standard to correct the measured concentrations of E1 and E2, since the higher polarity of E3 makes it chemically in-comparable during extraction. However, because the developed extraction method recovery is highly reproducible between natural and fluorescent estrogens, we can directly compare the biodegradation of both forms by extracting a control with the substrates spiked at the same concentration. Furthermore, if the fluorophore were deconjugated from the molecule, either enzymatically or abiotically, the now-untagged estrogen could be quantified in the very same extract. Because we have thoroughly evaluated the extraction and analysis methods, we can confidently measure the degradation of estrogens as well as their fluorescent analogues in bacteria cultures.

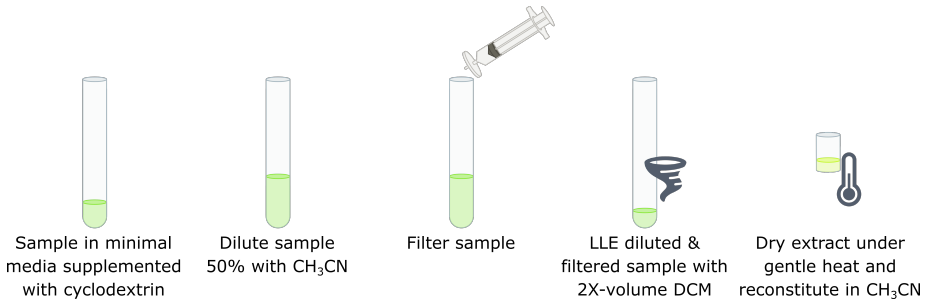

Figure 3.11: Optimised LLE method workflow for natural and BODIPY-labelled estrogens.

3.4 Conclusion

In summary, this study evaluated two traditional chromatographic platforms – GC-MS and HPLC-PDA – for quantifying estrogen micropollutants and developed an accompanying extraction method using LLE.

- The GC-MS method was unable to detect BODIPY-estrogens; however, it demonstrated acceptable accuracy and sub-optimal precision for E1 and E2.
- The HPLC-PDA method, which was capable of analyzing both natural and fluorescent estrogens, showed good precision, accuracy, and obtained an instrumental detection limit comparable to the GC-MS method. Notably, the BODIPY-estrogens exceeded the untagged estrogens on every figure of merit; this was attributed to enhanced sensitivity due to the fluorophore.

- Because the HPLC demonstrated better precision and could detect both natural and BODIPY-labelled estrogens, this platform was selected to be our method for measuring biodegradation of estrogens, as well as our benchmark to compare the spectroscopic assays against.

- Lastly, the impact of the BODIPY fluorophore on extraction recovery was explored in detail. A fit-for-purpose LLE method was developed, which accounts for the poor hydrosolubility and aggregative properties of our BODIPY analytes and is capable of co-extracting the fluorescent and natural estrogens with similar recovery.

The developed analytical workflow based on LLE and HPLC-PDA allows for concurrent analysis of both fluorescent and natural estrogens with comparable recovery, accuracy, and precision. Therefore, we can now confidently apply these methods towards measuring biodegradation of estrogens and their fluorescent analogues in bacteria cultures.

Chapter 4

Mechanisms of BODIPY-Estrogen Biodegradation by Individual and Consortium Bacteria Cultures

4.1 Introduction

The role of biological degradation in removing estrogen hormones from water treatment systems has been reported in numerous studies, including aerobic degradation through activated sludge [22, 59, 232] and biofilters [38] and anaerobic degradation in waste lagoons [233, 234]. Recently, the specific biodegradation pathways of estrogen-degrading environmental bacteria have been elucidated, including *Nitrosomonas europaea* [103, 235], *Novosphingobium* sp. [97], *Sphingomonas* sp. [82, 98], *Sphingobacterium* sp. [92], and *Novosphingobium tardaugens* [99]. However, identifying, isolating, and studying estrogen-degrading bacteria is often a time- and labour-intensive process, with lengthy enrichment culture periods ranging from several weeks up to a year, time-consuming sample preparation, and low throughput chromatographic analyses [75, 78, 120]. Furthermore, in contrast with biomedical research, isolating bacteria from the environment is extremely challenging, as most microorganisms are unculturable in lab settings [63]. These challenges in identifying and studying estrogen-degrading microbial communities are the motivation for developing a rapid analytical method based on fluorescently labelled estrogens.

Part of the work in this chapter has been published in "BODIPY-Labeled Estrogens for Fluorescence Analysis of Environmental Microbial Degradation", Felion, C., Lopez-Gonzalez, R., Sewell, A.L., Marquez, R. and Gauchotte-Lindsay, C. *ACS Omega* 2022 7 (45), 41284-41295 DOI: 10.1021/acsomega.2c05002.

As noted previously, fluorescently labelled substrates, including those conjugated with BODIPY, have long been used in assays for biological processes. The sensing mechanisms for these fluorescent probes are varied. In some cases, as the fluorescent substrate is taken up by the cell, the decrease in the extracellular concentration of the probe can be measured by spectrofluorometry [236]. Cellular uptake may also be measured by the increase of fluorescence within the cell. This approach usually requires a cell-impermeable quenching agent [237] or separating the cells from the media, for example, by washing [238], filtering [239], microscopy [209, 240], or flow cytometry [201, 202]. BODIPY-labelled substrates have been employed using these sensing mechanisms [209, 240, 241]. Another sensing mechanism is deconjugation of the probe, where the intensity of the free fluorophore markedly increases, although this application is limited to hydrolysing enzymes [205, 242]. However, hydrolysis has been identified as part of the biodegradation pathways of estrogen (see Figure 2.7 in Chapter 2). Thus, before BODIPY-estrogens can be used to investigate biodegradation in microbial communities, the mechanism of action must be elucidated.

For any sensing mechanism of the fluorescent probe, an important development step is to ensure that the mechanism is fit for the intended purpose of the assay with supporting evidence in biological systems – i.e., validating the technique. A variety of approaches used to validate the application of fluorescent substrates are reported in the literature. Yoshioka *et al.* (1996) established 2-NBDG as a fluorescent proxy for glucose metabolism by competitive inhibition assays with glucose and other simple sugars, as well as confirmation of uptake via fluorescence microscopy [236]. Additionally, fluorescent substrates based on 4-methylumbelliferone (4-MU)-conjugated glycans used to detect coliform bacteria were validated by comparison against traditional methods (i.e., direct colony count) [204, 205]. More robust examples of validation include chromatographic analyses of the biotransformation of fluorescent analogues compared to the natural molecule, as has been done for BODIPY-labelled glycans [202, 243] and BODIPY-labelled lipids [224, 230, 244].

One notable challenge in validating the use of fluorescently labelled micropollutants is procuring micropollutant-degrading bacteria. Since most published fluorescent probes are based on ordinary glycans, peptides and lipids, validation studies often use multiple bacteria strains or a mixed culture procured from environmental samples [204, 205, 239]. However, bacteria with a niche metabolic potential are not readily available, and as such, most published biodegradation studies independently isolate these rare bacteria. Fortunately, a small selection of estrogen-degrading isolates have been added to culture collections as reference strains which can be used to investigate estrogen biodegradation.

In this chapter, we evaluated and established a synthetic community of bacteria which would be used to validate the developed spectroscopic assays as fit for purpose for monitoring estrogen biodegradation in bacteria cultures. Two estrogen-degrading reference strains were used to

validate the spectroscopic methods developed in this thesis: *Caenibius tardaugens* DSM 16702 and *Nitrosomonas europaea* NCIMB 11850. The heterotrophic *C. tardaugens* catabolises E2 via the 4,5-*seco* pathway (i.e., oxidation to E1, followed by cleavage of the A-ring), while chemolithoautotrophic *N. europaea* cometabolises E2 into E0 by reduction at C17 of the D-ring [99, 103]. Additionally, a non-degrading reference bacteria, *Escherichia coli* K-12 strain MG1655, was used as a biological negative control for degradation. These three bacteria, which have distinct approaches to estrogen degradation (i.e., catabolism, cometabolism, and non-metabolism), comprised the synthetic microbial community used to validate the spectroscopic methods. However, before this synthetic community could be used for spectroscopic method validation, the conditions for bacterial growth and degradation had to be characterised, both individually and in co-culture. In this chapter, the bacterial growth conditions and degradation of E2 were characterised and compared to those with BODIPY-labelled E2. In addition, the fate and putative mechanisms of BODIPY-E2 biodegradation were determined, which would inform the approach used in the fluorometric assay (i.e., cellular uptake versus hydrolysis).

The aim of this work was to compare the degradation of BODIPY-estradiol with the natural 17β-estradiol (E2) using the traditional analytical workflow developed in Chapter 3 and a synthetic community of estrogen-degrading reference bacteria.

4.2 Materials & Methods

4.2.1 Reagents

The BODIPY-labelled estrogens' synthesis and natural estrogens were described in Chapter 3 Section 3.2.1. HPLC-grade solvents were purchased from Sigma Aldrich UK. Ultrapure (18.2 MΩ·cm) and deionised (DI) water were procured from a Milli-Q water system (Millipore UK) or a PURELAB water system (ELGA LabWater UK).

The salts used for minimal media AOBM 181 and MMB and LB medium were from Sigma Aldrich UK and Acros Organics (Fisher Scientific UK) and were of at least 98% purity. The LB medium reagents agar, tryptone, and yeast extract were from Formedium UK. Media supplements thiamine hydrochloride (B_1) and 2-hydroxypropyl-β-cyclodextrin (HPβ-CDX) were from Sigma Aldrich UK, and sodium pyruvate and D-glucose were from Fisher Scientific UK. The microscopy experiment reagents allylthiourea (ATU), sodium azide (NaN_3), DAPI Readymade Solution (1 mg/mL), and Fluoroshield mounting medium were from Sigma Aldrich UK, and Triton X100 and paraformaldehyde were from Fisher Scientific UK.

4.2.2 Reference Strains

Nitrosomonas europaea NCIMB 11850 was purchased from NCIMB Culture Collection; stocks were cryopreserved at -80°C as single-use aliquots in AOBM 181 media with 5% DMSO. *Caenibius tardaugens* DSM 16702 was purchased from DSMZ Culture Collection. *Escherichia coli* MG1655 was given by Dr Lucile Chatellard (University of Glasgow School of Engineering, formerly). Stocks of *C. tardaugens* and *E. coli* were cryopreserved at -80°C in LB media with 15% glycerol.

4.2.3 Culture Media

4.2.3.1 Ammonia-Oxidising Bacteria Medium 181 (AOBM 181)

Ammonia-oxidising bacteria medium 181 (AOBM 181) was prepared by dissolving 235 mg/L $(NH_4)_2SO_4$, 200 mg/L KH_2PO_4, 40 mg/L $CaCl_2{\cdot}2H_2O$, 40 mg/L $MgSO_4{\cdot}7H_2O$, 0.5 mg/L $FeSO_4{\cdot}7H_2O$, 0.5 mg/L $Na_2EDTA{\cdot}2H_2O$, and 0.5 mg/L phenol red in deionised water. The media was then sterilised by autoclaving for 15 min at 121°C. After the media cooled to room temperature, 5% (w/v) filter-sterilised Na_2CO_3 was added drop-wise until the yellow media turned pale pink. AOBM 181 was stored at room temperature in the dark.

4.2.3.2 Luria-Bertani (LB) Medium

Luria-Bertani (LB) both medium was prepared by dissolving 10 g/L tryptone, 10 g/L NaCl, and 5 g/L yeast extract in deionised water. LB agar was prepared by adding 15 g/L agar to LB broth. The media was then sterilised by autoclaving for 15 min at 121°C. LB broth was stored at room temperature, and LB agar was stored at 4°C.

4.2.3.3 Modified Medium B (MMB)

The minimal salts medium, Modified Medium B (MMB; 10 mM $(NH_4)_2SO_4$, 3 mM KH_2PO_4, 0.75 mM $MgSO_4{\cdot}7H_2O$, 0.2 mM $CaCl_2{\cdot}2H_2O$, 10 µM $FeSO_4{\cdot}7H_2O$, 16 µM $Na_2EDTA{\cdot}2H_2O$, 1 µM $CuSO_4{\cdot}5H_2O$, 43 mM $NaH_2PO_4{\cdot}2H_2O$, 4 mM K_2HPO_4, 0.04% Na_2CO_3), was prepared by dissolving salts in DI water and adjusting to pH 8.0 with 5 M NaOH. The media was filter-sterilised and stored at room temperature.

4.2.3.4 Media Supplements

Media supplements were prepared as stock solutions (Table 4.1) in DI water and filter-sterilised. Stock solutions were diluted to their working concentration in MMB media immediately prior to an experiment.

Table 4.1: Minimal media supplements used in this work.

Supplement	Stock Conc.	Working Conc.	Storage
HPβ-CDX	40% (w/v)	2% (w/v)	RT
Glucose	100 mg/mL	150 µg/mL[a] or 100 µg/mL	RT
Pyruvate	50 mg/mL	183 µg/mL[a] or 500 µg/mL	4°C
Thiamine HCl	0.25 mg/mL	2.5 µg/mL	4°C

[a]Concentration is equivalent to 5 mM carbon. RT – room temperature.

4.2.4 Culturing Reference Strains

4.2.4.1 Culturing *N. europaea*

N. europaea 11850 cultures were prepared from cryo-stocks. Prior to culturing, the DMSO cryoprotectant was removed by thawing a cryo-stock vial and centrifuging the contents at 2000*xg* for 10 minutes, then discarding the supernatant. The bacteria were then gently resuspended in 650 µL of fresh AOBM 181 media and then transferred to a flask of 25 mL AOBM 181 media. *N. europaea* was cultured in the dark at 30°C static or shaking at 150 rpm. When the media acidified due to bacterial growth, it turned pale yellow, and 5% Na_2CO_3 was added drop-wise until the media returned to pale pink. *N. europaea* growth was completed when the media no longer acidified, approximately 2 weeks. After growth was complete, 1 mL of the bacteria were subcultured into 25 mL of fresh AOBM 181 media. Bacteria were subcultured up to 3 times before preparing a new culture from cryo-stock. The maintenance cultures were regularly tested for heterotrophic contamination by plating on LB agar. Prior to experiments, *N. europaea* was pre-cultured in AOBM 181 media, either from cryo-stock or new subculture, for at least one week.

4.2.4.2 Culturing *C. tardaugens*

C. tardaugens 16702 cultures were prepared from cryo-stocks before each experiment. The bacteria were inoculated directly from the cryo-stocks into 25 mL of LB media. The bacteria were cultured in the dark at 30°C shaking at 150 rpm. Prior to experiments, *C. tardaugens* was pre-cultured in LB media for 5 days.

4.2.4.3 Culturing *E. coli*

E. coli MG1655 cultures were prepared from cryo-stocks. The bacteria were inoculated directly from the cryo-stocks onto LB agar. The agar plates were cultured at 30°C overnight then stored at 4°C for up to two weeks. Prior to each experiment, a single colony from the agar plate was inoculated into 10 mL of LB media and cultured at 30°C shaking at 150 rpm overnight.

4.2.5 Growth Assays

4.2.5.1 Growth Assays for *N. europaea*

The growth of chemolithoautorophic *N. europaea* in the presence of different organic carbon substrates was investigated (Table 4.2). The first experiment evaluated *N. europaea* growth without any organic carbon or in the presence of media supplements 2% HPβ-CDX and 2.5 µg/mL B_1 and 5 mM C of glucose or pyruvate. The second experiment evaluated *N. europaea* growth in the presence of 2% HPβ-CDX and 2.5 µg/mL B_1 and 0.01, 0.1, and 1 mg/L E2 or BODIPY-E2. The bacteria was pre-cultured as described in Section 4.2.4.1. Prior to each experiment, spent media was removed by centrifuging the pre-culture at 2000*xg* for 10 minutes and resuspending the pelleted bacteria in fresh MMB media. The bacteria were inoculated in the test media at an optical density at 600 nm (OD_{600}) of 0.0007 for both experiments. Abiotic controls for each test media were included in both experiments.

Table 4.2: N. europaea growth assay test conditions.

		Carbon Substrates					
Experiment	Test Condition	No Carbon	2% HPβ-CDX + 2.5 µg/mL B_1	Na Pyruvate 5 mM C	Glucose 5 mM C	E2 0.01-1 mg/L	BODIPY-E2 0.01-1 mg/L
1	1	✓					
	2		✓				
	3		✓	✓			
	4		✓		✓		
2	1		✓				
	2		✓			✓	
	3		✓				✓

Growth assays were conducted in triplicate foil-wrapped serum bottles under aerobic conditions (i.e. by sealing the bottles with a sterile cotton plug; an example is shown in Appendix A). The cultures (15 mL for Experiment 1 and 9 mL for Experiment 2) were incubated in the dark at 30°C, shaking at 150 rpm, and were sampled daily for one week. Samples were measured for growth by OD_{600}; additionally, NH_4^+ and NO_2^- concentrations were determined to measure ammonium oxidation.

4.2.5.2 Growth Assays for *C. tardaugens* and *E. coli*

The growth of heterotrophic *C. tardaugens* and *E. coli* in the presence of different organic carbon substrates was investigated (Table 4.3). The bacterial growth was evaluated in the presence of media supplements 2% HPβ-CDX and 2.5 µg/mL B_1 and 5 mM C of pyruvate, glucose, E2, or BODIPY-E2. The bacteria were pre-cultured as described in Sections 4.2.4.2 and 4.2.4.3. Prior to each experiment, spent media was removed by centrifuging the pre-culture at 2000*xg* for 10 minutes and resuspending the pelleted bacteria in fresh MMB media. The bacteria were inoculated in test media at an OD_{600} of 0.1. Abiotic controls for each test media were included.

Table 4.3: C. tardaugens and E. coli growth assay test conditions.

	Carbon Substrates				
Test Condition	2% HPβ-CDX + 2.5 µg/mL B_1	Na Pyruvate 5 mM C	Glucose 5 mM C	E2 5 mM C	BODIPY-E2 5 mM C
1	✓				
2	✓	✓			
3	✓		✓		
4	✓			✓	
5	✓				✓

Growth assays for heterotrophic bacteria were conducted in triplicate wells (150 µL) in a 96-well microplate (Sterilin, Thermo Scientific UK). The cultures were incubated in the dark at 30°C, shaking at 150 rpm, and the OD_{600} was measured daily for one week. In order to minimise evaporation, the perimeter wells of the microplate were filled with 200 µL of sterile water, and the plate was sealed with a BreathEasy gas-permeable membrane (Sigma Aldrich UK); an example is shown in Appendix A. The plate was incubated within an air-tight plastic box, humidified with a damp towel. The microplate growth assays were conducted in three repeat experiments.

4.2.5.3 Growth Assays for Bacteria Consortium

The ability to grow the three reference strains as a consortium was also investigated. The three bacteria each were cultured together pairwise and as a trio consortium in MMB media with the following media supplements: 2% HPβ-CDX, 2.5 µg/mL B_1, 0.1 mg/mL glucose, and 0.5 mg/mL sodium pyruvate. The bacteria were each pre-cultured individually according to Sections 4.2.4.1–4.2.4.3. As with the individual growth assays, prior to the experiment, spent media was removed by centrifuging the pre-culture at 2000*xg* for 10 minutes and resuspending the pelleted bacteria in fresh MMB media. The heterotrophic bacteria were inoculated at an

OD_{600} of 0.007, and *N. europaea* was inoculated at an OD_{600} of 0.0007.

Growth assays were conducted in triplicate foil-wrapped serum bottles under aerobic conditions. The cultures and abiotic controls (15 mL) were incubated in the dark at 30°C, shaking at 150 rpm, and were sampled daily for one week. Samples were measured for growth by OD_{600}, and NH_4^+ and NO_2^- concentrations were determined to measure ammonium oxidation.

4.2.5.4 Growth Analysis by OD_{600}

Growth was measured by the optical density at 600 nm (OD_{600}). An aliquot of liquid culture (0.75 mL) was measured in polystyrene semi-micro cuvettes (Fisherbrand, Fisher Scientific UK) using a Hach DR2800 spectrophotometer. Since the growth assays for *C. tardaugens* and *E. coli* were conducted in 96-well microplates, the OD_{600} for these experiments were measured using a Tecan Infinite M200 Pro plate reader.

4.2.5.5 NH_4^+ Measurement

Ammonium oxidation to nitrite was used to selectively confirm metabolic activity by *N. europaea*. Standard colorimetric assays were used to evaluate their concentrations.[245] The MMB culture media contains approximately 20 mM NH_4^+, so samples were diluted 1:200 with DI water. As *N. europaea* depleted ammonium, the dilution ratio was reduced to 1:100. The diluted samples (100 µL) were added to a clear 96-well microplate (#655101 Greiner Bio-One, UK) in duplicate, along with a blank (DI water) and a set of calibration standards prepared from $(NH_4)_2SO_4$ (5, 10, 20, 50, 100, and 200 µM NH_4^+).

Ammonium was measured by combining Solution A (12 g/L sodium hydroxide) with Solution B (85 g/L sodium nitroprusside and 0.6 g/L sodium salicylate) at a ratio of 2:1. Next, 50 µL of the 2A:1B mixture was added to each well of the microplate and mixed. Then, 25 µL of 0.2 g/L sodium dichloroisocyanurate was added to each well of the microplate and mixed. The plate was incubated in the dark for 30 minutes before recording the absorbance at 660 nm using the Tecan Infinite M200 Pro plate reader.

4.2.5.6 NO_2^- Measurement

Samples in MMB culture media were measured undiluted initially. As *N. europaea* released nitrite, the biotic samples were then diluted 1:100 or 1:200 with DI water. The samples (100 µL) were added to a clear 96-well microplate (#655101 Greiner Bio-One, UK) in duplicate, along with a blank (DI water) and a set of calibration standards prepared from KNO_2 (5, 10, 25, 50, and 100 µM NO_2^-).

A nitrite determination reagent was prepared by dissolving 10 g/L sulfanilamide, 0.5 g/L naphthylethylene diamine dihydrochloride into 10% (v/v) H_3PO_4. Nitrite was then measured by

adding 25 µL of the determination reagent to each well of the microplate and mixed. The plate was incubated in the dark for 10 minutes before recording the absorbance at 540 nm using the Tecan Infinite M200 Pro plate reader.

4.2.6 Biodegradation of E2 versus BODIPY-E2

The biodegradation of E2 and BODIPY-E2 by the three reference strains was evaluated in individual and co-cultures. First, an aliquot of E2 or BODIPY-E2 at 1 mg/mL (200 µL for single cultures or 480 µL for co-cultures) in methanol was added to a sterile bottle and air dried under a sterile biosafety cabinet. Estrogen-free controls were prepared by adding an equivalent volume of methanol to a separate bottle. The estrogens were redissolved in 40% HPβ-CDX (10 mL for single cultures or 24 mL for co-cultures) and diluted with MMB media (200 mL for single cultures or 480 mL for co-cultures) to a final concentration of 1 mg/L E2 or BODIPY-E2 and 2% HPβ-CDX. Thiamine HCl was added to a final concentration of 2.5 µg/mL. In addition, a growth substrate was included for each heterotrophic bacteria, as shown in Table 4.4. Both 0.5 mg/mL sodium pyruvate and 0.1 mg/mL glucose were added to the media for the co-cultures.

Table 4.4: Natural and BODIPY-estradiol biodegradation experiments test conditions.

	Carbon Substrates					
Bacteria	2% HPβ-CDX + 2.5 µg/mL B_1	Na Pyruvate 0.5 mg/mL	Na Pyruvate 0.1 mg/mL	Glucose 0.1 mg/mL	E2 1 mg/L	BODIPY-E2 1 mg/L
N. europaea	✓					
	✓				✓	
	✓					✓
C. tardaugens	✓	✓				
	✓	✓			✓	
	✓	✓				✓
	✓		✓			
	✓		✓		✓	
	✓		✓			✓
E. coli	✓			✓		
	✓			✓	✓	
	✓			✓		✓
Co-cultures	✓	✓		✓		
	✓	✓		✓	✓	
	✓	✓		✓		✓

The bacteria were all pre-cultured individually according to Sections 4.2.4.1–4.2.4.3. As with the growth assays, prior to each experiment, spent media was removed by centrifuging

the pre-culture at 2000*xg* for 10 minutes and resuspending the pelleted bacteria in fresh MMB media. The heterotrophic bacteria were inoculated at an OD_{600} of 0.005, and *N. europaea* was inoculated at an OD_{600} of 0.0005.

Biodegradation assays were conducted in triplicate foil-wrapped serum bottles under aerobic conditions. Abiotic controls were also cultured in triplicate, except for the estrogen-free abiotic control which was a single culture. The cultures were incubated in the dark at 30°C, shaking at 150 rpm for one week in individual cultures and 9 days for co-cultures. Samples were measured for estrogen concentrations, as well as growth by OD_{600}. NH_4^+ and NO_2^- concentrations were determined to measure ammonium oxidation.

4.2.7 Estrogen Analysis

Natural and fluorescent estrogen concentrations were measured according to the analytical workflow developed in Chapter 3. Briefly, 1.5 mL of liquid culture was sampled using aseptic technique and added to a 15-mL glass tube. The sample was immediately mixed with 1.5 mL of acetonitrile and filtered through 0.45-µm hydrophilic PTFE syringe filter into a fresh glass tube. Estrogens were then extracted by vortexing a 0.5-mL aliquot of the diluted and filtered sample with 1 mL of dichloromethane for 30 s. Exactly 0.8 mL of organic phase was recovered and evaporated to dryness at 37°C before resuspending in 0.2 mL of acetonitrile containing 1 mg L^{-1} of E3 and BODIPY-E3 internal standards. Extracts were stored at -20°C until analysis.

Estrogen quantification was conducted by HPLC analysis as described in Section 3.2.3 of Chapter 3. Each timepoint, which included 15-16 samples, was analysed as a batch. Samples were measured in duplicate injections. A standard curve (100, 200, 400, 600, 800, and 1000 µg/L each for E1, E2, BODIPY-E1, and BODIPY-E2) was run at the beginning of each batch. The limit for accurate quantitation was set at 100 µg/L, since this was the lowest standard measured.

4.2.8 Fluorescence Microscopy

The selective uptake of BODIPY-E2 was assessed by fluorescence microscopy. Bacteria were cultured in the presence of 1 µg/L of E2, BODIPY-E2 or BODIPY-azide. *C. tardaugens* was also grown with 0.5 mg/mL pyruvate, and *E. coli* was grown with 0.1 mg/mL glucose. The bacteria were cultured normally and with a cytostatic agent to determine if the fluorescent compounds were actively transported into the cells or simply adhering to the surface. *N. europaea* were made metabolically inactive with 10 µg/mL of allylthiourea (ATU). *C. tardaugens* and *E. coli* were inactivated with 2.5 mM sodium azide. Bacteria were cultured in duplicate in 24-well plates (1 mL per well) sealed with BreathEasy membrane (Sigma Aldrich UK) in a humidified air-tight container, shaking in the dark at 150 rpm, 30°C.

For each timepoint, bacteria were fixed with 2% (w/v) paraformaldehyde and stored at 4°C until filtration. The bacteria were filtered onto Millipore Nuclepore membrane filters (0.22-µm, Sigma Aldrich UK) and stained with 1 µg/mL DAPI and 0.1% Triton X100. Bacteria were visualised by Olympus X71 microscope. DAPI staining was captured by 0.5–1.5 s of exposure. BODIPY-E2 and BODIPY–azide were captured by 3.1 s or 5.1 s of exposure. The images were reviewed and processed with ImageJ software. The background fluorescence of each image was subtracted using a rolling ball radius of 50 pixels. The mean fluorescence intensity of each background-subtracted image was then calculated by the software, which used a scale of 0–255 units. A pilot test using flow cytometry to the detect selective uptake of BODIPY-E2 by the bacteria is described in Appendix B.

4.2.9 Statistical Analysis

Calibration curves and concentrations for estrogens or nitrogen species were calculated in Excel. Statistical analysis of the replicates were calculated in R; plots were generated in R using ggplot2 package [221]. The fluorescence intensity of the BODIPY/fluorescein filter images were compared by parametric pairwise independent t-test.

4.3 Results & Discussion

4.3.1 Growth Assays

Before evaluating the biodegradation and fate of BODIPY-labelled E2 as a surrogate for E2, the conditions for culturing the reference strains had to be established. Each strain had distinct substrate requirements, however, all three bacteria could be cultured at similar temperature (28–30°C) and pH (7.4–8.0) [72, 246, 247]. Since *N. europaea* is the most fastidious organism in the consortium, the minimal salts medium MMB was selected to be the culture media for studying E2 biodegradation, as it was used previously by Shi *et al.* (2004) to study the biodegradation of estrogens by *N. europaea* 11850 [72]. MMB media contains the necessary minerals for culturing most heterotophic bacteria, such as NH_4^+, PO_4^{3-}, SO_4^{2-}, Ca^{2+}, and Mg^{2+}.

In Chapter 3, it was established that HPβ-CDX is required to maintain hydrophobic BODIPY-E2 in solution; since 2% was the working concentration used previously, this was continued here. Additionally, thiamine is an essential co-factor for *E. coli* strain MG1655 and, therefore, must be included in the media, as well. However, in order to support growth of heterotrophic bacteria, an organic carbon substrate must be included. Thus, a series of growth assays were conducted to assess the ability to culture the consortium in a shared medium. The detailed growth assay results for each bacteria are described in the following sections and summarised in Table 4.5.

Table 4.5: Summary of growth assay results for the reference strains.

	Test Condition	*Bacterial Growth (Timepoint of log-phase Start/Log-phase Duration[a])*		
		N. europaea 11850	*C. tardaugens* 16702	*E. coli* MG1655
Carbon Substrate	None	+ (48h/120h)	nt	nt
	HPβ-CDX + B_1	+ (48h-72h/72h-120h)	–	–
	Pyruvate 5 mM C	++ (48h/72h)	+ (48h/72h)	+ (0h/24h)
	Glucose 5 mM C	+ (72h/>96h)	–	++ (0h/24h)
	E2 5 mM C	nt	++ (24h/48h)	–
	BDP-E2 5 mM C	nt	–	–
	E2 1 mg L^{-1}	+ (96h/>72h)	nt	nt
	E2 0.1 mg L^{-1}	++ (72h/96h)	nt	nt
	E2 0.01 mg L^{-1}	++ (72h/96h)	nt	nt
	BDP-E2 1 mg L^{-1}	+ (96h/>72h)	nt	nt
	BDP-E2 0.1 mg L^{-1}	++ (72h/96h)	nt	nt
	BDP-E2 0.01 mg L^{-1}	++ (72h/96h)	nt	nt
Co-culture	*N. europaea*		+	+
	C. tardaugens	+		+
	E. coli	+	Ind.	
	Consortium	+	Ind.	+

[a] Log-phase duration given in increments of 24 h. '++' – positive growth, highest OD_{600}; '+' – positive growth; '–' – negative for growth; 'Ind.' – indeterminate growth; nt – not tested.

4.3.1.1 Growth Assays for *N. europaea*

N. europaea was cultured in MMB media with and without additional carbon substrates (Figure 4.1); the results for all abiotic controls are given in Appendix A. When cultured with the requisite supplements, HPβ-CDX and B_1, the bacteria showed slightly more rapid growth but lower abundance than without any added carbon (Figure 4.1a). Interestingly, *N. europaea* showed marginally faster and more abundant growth in the presence of pyruvate at 5 mM C. However, growth was notably inhibited by 5 mM C glucose. A study by Hommes *et al.* (2003) on the growth of *N. europaea* in the presence of various organic substrates up to 50 mM showed

increased growth with pyruvate, no increased growth with glucose, and inhibited growth with mannose [248]. While pyruvate may be oxidised by *Nitrosomonas* directly into acetyl coenzyme A, an intermediate metabolite in many biochemical pathways, *N. europaea* lacks the enzymes to metabolise glucose. Inhibition of *Nitrosomonas* by glucose was not previously observed [248, 249].

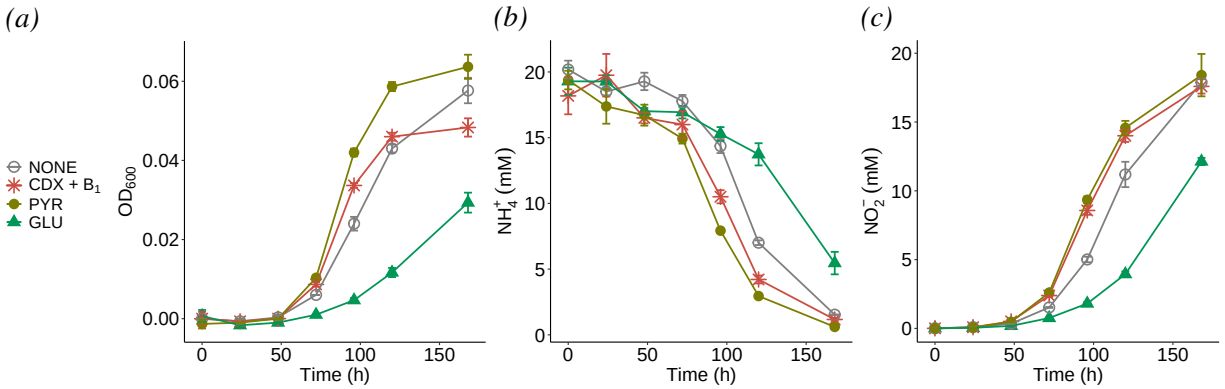

*Figure 4.1: Growth of N. europaea in the presence of different organic carbon sources: HP*β*-CDX and thiamine (CDX + B_1), pyruvate (PYR), and glucose (GLU) or no added organic carbon (NONE). Growth was assessed by (a) OD_{600} and the metabolism of (b) NH_4^+ into (c) NO_2^-. Error bars are the standard deviation (n=3).*

The impact of the organic substrates on nitrification was also evaluated (Figures 4.1b and 4.1c). The decrease in ammonium and increase in nitrite generally reflect the observations from the OD_{600} measurements, particularly the apparent growth and metabolic inhibition by glucose. Although pyruvate did not negatively impact growth, the working concentration of glucose should be considered as it appears to inhibit *N. europaea*. The lower growth rate in the absence of organic carbons (i.e., log-phase duration 120 h versus 72 h with pyruvate or supplements) appears to be reflected in the rate of NH_4^+ decrease and NO_2^- increase. Additional sampling points and calibration of the OD_{600} with microbial biomass would have enabled accurate calculation of the growth and metabolism rates. The obtained results are sufficient to determine that *N. europaea* can grow in MMB media in the presence of requisite culture supplements.

Since the presence of glucose hindered the growth of *N. europaea*, the presence of E2 and BODIPY-E2 was also evaluated to determine if there would be a similar effect (Figure 4.2). There was no difference in growth or ammonium metabolism between 0.1 and 0.01 mg/L of E2 (Figures 4.2a-4.2c) and only a very small difference in growth between 0.1 and 0.01 mg/L of BODIPY-E2 (Figures 4.2d-4.2f). The growth and nitrification at these concentrations were very similar to controls without any estrogen (Figures 4.2g -4.2i). However, at 1 mg/L of E2 and BODIPY-E2, there was a small decrease of growth and NH_4^+ oxidation. Interestingly, the level of inhibition appears to be comparable for both the natural and fluorescent estrogen, suggesting

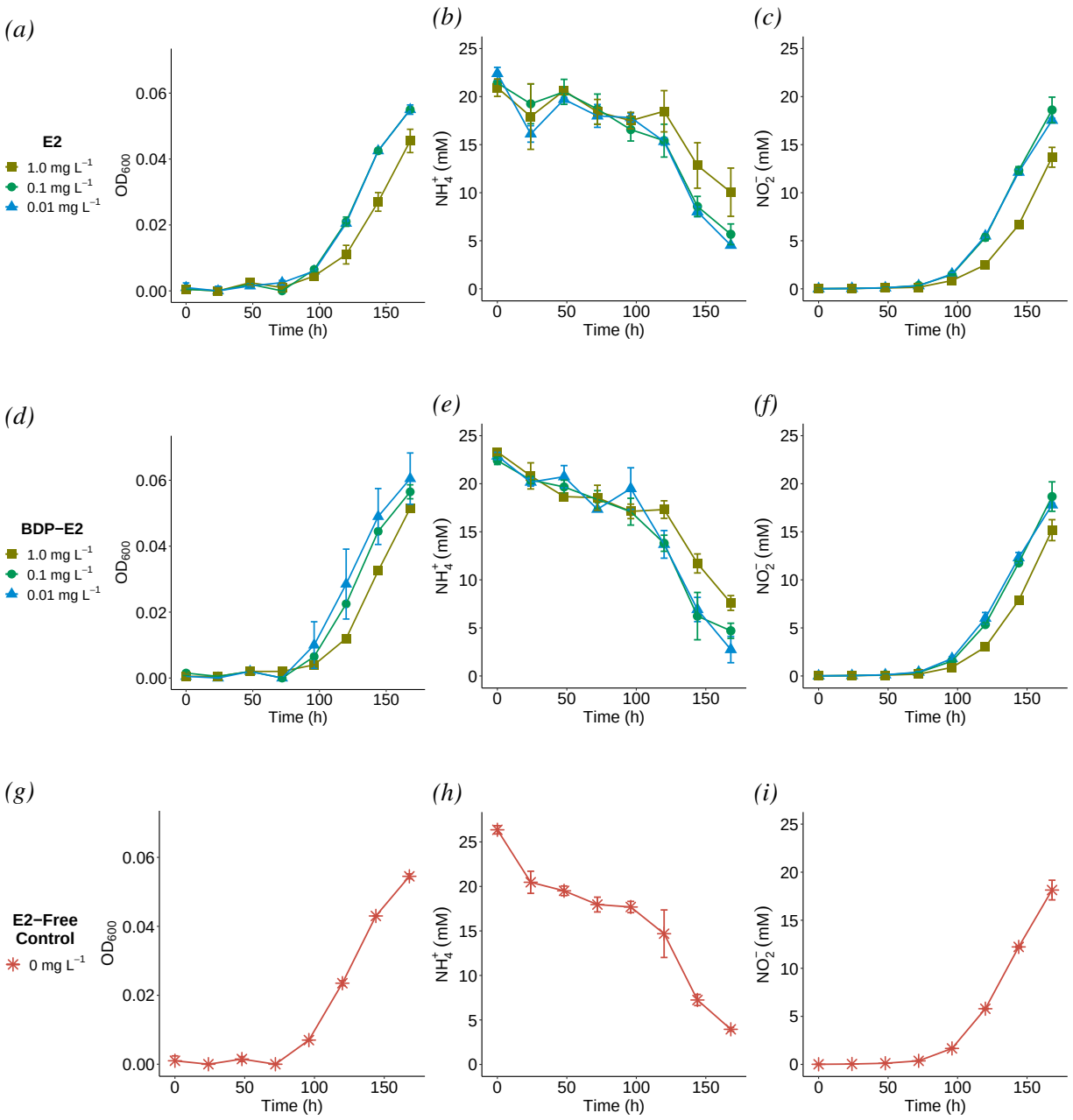

Figure 4.2: Growth of N. europaea in the presence of different concentrations of (a,b,c) E2 and (d,e,f) BODIPY-E2. (g,h,i) Controls with no added estrogen were also assessed. Growth was assessed by (a,d,g) OD_{600} and the metabolism of (b,e,h) NH_4^+ into (c,f,i) NO_2^-. Error bars are the standard deviation (n=3).

the BODIPY fluorophore doesn't have an effect on growth. A study by Li *et al.* (2020) reported NO_2^- production by *N. europaea* was inhibited up to 78% by 1 mg/L E2 [85]. Although the level of inhibition observed in this work was not as severe, the results show that certain organic substrates – including glucose, E2, and BODIPY-E2 – have an adverse effect on *N. europaea*.

4.3.1.2 Growth Assays for *C. tardaugens*

C. tardaugens was cultured with 5 mM of carbon using various substrates: pyruvate, glucose, E2, and BODIPY-E2. Although MMB media was not developed for heterotrophic bacteria, *C. tardaugens* was able to grow on both E2 and pyruvate in MMB (Figure 4.3). The bacteria grew more rapidly and to a greater abundance with E2, reaching stationary phase around 72 h compared to 120 h for pyruvate. Both E2 and pyruvate are known growth substrates for *C. tardaugens* strain 16702 [99]. However, since the working concentration of E2 should be as low as possible due to its toxicity on *N. europaea*, pyruvate is the more appropriate growth co-substrate for *C. tardaugens*. Media supplements HPβ-CDX and B_1 and glucose were not utilised by *C. tardaugens* as growth substrates. Notably, *C. tardaugens* was not able to grow with BODIPY-E2 as a carbon and energy source unlike the natural, untagged E2. This was anticipated due to the steric interference of the BODIPY conjugation at C3 of the estrogen, which is where *C. tardaugens* cleaves the A-ring [99].

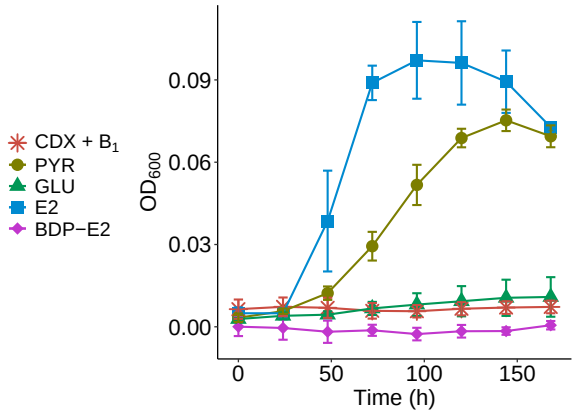

Figure 4.3: Growth (OD_{600}) of C. tardaugens in the presence of different organic carbon sources: HPβ-CDX and thiamine (CDX + B_1), pyruvate (PYR), glucose (GLU), E2, and BDP-E2. Points are the averages of 3 independent experiments, each containing 3 technical replicates, and error bars are the standard error.

4.3.1.3 Growth Assays for *E. coli*

E. coli growth was evaluated using the same substrates as *C. tardaugens*. *E. coli* strain MG1655 successfully grew on both glucose and pyruvate in MMB media, reaching stationary phase around 24 h (Figure 4.4). *E. coli* has previously been shown to grow more efficiently on glucose than pyruvate [250]. Media supplements HPβ-CDX and B_1 and the estrogens were not used by *E. coli* for growth. The results demonstrate that *E. coli* strain MG1655 is a suitable negative control bacteria for estrogen biodegradation. In addition, this strain is also capable of growing under the same conditions as the two estrogen-degrading reference strains, which allows for direct comparison and co-culture.

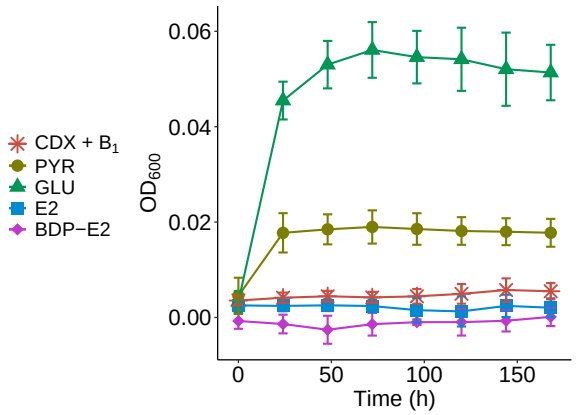

Figure 4.4: Growth (OD_{600}) of E. coli in the presence of different organic carbon sources: HPβ-CDX and thiamine (CDX + B_1), pyruvate (PYR), glucose (GLU), E2, and BDP-E2. Points are the averages of 3 independent experiments, each containing 3 technical replicates, and error bars are the standard error.

4.3.1.4 Growth Assays for Bacteria Consortium

The reference strains were co-cultured pairwise and as a trio consortium (Figure 4.5). In the *E. coli* co-cultures, a rapid growth within 24 hours was observed (Figure 4.5a), similar to its individual cultures with glucose and pyruvate (Figure 4.4). Since the two estrogen-degrading bacteria have a delayed and extended log-phase – initiating after 48 h and a duration of at least 72 h with pyruvate – the early, rapid growth is attributed to *E. coli* MG1655. A slight increase in turbidity (+0.04 OD_{600}) between 48–96 h was observed in the *N. europaea* + *E. coli* and trio co-cultures. In addition, the complete oxidation of ammonium to nitrite (Figures 4.5b-4.5c) indicated that *N. europaea* was metabolically active in all co-cultures. This is especially encouraging considering the sensitive nature of *N. europaea* to environmental stressors [251]. There have been very few examples of co-culturing *Nitrosomonas* in the literature, limited primarily to co-cultures with *Nitrobacter* in studying nitrification or with *P. aeruginosa* [252, 253].

The maximum OD_{600} in *N. europaea* + *C. tardaugens* co-culture is 3.6-times greater than *N. europaea* alone with pyruvate (0.235 versus 0.064 OD_{600}). Furthermore, the NO_2^- production in *N. europaea* + *C. tardaugens* co-culture increased later than the OD_{600} (72 h versus 48 h). This suggests that *C. tardaugens* is likely growing in co-culture with *N. europaea*, however, concurrently tested individual control cultures would provide stronger evidence. The apparent lack of growth by *C. tardaugens* in the presence of *E. coli* is likely due to competition for pyruvate. Since *E. coli* grows more rapidly than *C. tardaugens*, it is able to consume both glucose and pyruvate before the other bacteria reach log-phase. Although *N. europaea* is also capable of consuming pyruvate, it is the only strain which consumes NH_4^+ as an energy and growth substrate. These results represent conditions where individual species are competing for resources, which would be the case within a treatment facility. Thus, the selected strains can

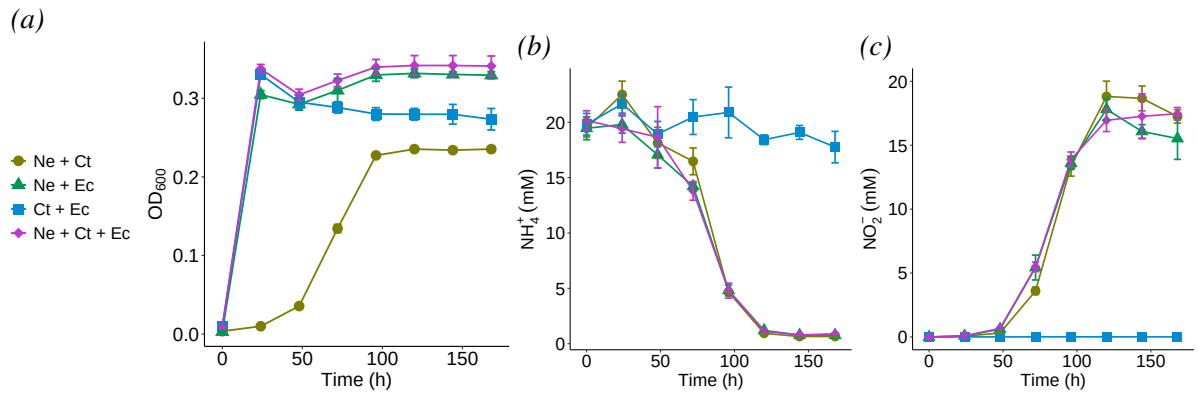

Figure 4.5: Growth of the three strains as pairwise and consortium co-cultures: N. europaea and C. tardaugens (Ne+Ct); N. europaea and E. coli (Ne+Ec); C. tardaugens and E. coli (Ct+Ec); and all three strains together (Ne+Ct+Ec). Growth was assessed by (a) OD_{600}; the metabolism of (b) NH_4^+ into (c) NO_2^- was also evaluated. Error bars are the standard deviation (n=3).

be successfully cultured both individually and as a consortium for evaluating biodegradation of estrogens.

4.3.2 Biodegradation of E2 versus BODIPY-E2

Next, the biodegradation of E2 and BODIPY-E2 were characterised, both individually and in co-culture. Although *N. europaea* was successfully cultured in the presence of E2 and BODIPY-E2, biodegradation via cometabolism is not discernible by growth. Therefore, chemical trace analysis with HPLC was used to confirm biodegradation of E2 by *N. europaea*, as well as confirm no cometabolism of E2 by *E. coli*. In addition, the fate and possible cometabolism of BODIPY-E2 was investigated. The growth experiments showed that *C. tardaugens* was unable to utilise BODIPY-E2 as a growth substrate. Therefore, the heterotrophic reference strains were supplemented with organic growth substrates – 0.5 mg/mL pyruvate for *C. tardaugens* and 0.1 mg/mL glucose for *E. coli*. The detailed biodegradation results for each bacteria are described in the following sections and summarised in Table 4.6.

4.3.2.1 Biodegradation by *N. europaea*

The growth assay samples for *N. europaea* containing 1 mg/L E2 and BODIPY-E2 were extracted and analysed for evidence of biodegradation after one week of growth (Figure 4.6). After 168 h, there was 92 ± 5% E2 and 84 ± 2% BODIPY-E2 in the biotic cultures relative to the abiotic control (measured as 879 ± 6 µg/L E2 and 705 ± 7 µg/L BODIPY-E2). The measured concentrations correspond to a degradation rate of 0.4 ± 0.3 µg/L h^{-1} for E2 and 0.65 ± 0.08 µg/L h^{-1} for BODIPY-E2 over 168 h, assuming zero-order degradation in accor-

Table 4.6: Summary of biodegradation results for the reference strains.

	Degradation Rate (µg/L h^{-1})		
	N. europaea 11850[a]	*C. tardaugens* 16702[b]	*E. coli* MG1655
E2 1 mg L^{-1}	0.4 ± 0.3	42 ± 6	–
BDP-E2 1 mg L^{-1}	0.65 ± 0.08	3.6 ± 0.6	–

[a]Degradation estimated from one endpoint measurement at 168 h (n=2). [b]Degradation estimated from 0-6 h for E2 and 72-168 h for BDP-E2 with 0.5 mg/mL Na pyruvate co-substrate (n=3).

dance with previous studies for E2 removal by *N. europaea* [72, 85]. While the degradation rates for E2 and BODIPY-E2 were similar, the estimated degradation rates in this work are much lower than 2 µg/L h^{-1} observed by Shi *et al.* (2004) or 4 µg/L h^{-1} observed by Li *et al.* (2020), which both reported zero-order degradation kinetics over 8 days [72, 85].

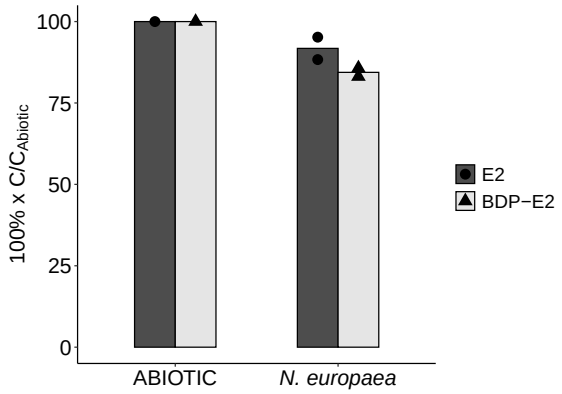

Figure 4.6: Biodegradation of E2 and BODIPY-E2 by N. europaea relative to the abiotic control. Bars are the mean of individual cultures, represented as points (n=2).

Since cyclodextrin was not used in the studies by Shi *et al.* (2004) and Li *et al.* (2020), one possible reason for the lower degradation rate is interference by HPβ-CDX. A study by Casali *et al.* (2022) reported that the β-cyclodextrin inclusion complex with ammonia monooxygenase (AMO) inhibitors had reduced inhibition of *N. europaea* respiration compared to the free inhibitor [254]. The authors proposed that the reason for this was the inclusion complex was slower passing through the bacterial membrane [254]. Although the E2 degradation efficiency and kinetics observed in the literature were not reproduced, HPβ-CDX was necessary to maintain BODIPY-E2 in solution at the working concentration for chromatographic analyses. Thus, while *N. europaea* is our model organism for estrogen cometabolism, it is important to note that estrogen degradation will be impeded by our culture methods.

After observing a modest decrease in E2 and BODIPY-E2 in the preliminary test, a more thorough biodegradation experiment was conducted (Figure 4.7). In this experiment, *N. eu-*

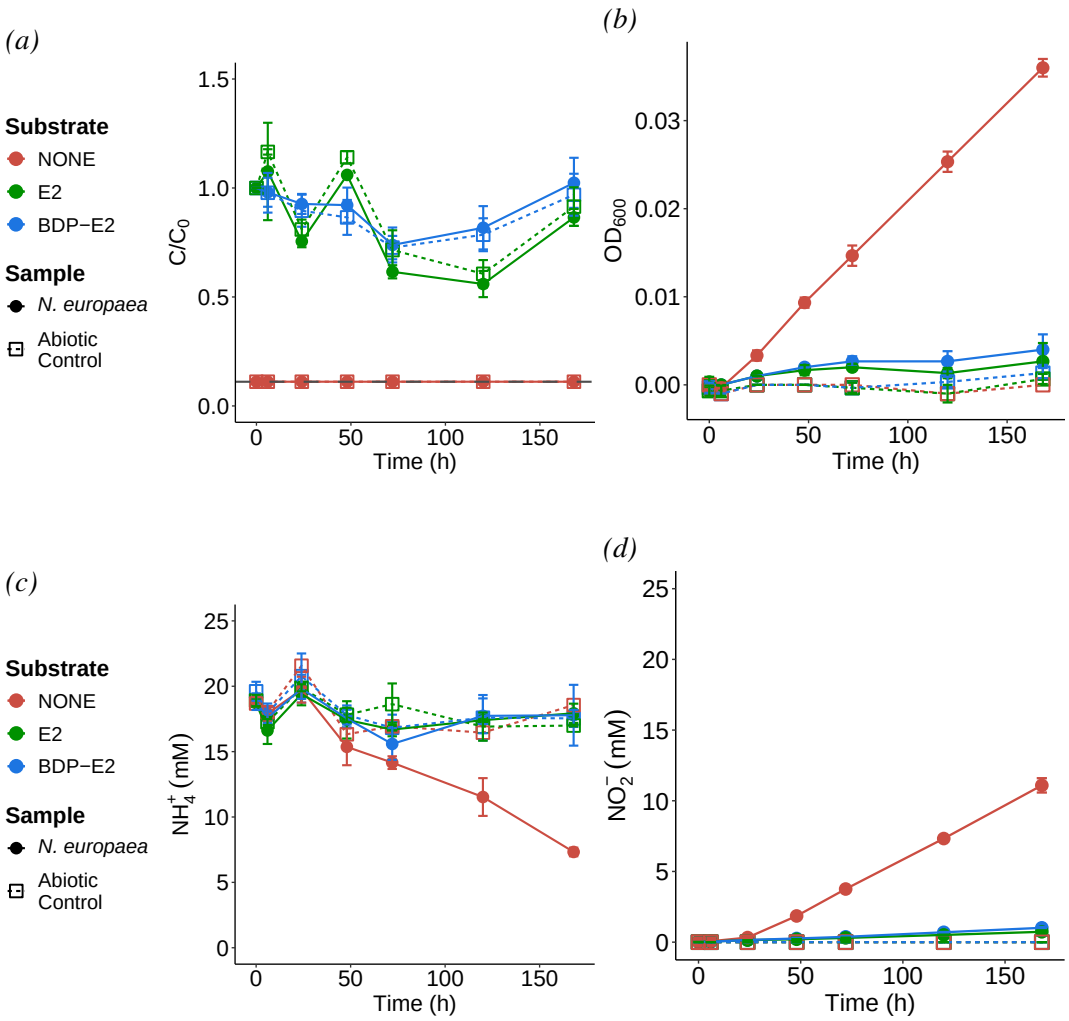

Figure 4.7: (a) Biodegradation of E2 (green) versus BODIPY-E2 (blue) by N. europaea (solid circle, solid lines). E2-free controls (red) and abiotic controls (open square, dashed lines) were also evaluated. The grey dashed line represents the LOQ (100 µg L^{-1}). (b) Growth was assessed by OD_{600}; the metabolism of (c) NH_4^+ into (d) NO_2^- was also evaluated. Error bars are the standard deviation (n=3).

ropaea was unable to grow in both E2 and BODIPY-E2 samples (Figure 4.7b). In the estrogen-free controls, *N. europaea* grew to approximately 62% of its expected yield after one week. The growth results were confirmed with NH_4^+ and NO_2^- measurements (Figures 4.7c–4.7d). Interestingly, both E2 and BODIPY-E2 cultures' inhibition were highly similar compared to the estrogen-free control. Since there was no observable growth, there was no evidence of biodegradation for E2 or BODIPY-E2 (Figure 4.7a).

N. europaea is a fastidious and slow-growing organism, and occasionally, even maintenance cultures failed to thrive for unknown reasons [253]. However, two deductions can still be made from the obtained results. First, there is evidence that *N. europaea* may perceive and respond

to the fluorescently labelled E2 in a similar fashion to the natural estrogen. In two separate and independent experiments, there was a similar inhibition of growth by E2 and BODIPY-E2 and a similar rate of biodegradation (although this was measured in only a single timepoint). The similar response of the bacteria strongly advocates for BODIPY-E2 as a viable, biologically active surrogate to the natural E2.

Second, the fate of BODIPY-E2 is unknown, since no metabolites (i.e., no other peaks in the chromatogram at 230 nm or 503 nm) for either E2 or BODIPY-E2 were detected. We explored using non-targeted exometabolomics by LC-MS/MS analysis with the University of Glasgow Polyomics facility to uncover the fate of the BODIPY-labelled estrogen. However, the pilot test did not recover enough metabolites to draw any conclusions; the results of this pilot test are provided in Appendix C. Since there were no degradation products observed with the BODIPY fluorophore, it is possible the bacteria is altering the fluorophore.

4.3.2.2 Biodegradation by *C. tardaugens*

We hypothesised that if *C. tardaugens* could metabolise BODIPY-E2, it would transform into BODIPY-E1 but no further because the fluorescent tag (Figure 4.8), which is conjugated at C3 of the estrogen A-ring, would sterically interfere with the remaining degradation steps (see Figure 2.7). The lack of BODIPY-E2 catabolism was confirmed by the growth assay, however, partial degradation had to be confirmed with HPLC analysis. Therefore, a preliminary experiment was conducted to determine if co-substrate for growth was necessary for biotransformation BODIPY-E2 or if transformation could occur without an energy source. No co-substrate was required to fully degrade E2, as both E2 and the metabolite E1 were undetectable (Figure 4.9a). However, only a small, un-quantifiable amount of BODIPY-E2 was transformed into BODIPY-E1 without a co-substrate after one week (Figure 4.9a).

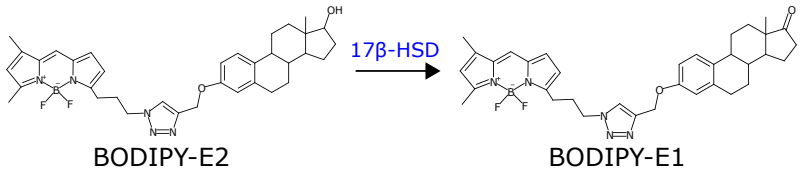

Figure 4.8: Proposed biotransformation of BODIPY-E2 by C. tardaugens via 17β- hydroxysteroid dehydrogenase (17β-HSD) enzyme.

When cultured with pyruvate as co-substrate, 43 ± 4% of BODIPY-E2 remained relative to the abiotic control (measured as 650 ± 10 µg/L). As a percentage of the abiotic control BODIPY-E2 concentration, 47 ± 3% of BODIPY-E1 was generated. There appeared to be a stoichiometric biotransformation of BODIPY-E2 into BODIPY-E1: 0.5 µM each BODIPY-E2 and BODIPY-E1 in the biotic samples and 1.1 µM BODIPY-E2 in the abiotic control (Figure 4.8). Thus, although the BODIPY fluorophore sterically interfered with the downstream metabolism of estrogen and

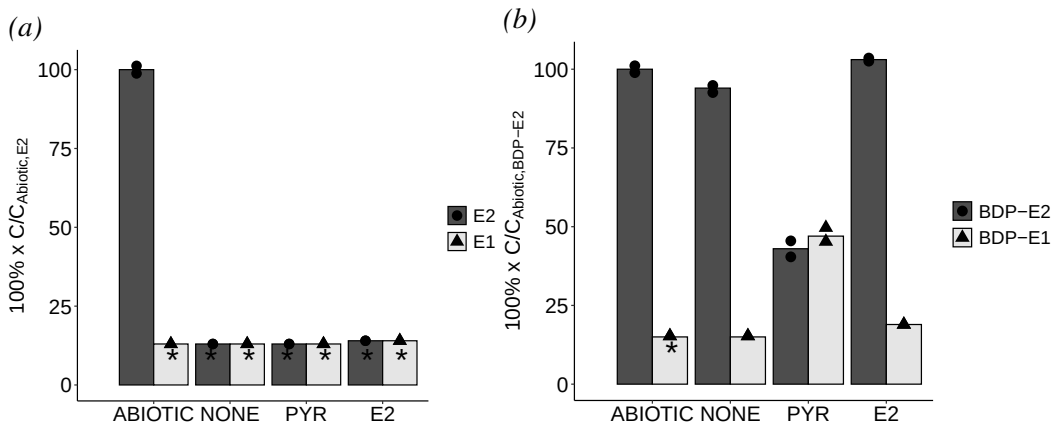

Figure 4.9: Biodegradation of (a) E2 and (b) BODIPY-E2 by C. tardaugens with various co-substrates: ABIOTIC–abiotic controls, no co-substrate; NONE–no co-substrate; PYR–0.5 mg/mL pyruvate; E2–1 mg/L E2. Bars are the mean of individual cultures, represented as points (n=2). Stars indicated analyte was not detected.

the metabolic rate, *C. tardaugens* successfully converted BODIPY-E2 to BODIPY-E1. The stoichiometric transformation of the probe also established that BODIPY was not enzymatically cleaved, and therefore, fluorophore hydrolysis did not occur. In addition, a small quantity of E2 (1 mg/L) was trialled as co-substrate, and this gave similar results as without co-substrate. Therefore, an abundant co-substrate – which could only be pyruvate, due to the toxicity of E2 on *Nitrosomonas* – was deemed necessary for the biotransformation of BODIPY-E2.

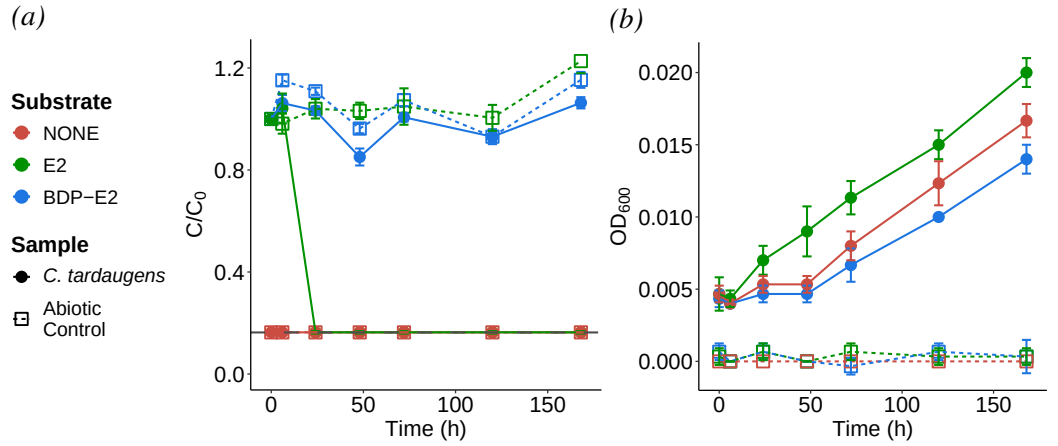

Figure 4.10: (a) Biodegradation of E2 (green) versus BODIPY-E2 (blue) by C. tardaugens (solid circle, solid lines) with 0.1 mg/mL Na pyruvate. E2-free controls (red) and abiotic controls (open square, dashed lines) were also evaluated. The grey dashed line represents the method LOQ (100 µg L^{-1}). (b) Growth was assessed by OD_{600}. Error bars are the standard deviation (n=3).

The preliminary test (Figure 4.9b) showed that a low concentration of E2 co-substrate (0.07 mM C) was unable to facilitate biotransformation of BODIPY-E2 to BODIPY-E1 as effectively as a higher concentration of pyruvate (13.6 mM C). In order to confirm the effects of co-substrate concentration on biotransformation, a lower concentration of pyruvate co-substrate (0.1 mg/mL, 2.7 mM C) was trialled (Figure 4.10). *C. tardaugens* cultured with a lower concentration of pyruvate showed complete E2 degradation within 24 h, however, there was no detectable biotransformation of BODIPY-E2 (Figure 4.10a). The bacteria grew very slowly and to a low abundance (Figure 4.10b), but the co-substrate was insufficient for transformation of the fluorescent estrogen. Thus, *C. tardaugens* requires a rich energy source to transform BODIPY-E2.

After confirming that a higher concentration of pyruvate was necessary to facilitate the biotransformation of BODIPY-E2, a more thorough biodegradation experiment was conducted using 0.5 mg/mL of Na pyruvate as a co-substrate. The biodegradation of 1 mg/L E2 by *C. tardaugens* was observable by 6 h and completed by 24 h (Figure 4.11a). The biotransformation of BODIPY-E2 was much slower (42 ± 6 µg/L h^{-1} for E2 versus 3.6 ± 0.6 µg/L h^{-1} for BODIPY-E2) and occurred primarily during log-phase growth (Figure 4.11b). Although *C. tardaugens* can rapidly and thoroughly degrade 1 mg/L E2, the transformation of the fluorescent surrogate was much slower and incomplete.

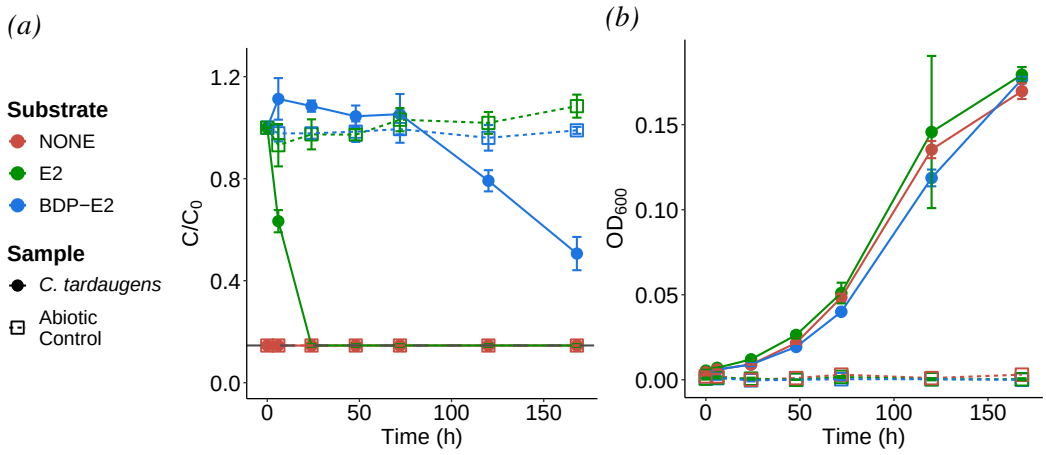

Figure 4.11: (a) Biodegradation of E2 (green) versus BODIPY-E2 (blue) by C. tardaugens (solid circle, solid lines) with 0.5 mg/mL Na pyruvate. E2-free controls (red) and abiotic controls (open square, dashed lines) were also evaluated. The grey dashed line represents the method LOQ (100 µg L^{-1}). (b) Growth was assessed by OD_{600}. Error bars are the standard deviation (n=3).

4.3.2.3 Biodegradation by *E. coli*

The absence of estrogen biodegradation by *E. coli* grown with glucose as a carbon and energy source was confirmed (Figures 4.12a and 4.12b). Thus, the results conclusively establish *E. coli* MG1655 as a suitable negative biological control for estrogen biodegradation.

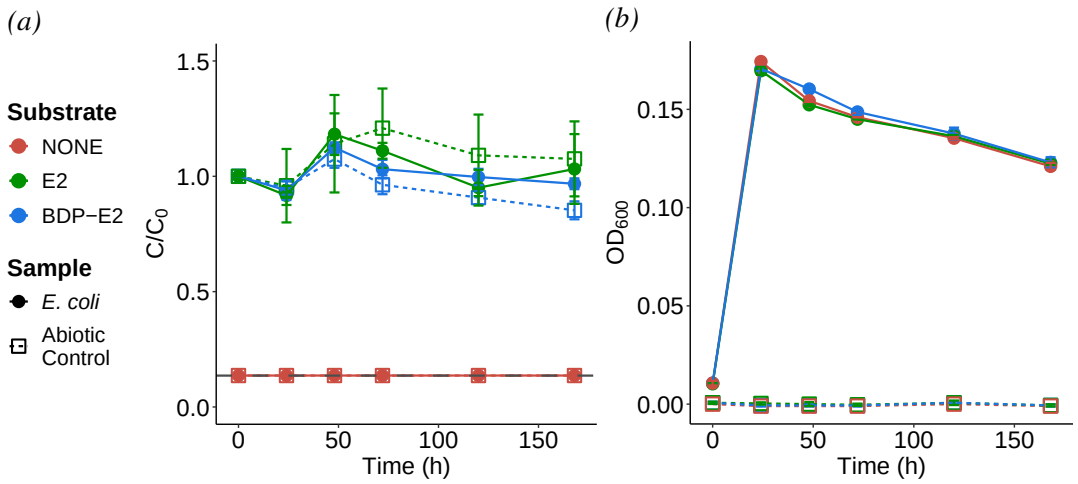

Figure 4.12: (a) Biodegradation of E2 (green) versus BODIPY-E2 (blue) by E. coli (solid circle, solid lines). E2-free controls (red) and abiotic controls (open square, dashed lines) were also evaluated. The grey dashed line represents the method LOQ (100 µg L^{-1}). (b) Growth was assessed by OD_{600}. Error bars are the standard deviation (n=3).

4.3.2.4 Biodegradation by Bacteria Consortium

Next, biodegradation as pairwise and trio consortium co-cultures was assessed (Figure 4.13). In this experiment, the media was contaminated, as evidenced by growth in the abiotic controls (Figures 4.13b and 4.13d). The contaminant organism formed flocs, which made OD_{600} measurements inaccurate and unreliable. Nonetheless, the results provide some useful insight into biodegradation in a mixed culture inoculated with estrogen-degrading bacteria.

The contaminant organism was not able to degrade E2 or BODIPY-E2, as evidenced by the lack of removal in the abiotic controls (Figures 4.13a and 4.13c). In addition, *N. europaea* proved non-viable again, and thus, no biodegradation of E2 or BODIPY-E2 was observed in the *N. europaea* + *E. coli* co-culture. Therefore, E2 degradation was attributed solely to *C. tardaugens*, since complete removal occurred only in co-cultures with *C. tardaugens* strain 16702. The biotransformation of BODIPY-E2 into BODIPY-E1 by *C. tardaugens* did not occur. Considering the lack of apparent growth in co-culture with *E. coli* and the lack of transformation without sufficient co-substrate, it is possible that *E. coli* or the contaminant organism consumed the pyruvate. These results reinforce observations from the individual cultures: *C. tardaugens*

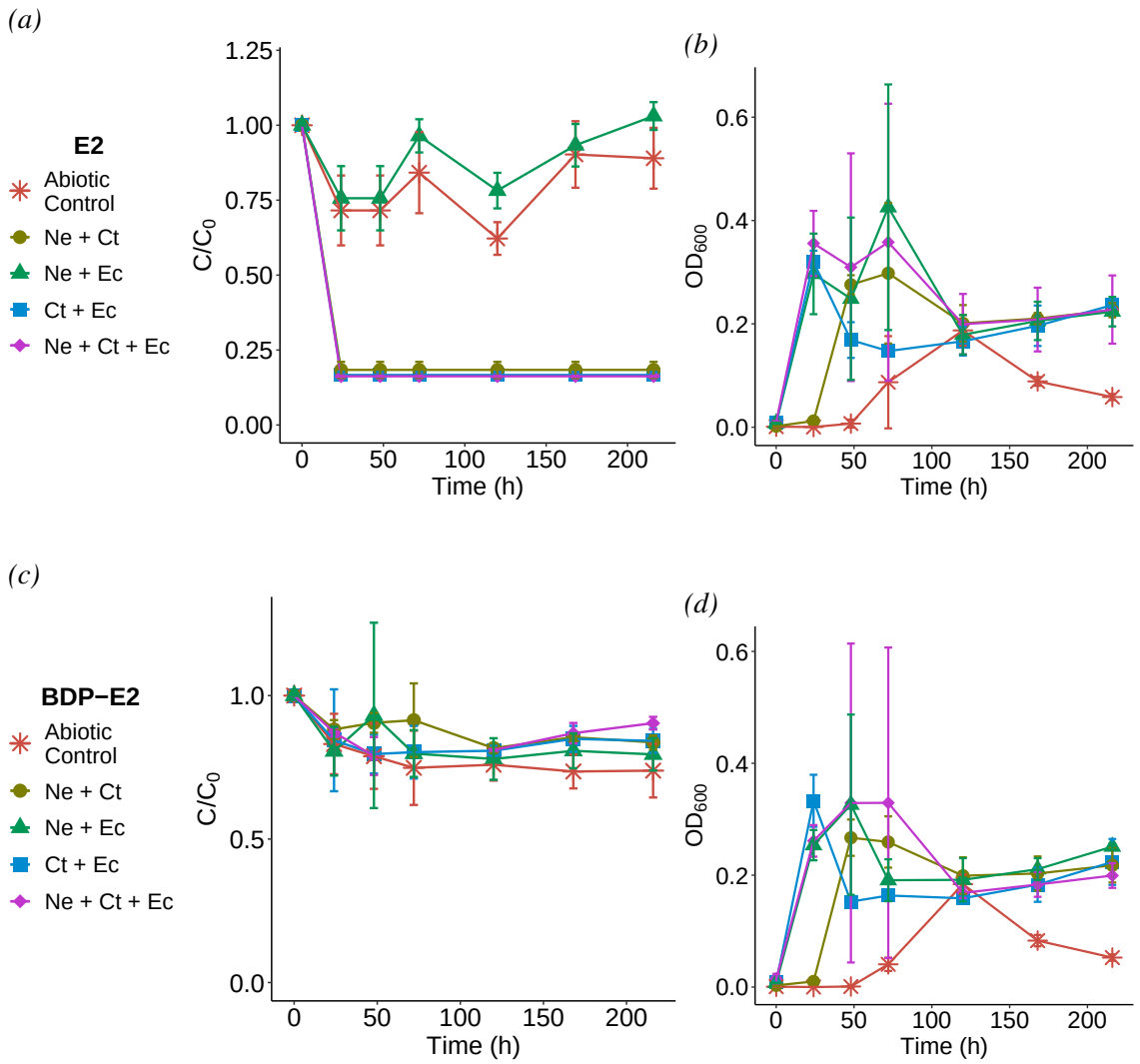

Figure 4.13: Biodegradation of (a) E2 and (c) BODIPY-E2 by the reference strains as pairwise and consortium co-cultures: abiotic controls (red star), N. europaea and C. tardaugens (Ne+Ct); N. europaea and E. coli (Ne+Ec); C. tardaugens and E. coli (Ct+Ec); and all three strains (Ne+Ct+Ec). Growth was assessed by OD_{600} for (b) E2 and (d) BODIPY-E2 cultures. Error bars are the standard deviation (n=3).

will readily mineralise E2, even in the absence of a co-substrate and in the presence of other microorganisms, but requires a rich energy source to transform BODIPY-E2 into BODIPY-E1.

4.3.3 Fluorescence Microscopy of BODIPY-E2 Uptake

Lastly, after characterising the biodegradation of E2 and BODIPY-E2 in batch cultures, uptake of the fluorescently labelled estrogen was evaluated by fluorescence microscopy. In order to verify that the observed fluorescence was from selective uptake of BODIPY-E2, several controls were

included. The autofluorescence of the bacteria was evaluated by imaging bacteria cultured with natural E2, and the selective uptake of BODIPY-E2 was evaluated by imaging the bacteria with BODIPY-azide tag (BODIPY-N3). Additionally, the bacteria were metabolically inactivated with ATU (an ammonia monooxygenase inhibitor) or NaN_3 (an ATPase inhibitor) to determine if the fluorescent compounds were actively transported into the bacteria or passively associating with the bacteria (e.g., adhering to the cell membrane or passively diffusing into the cell).

The microscopy images presented herein are unedited representative images captured using the filter for BODIPY fluorescence, which most clearly shows the fluorescence intensity. The merged, background subtracted filter images which localise the bacteria (via DAPI DNA staining) in relation to the green fluorescence are provided in Appendix A. The mean fluorescence intensity (MFI) between background subtracted images was compared statistically. Homogeneity between the number of bacteria imaged for each timepoint was confirmed by Kruskal-Wallis and Mann-Whitney U tests on the MFI of the DAPI filter images. The three timepoints which had different bacterial densities between the substrates – active *N. europaea* at 168 h, inactive *C. tardaugens* at 168 h, and active strain MG1655 at 168 h – were excluded from further comparison.

4.3.3.1 Uptake by *N. europaea*

Since a lower concentration of estrogens (1 µg/L) was used to avoid high background fluorescence, *N. europaea* was unaffected by the estrogens and grew without issue. *N. europaea* cultured with E2 showed negligible autofluorescence throughout the experiment (Figure 4.14). After 24 h, no fluorescence by either BODIPY-E2 or BODIPY-N3 was observed. However, there was a clear increase in fluorescence at 120 h for both BODIPY-E2 and BODIPY-N3, which had subsided by 168 h. In the inactivated controls cultured with ATU, an insufficient number of bacteria were present and imaged ($<$ 3 images per condition per duplicate well).

The results at 120 h showed a lack of selectivity for BODIPY-E2, with statistically higher fluorescence intensity in the fluorophore control (Figure 4.15). *Nitrosomonas* is known to cometabolise several organic micropollutants, including trihalomethanes [235]. Therefore, it is possible the dihalogenated BODIPY fluorophore was cometabolised. However, with insufficient data for the inactivated bacteria, the possibility that the fluorescence is simply due to passive association of the fluorophore with the bacteria can not be excluded. The trace fluorescence in the cultures with BODIPY-E2 corresponds with the low amount of biodegradation by *N. europaea* observed. In addition, the weak fluorescence within the viable bacteria supports the hypothesis that the HPβ-CDX-BODIPY-E2 inclusion complex may be too large to efficiently enter the cell. If the impeded degradation was simply due to interference by the inclusion complex for the enzyme active sites, we would have expected there to be greater intracellular fluorescence.

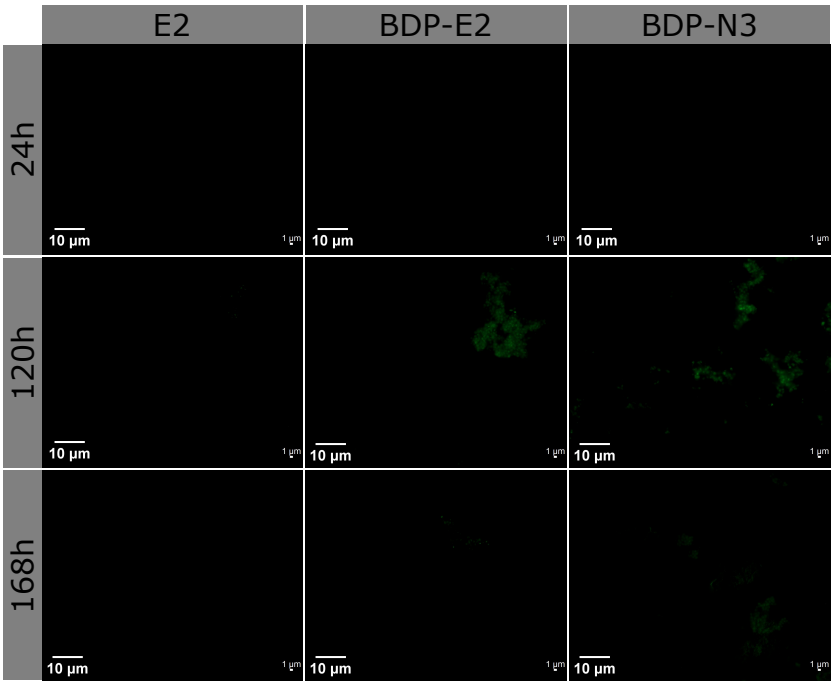

Figure 4.14: Representative fluorescence microscopy images of N. europaea cultured with natural and fluorescent estrogen or BODIPY-azide showing weak fluorescence intensity only at 120 h. Scale bars are 10 µm (lower left) and 1 µm (lower right).

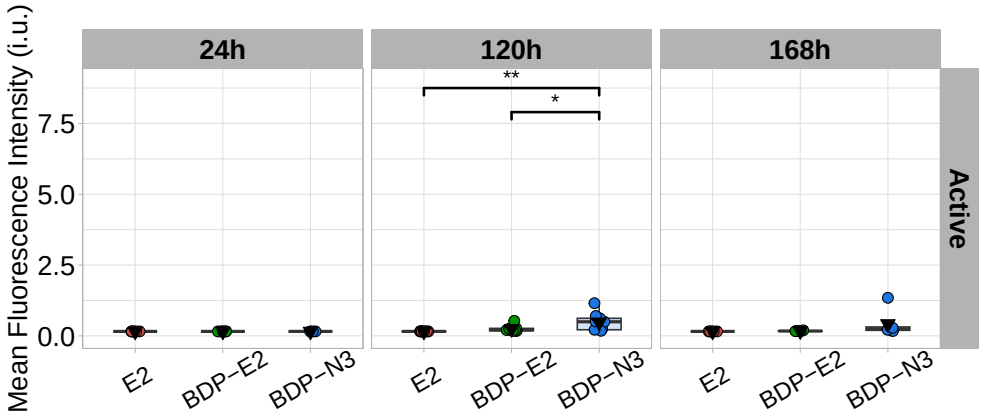

*Figure 4.15: Mean fluorescence intensity (MFI) for fluorescence microscopy of N. europaea cultured with natural and fluorescent estrogen or BODIPY-azide. Points are the MFI calculated for each image (max 255), and inverted triangles are the mean of the images. Boxes show 25%, 50%, and 75% quartiles, and whiskers show 1.5-times the IQR. p-values: * <0.05, ** <0.01. Note – y-axis scaling is kept consistent throughout the chapter for ease of comparison between figures.*

4.3.3.2 Uptake by *C. tardaugens*

The biodegradation experiments showed that *C. tardaugens* transformed BODIPY-E2 after 72 h, and thus, a clear uptake of BODIPY-E2 was anticipated (Figure 4.16). At 24 h, there was some

diffuse fluorescence in the BODIPY-N3, which was statistically significant compared to the natural and fluorescent E2. However, the culture with BODIPY-E2 showed bright fluorescence which was highly localised and present within very few of the bacteria (Figure 4.17). There was no observable autofluorescence in the culture with E2 at 24 h. After 72 h, the fluorescence with both BODIPY substrates increased substantially. While both fluorophores appeared diffusely fluorescent, the BODIPY-E2 culture showed pinpoints of high intensity throughout. The fluorescence peaked at 120 h, and the bacteria cultured with non-fluorescent E2 began to show autofluorescence. At this timepoint, the high intensity spots appeared with all substrates. At 168 h, the fluorescence intensity with all substrates had begun to decrease, and this was the only timepoint where BODIPY-E2 MFI was statistically greater than the other substrates.

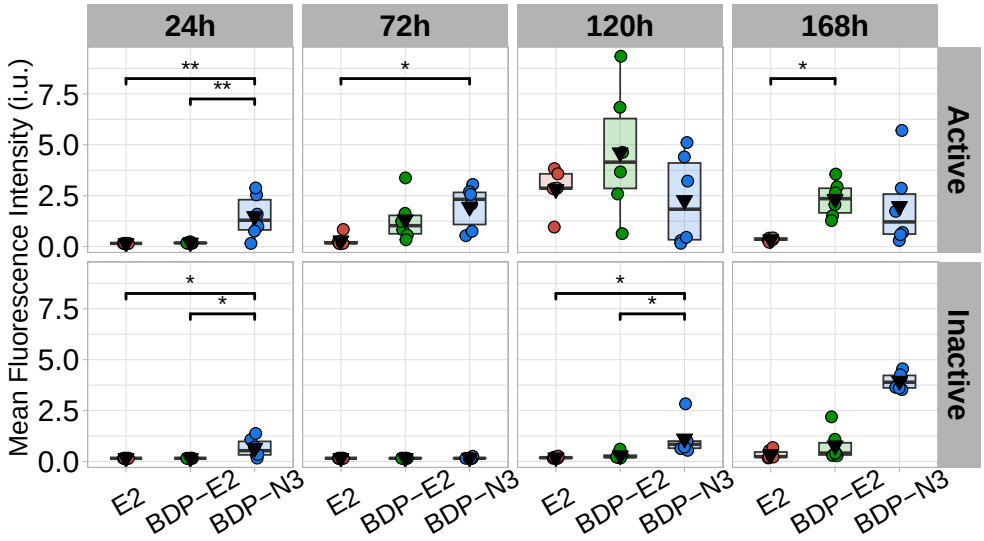

*Figure 4.16: Mean fluorescence intensity (MFI) for fluorescence microscopy of C. tardaugens cultured with natural and fluorescent estrogen or BODIPY-azide. Points are the MFI calculated for each image (max 255), and inverted triangles are the mean of the images. Boxes show 25%, 50%, and 75% quartiles, and whiskers show 1.5-times the IQR. p-values: * <0.05, ** <0.01.*

The autofluorescence appears to be an endogenous fluorescent metabolite whose emission overlaps with BODIPY emission at 512 nm (Figure 4.17). The inactive bacteria, including those cultured with natural E2, produced spots of high intensity starting at 120 h with all substrates. While sodium azide is a bacteriostatic agent that prevents growth, some metabolic activity may still be occurring which produced some fluorescent metabolite. The MFI measured for the inactive BODIPY-N3 cultures at 168 h was affected by overexposure which was not corrected by background subtraction, and since the bacterial density was dissimilar to the other substrates at this timepoint, a valid statistical comparison could not be performed. In all other timepoints, the measured MFI is clearly lower for the inactive bacteria for both BODIPY-E2 and BODIPY-N3. Therefore, it is likely the association of BODIPY molecules with *C. tardaugens* relies on active transport into the bacteria rather than passive binding or diffusion.

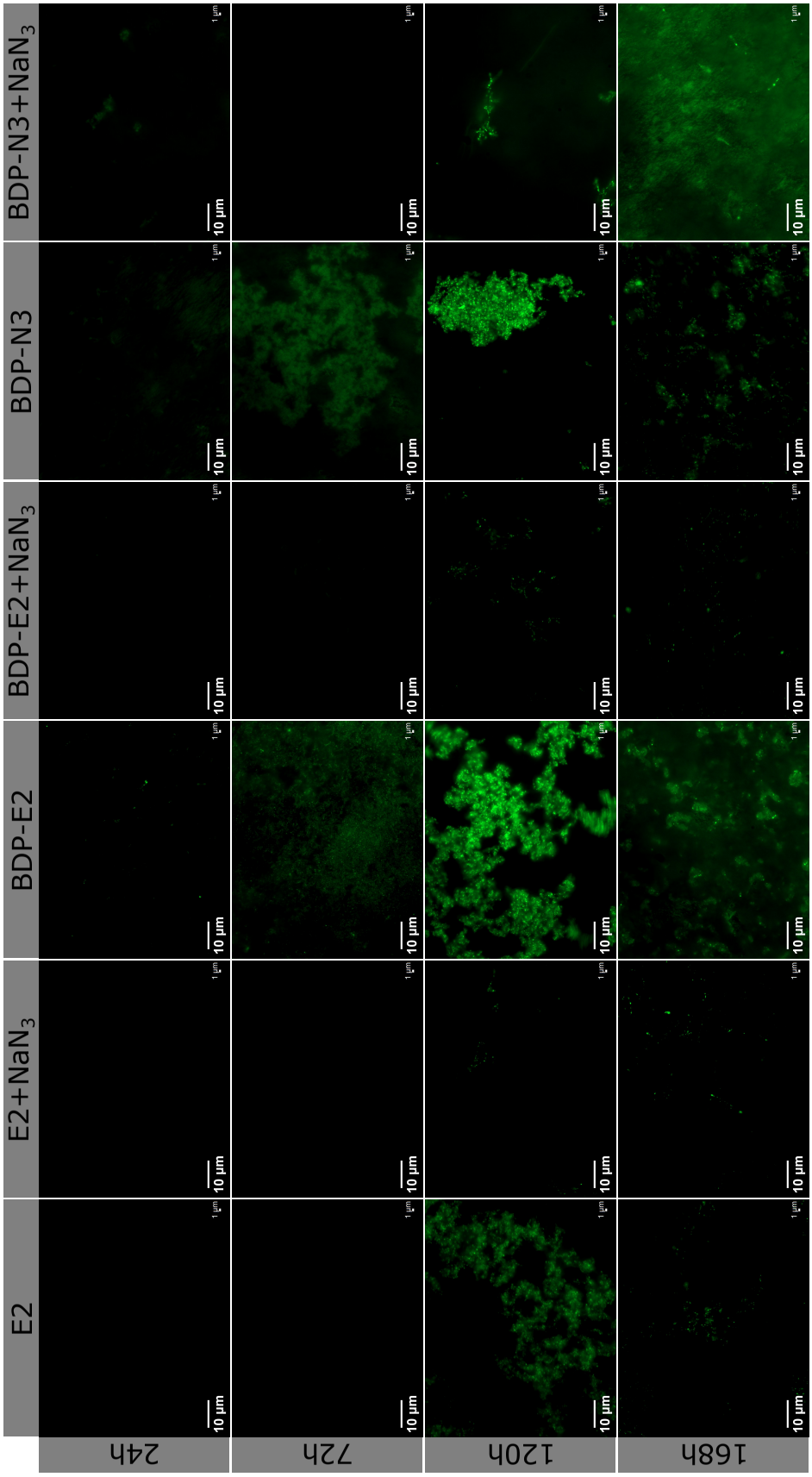

Figure 4.17: Representative fluorescence microscopy images of C. tardaugens cultured with natural and fluorescent estrogen or BODIPY-azide. Scale bars are 10 µm (lower left) and 1 µm (lower right).

4.3.3.3 Uptake by *E. coli*

The images showed clear and intense fluorescence with both BODIPY-E2 and BODIPY-N3 (Figure 4.18). Although the culture with natural E2 showed some autofluorescence, it was not of the same intensity as those cultures with the fluorescent molecules. The fluorescence intensity of BODIPY-E2 and BODIPY-N3 were statistically similar (Figure 4.19) for both timepoints. Since the biodegradation experiments showed no removal of BODIPY-E2, we anticipated that *E. coli* would not actively uptake the fluorescent estrogen. Unexpectedly, the bacteria appeared to grow in the presence of NaN_3. Since the bacteria were not metabolically inactive, the passive or active association of the fluorescent molecules with *E. coli* was undetermined.

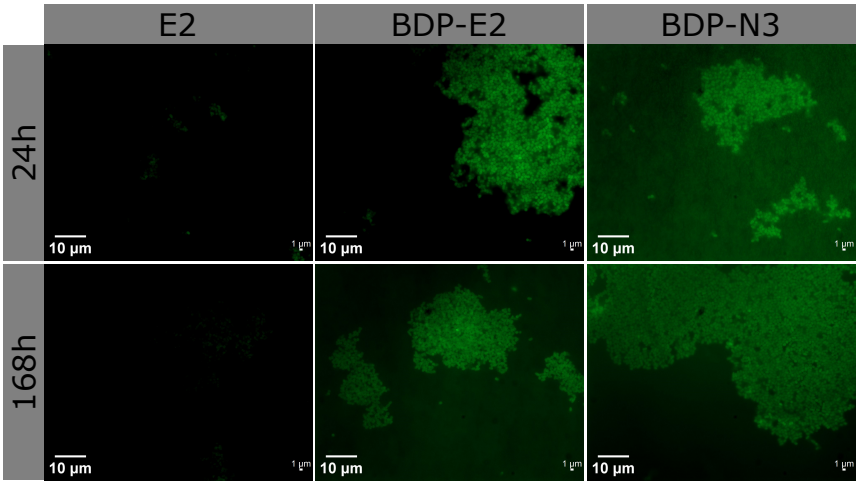

Figure 4.18: Representative fluorescence microscopy images of E. coli cultured with natural and fluorescent estrogen or BODIPY-azide. Scale bars are 10 µm (lower left) and 1 µm (lower right).

Fluorescence microscopy of the three reference strains showed non-specific fluorescence with BODIPY-N3, and the non-estrogen-degrading strain showed significant fluorescence with BODIPY-E2. These results suggest that although biodegradation of BODIPY-E2 is specific to the estrogen-degrading bacteria, the association of BODIPY fluorophore molecules with the bacteria is less specific. The fluorescence of *C. tardaugens* was more intense in the active bacteria than the bacteriostatic cultures, and therefore, it is likely the fluorophores are being actively transported into the cells. Conversely, the active or passive association of the fluorophores with *E. coli* remains uncertain. The green fluorescence of *E. coli* cultured with the BODIPY molecules showed clearly defined boundaries around the bacteria compared to the estrogen-degrading bacteria, which had more diffuse fluorescence (Figure 4.20). Additionally, the cell diameters appeared larger with the BODIPY fluorescence than the internalised DAPI DNA stain. Thus, it is possible the BODIPY molecules are associating with the *E. coli* cell membrane.

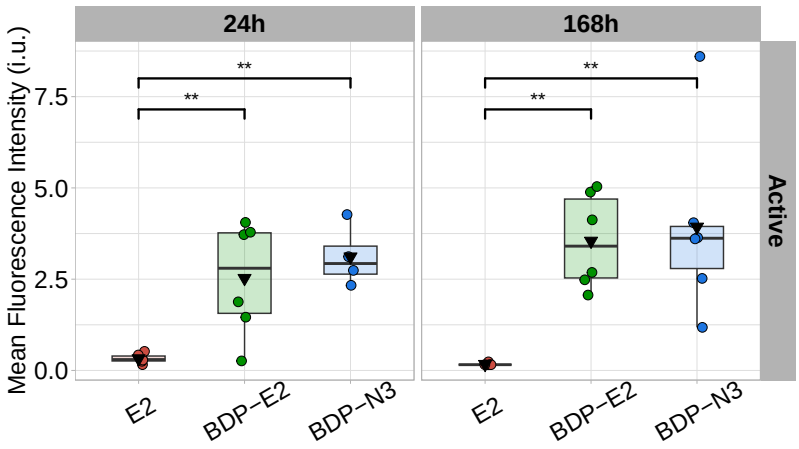

*Figure 4.19: Mean fluorescence intensity (MFI) for fluorescence microscopy of E. coli cultured with natural and fluorescent estrogen or BODIPY-azide. Points are the MFI calculated for each image (max 255), and inverted triangles are the mean of the images. Boxes show 25%, 50%, and 75% quartiles, and whiskers show 1.5-times the IQR. p-values ** <0.01.*

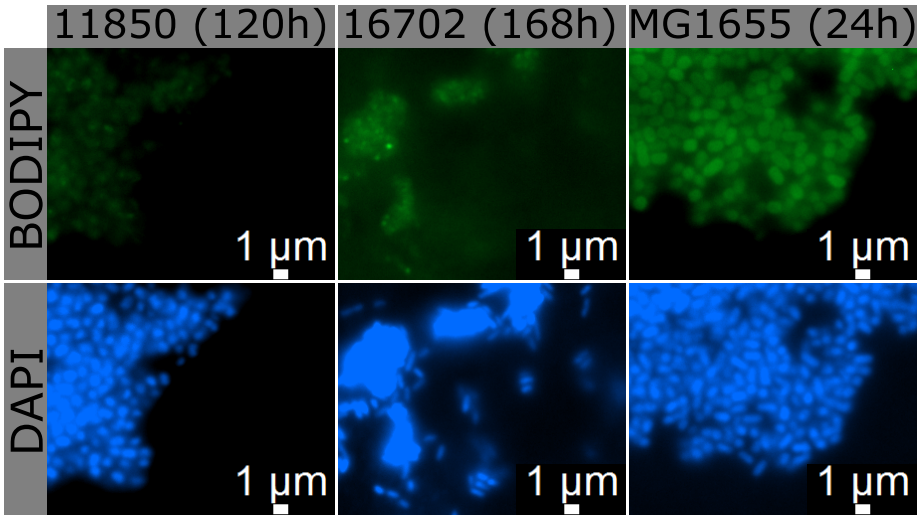

Figure 4.20: Magnified segments of representative fluorescence microscopy images of N. europaea, C. tardaugens, and E. coli cultured with BODIPY-E2. Images show the same field for each bacteria using DAPI and BODIPY/fluorescein filters without background correction.

4.4 Conclusion

In summary, this work evaluated the fate of BODIPY-labelled estradiol when cultured with a synthetic community of estrogen-degrading reference bacteria strains.

- Two estrogen-degrading bacteria, *N. europaea* 11850 and *C. tardaugens* 16702, and a non-degrading control bacteria, *E. coli* MG1655, were cultured in MMB medium supplemented with substrates tailored to each strains' growth requirements. The three bacteria were cultured both individually and as a consortium.

- The selective biodegradation of E2 was observed in cultures with the estrogen-degrading *C. tardaugens*.
- The partial metabolism of BODIPY-E2 by *C. tardaugens* into BODIPY-E1 was observed, but only in the presence of abundant co-substrate and at a much slower rate than E2.
- Cometabolism of E2 and BODIPY-E2 was possibly observed with *N. europaea*, however, this was not reproduced due to toxicity of the estrogen at the working concentration.
- We hypothesise that the low rate and efficiency of degradation by *N. europaea* compared to published studies is due to the cyclodextrin-estrogen inclusion complex interfering with entering the cell, which is supported by microscopy evidence.
- Fluorescence microscopy showed that *C. tardaugens* actively transports both BODIPY-E2 and BODIPY-azide tag. While the BODIPY-estrogen and tag appear to associate with *E. coli* cell membrane, this could not be confirmed.

The synthetic community of reference strains used in this work – which included E2 catabolism, cometabolism, and non-metabolism – were used to determine the growth and biodegradation of BODIPY-labelled estradiol compared to the natural hormone. The results of this chapter provide an understanding of the biochemical fate and spatial distribution of the fluorescent probe. These results will be used to inform the development of a fluorometric assay for the selective detection of estrogen-degrading bacteria using BODIPY-tagged estradiol.

Chapter 5

Development of a Fluorometric Assay for Estrogen-Degrading Bacteria

5.1 Introduction

In Chapter 2, the biological transformation and degradation of estrogen micropollutants were explored in detail, and the important role that chemical trace analysis plays in understanding these processes is apparent. In addition to directly monitoring pollutant levels in wastewater treatment systems and the environment, chemical analysis of estrogens has been instrumental in improving and developing biological treatment strategies *in vitro*. For example, numerous studies have used chromatographic techniques to explore the effects of lab-scale bioreactors and biofiltration systems' operating parameters on estrogen removal [121, 255–257]. Chemical analysis has also been used to confirm the enhanced removal of estrogens in bioaugmented treatment systems [105, 120, 258].

Although obtaining accurate concentrations of estrogen micropollutants is pertinent in many circumstances, preliminary screening to detect biodegradation does not necessarily require this degree of precision. Yet, chromatographic analysis of estrogens remains the most widely used analytical technique to detect estrogen biodegradation. In particular, chromatography has been used to detect biodegradation by cometabolism in nitrifying activated sludge [69, 72]. A study by Pauwels *et al.* (2008) screened cultures inoculated with compost, sludge, or faeces after one month for degrading bacteria by measuring EE2 removal using HPLC analysis [75].

While biodegradation may be directly observable as growth in chemically defined media with estrogen as the sole carbon source, such conditions are not representative of the natural settings where biodegradation occurs (e.g., biological treatment processes in a WWTP). In addition, the process of identifying estrogen-degrading bacteria can be time-consuming (refer to Table 2.4) and may require a large number of samples. For example, a study by Shi *et al.* (2002)

screened "hundreds of sediment, soil, and manure samples" for an EE2-degrading organism using enrichment cultures [122]. Therefore, a simpler technique based on a fluorescent BODIPY-estrogen derivative which can rapidly detect the activity of estrogen-degrading microorganisms would be beneficial.

The findings in Chapter 4 revealed that BODIPY-estradiol is a viable surrogate for E2 based on the selective biotransformation of the fluorescently labelled micropollutant by estrogen-degrading bacteria. A small, but comparable, degree of either natural E2 or BODIPY-E2 removal was observed by the cometabolising reference strain, *N. europaea* 11850. The estrogen-catabolising strain, *C. tardaugens* 16702, transformed BODIPY-E2 into BODIPY-E1 in accordance with its estradiol biodegradation pathway [99]. Therefore, these reference strains will again be used to demonstrate proof-of-concept for the fluorometric assay. Since hydrolysis of the fluorophore conjugation was not observed, the best candidate for a fluorometric response is detecting uptake of the BODIPY-E2 by the estrogen-degrading bacteria rather than biodegradation of the fluorescent estrogen.

Fluorescent assays which measure the internalisation of fluorescent probes using a spectrofluorometer have been developed primarily with eukaryotic cell lines in biomedical applications. A selection of such assays from the literature is provided in Table 5.1. The majority of cell lines are adherent, i.e., where the cells adhere to the surface of the culture vessel as they grow. In these cases, detection is achieved by removing the spent media containing the free fluorescent probe and recording the fluorescence of the cells attached to the multi-well culture plate [174, 259]. Alternatively, intracellular fluorescence can be detected by using a cell-impermeable quenching agent to suppress the extracellular fluorophore fluorescence [241, 260]. The concentrations of the fluorescently labelled substrates used in these assays are micromolar, while 1.6 nM BODIPY-E2 was used to detect uptake by microscopy in Chapter 4. However, it should be noted eukaryotic cells are 100 times larger than bacteria, which may influence uptake sensitivity.

Non-adherent cell lines are often analysed by flow cytometry, however, there are a few examples of spectrofluorometric assays with bacteria which used physical separation indicated in Table 5.1. Phetsang *et al.* (2016) measured the internalised fluorescently labelled trimethoprim (TMP) antibiotic by centrifuging the bacteria to remove the media containing the free probe, then recording the fluorescence intensity of resuspended cell pellets [238]. Alternatively, Tao *et al.* (2016) filtered bacteria cultured with 2-NBDG (a fluorescent glucose analogue) to remove the media and then dissolved the filter containing the bacteria for analysis by spectrofluorometer [239]. Based on these two simple detection mechanisms (separating of the cells from the media and fluorescence quenching), there are a variety of approaches to detect the uptake of a fluorescent probe. Thus, these approaches can applied towards detecting the uptake of BODIPY-E2 by estrogen-degrading bacteria.

Table 5.1: A selection of methods from the literature which measured the uptake of fluorescent probes by spectrofluorometry.

Sample Type	Detection Mechanism	Fluorescent Probe	Conc. (μM)	ε ($M^{-1}cm^{-1}$)	Φ_f	Ref.
Adherent cells NHLF	Separation	2-NBDG	1–100	2.4×10^{4a}	0.55^a	[174]
Adherent cells HEK	Separation	FFN206	20	No data	0.74^b	[259]
Multiple *E. coli* strains	Separation	NBD-TMP	12.5–100	8×10^{3c}	0.03^c	[238]
Rumen bacteria strains	Separation	2-NBDG	100	2.4×10^{4a}	0.55^a	[239]
Adherent cells 3T3-L1	Quenching	BODIPY-C12	2	9×10^{4d}	No data	[241]
Adherent cells HEK and CHO	Quenching	No data[e]	No data[e]	No data[e]	No data[e]	[260]

References for the molar extinction coefficient (ε) and quantum yield (Φ_f) of the fluorophore: [a] [201], [b][259], [c][261], [d][262]. [e]The method used a commercial kit with a "fluorescent substrate that mimics the biogenic amine neurotransmitters".

The aim of this chapter was to develop a high-throughput fluorometric assay for identifying estrogen-degrading bacteria via the uptake of BODIPY-E2, a fluorescent analogue of estradiol, using estrogen-degrading reference strains in individual and mixed cultures.

5.2 Materials & Methods

5.2.1 Reagents

The reagents for this work are the same as those in Chapter 4 Section 4.2.1. Potassium iodide (reagent-grade) was from Sigma-Aldrich UK.

5.2.2 Fluorescence Analysis

Fluorescence measurements were conducted using the Tecan Infinite M200 Pro plate reader. Samples were measured in triplicate wells (100 μL) in black μClear® 96-well microplates (#655096, Greiner Bio-One, UK). The general instrument parameters, unless specified otherwise, are given in Table 5.2.

During method development, an initial working concentration of 1 mg/L of individual BODIPY-estrogens was used. Absorption spectra were obtained by recording absorbance from 300–650 nm in 5-nm steps. Emission spectra were obtained by recording the fluorescence intensity from 495–650 nm in 5-nm steps, using a fixed excitation wavelength at 470 nm and a gain value of 60. The optimum excitation/emission wavelength combination was determined by measuring the fluorescence excitation spectra from 470–500 nm in 2-nm steps with a fixed emission

Table 5.2: Instrument parameters for spectrofluorometric analysis.

Parameter	Value
Z-position	17419 µm
Integration time	20 µs
Flash number	20
Ex. Bandwidth	9 nm
Em. Bandwidth	20 nm
Ex. Wavelength	482 nm
Em. Wavelength	514 nm
Gain	142 (Low) or 50 (High)

wavelength at 510, 512, 514 and 516 nm and a gain value of 30.

5.2.3 Standards Preparation

Six calibration standards and three quality control (QC) samples were prepared by diluting BODIPY-E2 stock solution (1 mg/mL in methanol) in MMB supplemented with 2% HPβ-CDX. A set of standards and QCs (Table 5.3) were prepared at a high concentration range (100–2500 µg/L) to compare with the HPLC-PDA method (Chapter 3) and at a low concentration range (100–2500 ng/L) to test the lower limits of the plate reader.

5.2.4 Fluorometric Method Evaluation

As with the chromatographic methods, the fluorometric method was evaluated according to the ICH Guidelines Q2 (R1) for method validation in terms of precision, linearity, range, accuracy, and instrument limits of detection and quantitation [140]. Method evaluation was carried out by running a batch of six calibration standards and three QC samples on three separate days. The calculations for each figure of merit are described below. Accuracy and instrument limits of detection and quantitation were determined as per Sections 3.2.7.3 and 3.2.7.4, respectively.

5.2.4.1 Linearity

Linearity for each batch was determined using unweighted linear regression of the concentration (x) versus the blank-corrected fluorescence intensity (y) of the calibration standards analysed in triplicate. The coefficient of determination (R^2) of the linear regression and the percent error

Table 5.3: Standards and quality controls used for fluorometric method evaluation.

	Low		*High*	
Std or QC	ng/L	nM	µg/L	µM
S1	100	0.16	100	0.16
S2	300	0.49	300	0.49
S3	600	0.98	600	0.98
S4	1000	1.63	1000	1.63
S5	1750	2.85	1750	2.85
S6	2500	4.07	2500	4.07
QC H	200	0.33	200	0.33
QC M	800	1.30	800	1.30
QC L	2000	3.26	2000	3.26

of the standard concentrations were used to evaluate the linearity of the method, as per Section 3.2.7.1.

5.2.4.2 Precision

Precision was determined by the percent relative standard deviation (%RSD) of the three QCs measured as six replicates in three separate batches. Repeatability was evaluated by %RSD for the QCs within a single batch; the value reported is the mean repeatability for all three batches. Since the spectrofluorometer readings are rapid (e.g., a 96-well plate in approximately 1 min.) and would occur immediately after sampling, repeatability was deemed a sufficient metric for intra-assay precision. Inter-assay precision was evaluated by the %RSD for the QCs across all three batches.

5.2.5 Biodegradation Cultures with BODIPY-E2

The selective uptake of BODIPY-E2 by estrogen-degrading bacteria was evaluated by a series of biodegradation experiments with the three reference strains: *N. europaea* 11850, *C. tardaugens* 16702, and *E. coli* MG1655. The bacteria were all pre-cultured individually according to Sections 4.2.4.1–4.2.4.3 and washed according to Section 4.2.6. The heterotrophic bacteria were inoculated at OD_{600} 0.005, and *N. europaea* was inoculated at OD_{600} 0.00025.

The media was prepared similarly to the biodegradation experiments described in Section

4.2.6. The estrogens were redissolved in 40% HPβ-CDX and diluted with MMB media to a final working concentration of 1 µg/L or 1 mg/L E2 or BODIPY-E2 and 2% HPβ-CDX. Media was supplemented with 2.5 µg/mL thiamine HCl, 0.5 mg/mL sodium pyruvate, and 0.1 mg/mL glucose.

Biodegradation experiments were conducted in triplicate foil-wrapped serum bottles under aerobic conditions. Abiotic controls and cultures (20 mL) were incubated in the dark at 30°C, shaking at 150 rpm for one week. Samples (1 mL, 2X) were collected at each timepoint for fluorescence and growth analysis. For fluorometric analysis, an aliquot of culture was collected in a 1.5-mL microcentrifuge tube and analysed immediately. The fluorescence of each sample was measured in three replicate wells (100 µL) according to Section 5.2.2. Growth was measured by OD_{600} per Section 4.2.5.4. NO_2^- concentrations were measured to detect nitrification in *N. europaea* cultures per Section 4.2.5.6. Growth and nitrite results are provided in Appendix D.

5.2.5.1 Low Concentration with Physical Separation

The uptake of BODIPY-E2 was evaluated at an environmentally relevant working concentration (1 µg/L) with all three bacteria individually. In order to measure uptake, bacteria were separated from the media by centrifuging the samples at $2000\times g$ for 10 minutes. The fluorescence intensity was measured for the whole culture (i.e., cells in media prior to centrifugation) and the cell-free supernatant using the gain parameter for the low analytical range.

5.2.5.2 High Concentration with Physical Separation

The uptake of BODIPY-E2 was also evaluated at 1 mg/L with *C. tardaugens* and *E. coli*. Here, uptake was also measured by physically separating bacteria from the media by centrifuging the samples at $2000\times g$ for 10 minutes. The fluorescence intensity was measured for the whole culture (i.e., cells in media prior to centrifugation) and the cell-free supernatant using the gain parameter for the high analytical range.

5.2.5.3 High Concentration with Quenching Agent

Finally, the uptake of BODIPY-E2 was evaluated with KI as a quenching agent. The extracellular fluorescence was quenched by adding 25 µL of 5 M KI to each well. The plate was gently agitated and incubated in the dark for 5 minutes before measuring the fluorescence intensity using the gain parameter for the high analytical range. This experiment was conducted with 1 mg/L BODIPY-E2 and all three bacteria both individually and in co-cultures. Since the extracellular fluorescence was chemically quenched, the fluorescence-free control (1 mg/L E2) was only measured at 168 h in single-strain cultures. Additionally, BODIPY-azide (0.5 mg/L

BODIPY-N3) was also included as a fluorescent estrogen-free control and measured at 168 h in single-strain cultures.

5.2.6 Statistical Analysis

Analytical figures of merit, calibration curves, and concentrations for BODIPY-E2 or NO_2^- were calculated in MS Excel. Statistical analysis of the replicates (i.e., mean and standard deviation) were calculated in R. When ANOVA was performed, significant *p*-values were calculated using Tukey's HSD ($\alpha = 0.05$). Plots were generated in R using ggplot2 package [221].

5.3 Results & Discussion

5.3.1 Method Development

A fluorometric method for detecting the uptake of BODIPY-E2 was developed by first understanding the effects of the solvent environment and the polarity of the estrogen molecule on the fluorophore's photophysical properties. The fluorescence intensity of fluorophores, including BODIPY, may be influenced by the solvent polarity [263]. The absorbance and fluorescence intensity of BODIPY-E2 was notably greater in methanol compared to water or MMB media (Figure 5.1a). In MMB media, the addition of 2% HPβ-CDX increased the absorbance and fluorescence intensity.

The lower molar extinction (i.e., absorbance), fluorescence quenching, and spectral broadening in an aqueous environment without cyclodextrin (Figure 5.1b) are explained by aggregation-caused quenching of BODIPY [216]. In Chapter 3, we demonstrated that HPβ-CDX improved the solubility of BODIPY-estrogens. These results show the improved solubility and stability afforded by including cyclodextrin increased the fluorescence intensity of BODIPY-estrogens.

Next, the spectral profiles of different estrogen conjugates in MMB with 2% HPβ-CDX were investigated. The absorbance and fluorescence intensity were negatively correlated with the hydrophobicity of the BODIPY-estrogen conjugate (BODIPY-E1 > BODIPY-E2 > BODIPY-E3), based on the elution order observed in Chapter 3 (Figure 5.2a). The maximum fluorescence intensity of BODIPY-E1 and BODIPY-E2 were 37% and 82% of BODIPY-E3, respectively.

Spectral broadening was apparent in the absorbance for BODIPY-E1, but not for BODIPY-E2 or BODIPY-E3 (Figure 5.2b). The results demonstrate that even small changes in oxidation level of the fluorescent estrogen can have a profound impact on the fluorescence intensity of the probe. Since the transformation of BODIPY-E2 into BODIPY-E1 by *C. tardaugens* was confirmed in Chapter 4, decreases in fluorescence intensity in *C. tardaugens* cultures could be attributed to the oxidation of BODIPY-E2 into BODIPY-E1.

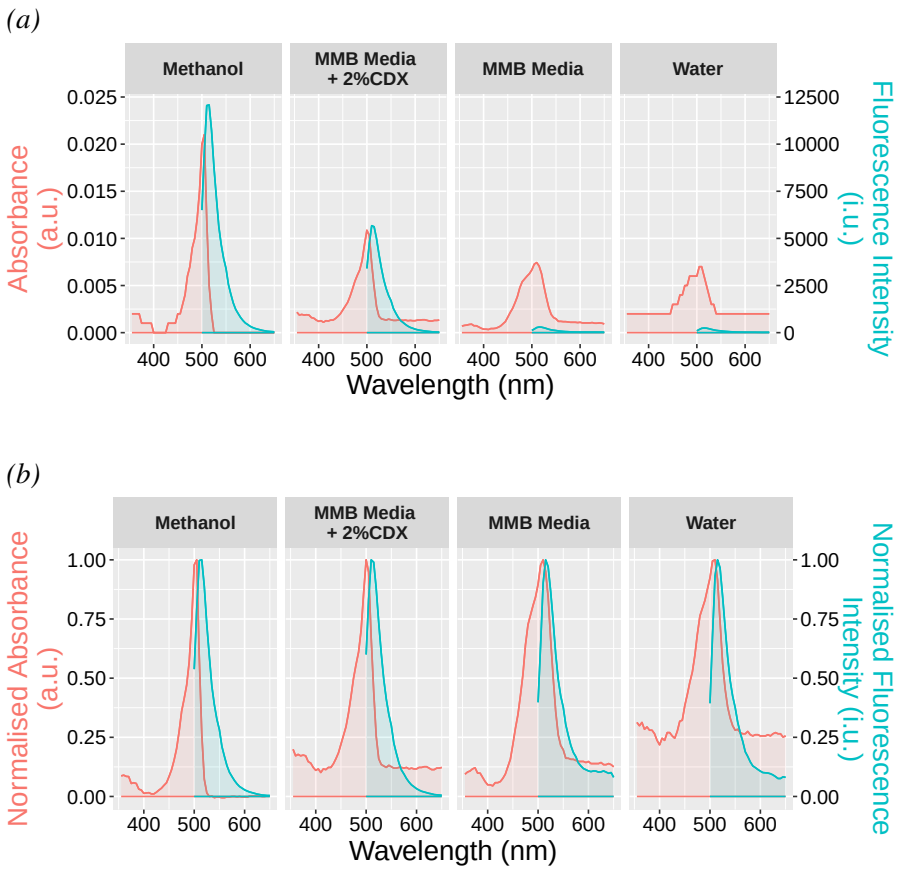

Figure 5.1: Absorbance and fluorescence emission spectra of 1 mg/L BODIPY-E2 in different solvents, given as (a) blank-corrected measurements and (b) normalised to the maximum. Results are the mean of triplicate wells.

Although the absorbance and emission maxima would be the optimal wavelengths (λ) for fluorometric detection, the instrument's excitation and emission bandwidths (Table 5.2) would overlap the extremely small Stokes shift for BODIPY (<10 nm). Therefore, the optimal excitation and emission wavelength pair for detection was empirically determined using the three BODIPY-estrogens (Figure 5.3). The optimal combinations for each BODIPY-estrogen were generally between 482–488 nm and 512–514 nm for excitation and emission, respectively. The excitation laser interfered with detection of fluorescence emission for combinations $\leq$24 nm apart. Fluorescence intensity notably decreased for excitation wavelengths <480 nm. The combination of 482 nm and 514 nm was selected for detection of BODIPY-E2 to comfortably avoid bandwidth overlap. After selecting the optimal excitation and emission pair, the sensitivity of the instrument was further optimised for the lowest detectable range. The instrument's software determined an optimal gain value of 142 to detect 1 µg/L BODIPY-E2.

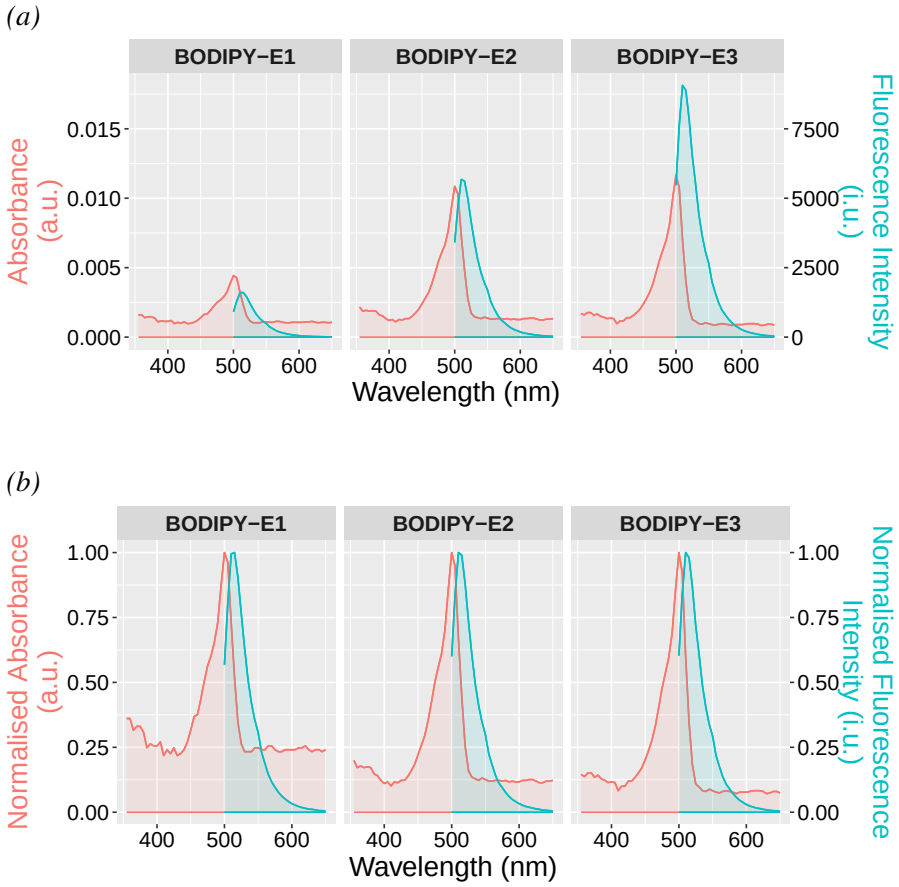

Figure 5.2: Absorbance and fluorescence emission spectra of 1 mg/L BODIPY-E1, BODIPY-E2, and BODIPY-E3 in MMB media with 2% HPβ-CDX, given as (a) blank-corrected measurements and (b) normalised to the maximum. Results are the mean of triplicate wells.

5.3.2 Method Evaluation

Next, the analytical figures of merit were determined for the spectrofluorometer (Table 5.4); the calibration curves are provided in Appendix D. Two analytical measurement ranges were evaluated by adjusting the instrument gain: 100–2500 ng/L and 100–2500 µg/L, referred to herein as "low" and "high", respectively. The low range, which is near the spectrofluorometer detector limits, was used to test biodegradation at environmentally relevant concentrations. The high range was included to directly compare the fluorometric results with the biotransformation results of Chapter 4. The instrument gain for the high range (50) was selected by conjecture. The upper limit of the analytical range was set 150% higher than the HPLC-PDA method (1 mg/L) to account for potential background fluorescence in the cultures.

The analytical performance of the spectrofluorometer was notably different between the low and high measurement ranges. The high range demonstrated very good precision and accuracy

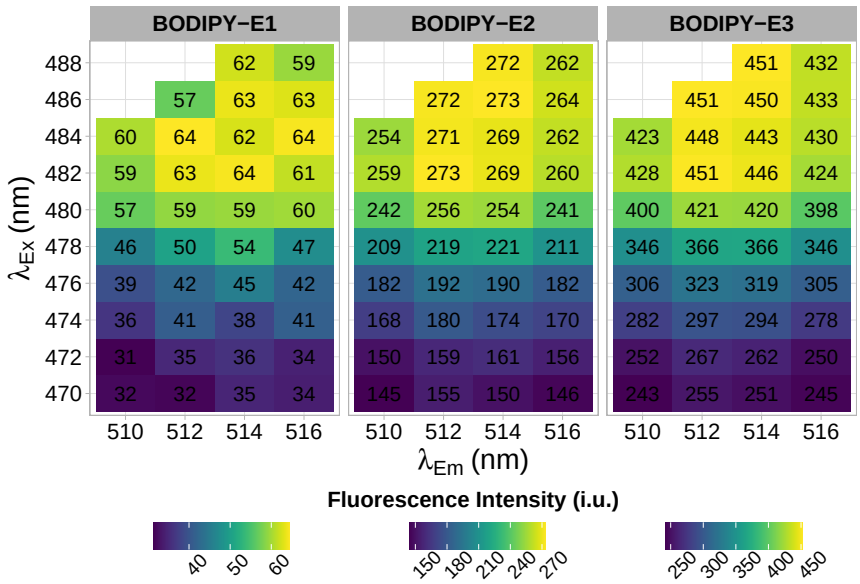

Figure 5.3: Fluorescence excitation/emission matrices for 1 mg/L BODIPY-E1, BODIPY-E2, and BODIPY-E3 in MMB media with 2% HPβ-CDX. Values are the mean fluorescence intensity for triplicate wells.

Table 5.4: Results of spectrofluorometric method evaluation.

		Precision		*Accuracy*		*Calibration Statistics*		
Analytical Range	QC	Repeat.	Inter-Assay	% Recovery	% Error	LOD	LOQ	R^2
100–2500 µg/L	L	5	5	100	9.2	**0.08 ± 0.02** 50.0 ± 10	**0.24 ± 0.06** 150 ± 30	0.998 ± 0.001
	M	5	5	110	7.7			
	H	4	5	110	11			
100–2500 ng/L	L	70	90	63	46	**0.17 ± 0.05** 100 ± 30	**0.50 ± 0.10** 310 ± 90	0.996 ± 0.003
	M	30	50	87	31			
	H	10	40	130	26			

Precision values are percent relative standard deviation. Limits of detection (LOD) and quantitation (LOQ) are reported in micromolar (**bold**, top values) and µg/L (bottom values) for the high analytical range and nanomolar (**bold**, top values) and ng/L (bottom values) for the low analytical range. Linearity and limit values are the means of the three different batches (n=3) and include standard deviation (± value).

(<6% RSD and <11% error) and high degree of linearity (0.998 ± 0.001). In contrast, the low range showed very poor precision of the response (7.3–66.0% repeatability, 39.8–94.4% inter-assay precision), particularly over different days. The accuracy of the low range was also poor (>15% error). However, the linearity was good quality (0.996 ± 0.003). Since precision and accuracy improved as concentrations increased and the calibration standards consistently produced a linear response, even in the low range, the weak performance is primarily attributed to the limitations of the instrument at the lower range. Thus, error propagation for the technical

replicates will be particularly pertinent for the low range.

Comparing the high analytical range on the spectrofluorometer with the HPLC-PDA method for BODIPY-E2, the chromatographic method showed better precision and accuracy (Chapter 3 Table 3.8). The chromatographic method achieved 0.4% and 0.3% RSD for repeatability and inter-assay precision, respectively, and 4.9% error for accuracy. However, the estimated LOD and LOQ for both platforms were very similar: 68 $\pm$ 50 µg/L and 208 $\pm$ 152 µg/L for the HPLC, and 50 $\pm$ 11 µg/L and 148 $\pm$ 34 µg/L for the spectrofluorometer. Although the fluorometer can semi-quantitatively detect BODIPY-E2 three orders of magnitude lower than the HPLC by increasing the gain setting, the overall analytical performance is significantly reduced at this low range. In addition, the fluorometer was not selective between the different BODIPY-estrogens, whereas each compound has a unique retention time on the HPLC.

However, the loss in quantitative accuracy, precision, and selectivity must be balanced against cost and time efficiency gained. While the HPLC-PDA required 28 minutes of run-time per sample, the spectrofluorometer could measure a 96-well plate – i.e., up to 25 samples, a calibration curve and a blank in triplicate – in less than 2 minutes. Furthermore, the spectrofluorometer can directly measure nearly environmentally relevant concentrations without requiring analyte enrichment (i.e., sampling a large volume to be concentrated down into a small extract). As noted in Chapter 2, the environmentally relevant concentrations of estrogen in water are approximately 0.001–30 ng/L – one order of magnitude below the low analytical range of the spectrofluorometer. However, this is a substantial improvement upon the working concentrations for laboratory-based biodegradation studies, which used estrogen concentrations up to five orders of magnitude higher than environmentally relevant [99].

Although comparing the analytical performance of the plate reader with the chromatography system is informative from a chemometric perspective, the method evaluation of the two platforms served different purposes towards the primary objective of developing a fluorometric assay for selecting estrogen-degrading microbial communities. The HPLC-PDA method was developed and validated in Chapter 3 to ensure the concentrations of natural and BODIPY-labelled estrogens could be reliably measured in cultures with estrogen-degrading bacteria, as done in Chapter 4. Conversely, a selective fluorometric response to the uptake of BODIPY-E2 will rely on the approach to distinguish intracellular fluorescence from the extracellular or whole-culture fluorescence, not the exact concentration derived from the measured intensity. Here, the method evaluation provides two key pieces of information that aid the development of a fluorometric assay. First, the evaluation confirmed there is a linear, proportionate response to the concentration of BODIPY-E2 by the fluorometer at two different analytical measurement ranges. Second, the response of the low range is more sensitive but much less precise and accurate than the high range.

5.3.3 Selection of Estrogen-Degrading Bacteria with BODIPY-E2

As previously stated, a selective response to the uptake of BODIPY-labelled estrogen requires distinguishing fluorescence from within the bacteria from the bulk fluorescent signal. Two different approaches were used to differentiate the intracellular versus extracellular fluorescence. First, the bacteria were removed from the media by centrifugation, whereby the cell-free media was expected to have a lower fluorescence due to the BODIPY-E2 being taken up by the bacteria (Figure 5.4). Since the method evaluation showed different sensitivities and variances across the analytical measurement range, this simple approach to separating the bacteria was tested using two working conditions, 1 µg/L and 1 mg/L BODIPY-E2. BODIPY-free controls using natural E2 were included to account for innate fluorescence of the cultures. For the second approach a cell-impermeable quenching agent, KI, was used to suppress extracellular fluorescence (Figure 5.8).

5.3.3.1 Low Concentration with Physical Separation

When centrifugation was used to physically separate the cells cultured with the 1 µg/L E2 and BODIPY-E2, innate fluorescence by the heterotrophic bacteria exceeded the signal of the fluorescent probe at environmentally relevant concentrations (Figure 5.5a). The increase in background fluorescence was clearly observed even in non-fluorescent cultures with natural E2 for *C. tardaugens* and *E. coli*. The background fluorescence was also observed in the cell-free culture. This suggests that the bacteria are secreting a metabolite during growth which is interfering with detection of BODIPY. The most plausible compound is riboflavin, a metabolite of *E. coli* K-12 which has an emission peak around 450–520 nm [264]. Nonetheless, the high background fluorescence of the cultures greatly impedes detection of selective BODIPY-E2 uptake.

Since growth was identical between E2 versus BODIPY-E2 at 1 µg/L for all three bacteria (Figure 5.6), the background fluorescence from the E2 cultures (F_{E2}) was subtracted from the corresponding BODIPY-E2 cultures ($F_{\text{BDP-E2}}$) for each timepoint (t_i). Here, we will refer to this as the blank-corrected signal (F_{BC}), since the "blank" (i.e., BODIPY-free) signal is removed. This was done for the abiotic controls (a) and for each bacteria individually (b, representing *N. europaea*, *C. tardaugens*, or *E. coli*). This blank-correction procedure is summarised in Equations 5.1 and 5.2:

$$F_{\text{BC},a,t_i} = F_{\text{BDP-E2},a,t_i} - F_{\text{E2},a,t_i} \,, \tag{5.1}$$

$$F_{\text{BC},b,t_i} = F_{\text{BDP-E2},b,t_i} - F_{\text{E2},b,t_i} \,. \tag{5.2}$$

This approach to background subtraction was possible due to the availability of an abundant growth substrate for each of the bacteria: pyruvate for *E. coli* and *C. tardaugens*, glucose for *E. coli*, and ammonium for *N. europaea*. Since the estrogen concentrations are so low,

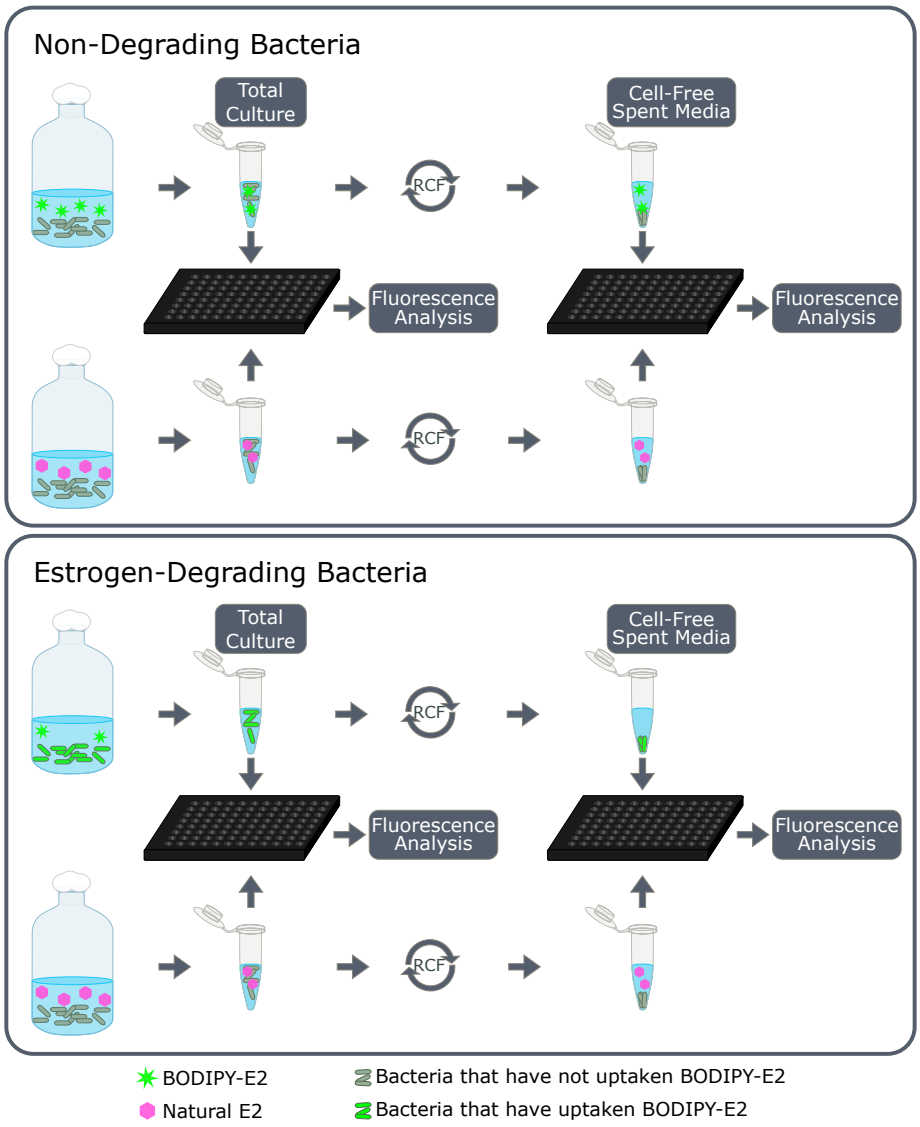

Figure 5.4: Workflow of the fluorometric method based on physical separation of the bacteria from the culture media.

catabolism of E2 had no influence on the growth *C. tardaugens*.

The blank-corrected fluorescence intensity did not clearly indicate uptake of BODIPY-E2 by either estrogen-degrading strain (Figure 5.5b). The variances of the measurements were considerable, and there were no clear differences between cultures and the abiotic controls. Traditionally, fluorescent probes are not used for extended periods due to degradation of the fluorophore by photobleaching. Extensive care was taken to prevent exposure to unnatural light during sampling and incubation. The abiotic controls of the total cultures do not show evidence of photobleaching, since the fluorescent signal does not decrease over the duration of the experiment.

However, the fluorescent signal of the blank-corrected cell-free samples are more variable

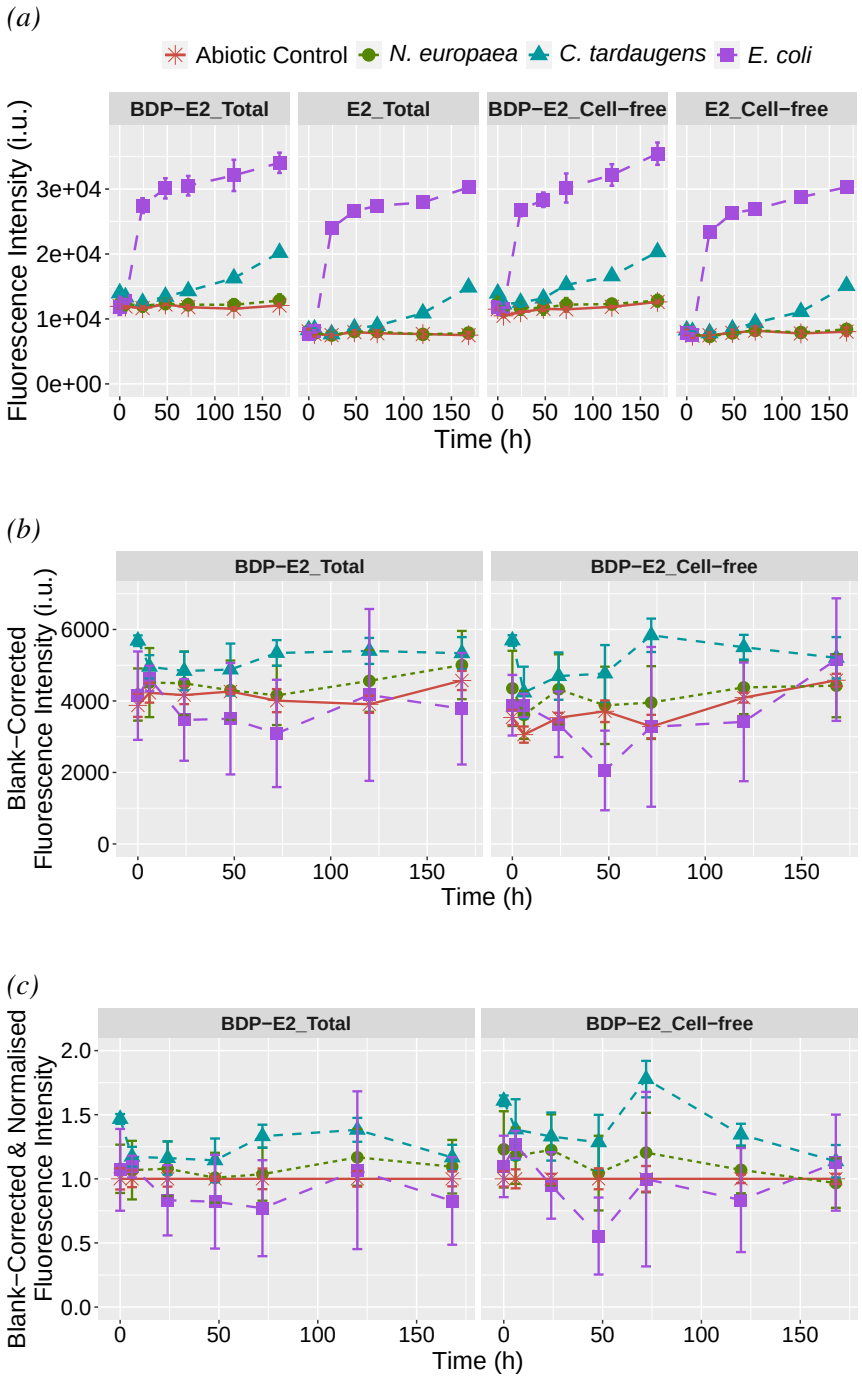

Figure 5.5: Fluorometric measurements of estrogen-degrading cultures with 1 µg/L E2 or BODIPY-E2. Results are given for the total culture ("Total") and the media with the bacteria removed ("Cell-free"). (a) The raw fluorescence values for E2 and BODIPY-E2 cultures. (b) Blank-corrected fluorescence obtained by subtracting the raw fluorescence for E2 cultures from the raw fluorescence of the BODIPY-E2 cultures. (c) Normalised fluorescence obtained by dividing the blank-corrected fluorescence by the abiotic control's fluorescence. Results are the mean and standard deviation of triplicate cultures.

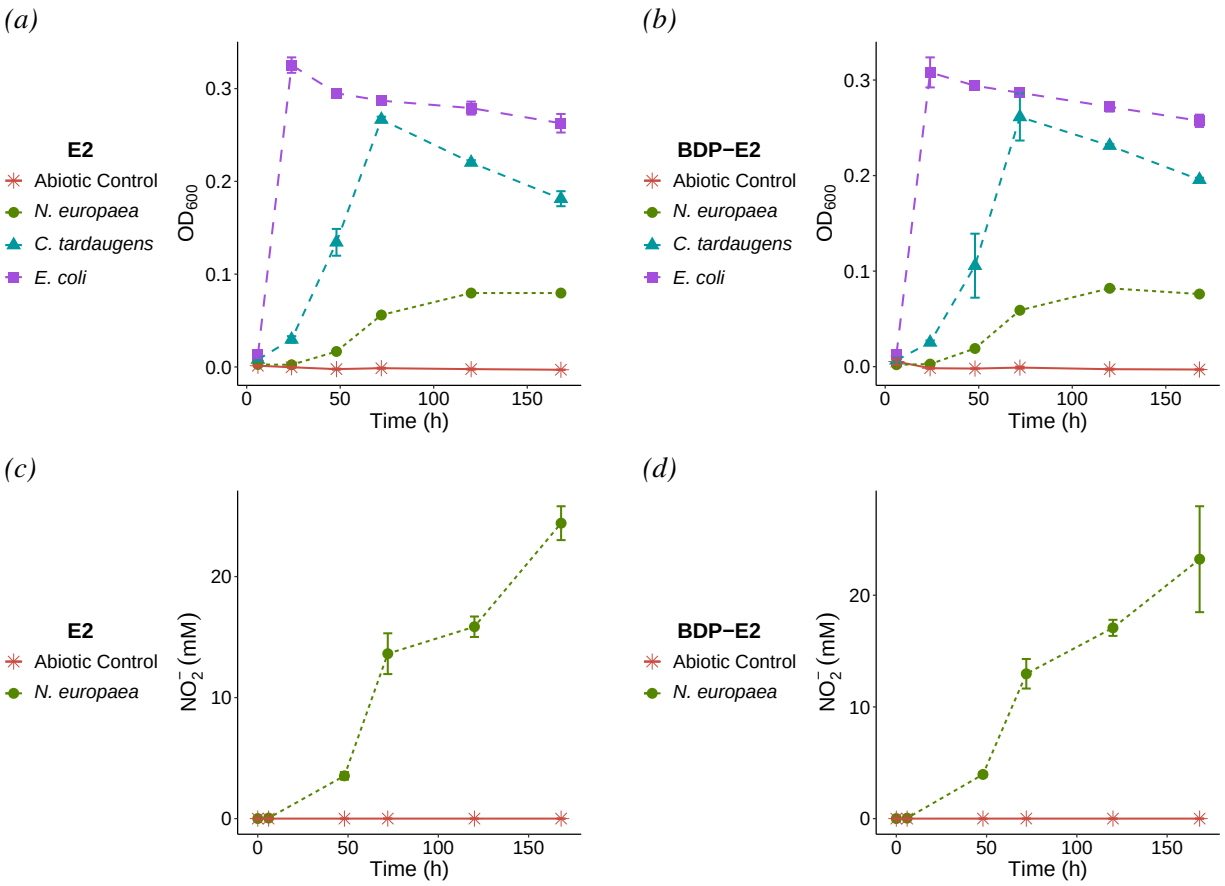

Figure 5.6: Growth results (OD_{600}) for testing 1 µg/L E2 (a) and BODIPY-E2 (b) with physical separation. The production of NO_2^- by N europaea was also measured for (c) E2 and (d) BODIPY-E2 cultures. Error bars are the standard deviation (n=3).

than the total cultures between timepoints, which is evident in both the biotic cultures and the abiotic control. This is probably due to light exposure while loading and unloading the centrifuge. Therefore, the blank-corrected fluorescent signal of the biological samples was also normalised against the abiotic control's for each timepoint, as it can be safely assumed the controls and bacteria samples suffered an equivalent degree of light exposure during handling. Normalisation was selected instead of subtraction to compare the change in fluorescence against a reference (i.e., the abiotic control). The blank-corrected fluorescence normalised for abiotic decay (F_D) for each timepoint was calculated by Equation 5.3:

$$F_{D,t_i} = \frac{F_{BC,b,t_i}}{F_{BC,a,t_i}} . \tag{5.3}$$

The blank-corrected and normalised results did not reveal a decrease in fluorescence in cell-free media for the estrogen-degrading strains, which we would have expected due to uptake of the fluorophore (Figure 5.5c). At 72 h, there was an increase in fluorescence in the *C. tardaugens*

cell-free media, however, it was not observed at any other time. The increase in fluorescence, particularly compared to the abiotic control, could not be explained and contradicts the expected response of bacteria uptake of BODIPY-E2 (i.e., a decrease in extracellular fluorescence).

Based on the results from Chapter 4, we expected that the estrogen-catabolising organism, *C. tardaugens*, would uptake the fluorescent probe, while it was inconclusive whether the BODIPY-E2 was internalised or adsorbed to *E. coli*. However, this uptake was not observed through physically separating the bacteria from the spent media containing a low concentration of BODIPY-E2. Conversely, the cometabolising organism, *N. europaea*, did not degrade BODIPY-E2 rapidly or uptake a significant amount of BODIPY-E2 when analysed by fluorescence microscopy in the previous chapter. Therefore, uptake by *N. europaea* was not expected to be readily detectable by spectrofluorometry.

In addition, a clear decrease in fluorescence for *C. tardaugens* over 168 h was not observed in either the total culture or cell-free media. Since *C. tardaugens* does not further transform BODIPY-E2 beyond BODIPY-E1, we expected that fluorescence might decrease in the total culture due to the lower fluorescent yield of the metabolite (Figure 5.2a). Although the low analytical measurement range detects more environmentally relevant concentrations, the high error in measurement combined with the corrections for high background fluorescence impede detection of a response to either the uptake of BODIPY-E2 or its biotransformation to BODIPY-E1 by estrogen-degrading bacteria.

5.3.3.2 High Concentration with Physical Separation

The cultures with 1 mg/L natural E2 and BODIPY-E2 were analysed using the spectrofluorometer settings for the high analytical range (Figure 5.7a). At this working concentration and gain settings, the background fluorescence from the bacteria was negligible. Following the same blank-correction procedures as performed on the low concentration experiment (Equations 5.1 and 5.2), there was no difference between the non-corrected fluorescence measurements and the blank-corrected fluorescence (Figure 5.7b). The variance of the measurements in the high analytical range was markedly less than the variance for the low range. There was some variability in the fluorescence of the "cell-free" abiotic control, so normalisation (Equation 5.3) was applied here as well (Figure 5.7c). The results did not show a decrease in the cell-free samples of *C. tardaugens* cultures. Indeed, there was no clear difference in the fluorescence between the abiotic control, the estrogen-degrading bacteria, and the non-estrogen-degrading bacteria.

Surprisingly, the fluorescence of the total culture did not decrease with *C. tardaugens*. In Chapter 4, *C. tardaugens* was repeatedly shown to transform BODIPY-E2 into BODIPY-E1 at the same working concentration. The fluorescence intensity of BODIPY-E1 was measured as 23% and 29% that of BODIPY-E2 in MMB with 2% HPβ-CDX (Figures 5.2a and 5.3). However,

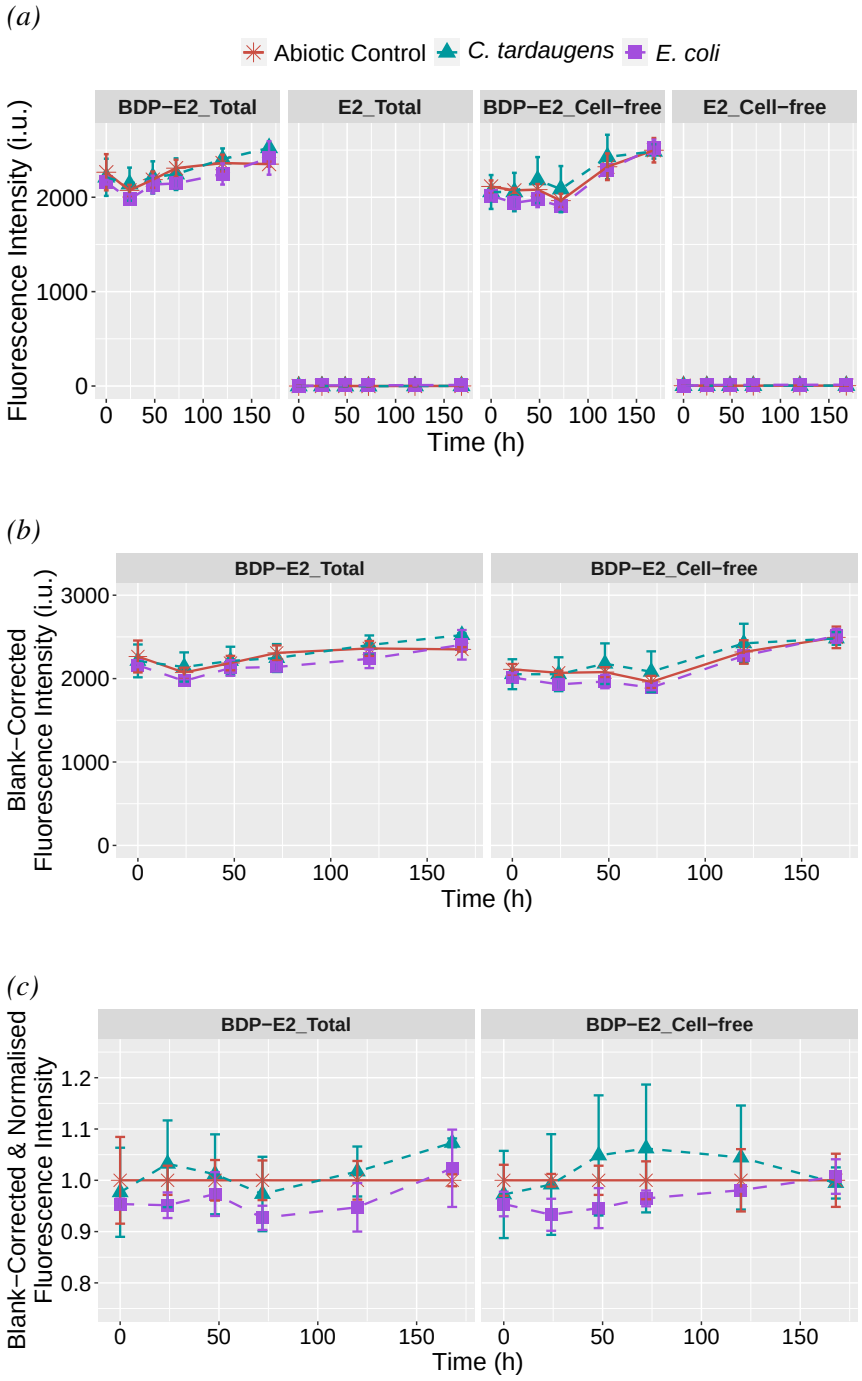

Figure 5.7: Fluorometric measurements of estrogen-degrading cultures with 1 mg/L E2 or BODIPY-E2. Results are given for the total culture ("Total") and the media with the bacteria removed ("Cell-free"). (a) The raw fluorescence values for E2 and BODIPY-E2 cultures. (b) Blank-corrected fluorescence obtained by subtracting the raw fluorescence for E2 cultures from the raw fluorescence of the BODIPY-E2 cultures. (c) Normalised fluorescence obtained by dividing the blank-corrected fluorescence by the abiotic control's fluorescence. Results are the mean and standard deviation of triplicate cultures.

these intensities were measured with gain settings of 30 and 60, respectively, while the method here used a gain of 50. A set of calibration standards determined the concentration of BODIPY-E2 in the total cultures at 168 h as 640 ± 5 µg/L in the *C. tardaugens* cultures and 596 ± 7 µg/L in the abiotic control. Assuming 50% of BODIPY-E2 was transformed to BODIPY-E1 (based on the biotransformation results) and applying 29% fluorescence intensity towards BODIPY-E1, we would expect a fluorescence intensity around 1680 i.u. – 33% less than actual measured value. Although this particular result cannot be explained, the absence of a fluorometric response to the biotransformation of BODIPY-E2 is a favourable outcome, as it means the fluorescent signal may remain stable even after partial metabolism.

As discussed in Chapter 2, one of the key advantages of fluorescence over UV-Vis absorbance spectroscopy is the analytical sensitivity. While absorbance measures the proportion of transmitted light (i.e., the difference between two non-zero values), fluorescence measures emitted light from a dark background (i.e., an increase from zero). However, this approach of measuring uptake by the decrease in extracellular BODIPY-E2 fluorescence relative to a control is effectively tantamount to the principles of absorbance spectroscopy. Thus, the extracellular fluorescence is not sensitive to the uptake of BODIPY-E2. Therefore, a different approach is needed to differentiate the intracellular BODIPY.

5.3.3.3 High Concentration with Quenching Agent

The second approach to distinguish the uptake of fluorescently labelled estrogen by estrogen-degrading bacteria was by quenching the extracellular BODIPY-E2 with iodide (Figure 5.8). Halide ions are well-established fluorescence quenchers, where I^- is much more effective at quenching than Br^- or Cl^- [265]. Iodide quenching is achieved by collisional interactions, where proximal quenching ions mediate intersystem crossing of the fluorophore as well as deactivation of the triplet state [265, 266]. The kinetics of intermolecular quenching are described by the Stern-Volmer relationship:

$$\frac{F_0}{F} = 1 + k_q \tau_0 [Q] \,, \tag{5.4}$$

where F is the fluorescence intensity of the fluorophore, F_0 is the fluorescence intensity in the absence of quencher, τ_0 is the excited state lifetime of the fluorophore in the absence of quencher, k_q is the quencher rate coefficient, and $[Q]$ is the concentration of quenching agent. Based on the Stern-Volmer relationship with 1 mg/L BODIPY-E2 (Figure 5.9), the iodide quenching constant ($K_q = k_q \tau_0$) is 1.73 M^{-1}. However, the highest concentration of quencher tested did not completely suppress fluorescence emission of 1 mg/L BODIPY-E2. In the presence of 1 M KI, the fluorescence intensity was significantly reduced, however, the linear relationship between intensity and concentration remains (Appendix D).

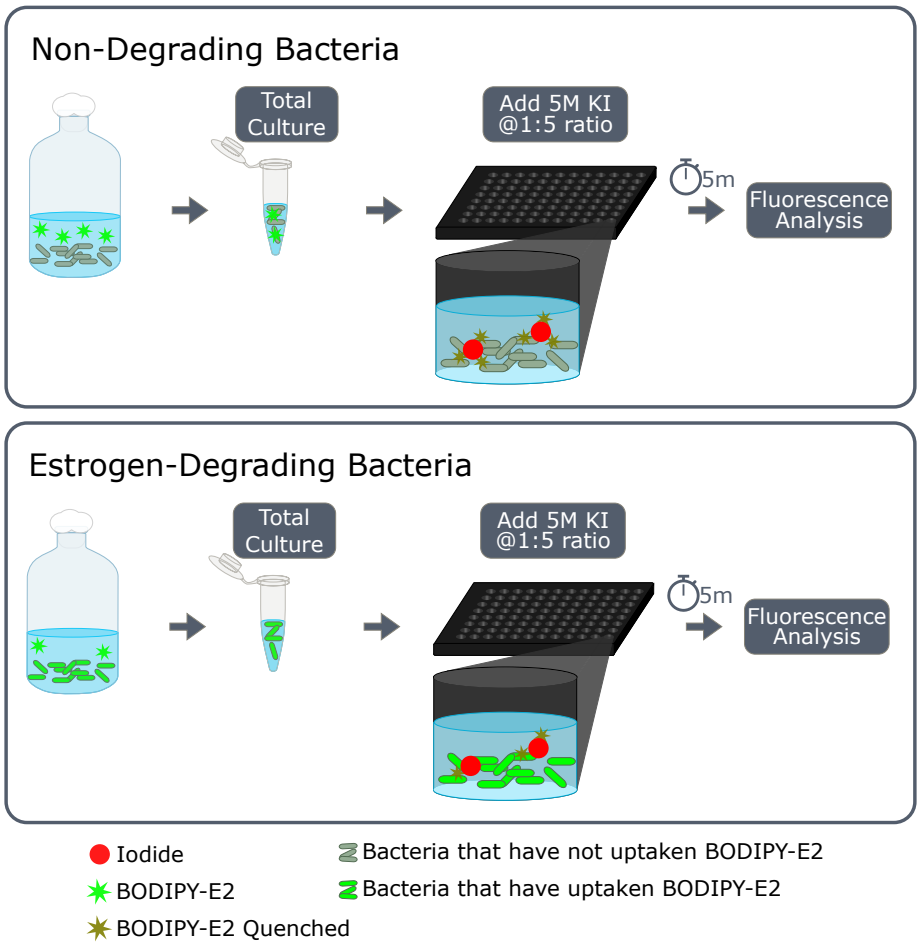

Figure 5.8: Workflow of the fluorometric method based on quenching the extracellular BODIPY-E2 with iodide ions.

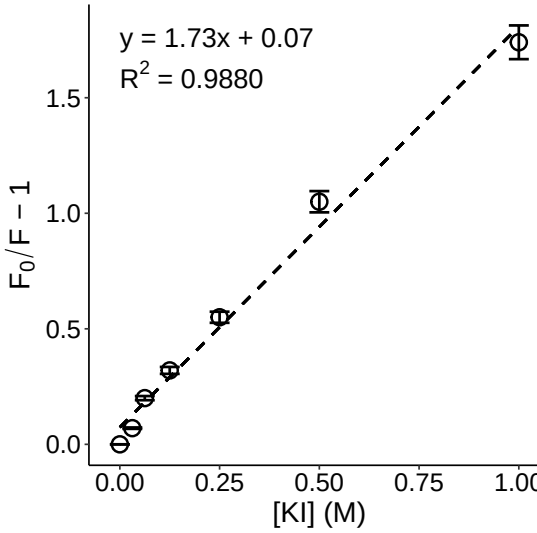

Figure 5.9: Stern-Volmer plot of fluorescence quenching of 1 mg/L BODIPY-E2 by KI.

Since the innate background fluorescence by the bacteria was not detectable by the high range gain settings (Figure 5.7a), the fluorescence intensity was simply blank-corrected with blank media. The results showed a clear increase in the fluorescence intensity of the *C. tardaugens* cultures at 72–168 h (Figure 5.10a). When normalised for abiotic decay, the distinction of the estrogen-catabolising bacteria was even more apparent (Figure 5.10b). Since iodide is impermeable to the bacteria, the increase in fluorescence is attributed to the intracellular uptake of BODIPY-E2, where it is not exposed to the quenching agent. As expected, there was no fluorescence response to uptake detected by the estrogen-cometabolising or non-degrading bacteria.

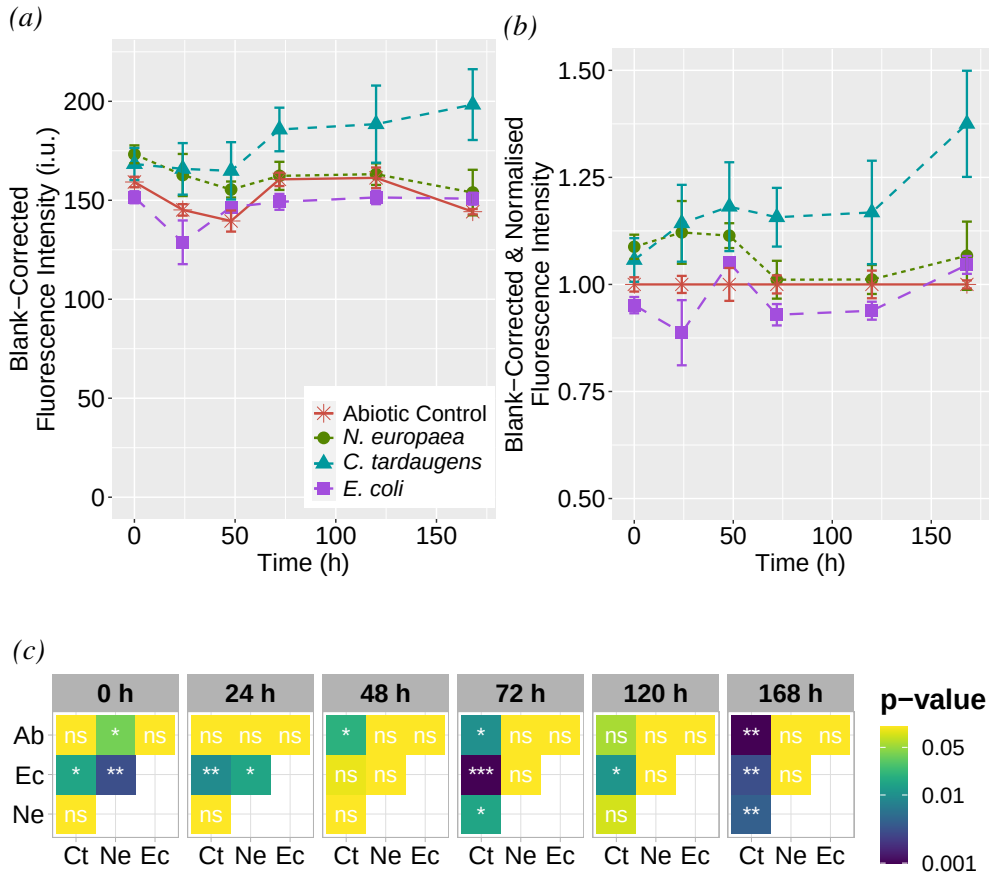

Figure 5.10: Fluorometric measurements of estrogen-degrading bacteria cultures with 1 mg/L BODIPY-E2 and 1 M KI. (a) Blank-corrected fluorescence with MMB media with 2% HPβ-CDX. (b) Normalised fluorescence obtained by dividing the blank-corrected fluorescence by the abiotic control's fluorescence. Results are the mean and standard deviation of triplicate cultures. (c) Tukey's HSD pairwise comparisons of the fluorescence values at each timepoint. Ab–abiotic control, Ct–C. tardaugens, Ne–N. europaea, Ec–E. coli.

Pairwise statistical comparisons of the cultures showed a significant difference for *C. tardaugens* cultures compared to the other bacteria and abiotic controls at 72 and 168 h (Figure 5.10c).

Significant differences were also observed for *N. europaea* at the start of the experiment. However, since sampling occurred just after inoculation for 0 h, this increase was not considered meaningful. Despite the strong fluorescence detected by microscopy in Chapter 4, the lack of intracellular fluorescence for *E. coli* at each timepoint supports our theory that the BODIPY molecules were interacting with the cell membrane.

In order to verify that the signal increase in *C. tardaugens* cultures was indeed due to uptake of the fluorescent estrogen, two control conditions were cultured in tandem with the BODIPY-E2 cultures and measured at 168 h. First, cultures with 1 mg/L of non-fluorescent E2 were measured with 1 M KI to confirm there was still no background fluorescence. Second, the bacteria were cultured with 0.5 mg/L BODIPY-azide to determine substrate selectivity. Compared to BODIPY-E2, BODIPY-azide showed a much lower, yet still slightly significant, increase in fluorescence by *C. tardaugens* (Figure 5.11). The low level of intracellular fluorescence by BODIPY-azide is supported by fluorescence microscopy observations in Chapter 4.

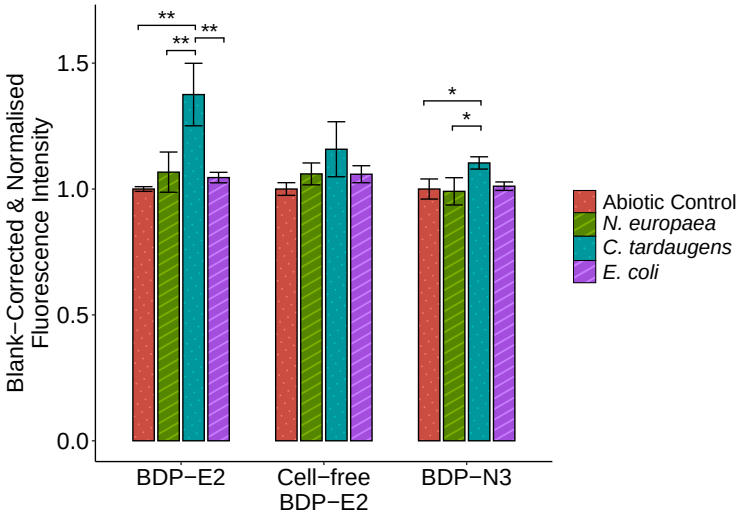

Figure 5.11: Abiotic control-normalised fluorescence of estrogen-degrading cultures with 1 mg/L BODIPY-E2 (total and cell-free) or 0.5 mg/L BODIPY-azide: abiotic controls (dotted red), N. europaea (striped green), C. tardaugens (dotted blue), and E. coli (striped purple). Results are the mean and standard deviation of triplicate cultures.

In addition, we confirmed that the increase in fluorescence was due to cellular uptake and not due to the loss of quenching in the culture medium. The bacteria were separated from the media by centrifugation, and the cell-free media was analysed following the addition of the quenching agent. The results showed no significant difference between *C. tardaugens* and the other bacteria or abiotic control. Thus, the observed fluorescence increase can be attributed to the selective uptake of BODIPY-E2 by estrogen-catabolising bacteria. These results confirm that BODIPY-labelled estrogen and cell-impermeable iodide quencher can be used together in a fluorometric assay for the selective detection of estrogen-degrading bacteria in pure cultures. The developed

assay detects an increase in fluorescence (relative to abiotic controls) that represents the internalisation of BODIPY-estrogen. Through collisional quenching of the extracellular fluorescence, the assay is much more sensitive in detecting changes in intracellular fluorescence compared to the previous approach of attempting to capture minute changes in extracellular fluorescence by physical separation of the cells.

5.3.3.4 Mixed Cultures with Quenching Agent

A high-throughput fluorometric assay for selecting estrogen-degrading bacteria was developed using pure cultures of reference strains. However, the method is ultimately intended for natural microbial communities, comprised of mostly unculturable microorganisms. If the assay can detect uptake of BODIPY-E2 by *C. tardaugens* in highly controlled, synthetic microbial communities, we can be more confident in deploying the developed method on environmental samples. Therefore, the developed assay was applied to pairwise and trio consortium co-cultures of the reference strains.

The co-culture of two heterotrophic bacteria showed an unambiguous increase in fluorescence compared to the abiotic control (Figures 5.12a and 5.12b). Since the increase in fluorescence did not occur with *E. coli* in any other mixed culture or its individual culture, this is attributed to *C. tardaugens*'s uptake of BODIPY-E2. The uptake of BODIPY-E2 by *C. tardaugens* in co-culture with *E. coli* was highly significant compared to the abiotic controls (Figure 5.12c). However, there was no significant increase in fluorescence when *C. tardaugens* was co-cultured with *N. europaea*. The presence of the estrogen cometabolising organism appeared to impede the increase in fluorescence associated with the uptake of BODIPY-E2 by *C. tardaugens*.

The culture media used in this work is optimised for *Nitrosomonas* growth, and *N. europaea* was cultured here to a greater relative abundance than what is expected in environmental samples. In nitrifying activated sludge, *Nitrosomonas* and other nitrifying bacteria have been estimated as 0.5–3% relative abundance of the community [267, 268]. Therefore, *N. europaea* in environmental samples are not expected to have an impact on BODIPY-estrogen uptake. In natural communities, the majority of bacteria are heterotrophic. Since the uptake of BODIPY-E2 by *C. tardaugens* was successfully detected in co-culture with a competitive heterotrophic bacteria, we can be reasonably confident that this simple fluorometric method can be used for detecting estrogen-degrading bacteria in environmental samples. Fluorescence quenching by nitrite – a product of ammonia oxidation by *N. europaea* – is another possible reason for the loss of intracellular fluorescence in *C. tardaugens* [160]. Although nitrite does not passively diffuse into the bacteria cytoplasm, it is possible that *C. tardaugens* transports NO_2^- into the cell where it quenches intracellular BODIPY-E2 [269].

The increase in fluorescence for *C. tardaugens* alone and in co-culture with *E. coli* was com-

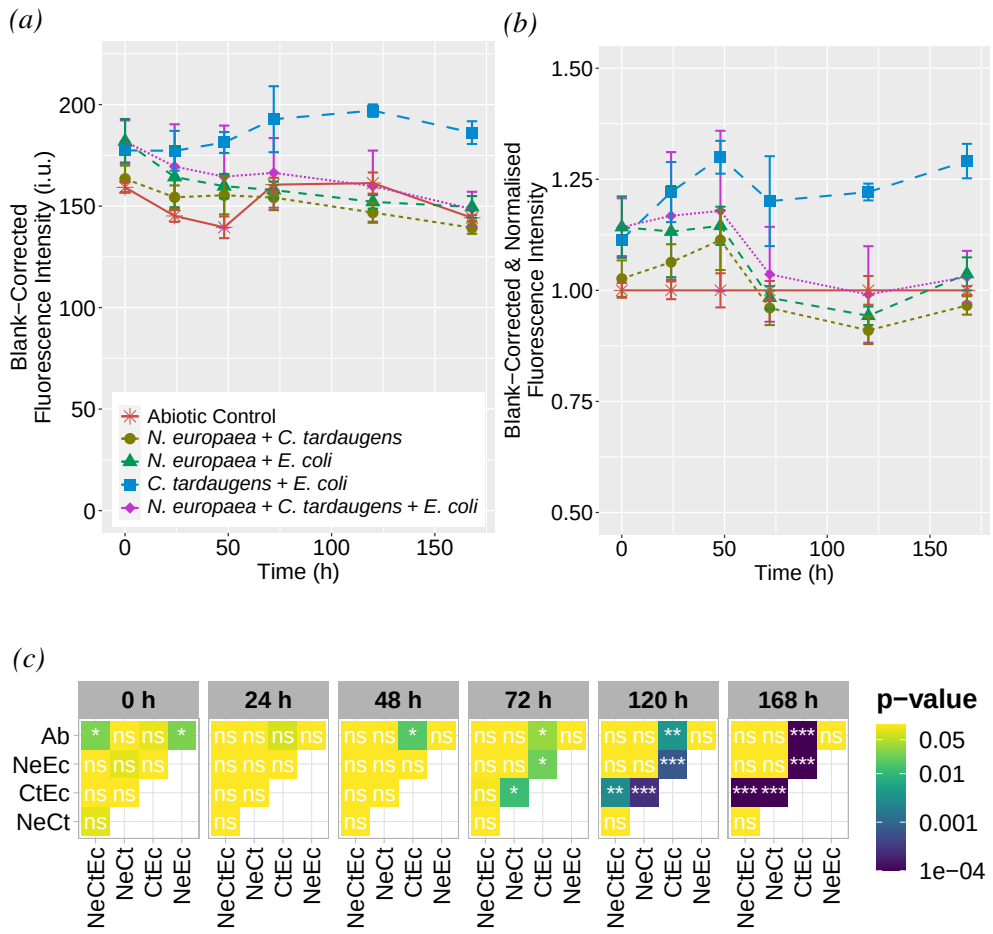

Figure 5.12: Fluorometric measurements of the three reference strains as pairwise and consortium co-cultures with 1 mg/L BODIPY-E2 and 1 M KI. (a) Blank-corrected fluorescence with MMB media with 2% HPβ-CDX. (b) Normalised fluorescence obtained by dividing the blank-corrected fluorescence by the abiotic control's fluorescence. Results are the mean and standard deviation of triplicate cultures. (c) Tukey's HSD pairwise comparisons of the fluorescence values at each timepoint. Ab–abiotic control, Ct–C. tardaugens, Ne–N. europaea, Ec–E. coli.

parable (Figures 5.10a and 5.12a). This is particularly interesting considering that *C. tardaugens* did not transform BODIPY-E2 with insufficient co-substrate (see Section 4.3.2.2), which suggests that the bacteria do not require an energy source to internalise the probe. However, the abundance of *C. tardaugens* in co-culture is most likely much less than *E. coli* or that of itself in pure culture. Therefore, the correlation between fluorescence intensity and bacterial growth was assessed (Figure 5.13). In individual cultures, only *C. tardaugens* showed a moderate-to-strongly positive correlation between fluorescence intensity and bacterial abundance (Figure 5.13a). The other bacteria and abiotic controls showed a negligible-to-weakly negative correlation. However, the correlation between bacterial density and fluorescence was much weaker in the *C. tardaugens* and *E. coli* co-culture (Figure 5.13b). Thus, it can be inferred that

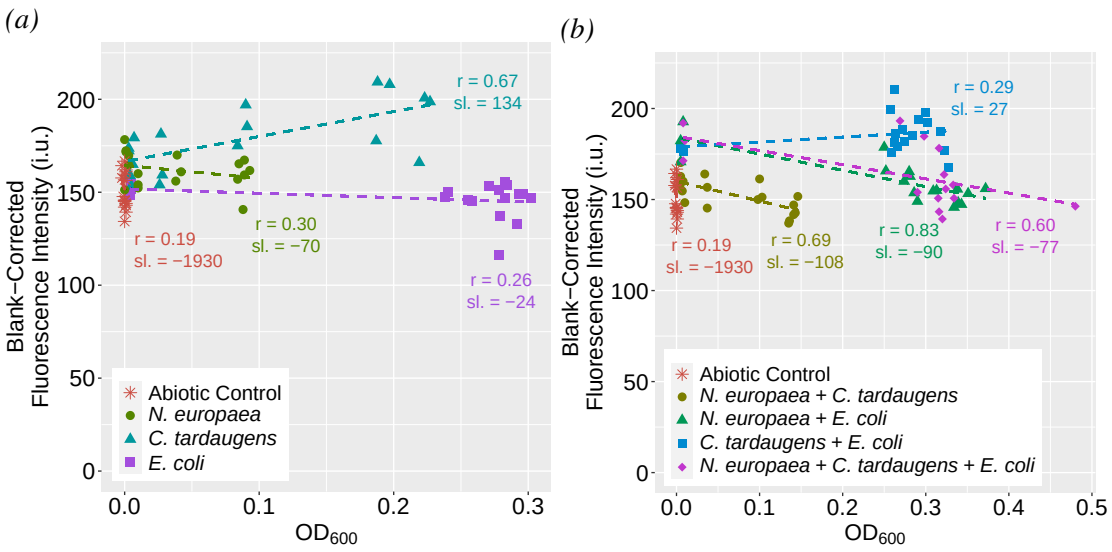

Figure 5.13: Correlation between the measured blank-corrected fluorescence intensity with 1 M KI and bacterial abundance (OD_{600}) for (a) individual and (b) mixed cultures. The dashed lines are the unweighted linear regression for each bacteria or combination of bacteria. The slope (sl.) and Pearson's correlation coefficient (r) are also shown. Note – the single and mixed cultures are from the same experiment and share the same abiotic controls.

the increase in intracellular fluorescence is not explicitly related to the density of the estrogen-degrading bacteria. In this experiment, the fluorescent substrate was introduced at inoculation, when the bacteria density was very low and not in log-phase growth. However, adding the probe while bacteria are growing in steady-state would be a more practical application of the method.

5.4 Conclusion

In this chapter, we developed a high-throughput fluorometric assay which can be used to detect the uptake of BODIPY-estradiol by estrogen-catabolising bacteria *C. tardaugens*.

- A fluorometric method for BODIPY-E2 was developed for a standard spectrophotometer plate reader. The instrument's analytical performance was comparable to the HPLC-PDA at the same working concentration. Although the spectrofluorometer could detect three orders of magnitude lower than the HPLC, the quantitative accuracy and precision at the lower limits of the detector were poorer at this concentration range.

- In addition, the effects of the solvent and analyte polarity on fluorescence of the BODIPY fluorophore were explored. These results were used to help provide context to the results of the biodegradation experiments.

- Two different approaches were tested to identify uptake of BODIPY-E2. The first approach sought to detect a decrease in free BODIPY-E2 in the media by physically removing the bacteria. This was tested at two different working concentrations – one more environmentally relevant but in the less accurate range of the instrument, the other at the same working concentration as the preliminary biodegradation experiments (Chapter 4) but in the more accurate range of the instrument. This method was not sensitive enough at either working concentration to detect a meaningful response.

- The second approach used cell-impermeable iodide to quench extracellular BODIPY-E2. This strategy successfully detected an increase in fluorescence in *C. tardaugens* cultures.

- The selective uptake of BODIPY-E2 (as well as some non-selective uptake of BODIPY-N3) by *C. tardaugens* and the lack of uptake by the other strains are supported by the biodegradation and microscopy results of Chapter 4.

- The increase in fluorescence by *C. tardaugens* was attributed to the uptake of BODIPY-E2 into the bacteria where the quencher cannot affect the fluorescent probe. Uptake was confirmed to be moderately selective for BODIPY-labelled estrogen over the BODIPY tag alone.

- The fluorometric method based on extracellular quenching was also evaluated in pairwise and trio consortium cultures with the reference strains. A clear response to BODIPY-E2 uptake by *C. tardaugens* was detected in co-culture with competitive bacteria, *E. coli*. However, uptake by *C. tardaugens* was not detected when co-cultured with *N. europaea*. Since *Nitrosomonas* does not have a high relative abundance in treatment system communities, this is not anticipated to be a concern in applications with field samples.

The developed fluorometric assay represents a significant step towards addressing the methodological gap of screening microbial communities for metabolically competent bacteria. The method was validated with at least two bacteria strains: estrogen-catabolising *C tardaugens* and the non-degrading control *E. coli*. The method mechanism is supported by biochemical evidence of the transformation of BODIPY-E2 into BODIPY-E1 and visual confirmation of the active uptake of the probe by *C. tardaugens*. However, our hypothesis that the fluorophores are passively interacting with the *E. coli* membrane remains to be confirmed.

In order to develop the fluorometric method, a mixotrophic culture media designed for co-culturing chemolithoautotrophic and heterotrophic bacteria was used. However, the method can be readily adapted for other sample types, provided the sample matrix does not interfere with the detection of the fluorescent probe. Controls for background fluorescence using non-fluorescent estrogen should also be assessed when using this method. In addition, the use of a cyclodextrin, such as HPβ-CDX, to maintain BODIPY-estrogen in solution is strongly recommended.

Chapter 6

Development of a Colorimetric Aptasensor for Monitoring Estrogen Biodegradation

6.1 Introduction

In Chapter 5, a high-throughput fluorometric assay was successfully developed to detect the uptake of BODIPY-labelled estradiol by estrogen-catabolising *C. tardaugens* in individual and mixed cultures under mixotrophic growth conditions. The developed fluorometric method for identifying estrogen-degrading microbial communities, which addresses one of the methodological gaps identified in this thesis, has the potential to be particularly useful in bioaugmentation. However, efforts towards engineering biological treatment systems for enhanced estrogen removal would greatly benefit from a rapid, high-throughput platform to directly measure estrogen concentrations. Indeed, the second methodological gap identified in Chapter 2 was the need for a rapid, scalable analytical method to quantify estrogen removal rates and efficiencies. These concentration values are necessary to optimise or predict the parameters which enhance estrogen biodegradation using computational methods.

While the developed fluorometric assay detects the intracellular distribution of fluorescently-labelled estrogen, the measured response does not represent the biodegradation of BODIPY-E2, as it is indistinguishable from the BODIPY-E1 transformation product. Furthermore, in Chapter 4, the biotransformation kinetics of BODIPY-E2 by *C. tardaugens* were shown to be dissimilar to natural E2, and estrogen cometabolism by *N. europaea* was impeded by the cyclodextrin-estrogen inclusion complex. Although uptake of the fluorescent surrogate was selective for estrogen biodegradation activity, the fluorescent tag sterically hindered the rate and extent of degradation by *C. tardaugens*. Thus, BODIPY-E2 is not a suitable surrogate for measuring estrogen removal rates and efficiencies.

In Chapter 2, the literature review highlighted that trace analysis of estrogen micropollu-

tants in the environment and laboratory degradation studies primarily relies on chromatographic methods. A review by Du *et al.* (2020) of estrogens measured in environmental surface waters published from 2015–2020 showed analysis was performed almost exclusively by mass spectrometry with liquid or gas chromatography [6]. In order to directly measure natural E2 during biodegradation without the use of chromatography or a fluorescent estrogen derivative, we explored an alternative approach based on a colorimetric nanoparticle-based biosensor.

Gold nanoparticles (AuNPs) have been used extensively in nanobiosensors [178]. Nanoparticles made from gold and other noble metals have unique physicochemical properties which can be exploited for receptor immobilisation, electron migration, reaction catalysis, and signal amplification [270, 271]. Signal enhancement by AuNPs has been particularly applicable across a range of sensing platforms, including optical, electrical, and micro-mechanical detection [270, 271].

The specific sensing mechanisms of AuNPs in colorimetric nanobiosensors were previously described in Section 2.8 of Chapter 2. Briefly, AuNPs are used in colorimetric sensing primarily through exploiting or manipulating the localised surface plasmon resonance (LSPR), a tunable property dependent on the particle size, the refractive index of the medium, and inter-particle distance [178]. In colorimetric assays, the inter-particle distance can be controlled by cross-linking the AuNPs via a biological receptor (e.g. antibodies or aptamers) or by adding electrolytes to the surrounding medium, disrupting the electrostatic stability of the colloid suspension [178, 272].

Numerous AuNP-based nanobiosensors have been designed for detecting estrogens in milk, meat, drinking water, surface waters, and wastewaters [199, 273–275]. Nanobiosensor method development studies often include spiked recovery tests to demonstrate accuracy and robustness, where a known quantity of target micropollutant is spiked into a sample matrix such as food or environmental waters. However, nanobiosensors for organic micropollutants have not yet been applied towards microbial cultures.

The ICH and U.S. Department of Health bioanalytical method validation guidelines for ligand-binding assays (including nanobiosensors) distinguish the influence of exogenous substances (e.g., structurally similar compounds, metabolites, and impurities) and the biological matrix as specificity and selectivity, respectively [140, 145]. The ICH Guideline M10 defines selectivity as the "ability of an analytical method to differentiate and measure the analyte in the presence of interfering substances in the biological matrix" and is tested by measuring the response of the assay using multiple sources of matrix, with and without a known concentration of analyte spiked in [140]. While the guidelines list blood, plasma, and urine as examples of biological matrices, the relevant biological matrix for *in vitro* biodegradation would be microbial cultures [140, 145]. Therefore, the suitability of the AuNP-based colorimetric aptasensor for measuring micropollutant biodegradation is contingent upon demonstrating biological selectivity in bacteria cultures.

The aim of this chapter was to develop and validate a high-throughput colorimetric aptasensor for directly measuring natural 17β-estradiol concentrations during biodegradation by estrogen-degrading reference strains.

6.2 Materials & Methods

6.2.1 Systematic Literature Review

A quantitative systematic review of published nanobiosensors for emerging contaminants was used to determine the most suitable platform for quantifying estrogen in bacteria samples. In order to capture as many unique methods as possible, the search included all non-pesticide contaminants in the 2018 EU Watch List of Substances (the most recent version at the time of this survey) [12]. A list of publications was obtained from Scopus and Web of Science (WoS) by searching the title, abstract or keywords containing the following: *(biosensor OR sensor) AND nano AND (aptamer OR antibody) AND (ethinylestradiol OR estradiol OR estrone OR erythromycin OR clarithromycin OR azithromycin OR amoxicillin OR ciprofloxacin)*. The list was further screened for the following inclusion criteria: original research articles in English using nanomaterials with either an aptamer or antibody targeting at least one of the listed contaminants.

6.2.2 Reagents

The reagents for this work pertaining to the culture media are the same as those in Chapter 4 Section 4.2.1. Hydrogen tetrachloroaurate(III) trihydrate (99.99%, Au 49.0%) was purchased from Alfa Aesar (Thermo Fisher Scientific UK) and stored in a desiccator. Sodium citrate trihydrate and sodium chloride were procured from Sigma-Aldrich UK. The E2-binding aptamers (Table 6.1) were synthesized by Eurofins Genomics and were stored in 10 μM aliquots (Milli-Q water) at -20°C.

Table 6.1: The E2-binding aptamers used in this work.

Aptamer Sequence	Length	Ref
5'- GCTTCCAGCTTATTGAATTACACGCAGAGGGTAGCGGCTC TGCGCATTCAATTGCTGCGCGCTGAAGCGCGGAAGC -3'	76 bases	[191]
5'-AAGGGATGCCGTTTGGGCCCAAGTTCGGCATAGTG-3'	35 bases	[192]

6.2.3 Absorbance Analysis

Absorbance measurements were primarily conducted using the Tecan Infinite M200 Pro plate reader. Samples were analysed in 96-well microplates (#655101, Greiner Bio-One UK); the specific volumes and number of replicates measured are specified throughout the text. Absorbance measurements using the Hach DR2800 spectrophotometer (Hach UK) were analysed in polystyrene semi-micro (1.6 mL) cuvettes (Fisherbrand, Fisher Scientific UK).

6.2.4 AuNP Synthesis & Characterisation

Citrate-stabilised AuNPs were synthesised according to Liu and Liu (2006) [276]. Prior to synthesis, all glassware and stir bars were cleaned using Decon90 detergent (2%) and soaked in a dilute acid bath (0.2 M HCl) overnight, before being rinsed thrice with Milli-Q water. AuNPs were synthesised by adding 10 mL of sodium citrate (38.8 mM) to a boiling solution of $HAuCl_4$ (100 mL, 1 mM) with vigorous stirring. After the addition of citrate, the solution changed from pale yellow to gray blue and, finally, wine red. After 10 minutes, the heat was turned off and the solution was allowed to cool under continuous stirring for 20 minutes. The colloidal gold nanoparticles were then filtered (0.22-µm pore) and stored at 4°C.

6.2.4.1 Dynamic Light Scattering

Dynamic light scattering (DLS) was used to evaluate the size and distribution of the prepared nanoparticles. DLS size analysis was performed using the Zetasizer Nano ZSP (Malvern Panalytical Ltd., UK). The refractive index and absorption parameters were 0.2 and 3.32, respectively. DLS measurements were obtained by Dr James Minto at the University of Strathclyde.

6.2.4.2 Localised Surface Plasmon Resonance

The AuNP size and concentration were also estimated using the LSPR peak wavelength and the reference tables from Haiss *et al.* (2007) [277]. The LSPR peak wavelength (λ_{SPR}) was determined by measuring the absorption spectrum, which was then matched with reference values for AuNP sizing. The absorption spectrum was measured on the plate reader in triplicate wells containing 25 µL of the prepared AuNPs diluted to 80 µL with Milli-Q water from 450–850 nm in 5-nm steps. The λ_{SPR} was then determined from absorbance values measured from 510–530 nm in 1 nm steps.

The absorption ratio $A_{\lambda_{SPR}}/A_{450}$ – where $A_{\lambda_{SPR}}$ and A_{450} are the absorbance values at λ_{SPR} and 450 nm, respectively – was used to estimate the concentration of nanoparticles according to reference values. The $A_{\lambda_{SPR}}$ and A_{450} values were measured using 0.5 mL of the prepared AuNPs (neat) in triplicate with the Hach spectrophotometer with 1 cm path length.

6.2.5 Aptasensor Method Development

The aptasensor was adapted from a published method by Liu *et al.* (2015) for samples in minimal salts media [278]. Accordingly, the relevant parameters were optimised, including: the λ_{SPR} shift following aggregation, ionic strength (i.e., the sample volume) to induce aggregation, E2-binding aptamer, and reaction times. All reactions were conducted at room temperature and analysed by the plate reader. Unless specified otherwise, reactions contained 25 µL of the prepared AuNPs in a fixed total reaction volume of 80 µL.

6.2.5.1 Salt-Induced Aggregation

The λ_{SPR} shift following aggregation (λ_{Agg}) was determined by measuring the absorbance of triplicate wells from 450–850 nm in 5-nm steps. Initial estimates of λ_{Agg} were made using either 125 mM NaCl or 25 µL of MMB media to induce aggregation. The optimal ionic strength (I) was determined by adding a range of volumes of MMB to the AuNPs (Table 6.2). In addition, different volumes of NaCl were tested to capture a similar range of ionic strengths. Absorbance was recorded for triplicate wells at 519 nm and 700 nm every 5 minutes for 60 minutes to determine optimal aggregation time.

Table 6.2: The ionic strengths (I) tested for aggregation of AuNPs and the equivalent volume of sample (MMB media) or 250 mM NaCl solution required for an 80 µL reaction.

MMB Media (I = 345 mM)		NaCl (I = 250 mM)	
I (mM)	Vol. (µL)	I (mM)	Vol. (µL)
0	0	0	0
22	5	20	17.4
32	7.5	30	18.4
43	10	40	19.4
54	12.5	50	20.4
65	15	60	21.4
76	17.5	70	22.4

6.2.5.2 Aptamer Selection

Two aptamer sequences from the literature were evaluated (Table 6.1). Before selecting the optimal aptamer for E2 detection, the relationship between sample volume and the concentration of each aptamer was assessed. Three sample volumes (15, 20, and 25 µL) and four aptamer concentrations (0, 50, 100, and 150 nM, final conc.) were tested pairwise and in duplicate. Briefly, aptamer-stabilised AuNPs were prepared in microcentrifuge tubes by combining different concentrations of E2 aptamer with AuNPs and incubating for 10 minutes. The aptamer-AuNP mixtures were then added to a 96-well plate. Next, the appropriate volumes of Milli-Q water and MMB media were added to the wells for a total reaction volume of 80 µL. The reactions incubated for 30 minutes before recording absorbance at 519 nm and 700 nm.

After determining the aptamer-sample volume combinations which yielded the most similar stabilisation of the AuNPs against salt-induced aggregation, the dynamic range of the assay was estimated using a 10-fold dilution series of E2 (3.2 nM–320 µM) in MMB media. Preparation of aptamer-stabilised AuNPs and the aggregation reaction was conducted as per above. Absorbance was recorded at 519 nm and the λ_{SPR} specific to each sample volume/aptamer combination. The most suitable aptamer sequence was selected by comparing the dynamic ranges produced by each aptamer sequence. Finally, the amount of the selected aptamer required to stabilise the AuNPs against salt-induced aggregation was determined using a range of concentrations (25, 50, 75, 100, 125, and 150 nM).

According to the literature, the 35-base aptamer was expected to have a limit of detection several orders of magnitude lower than the 76-base aptamer [192, 279]. Therefore, a face-centered central composite design of experiments and optimisation by response surface methodology were used to confirm the ratios of AuNPs, sample volume, and aptamer concentration used were appropriate. The findings were ultimately inconsequential to the objectives of this chapter. Therefore, the detailed methodology and results for the aptasensor optimisation by design of experiments are provided in Appendix F for completeness.

6.2.5.3 Reaction Time

The optimal reaction time for concurrent E2-aptamer binding and AuNP aggregation was determined from the aggregation of a five-point calibration curve (20, 40, 80, 160, and 320 µM, duplicate wells), measured every 5 minutes for 30 minutes. The reaction time was optimised using 50 nM of 76-base aptamer and 15 µL of E2 calibration standards in MMB media. After optimising the reaction time, the linear range of the assay for E2 was further refined through trial and error.

6.2.5.4 Cyclodextrin Supplementation

Hydroxypropyl-β-cyclodextrin was added to increase the solubility of E2 in the working range of the assay. The effects of HPβ-CDX supplementation in MMB media on AuNPs and the aptasensor were first investigated by recording the absorbance spectrum (450–850 nm, 5-nm steps in duplicate wells) of the nanoparticles under different conditions: AuNPs stabilised with 50 nM of 76-base aptamer, with and without 160 nM E2, and AuNPs alone.

The optimal concentration of HPβ-CDX was then determined using a phase solubility test. The phase solubility test was conducted by adding 500 µM E2 to 2 mL of MMB media with the different HPβ-CDX concentrations (0, 0.1, 0.2, 0.5, 1, and 2%) in duplicate 15-mL glass test tubes. The tubes were incubated overnight (approximately 18 h), shaking 150 rpm at 30°C. The next day, the solutions were filtered through 0.45-µm PTFE syringe filters. The soluble E2 in the filtrate was measured in duplicate wells (100 µL) by fluorescence spectroscopy (280 nm excitation, 310 nm emission). Soluble E2 concentrations were determined using a calibration curve (0, 50, 100, 200, 300, 400, 500 µM E2 in MMB media without cyclodextrin), also measured in duplicate. Fluorescence spectroscopy was performed using the Tecan Infinite M200 Pro plate reader in black µClear® 96-well microplates (#655096, Greiner Bio-One, UK).

6.2.6 E2 Detection with Aptasensor

The finalised aptasensor method for measuring E2 was performed as follows. A stock of aptamer-stabilised AuNPs was prepared in a microcentrifuge tube by adding 100 nM E2 aptamer (40 µL per reaction) to the AuNPs (25 µL per reaction) and incubating for 10 minutes at room temperature. The aptamer-AuNP mixture was then added to a 96-well plate (65 µL per well). Next, 15 µL of sample or calibration standard in MMB media was added to the wells for a total reaction volume of 80 µL in duplicate and incubated for 30 minutes. The absorbance ratio at 620 nm and 519 nm (A_{620}/A_{519}) was used to evaluate aggregation from E2 detection in MMB media. The absorbance ratio at 615 nm and 519 nm (A_{615}/A_{519}) was used for detection in MMB media supplemented with 2% HPβ-CDX. Six calibration standards (5, 10, 20, 40, 80, and 160 µM E2) were used for quantification.

6.2.7 Standards Preparation

Six calibration standards and five QCs were prepared by diluting E2 stock solution (1 mg/mL in methanol) in MMB, with or without 2% HPβ-CDX (Table 6.3).

Table 6.3: Standards and quality controls used for the aptasensor method evaluation.

Std			QC		
Level	µM	mg/L	Level	µM	mg/L
S1	5	1.37	QC vH	160	43.58
S2	10	2.72	QC H	120	32.69
S3	20	5.45	QC M	30	8.17
S4	40	10.90	QC L	15	4.09
S5	80	21.79	QC vL	5	1.37
S6	160	43.58			

6.2.8 Aptasensor Method Evaluation

The aptasensor method was evaluated according to the International Conference on Harmonization (ICH) Guidelines M10 for method validation of ligand-binding assays [140]. Specific figures of merit included specificity, precision, linearity, range, accuracy and limits of detection and quantitation. Method evaluation was carried out by running a batch of six calibration standards in duplicate and five QC samples in triplicate, repeated on three separate days. Instrument limits of detection and quantitation were determined as per Section 3.2.7.4. Accuracy was determined by the percent error and the percent recovery of the five QCs measured in triplicate in three separate batches, as per Section 3.2.7.3.

6.2.8.1 Linearity

Linearity for each batch was determined using linear regression of the logarithm of the concentration ($\log_{10}(x)$) versus the absorbance ratio (y) of the calibration standards. The coefficient of determination (R^2) of the linear regression and the percent error of the standard concentrations were used to evaluate the linearity of the method, as per Section 3.2.7.1.

6.2.8.2 Precision

Precision was determined by the percent relative standard deviation (%RSD) of the five QCs measured in triplicate in three separate batches. Repeatability was evaluated by %RSD for the QCs within a single batch; the value reported is the mean repeatability for all three batches. Since the spectrophotometer readings are rapid (e.g., a 96-well plate in approximately 1 min.) and would occur immediately after sampling, repeatability was deemed a sufficient metric for

intra-assay precision. Inter-assay precision was evaluated by the %RSD for the QCs across all three batches.

6.2.8.3 Chemical Specificity

The chemical specificity of the aptasensor was tested against estrogens E1 and E3 at 160 µM. In addition, specificity was evaluated against the essential minimal media supplements established in Chapter 4: 2.5 µg/mL thiamine HCl, 0.1 mg/mL glucose, and 0.5 mg/mL sodium pyruvate.

6.2.8.4 Biological Selectivity

The selectivity of the aptasensor in the presence of potential interferences from biological samples was also evaluated. *C. tardaugens* 16702 and *N. europaea* 11850 were first pre-cultured individually as per Sections 4.2.4.1 and 4.2.4.2. *E. coli* MG1655 was not used in this work. The pre-cultured bacteria were then inoculated 1:100 into 10 mL of MMB media supplemented with 2% HPβ-CDX and 0.5 mg/mL pyruvate. Bacteria were cultured in serum bottles under aerobic conditions in the dark at 30°C, shaking at 150 rpm for one week. To evaluate selectivity, 15 µL samples of the cultures were analysed by the aptasensor in duplicate, with and without 160 µM E2 spiked in before analysis.

6.2.9 Effects of Bacteria on Aptasensor Response

The effects of the bacteria cultures on the aptasensor were further characterised. The absorption spectra and λ_{SPR} in the presence of the cultures were analysed as per Section 6.2.4.2. The pH and conductivity of the cultures were measured in triplicate using the Orion 5 Star multi-meter, the Orion 8156BNUWP pH probe, and Orion 013605MD conductivity cell (Thermo Fisher Scientific, UK).

6.2.10 Statistical Analysis

Analytical figures of merit and statistical analysis of the replicates (i.e., mean and standard deviation) were calculated in MS Excel. Plots were generated in R using ggplot2 package [221]. Optimisation by design of experiments were calculated in R using the rsm and nplr packages [280, 281].

6.3 Results & Discussion

6.3.1 Systematic Literature Review

A systematic literature review was performed to validate the decision to use AuNP-based biosensor with aptamer detection, as well as identify a suitable method from literature to adapt for our specific application of measuring estrogen concentrations in microbial cultures with degrading bacteria. A total of 73 articles were returned from Scopus and 119 articles were returned from WoS. The list of publications was further screened for the following inclusion criteria: original research articles in English using nanomaterials with either an aptamer or antibody targeting at least one of the listed contaminants; 51 Scopus articles and 72 WoS satisfied the inclusion criteria. After removing the duplicate articles returned by both databases, there were a total of 83 unique research articles. Publications which had cited the 83 articles were also independently reviewed, and an additional 24 articles were included. In the end, a total of 107 unique research articles for the EU Watch List's 8 non-pesticide contaminants of emerging concern from 2005–2020 were analysed. Articles studying more than one contaminant from the list were counted as a separate methods, resulting in 122 nanobiosensor methods.

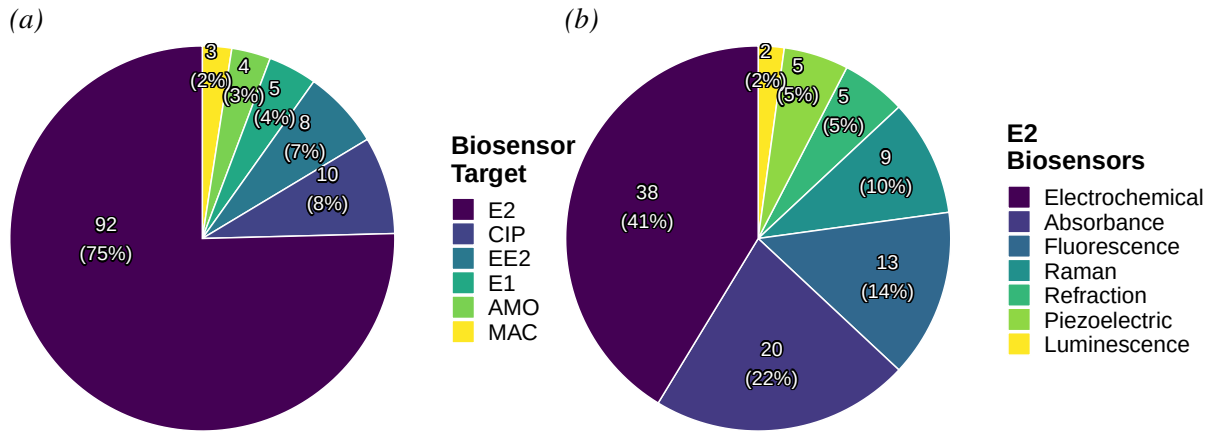

Figure 6.1: (a) The distribution of the target analytes for the nanobiosensor methods identified in the systematic literature review and (b) the distribution of detection methods used for E2. CIP – ciprofloxacin; AMO – amoxicillin; MAC – macrolide antibiotics.

The vast majority of emerging contaminant nanobiosensors were developed to target E2 (75%) (Figure 6.1a). Since the overwhelming majority of methods targeted the analyte of interest in this work, the remaining comparisons were done only with E2 nanobiosensors. The complete list of methods and associated metadata is provided in Appendix E. Most of the E2 nanobiosensor methods used a form of optical detection (53%), with absorbance (i.e., colorimetric) detection being the most prevalent (Figure 6.1b). However, electrochemical detection

was more common than any single optical detection technique (41%).

The number of publications which used antibodies marginally increased over time, with an average of one article per year from 2007–2013 and 3 articles per year from 2014–2020 (Figure 6.2a). After 2013, the number of publications which used aptamers greatly increased, with an average of 8 per year from 2014–2020. Aptamers were first developed in 1990 and had been used in biosensors since before 2014 [282]. However, the EU published several water policy documents relating to priority substances between 2012–2015, which was likely the impetus for publishing new nanobiosensor methods for emerging contaminants, including E2 [283–285]. In 2014 and 2015, E2 nanobiosensors primarily used electrochemical and absorbance detection, and the diversity in the detection methods increased over the next five years (Figure 6.2b).

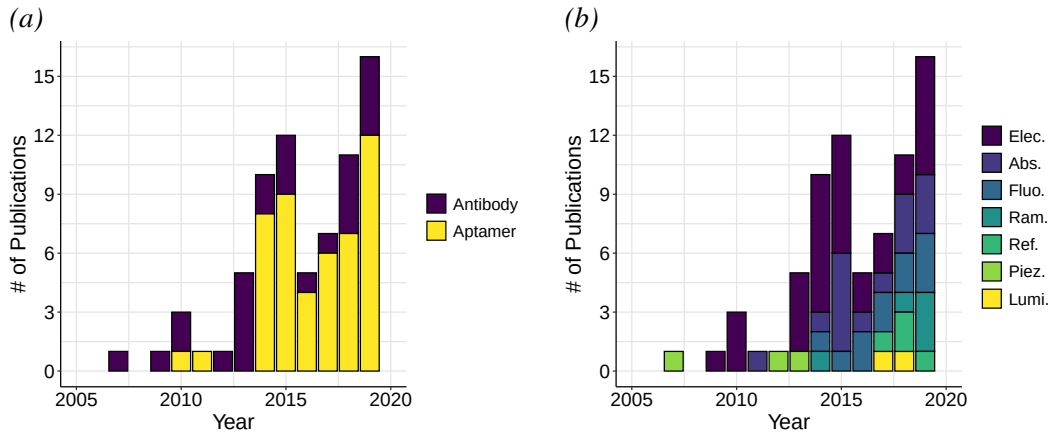

Figure 6.2: Number of E2 nanobiosensor publications from the systematic literature review by (a) bioreceptor and (b) detection method over time.

Overall, aptamers were used much more frequently than antibodies for E2 nanobiosensors ($n = 57$ versus $n = 28$; one study used both, Figure 6.3). Although antibodies possess high target affinity, DNA aptamers have a longer shelf-life and are easier to produce [282]. When aptamers were used as bioreceptors for E2, fluorometric sensors ($n = 12$) were about as common as colorimetric sensors ($n = 10$). Additionally, the reported limits of detection (LOD) for the absorbance methods were at least an order of magnitude greater than fluorescence and several orders of magnitude greater than electrochemical methods. A variety of methods were used to estimate LOD, including 3 times the signal-to-noise or 3 times the standard deviation of the blank (Appendix E). However, "noise" was usually not clearly defined (i.e., the mean or the standard deviation of the blank response). The majority of E2 nanobiosensors (55%) did not define how LOD was calculated, and in six cases, only visual observation was used.

The aptamer-based nanobiosensors ("aptasensors") which used fluorescence detection were highly diverse in the nanomaterials used, including graphene oxide [286], quantum dots [287],

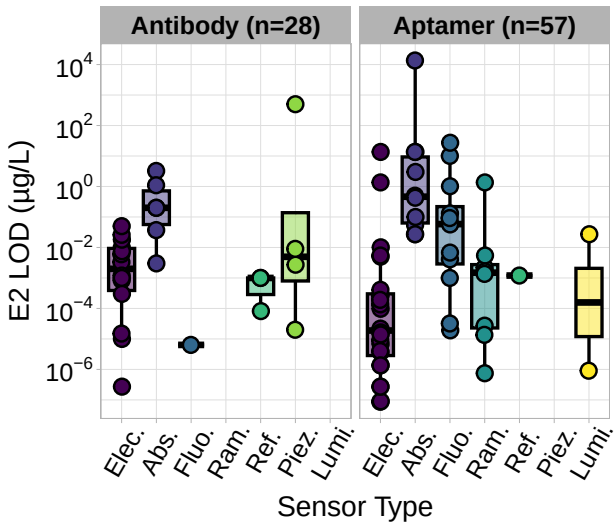

Figure 6.3: Reported limits of detection from the systematic literature review for E2 nanobiosensors. Points are the LOD of the individual nanobiosensor methods. Box plots show the median and the 25th and 75th percentile; whiskers show 1.5 times the IQR.

gold nanoparticles in conjunction with other nanomaterials [288–290], and silver nanoclusters [291]. In contrast, absorbance aptasensors for E2 were exclusively based on AuNPs (Appendix E). Although the reported LODs for E2 by fluorescence were generally lower than absorbance, the nanotechnology used for colorimetric aptasensors has clearly converged upon the use of AuNPs. Therefore, we expect that the colorimetric aptasensors for E2 should be reproducible.

The publications for colorimetric AuNP aptasensors used one of two available aptamers for E2. The first aptamer is a 76-base aptamer which was originally designed by Kim *et al.* (2007) for an electrochemical sensor [191]. The second is a 35-base aptamer which was designed by Alsager *et al.* (2015) for a colorimetric sensor [192]. In the study by Alsager *et al.* (2015), the authors showed that shorter aptamers were more sensitive in colorimetric AuNP sensors. Studies by Liu *et al.* (2015) and Alsager *et al.* (2015) tested other aptamers in parallel, but these were not used in further publications [192, 278]. At the time of this literature review, only three publications had used the 35-base aptamer, two of which were from the group which originally designed the aptamer [192, 200, 292].

Seven of the colorimetric E2 aptasensors were based on aggregation of colloidal AuNPs. The most common sensor design adsorbed single-stranded DNA (ssDNA) aptamers to the AuNPs before introducing the sample [192, 197, 200, 293]. As the aptamers preferentially bound to the target, they dissociated from the AuNPs, leaving the particles susceptible to salt-induced aggregation. Other method designs added sample containing the target to the aptamers before introducing the AuNPs [199, 278, 294]. In contrast, the study by Li *et al.* (2018) used dual AuNPs and upconversion nanoparticles (UCNPs) modified with either thiolated aptamers or comple-

mentary ssDNA (cDNA), cross-linking the particles into a pseudo-aggregated state [295]. The aptamer, which was immobilised onto the nanoparticle by covalent Au-SH bond, preferentially bound to the target and dissociated from the hybridisation complex. While the study by Li *et al.* (2018) used a more complex sensor design with UCNPs, the basic mechanism of deaggregation has been used for other colorimetric AuNP aptasensors [296]. The general mechanisms for AuNP aptasensors by deaggregation and aggregation are shown in Figure 6.4.

The E2 colorimetric aptasensors were primarily developed for samples in water. Alsager *et al.* (2015) demonstrated good assay performance using 100 µM E2 spiked in rat urine [192]. In addition, Chavez *et al.* (2014) developed a sensor which analysed E2 in buffer containing 33.3 mM Tris–HCl and 66.7 mM NaCl amongst other trace salts [293]. While the aptamer-target binding and AuNP aggregation are separate steps in the published methods, this approach is not suited for culture media buffered to support microbial growth. Therefore, we attempted to exploit the ionic strength of the culture media and combine sample addition and aggregation processes into a single step (Figure 6.5). In order to avoid prematurely aggregating the particles, the aptamers were added to the nanoparticles before sample addition.

The method by Liu *et al.* (2015) used the simplest approach of 1:1:1 volume ratios of AuNP/aptamer/sample, for a total reaction volume of 150 µL before aggregating with 10 µL of 2 M NaCl [278]. Therefore, a similar ratio – i.e., 31.25% (v/v) AuNPs with 68.75% (v/v) diluent – was used as the starting point for method development. Lastly, although the 76-base E2 aptamer has been used more frequently, the literature argues that shorter aptamers have better sensitivity [192, 278]. Therefore, both aptamers were evaluated empirically.

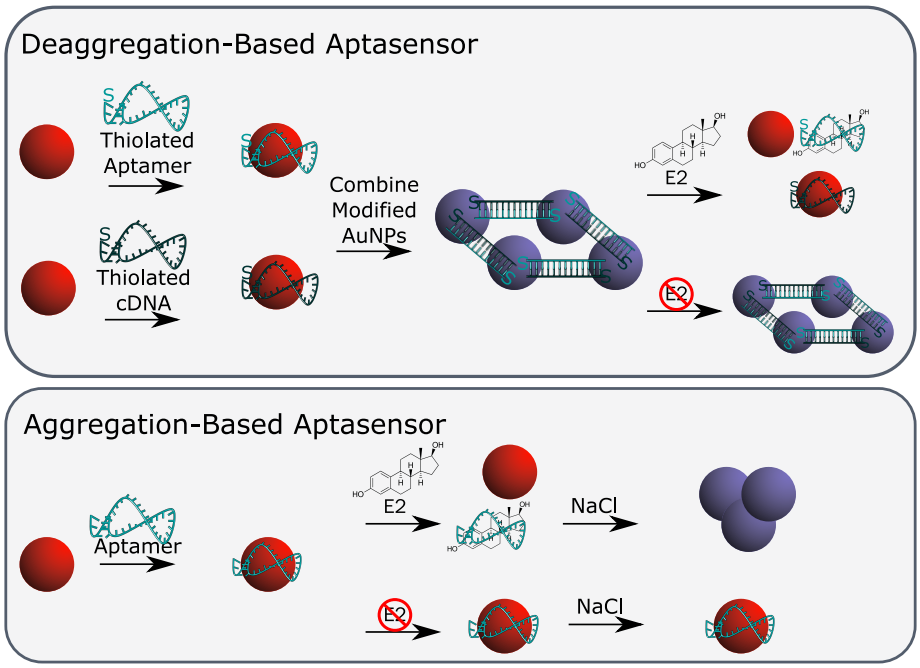

Figure 6.4: General mechanisms of colorimetric AuNP aptasensors. In the top panel, thiolated aptamers and cDNA are immobilised onto the AuNP surface. The aptamer and cDNA hybridise, cross-linking the AuNPs. The aptamer will bind to the present target (E2), separating from the cDNA and dispersing the particles. In the absence of E2, AuNPs remain cross-linked. In the bottom panel, the aptamer non-covalently adsorbs to the AuNP surface. The aptamer will bind to the present target, dissociating from the AuNP. The particles become susceptible to salt-induced aggregation. In the absence of E2, the AuNPs are stabilised against aggregation and remain dispersed.

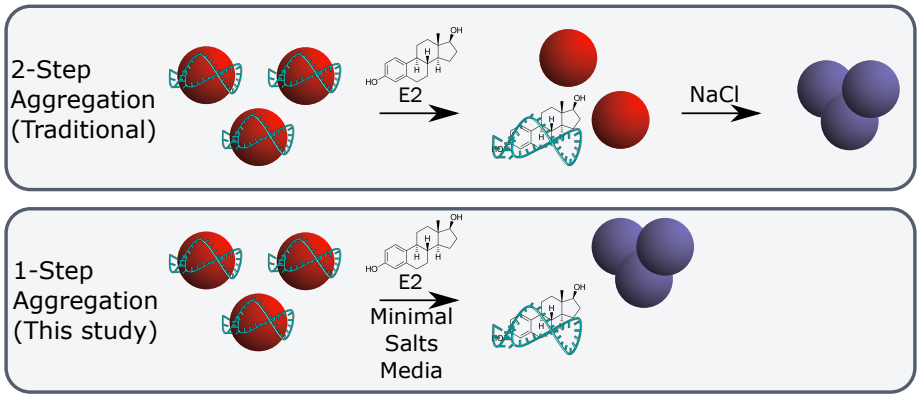

Figure 6.5: Mechanism of the proposed colorimetric AuNP aptasensor. In the top panel, the traditional method for colorimetric E2 sensing by aggregation following aptamer-E2 binding. In the bottom panel, the proposed method combines E2 detection with salt-induced aggregation by the sample of minimal salts media.

6.3.2 AuNP Characterisation

The size and concentration of the AuNPs were determined by several techniques. DLS analysis determined the cumulative average size of the nanoparticles to be 25 $\pm$ 5 nm and the polydispersity index (PDI) as 0.34 $\pm$ 0.06 ($n = 9$). The average particle size of the dominant peak (84 $\pm$ 9%) was measured as 25 $\pm$ 2 nm. Based on this index value, the AuNPs are classed as moderately polydispersed [297]. Although monodispersed particles (PDI < 0.1) are preferable, this did not appear to impact assay performance. The LSPR wavelength was determined to be 519 nm from the absorption spectrum (Figure 6.6). In addition, the absorbance ratio $A_{\lambda_{SPR}}/A_{450}$ was determined to be 1.50, which correlates with a particle diameter of 10 nm [277]. However, Haiss *et al.* (2007) measured the λ_{SPR} near 520 nm for 25 nm particles. The concentration was estimated using $A_{450}/\varepsilon_{450}$ to be 25.8 nM, where ε_{450} is the molar absorptivity for AuNPs of the calculated particle diameter (6.15×10^7 $M^{-1}cm^{-1}$ for 10 nm) [277]. The protocol used to synthesise the nanoparticles was designed to produce particles with 13 nm diameter and λ_{SPR} of 520 nm [276]. Although the true diameter could not be ascertained due to variable results depending on the sizing method, the intended λ_{SPR} for the gold nanoparticles was successfully obtained.

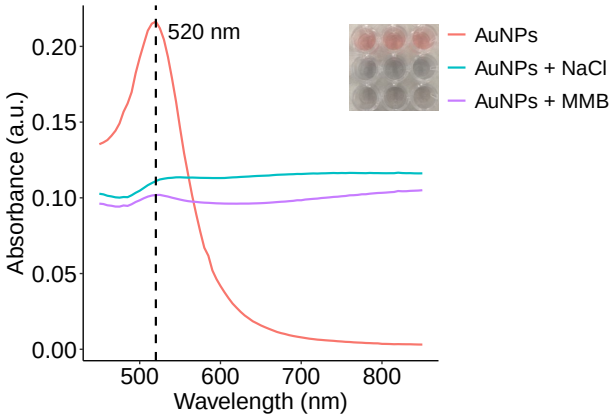

Figure 6.6: Absorption spectra of stable and aggregated AuNPs (mean, n=3). The red line represents stable nanoparticles, the blue line is AuNPs aggregated with 125 mM NaCl, and the purple line is AuNPs aggregated with 25 µL MMB (108 mM). Inset photo shows microplate wells containing stable AuNPs (top row), NaCl-aggregated (middle), and MMB-aggregated (bottom). The closest measured wavelength to λ_{SPR} (519 nm) is noted with the dashed line.

6.3.3 Aptasensor Method Development

The colorimetric aptasensor was developed for simultaneous target binding and gold nanoparticle aggregation. The approach in method development was generally consistent with colorimetric estrogen aptasensors from the literature [200, 278]. The λ_{SPR} and λ_{Agg} used for measuring

absorbance during method development varied depending on the analysis and reactions conditions. The rationale for the selected wavelengths are explained in the sections below, however, a summary is provided in Table 6.4 for convenience.

Table 6.4: Absorbance wavelengths used for the different analyses during method development.

Analysis	Reaction Reagents	λ_{SPR}	λ_{Agg}
Absorbance Spectra	AuNPs only AuNPs + Aptamer	520 nm	700 nm
	AuNPs + Aptamer + E2	520 nm	Varies[a]
Aggregation Response (A_{Agg}/A_{SPR})	AuNPs only AuNPs + Aptamer	519 nm	700 nm
	AuNPs + Aptamer + E2	519 nm	Varies[a]

[a]The λ_{Agg} for E2 detection was optimised for each aptamer concentration and sample volume. The different wavelengths used were 615 nm, 620 nm, 630 nm, 640 nm, or 645 nm.

6.3.3.1 LSPR Shift Determination

The first parameter optimised for the aptasensor method was selecting the absorbance wavelength which would capture aggregation of the nanoparticles. After adding an excess of NaCl and MMB to the particles, the resulting absorbance spectra did not reveal a clear LSPR band for the aggregated particles (Figure 6.6). This broadening of the LSPR is observed when particle aggregates exceed 100 nm, at which point peak wavelengths of the aggregates overlap and there is radiative damping of the electron oscillations [298]. Aggregation in colorimetric AuNP assays is often measured as A_{Agg}/A_{SPR}, where A_{Agg} is the absorbance at the red-shifted wavelength (λ_{Agg}) that increases in intensity with aggregation. To determine the optimum λ_{Agg}, first, the ratio A_λ/A_{520} was calculated for the absorbance across the spectrum (here, λ is 450 to 850 nm in 5-nm steps) for both stable and aggregated AuNPs (Figure 6.7a). Next, the difference between the NaCl- or MMB-aggregated and stable AuNPs was calculated (Figure 6.7b) as follows:

$$\Delta(A_\lambda/A_{520})_{\{\text{NaCl} \mid \text{MMB}\}} = \frac{A_{\lambda,\{\text{NaCl} \mid \text{MMB}\}}}{A_{520,\{\text{NaCl} \mid \text{MMB}\}}} - \frac{A_{\lambda,\text{ Stable}}}{A_{520,\text{ Stable}}}, \tag{6.1}$$

where {NaCl | MMB} indicates the calculation is performed for either NaCl or MMB aggregated particles. The difference between the absorbance ratio of between the aggregated and stable particles was used to ensure the largest dynamic range was used. Based on the results, 700 nm was selected as the optimum λ_{Agg}.

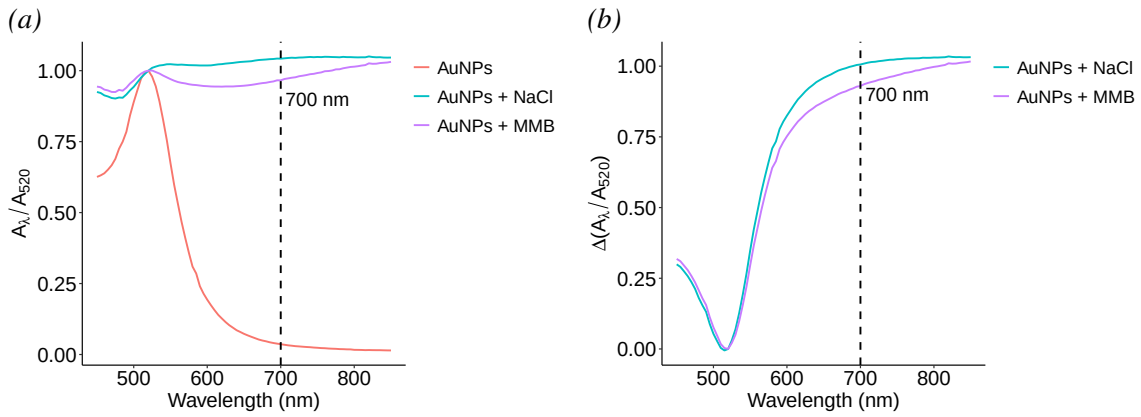

Figure 6.7: (a) Absorbance spectra normalised to the absorbance at 520 nm. (b) The normalised spectral difference between aggregated and stable particles. The red line represents stable AuNPs, blue lines show AuNPs aggregated with 125 mM NaCl, and purple lines show AuNPs aggregated with 25 µL MMB (108 mM). The selected λ_{Agg} is noted with the dashed line.

6.3.3.2 Salt Induced-Aggregation

This aptasensor design uses the ionic strength of the culture media to induce aggregation of the AuNPs. The ionic strength of the media (I_{MMB}) was calculated to be 345 mM by Equation 6.2:

$$I = 0.5 \sum_{i=1}^{n} c_i z_i^2, \tag{6.2}$$

where c is the molar concentration and z is the charge of each electrolyte (i). Based on this value, the ionic strengths in the AuNP aggregation reaction (I_{Rxn}) were calculated from the volume of MMB media sample (v_{MMB}):

$$I_{\mathrm{Rxn}} = \frac{I_{\mathrm{MMB}} \cdot v_{\mathrm{MMB}}}{v_{\mathrm{Rxn}}}, \tag{6.3}$$

with a total reaction volume (v_{Rxn}) of 80 µL. Thus, the optimal sample volume (and ionic strength) required to induce AuNP aggregation was determined from a range of 5–17.5 µL MMB (Figure 6.8). The minimum volume of sample required to rapidly induce aggregation was 15 µL, with an approximate I_{Rxn} of 65 mM (Figure 6.8c). A similar ionic strength of NaCl (60 mM) was required to induce complete aggregation. Interestingly, MMB of higher ionic strengths did not completely aggregate immediately as with NaCl (Figures 6.8a and 6.8b). Instead, aggregation gradually progressed for 30 minutes before plateauing. It is understood that different electrolyte properties – such as asymmetry, valency, and mixtures – can impact aggregation, which might explain the different kinetics from NaCl [299]. However, in this case, the critical coagulation concentration was roughly conserved regardless of the complexity of the ion solution.

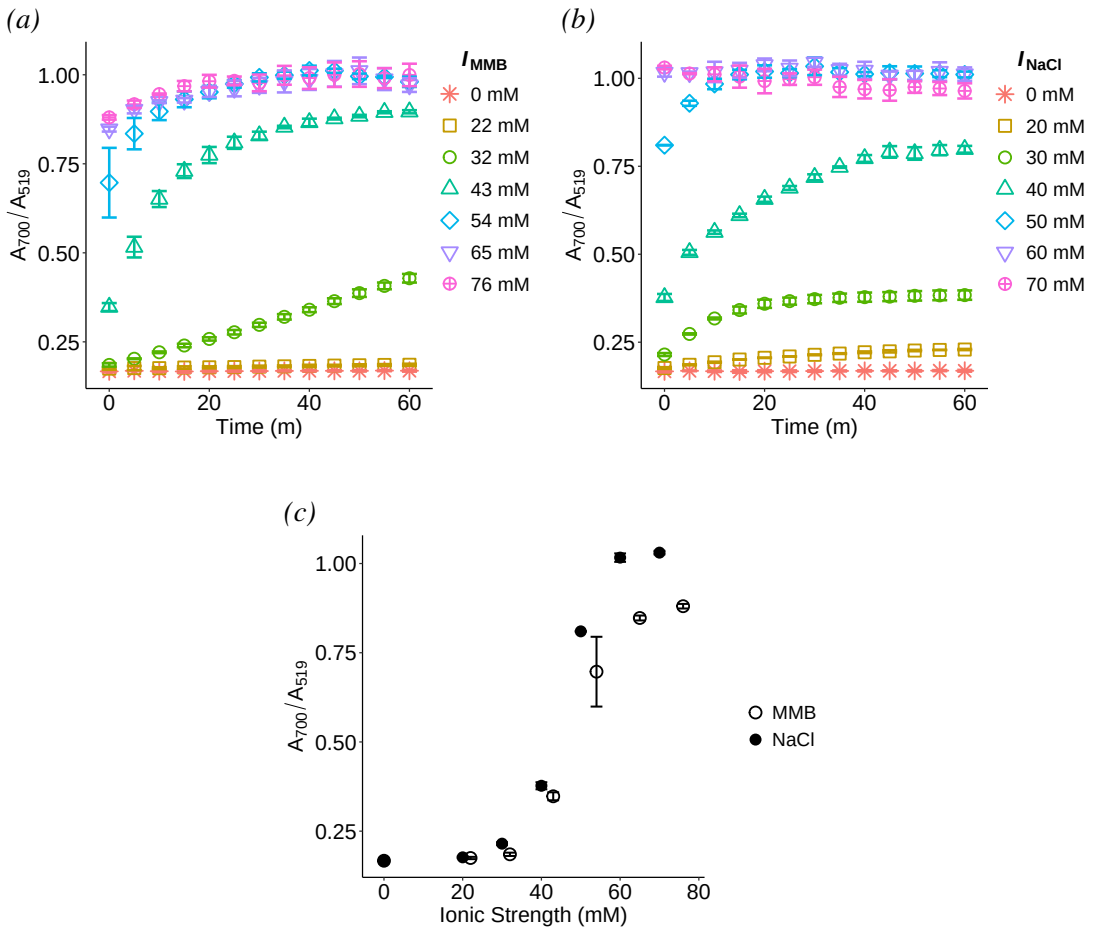

Figure 6.8: Salt-induced aggregation of AuNPs at different ionic strengths (a) of MMB or (b) NaCl over time. (c) Immediate (0 min) aggregation of AuNPs. Points are mean and error bars are standard deviation (n=3).

6.3.3.3 Aptamer Selection

The optimal volume of minimal salts media to induce rapid aggregation of the AuNPs (15 µL) was just 18.8% of the total reaction volume. This is considerably less than sample volume for the colorimetric E2 aptasensor developed by Liu *et al.* (2015), which used 50 µL of sample in a total reaction volume of 160 µL (31.25%) [278]. A smaller quantity of sample used for the aptasensor would mean that a smaller amount of analyte would be available for detection. In order to determine if the low sample volume would have an impact on sensitivity and the detection limit, a range of sample volumes and aptamer concentrations were compared for each aptamer (Figures 6.9 and 6.10).

The aptamer-sample volume combinations with the most similar degree stabilisation (i.e., the most similar A_{700}/A_{519} values) were selected to evaluate the effects of these reagents on the dynamic range. Here, "dynamic range" is the broad range of concentrations which produce a

concentration-dependent response, in contrast to the analytical range which is bounded by the calibration standards and is fit to the calibration equation. In analytical instrument detectors, high sensitivity (i.e., the slope of the response versus concentration) and low variance in the baseline (i.e., noise) improve the limit of detection [151]. For the aptasensor, the response of the blank is equivalent to an instrument baseline response. By using the combinations with a similar blank response, we are eliminating one of the variables which influences the limit of detection.

Of the 12 combinations tested using the 76-base aptamer (Figure 6.9a), 15 µL MMB with 50 nM of aptamer and 20 µL MMB with 100 nM of aptamer had the most similar stabilisation from aggregation in the absence of E2. These two conditions were further tested with a 10-fold dilution series of E2 (3.2 nM–320 µM) to determine the dynamic range (Figure 6.9b), i.e., the range between the maximum and minimum analyte concentrations which generate a detectable response.

In the presence of E2, aggregation following aptamer-target binding produced a clear shift in the LSPR peak wavelength (Figure 6.9c). This is in contrast to aggregation of AuNPs solely by MMB or NaCl, where no clear peak was observed (Figure 6.6). Following the same approach to determine λ_{Agg} as before, the aggregation wavelength was determined to be 620 nm for 15 µL MMB/50 nM aptamer combination and 645 nm for 20 µL MMB/100 nM aptamer combination (Figure 6.9c). Therefore, the optimal λ_{Agg} for each aptamer concentration/sample volume combination was used in estimating the dynamic range.

The dynamic range was estimated as the concentrations which generated a change in response (A_{Agg}/A_{519}), and the baseline was the concentrations which did not induce a change in response. Both aptamer concentration/sample volume combinations presented a dynamic range from 3.2–320 µM E2, which was linear using the logarithm of concentration (Figure 6.9b). The dynamic range for both conditions was comparable to the range reported in the study by Liu *et al.* (2015) for the same 76-base aptamer, which also used the log concentration to linearise the response [278]. While the dynamic ranges were similar, the 20 µL MMB/100 nM aptamer combination showed slightly higher sensitivity.

For the 35-base aptamer (Figure 6.10a), three combinations produced a similar stabilisation of the nanoparticles: 15 µL MMB/50 nM of aptamer; 20 µL MMB/100 nM of aptamer; 25 µL MMB/150 nM of aptamer. The conditions were tested with the same dilution series of E2 to determine the dynamic range (Figure 6.10b). The 15 µL MMB/50 nM aptamer and 25 µL MMB /150 nM aptamer combinations produced a similar dynamic range at 3.2–320 µM E2. However, the dynamic range for 20 µL/100 nM was only apparent from 32–320 µM E2. As with the 76-base aptamer, aggregation following E2 binding the 35-base aptamer produced unique LSPR shift for each sample volume/aptamer concentration combination (Figure 6.10c).

Broadly, the two aptamers had a very similar dynamic range and sensitivity (Table 6.5). The response range – i.e., the difference of the maximum and minimum A_{Agg}/A_{519} obtained

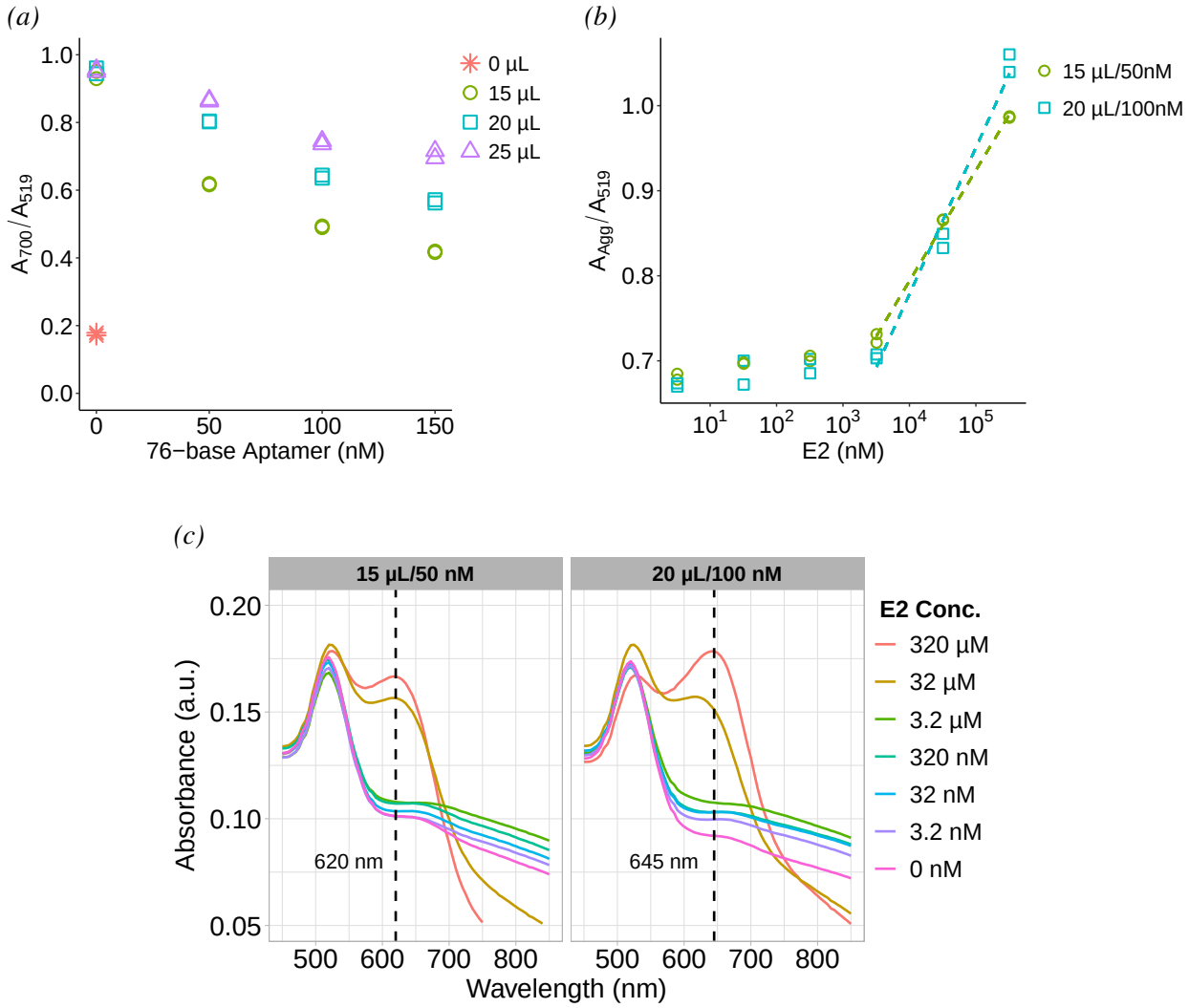

Figure 6.9: Effects of the 76-base aptamer concentration and sample volume on aptasensor dynamic range. (a) Aggregation of AuNPs varying aptamer concentration and MMB volume. (b) E2 dilutions using selected MMB volume/aptamer concentration combinations, shown with least-squares regression (dashed lines) to illustrate the dynamic range. Points are the individual measurements (n=2). (c) Absorbance spectra of AuNPs with E2 for the selected media volume/aptamer combinations. The λ_{Agg} for E2 detection by the specific sample volume-aptamer combination is indicated with the dashed line.

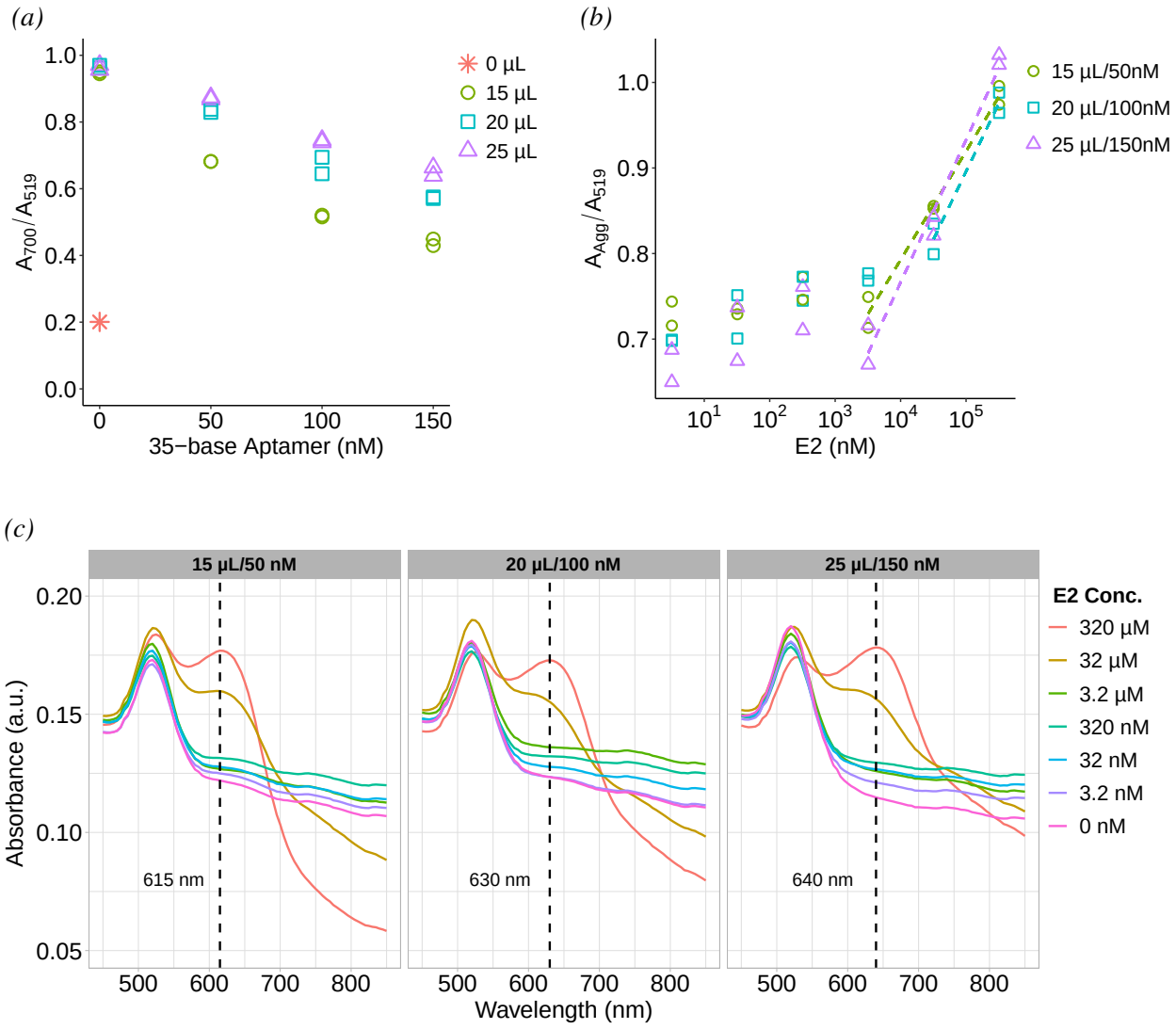

Figure 6.10: Effects of the 35-base aptamer concentration and sample volume on aptasensor dynamic range. (a) Aggregation of AuNPs varying aptamer concentration and MMB volume. (b) E2 dilutions using selected MMB volume/aptamer concentration combinations, shown with least-squares regression (dashed lines) to illustrate the dynamic range. Points are the individual measurements (n=2). (c) Absorbance spectra of AuNPs with E2 for the selected media volume/aptamer combinations. The λ_{Agg} for E2 detection by the specific sample volume-aptamer combination is indicated with the dashed line.

for the dynamic range – improved with higher sample volume and aptamer concentration. The sensitivity (i.e., the linear regression slope of the dynamic range) also increased with greater sample volumes and aptamer concentrations. However, increasing sample volume and aptamer increased the variability of the baseline. This would have a detrimental effect on the limit of detection, which is proportional to the error of the blank.

Table 6.5: Dynamic range properties for the sample volume/aptamer concentration combinations evaluated.

E2 Aptamer	Volume/Aptamer Comb.	Dynamic Range	Response Range	Sensitivity	Baseline %RSD
76-base	15 µL/50 nM	3.2 – 320 µM	0.260	0.130	3.00
	20 µL/100 nM	3.2 – 320 µM	0.345	0.172	4.68
35-base	15 µL/50 nM	3.2 – 320 µM	0.254	0.127	3.25
	20 µL/100 nM	32 – 320 µM	0.159	0.159	5.52
	25 µL/150 nM	3.2 – 320 µM	0.333	0.167	8.29

In the literature, the aptamer and salt concentrations are optimised separately, since salt-induced aggregation is a distinct step from sample addition [278]. Since this is a novel attempt at concurrent aptamer-ligand binding and salt-induced aggregation, the combined effects of aptamer concentration and ionic strength/sample volume were explored in detail. The relationship between AuNP concentration, aptamer concentration, and sample volume was investigated further with the 35-base aptamer in Appendix F by design of experiments. The results, which are presented in full in Appendix F, established that while the combination of 25 µL AuNPs, 25 µL sample volume, and 100 nM of 35-base aptamer produced the best sensitivity, the lowest estimated detection limit (582 nM) was three orders of magnitude greater than the literature – 0.2 nM E2 reported by Alsager *et al.* (2015) and 0.1 nM E2 by Pu *et al.* (2019) [192, 200].

Although the dynamic range for both aptamers was comparable, the 76-base aptamer was selected to carry forward in method development, as it has been used more widely in the literature [197, 278]. In addition, the 76-base aptamer performed better than the 35-base aptamer in the dynamic range metrics (Table 6.5). Lastly, the concentration of 50 nM of 76-base aptamer was confirmed as suitable for AuNP stabilisation against salt-induced aggregation (Figure 6.11a).

6.3.3.4 Reaction Time

This aptasensor method was designed for buffered samples where the ligand-aptamer binding occurs simultaneously with aggregation of the particles. The optimal colour development time was determined by evaluating the aggregation of 5 different concentrations of E2. Aggregation at the lowest concentration (20 µM) had stabilised by five minutes, however, higher concentrations continued to aggregate for up to 25 minutes (Figure 6.12a). In addition, linear regression

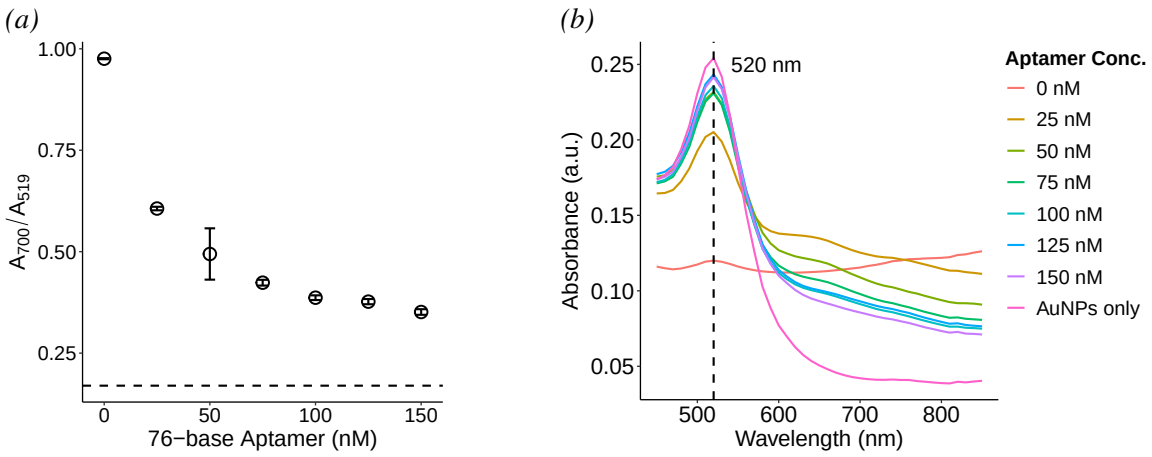

Figure 6.11: (a) Stabilisation of the AuNPs with 76-base aptamer against 15 µL MMB. Points are mean and error bars are standard deviation (n=3). The dashed line indicates the response of AuNPs without MMB. (b) Spectra of the aptamer-stabilised nanoparticles in the presence of 15 µL MMB; control AuNPs without added MMB are included for comparison (mean, n=3).

was performed at each time-point, and good linearity (R^2 >0.97) of the concentrations versus response was achieved within 10 minutes after sample addition (Figure 6.12b).

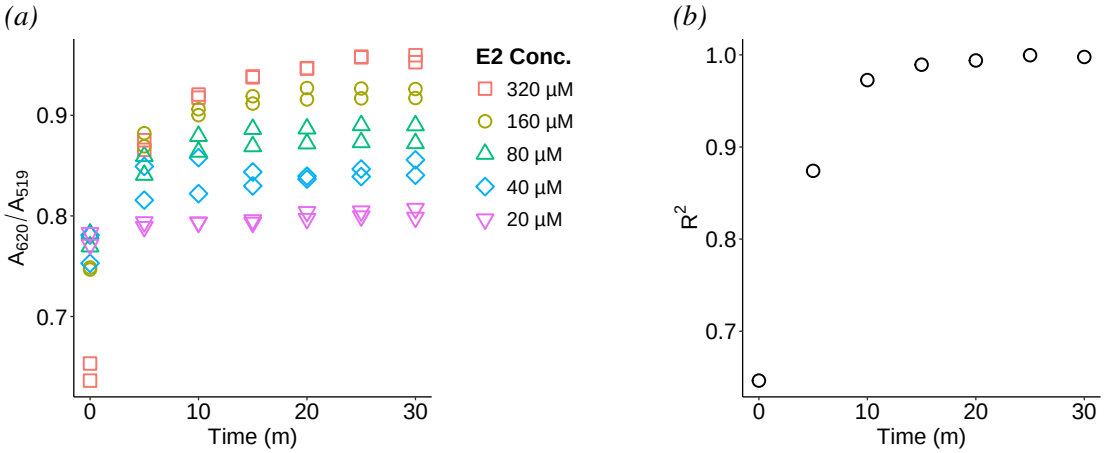

Figure 6.12: Optimisation of the color development time. (a) Aggregation of 5 concentrations of E2 over time. Points are the individual measurements (n=2). (b) The R^2 values from linear regression of the same five E2 concentrations.

The spectrophotometer requires about 2 min to record a full 96-well plate, and the time delay between the calibration standards' measurement and the samples could affect the accuracy of higher concentrations if the reaction has not concluded. Although good linearity was achieved within 10 minutes, a 30-minute incubation following sample addition was selected to ensure complete aggregation without sacrificing the speed of the assay to an appreciable extent.

This decision was motivated by the time required for bare AuNPs (i.e., no bound aptamers) to completely aggregate in the presence of MMB, with no observable change in $A_{\text{Agg}}/A_{\text{SPR}}$ after 30 minutes (Figure 6.8a).

6.3.3.5 Cyclodextrin Supplementation

The dynamic ranges observed during the aptamer selection process revealed that the working range of the assay is largely above the solubility limit of E2. The reported solubility limit of E2 in water is 3.6 mg/L (13.2 μM) [300]. Preliminary work showed that while higher concentrations of E2 could be analysed immediately, 100 μM E2 in MMB media precipitated within 24 h. This presented an obstacle for the intended application, as biodegradation experiments may be conducted over extended periods. Therefore, in order for the aptasensor to be fit for purpose, a cyclodextrin (CDX) was included to provide E2 solubility and stability at high concentrations. Since 2% (w/v) HPβ-CDX was shown to not interfere with E2 biodegradation (see Chapter 4), this cyclodextrin was included here to solubilise E2 above its natural limit in aqueous solution.

Media supplemented with 2% HPβ-CDX did not aggregate the gold nanoparticles, even without aptamer (Figure 6.13). Thus, E2 was not detectable when 2% HPβ-CDX was added to the media. A ten-fold dilution of HPβ-CDX permitted aggregation of the AuNPs and detection of E2. However, the absorbance intensity at λ_{SPR} was reduced compared to MMB media without cyclodextrin. The modification of AuNPs with CDX is well-documented in the literature; it is used as a capping agent to stabilise AuNPs and to aid in controlling particle size distribution during synthesis [301–303]. Colorimetric assays based on CDX-capped AuNPs – i.e., where the cyclodextrin has been immobilised onto the particle surface – were based on aggregating AuNPs by cross-linking the target analyte-CDX inclusion complexes[301, 302]. This mechanism was not considered for this application since CDX is a non-specific receptor. However, there is limited information available about the effects of CDX as a mediator for target analyte solubility within an AuNP-based colorimetric aptasensor.

The phase solubility test showed 0.2% HPβ-CDX maintained a solution of 360 ± 10 μM E2 (Figure 6.14). The next lowest concentration tested (0.1%) maintained 190 ± 10 μM E2 in solution, and 12 ± 3 μM E2 was recovered without any added cyclodextrin. Although 0.1% HPβ-CDX would be sufficient for the aptasensor linear range (5–160 μM E2), a working concentration at 0.2% HPβ-CDX was selected to ensure E2 solubility in the presence of biological material and potential interferences. In addition, the λ_{Agg} shifted slightly to 615 nm for detecting E2 in MMB with 0.2% HPβ-CDX (Figure 6.15a). The dynamic range of the aptasensor was unaffected by including the selected concentration of CDX (Figure 6.15b).

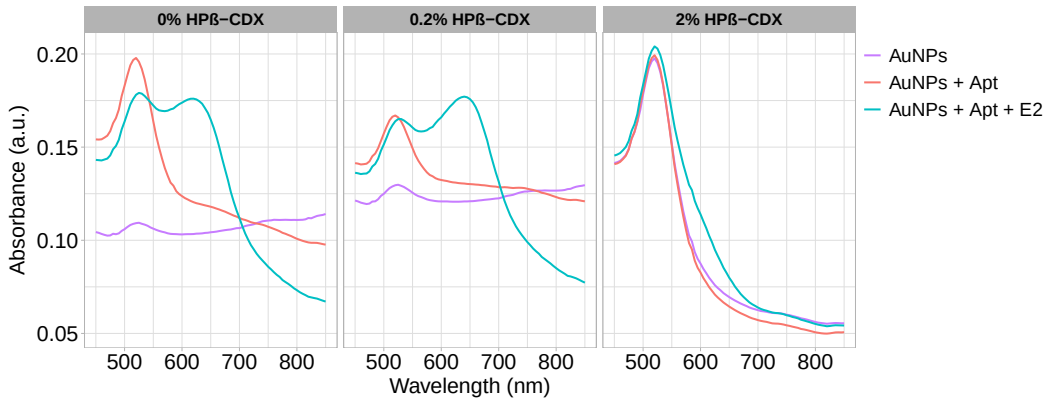

Figure 6.13: Absorbance spectra demonstrating the effects of HPβ-CDX on the aptasensor. MMB media containing 0, 0.2, or 2% HPβ-CDX was added to the following conditions in duplicate: AuNPs only; AuNPs with 50 nM aptamer; or AuNPs with aptamer and 160 µM E2.

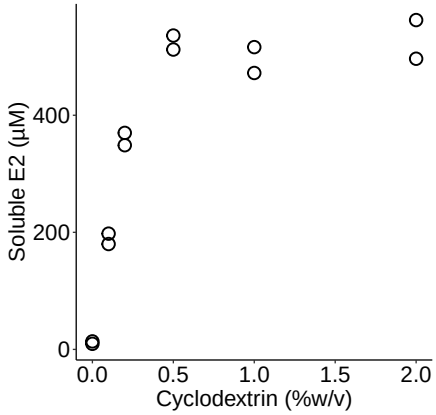

Figure 6.14: Phase solubility test of 500 µM E2 in MMB media with HPβ-CDX. Points are individual measurements (n=2).

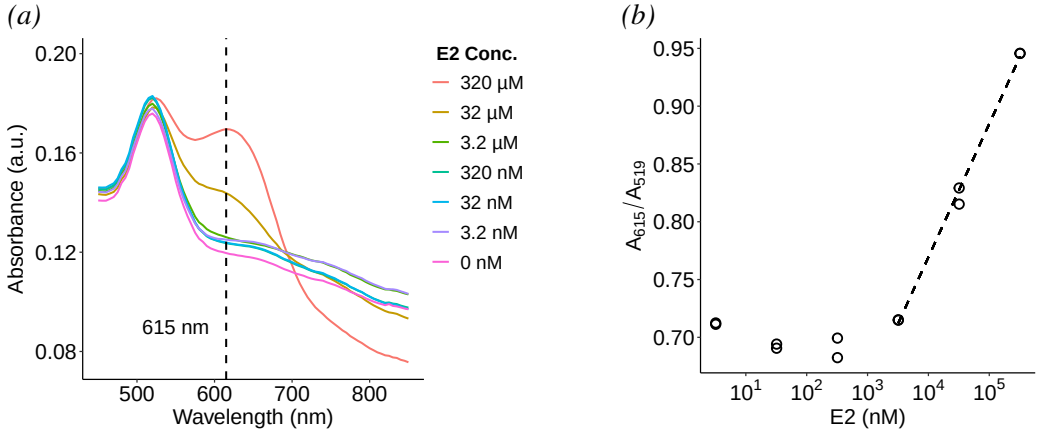

Figure 6.15: (a) Absorbance spectra of AuNPs with E2 in MMB with 0.2% HPβ-CDX. The new λ_{Agg} is indicated with the dashed line. (b) E2 dilutions in 0.2% HPβ-CDX, shown with regression (dashed line) to illustrate the dynamic range. Points are individual measurements (n=2).

6.3.4 Aptasensor Method Evaluation

The aptasensor method was evaluated following the ICH Guidelines M10 for ligand binding assays [140]. Although the developed aptasensor method requires an additive to fully solubilise E2 in the working range of the assay, concurrent target binding and AuNP aggregation has not yet (to our knowledge) been reported in the literature. Therefore, the method was evaluated both with and without the use of 2% HPβ-CDX using the appropriate λ_{Agg} – 620 nm for neat MMB and 615 nm for MMB with 2% HPβ-CDX. The figures of merit for the aptasensor method using only MMB media or MMB supplemented with cyclodextrin are summarised in Table 6.6. The aptasensor has a logarithmic relationship between response and concentration and is linearised by using the log of the concentration. Therefore, the figures of merit for accuracy and calibration statistics are given for the log value of the concentration, where the reported LOD and LOQ are the antilog concentration values.

Table 6.6: Results of E2 aptasensor method evaluation using standards in MMB media, with and without 2% HPβ-CDX supplement.

		Precision		*Accuracy*		*Calibration Statistics*		
Sample Matrix	QC	Repeat.	Inter-Assay	% Recovery	% Error	LOD	LOQ	R^2
Neat MMB	vH	0.2–2	1	97	4.8	**2.0 ± 0.3** 0.5 ± 0.1	**9 ± 4** 2 ± 1	0.986 ± 0.006
	H	0.3–1	2	99	3.6			
	M	0.3–3	3	96	6.5			
	L	1–3	3	100	8.9			
	vL	7–20	10	10	90			
MMB with 2% HPβ-CDX	vH	0.2–2	2	94	5.7	**3 ± 1** 0.9 ± 0.3	**50 ± 50** 10 ± 10	0.96 ± 0.02
	H	0.5–2	1	95	5.5			
	M	2–6	4	110	10			
	L	1–6	4	110	11			
	vL	4–6	4	120	37			

Precision values are percent relative standard deviation; repeatability is the range of %RSD within the three individual batches. Limits of detection (LOD) and quantitation (LOQ) are reported in micromolar (**bold**, top values) and mg/L (bottom values). Linearity and limit values are the means of the three different batches (n=3) and include standard deviation (± value).

The analytical performance of the aptasensor showed good precision and accuracy for most of the linear range, except for the lowest QC at 5 µM. Per the ICH Guidelines, ligand binding

assays should have a precision and accuracy within 20% RSD or error (25% permitted for lowest QC), respectively. In addition, the aptasensor showed linearity on three different batches, with an average $R^2 > 0.96$, however, not to the degree observed with the chromatographic ($R^2 > 0.992$) or fluorometric methods ($R^2 > 0.996$) from the previous chapters. A pooled calibration curve for the three batches is shown in Figure 6.16. In the literature, AuNP-based aptasensor responses are fitted using linear regression, however, other ligand-binding assays are commonly fitted using 4- or 5-parameter logistic models [140]. Since anchor calibration points near the upper and lower limits were not included, a nonlinear curve could not be accurately fit for comparison.

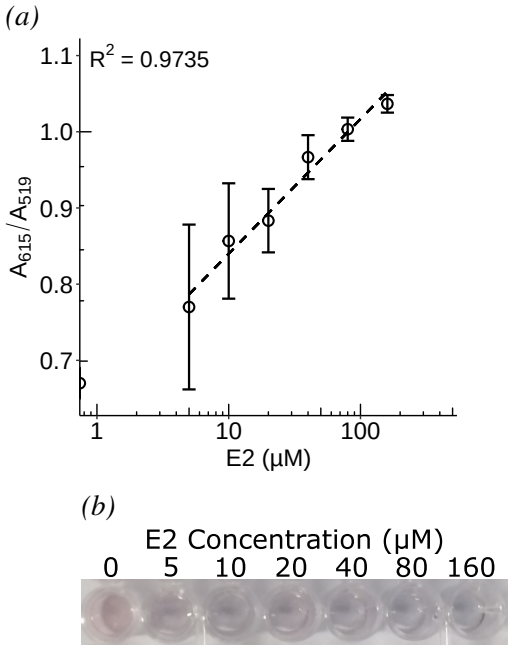

*Figure 6.16: (a) Calibration curve of the developed aptasensor for E2 in MMB media with 2% HP*β*-CDX. Points are the mean of calibration standards measured in three batches and error bars are standard deviation. Point on the y-axis represents the the blank. (b) Photo of the calibration standards' microplate wells.*

The method detection limits were comparable for MMB media with (3 ± 1 μM) and without cyclodextrin (2.0 ± 0.3 μM). The LOD and LOQ values obtained in this work are greater than some colorimetric aptasensor methods using the same 76-base E2 aptamer from the literature. This may be due to different approaches used in establishing the detection limit. In the study by Liu *et al.* (2015) – which this assay design drew heavily upon – the reported LOD is 0.01 mg/L (0.037 μM). However, their LOD determination was done primarily by visual observation, and the presented linear dynamic range actually appears to fall between 1–100 mg/L (3.7–367 μM), which would be in closer agreement with our results [278]. The method by Li *et al.* (2015) used a more conservative NaCl concentration (10 mM) and whose response was the decrease in A_{SPR}

rather than the more prevalent A_{Agg}/A_{SPR}, reported an LOD of 3 µg/L (0.01 µM) [199]. However, this approach had a narrower concentration range (10-90 µg/L) and response range (<0.1 units). The dynamic range observed by Kim *et al.* (2011) was between 10–100 µM, with a visual LOD of 50 µM [197]. Thus, we can conclude the developed method's detection limit approximately corresponded with at least two independent studies from the literature [197, 278].

6.3.4.1 Chemical Specificity

According to ICH Guideline M10, ligand-binding assay specificity is where "the binding reagent specifically binds to the target analyte but does not cross-react with coexisting structurally related molecules" [140]. Therefore, other estrogens, as well as the specific media supplements used in culturing the bacteria, were used to assess chemical specificity against potential abiotic interferences. The aptasensor responded to the major natural forms of estrogen, with a comparable response between 160 µM E2 and E1 (Figure 6.17). This aptamer has been shown to bind specifically to E2 compared to E1 and E3 in several published aptasensors from the literature [199, 278, 294, 304], however, previous observations from Nasri (2020) found that the aptamer responds to other estrogens [305]. Although the aptamer was not specific for E2, the aptasensor could be used as a general estrogen sensor which could detect estrogenic metabolites.

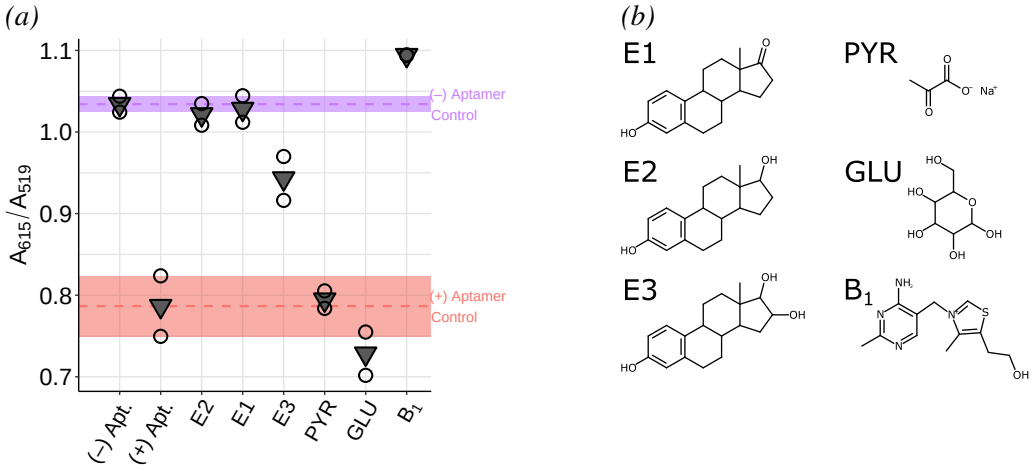

Figure 6.17: (a) Chemical specificity of the developed E2 aptasensor against other estrogens and media supplements. Empty circles are the individual measurements (n=2), and the inverted triangles are the mean of the two points. Blank media added to AuNPs with (+) or without aptamer (−) were included as controls; the control responses' means and standard deviations are indicated with the dashed line and shaded region, respectively. (b) Structures of the chemicals tested for selectivity.

In addition, the aptasensor produced a strong response for thiamine (B_1). Interestingly, the response to thiamine was greater than the aptamer-free control for aggregation. Thiamine is capable of inducing aggregation of bare citrate-capped AuNPs [306]. Thus, the energy barrier

for aptamer-bound particle aggregation appears to be surpassed by the combination of thiamine and the media salts. Because thiamine is an essential vitamin for *E. coli* MG1655 growth, this strain could not be used to evaluate biological selectivity.

6.3.4.2 Biological Selectivity

The ability of the aptasensor to detect E2 in the presence of biological interferences – such as bacteria cells and the biomolecules bacteria secrete into the media – was assessed using estrogen-degrading reference strains *C. tardaugens* 16702 and *N. europaea* 11850, with and without 160 µM E2 spiked in immediately before measurement. Without the addition of E2, the bacteria culture showed a reduced response compared to sterile MMB media, as evidenced by the A_{615}/A_{519} values below the E2-free media control (Figures 6.18b and 6.18c).

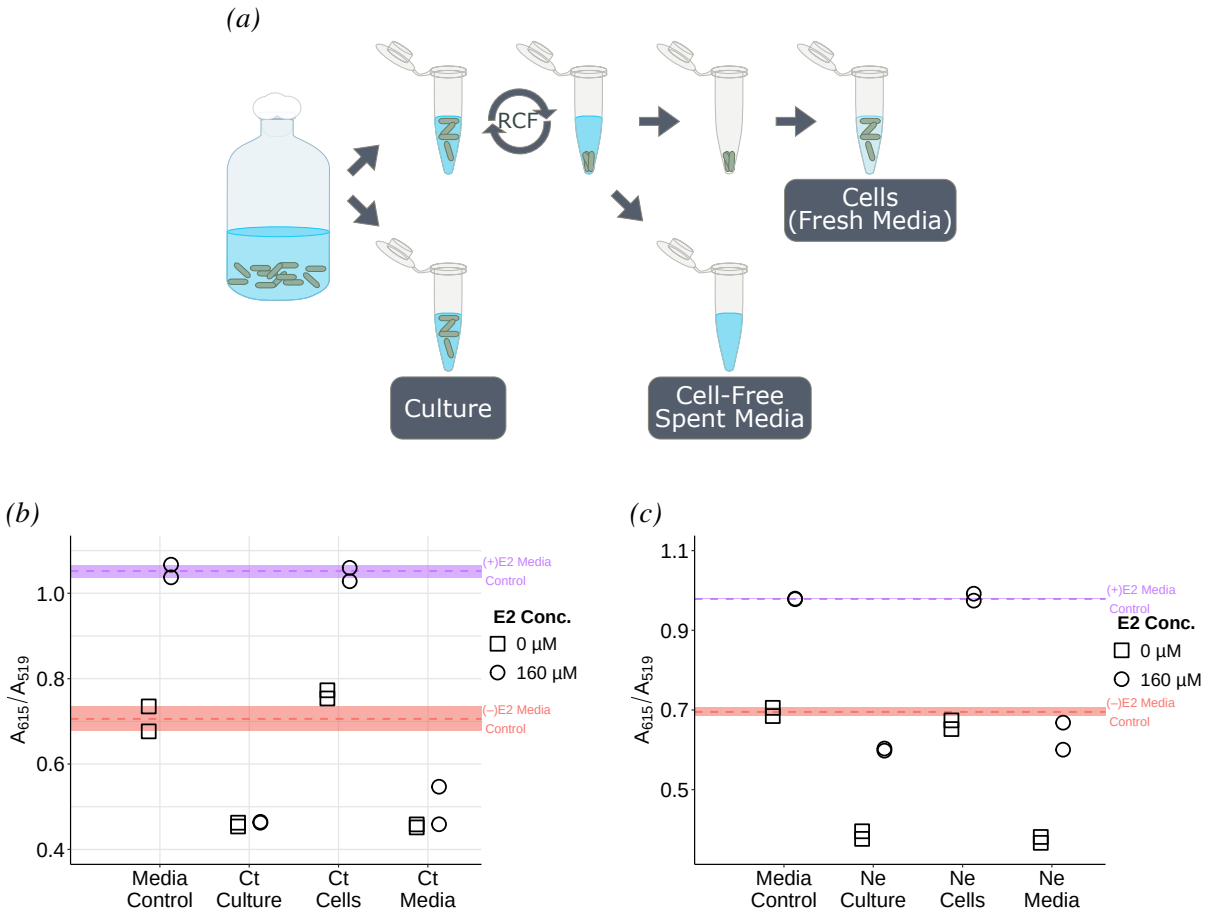

Figure 6.18: (a) Schematic of preparing samples for selectivity; (RCF–centrifugation). Aptasensor selectivity of E2 detection in the presence of (b) C. tardaugens or (c) N. europaea culture components. Points are individual measurements (n=2). The media control responses' mean and standard deviation are indicated with the dashed line and shaded region, respectively. Ct–C. tardaugens, Ne–N. europaea.

In the presence of MMB media, aptamer-bound AuNPs destabilise to a small degree, as evidenced by the increase in absorbance >600 nm shown in Figure 6.11b. However, the bacteria cultures showed an impeded ability to induce aggregation of the AuNPs. By separating the bacteria from the spent media, it was revealed that this was due to changes to the culture media rather than the bacteria cells.

After spiking the cultures with E2, there was a reduced response to E2 compared to the E2-negative bacteria cultures, particularly for *C. tardaugens*. In *C. tardaugens* culture, E2 was completely undetectable, while in the cell-free media, a weak response was observed (Figures 6.18b). The aptasensor produced a slightly greater response to E2 when spiked in *N. europaea* culture; however, the response was substantially lower than an equivalent concentration of E2 in sterile MMB (Figures 6.18c). Interestingly, the mechanisms for disruption appear different for the two strains.

6.3.5 Effects of Bacteria on Aptasensor Response

The inhibition of the aptasensor response by bacteria cultures was further investigated. First, the λ_{SPR} of the AuNPs in the presence of culture media with the bacteria removed was confirmed as unchanged (Figure 6.19a). Neither the aptamer nor cyclodextrin were included to exclude any other sources of stability for the gold nanoparticles. Thus, we can confirm the λ_{SPR} of 519 nm remains appropriate for the aptasensor response.

Since the AuNPs failed to aggregate even without aptamer stabilisation, two potential reasons were explored: the loss of ionic strength in the media or the release of some metabolite by the bacteria which increases the stability of the AuNPs against salt-induced aggregation. Both possibilities could account for the increased energy barrier to aggregation. The loss of ionic strength was tested by adding an excess of salt with 15 µL of sterile MMB media to the AuNPs in addition to 15 µL of culture sample (Figure 6.19b). The AuNPs with *N. europaea* culture media successfully aggregated with excess MMB media (a total of 30 µL of MMB media in 110 µL reaction), which suggests that there was a loss of ionic strength in the *Nitrosomonas* culture. This theory is supported by the impeded response to E2 observed in Figure 6.18c.

Conversely, aggregation remained inhibited with the *C. tardaugens* culture media when an excess of MMB media was added. This suggests that *C. tardaugens* had likely introduced something into the media which prevented the nanoparticles from aggregating. The different mechanisms for aptasensor inhibition explain the difference in the responses by the two strains observed in Figures 6.18b and 6.18c. Unlike with *N. europaea*, the aptasensor response did not change with E2 spiked in the *C. tardaugens* culture and spent media.

After the general mechanisms for aptasensor interference by *N. europaea* and *C. tardaugens* were identified, the specific causes for loss of ionic strength or AuNP passivation by bacterial

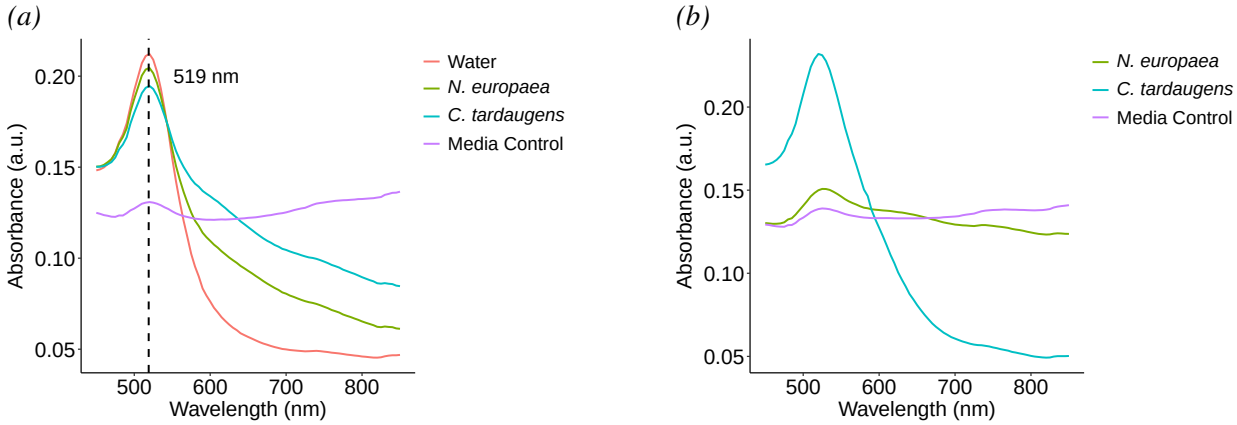

Figure 6.19: (a) Absorbance spectra of bare AuNPs in the presence of water, MMB media, or the cell-free media of bacteria cultures (mean, n=3). (b) Absorbance spectra of bare AuNPs in the presence of the cell-free media after supplementing with an additional 15 µL MMB (mean, n=3).

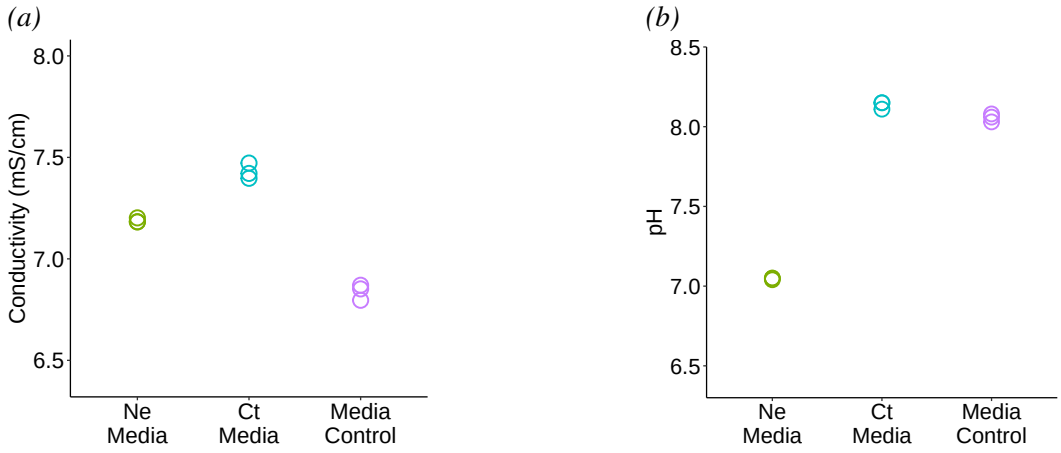

Figure 6.20: (a) Conductivity and (b) pH of the spent media. Points are the individual measurements (n=3). Ne–N. europaea, Ct–C. tardaugens.

metabolites were investigated. The loss of ionic strength was first evaluated by measuring conductivity and pH of the culture media. *C. tardaugens*'s culture media had greater conductivity than *N. europaea*, however, the conductivity of the two cultures were greater than the sterile media control. This may be due to the evaporation of the media increasing the salt concentrations; the sterile media was not incubated alongside the cultures. Since the sterile media was capable of aggregating the AuNPs, conductivity was not linked to the loss of aggregation potential. The pH of *N. europaea* was approximately one unit less than both the control and *C. tardaugens*'s culture media. Ammonia oxidation into nitrite by *Nitrosomonas* is an acidifying process which is mediated by ammonia monooxygenase (AMO) and hydroxylamine oxidoreductase (HAO)

enzymes [307]:

$$NH_3 + O_2 + 2H^+ + 2e^- \xrightarrow{AMO} NH_2OH + H_2O \xrightarrow{HAO} NO_2{}^- + 5H^+ + 4e^- \cdot \quad \text{(R6.7)}$$

The main components of MMB media are ammonium sulphate (10 mM) and potassium phosphate (43 mM), with a total [PO_4^-] of 50 mM. While NH_4^+ and SO_4^- would not be affected by the pH change, $H_2PO_4^-$ has a pKa of 7.20. Solvent composition – particularly, the types and concentrations of constituent electrolytes – has a significant impact on nanoparticles' surface charges and colloidal stability. A study by Afshinnia and Baalousha (2017) noted that phosphate ions can substitute with citrate ions on citrate-stabilised silver nanoparticles [308]. As ammonia oxidation decreased the media pH below 7.20, the charge of the dominant phosphate species changed from -2 to -1, altering the surface charge of the AuNPs.

The surface charge of nanoparticles affects their energy barrier to aggregation. A review by Wagner *et al.* (2014) on nanoparticle behaviour specifically noted that "adsorption of ions onto the NP surface can modify the surface charge of a particle, even if the ionic strength does not change" [309]. Therefore, we can reasonably conclude that the decreased sensitivity of the AuNPs to aggregation by *N. europaea*'s culture media was due to changes of the surface charge of the phosphate anions as a result of media acidification by microbial metabolism. Bacteria commonly alter the pH of their environment during growth, and therefore, this interference presents broad implications for the application of this aptasensor design in microbial samples [310].

Next, we revisited the literature for possible explanations of the interference by *C. tardaugens*. However, nanobiosensors for estrogens and other organic micropollutants are usually studied in the context of environmental and food matrices, not microbiological samples. Therefore, we looked specifically for colorimetric nanobiosensors of microbial metabolites; microbial toxins, in particular, are a popular target for nanobiosensors. Using a recent review by Geleta (2022) of colorimetric sensors for microbial toxins as a resource, no examples of colorimetric nanobiosensors were identified which measured a target in a microbiological sample without removing the sample matrix [311]. Most studies procured the toxins from commercial vendors and investigated matrix effects without including microorganisms [312–315].

One notable exception was a study by Mondal *et al.* (2018), which conducted a rigorous validation of a colorimetric aptasensor for enterotoxin B and was the only study which explicitly tested for biological interference [316]. However, their method used an extraction procedure to remove the sample matrix – in this case, the bacteria culture or food product – prior to analysis [316]. Although Mondal *et al.* (2018) did not explicitly state their motivations for including an extraction procedure, the reason could be related to the biological interferences observed with *C. tardaugens*. Thus, biological interference may be a known issue, however, it has not been

explicitly reported. The majority of published methods from the Geleta (2022) review did not evaluate biological selectivity and interference, by neither the culpable organism nor control organisms [311–315]. Therefore, in order for colorimetric AuNP-based aptasensors to be fit for the purpose of directly measuring organic micropollutants in microbial cultures, biological selectivity must be addressed.

6.4 Conclusion

In this chapter, a simple nanobiosensor, constructed from gold nanoparticles and an aptamer for E2, was developed and evaluated for the purposes of measuring estrogen biodegradation.

- A colorimetric AuNP-based aptasensor for quantifying E2 by Liu *et al.* (2015) was selected from the literature to adapt for our purposes of measuring E2 biodegradation in bacteria cultures.
- The aptasensor was adapted from the original published method for measuring E2 in water samples to buffered bacterial culture media. Building upon the methods in the literature, two novel changes were incorporated for this application:
  - First, the developed method combined aptamer-target binding and the colorimetric response into a single step by exploiting the high ionic strength of the culture media.
  - Second, HPβ-CDX was added to the media to solubilise E2 within the working range of the assay.
- The aptasensor was evaluated according to ICH Guidelines for ligand-binding assays and demonstrated good analytical performance overall. While the aptasensor was considerably faster than analysis by HPLC-PDA, the method working range was much higher.
- The aptasensor showed broad reactivity for all three natural estrogens, and thus, the platform could be used as a general estrogen sensor. However, thiamine – a well-known media supplement – interfered with the assay by causing the nanoparticles to aggregate.
- The aptasensor suffered from biological interferences by the estrogen-degrading bacteria *N. europaea* and *C. tardaugens*. Interestingly, the two bacteria each used a different mechanism to interfere with E2 detection.
- The causes for biological interference from the bacteria were broadly identified. *N. europaea* altered the pH of the culture media, which impacted AuNP aggregation. Conversely, *C. tardaugens* likely introduced a metabolite into the culture media which completely inhibited aggregation.

While the aptasensor developed in this chapter was not fit for the purpose of measuring E2 concentrations in bacteria cultures, this study took a rigorous approach towards a novel application in micropollutant nanobiosensors. In particular, two different mechanisms of biological interference by two estrogen-degrading bacteria were identified. While the aptasensor generally satisfied the analytical figures of merit for quantitation when using the abiotic biological matrix (i.e., the inherent ionic strength of the media) to induce the colorimetric response, the response mechanism was impacted by changes in the media caused by the bacteria. Thus, this study highlights the importance in evaluating biological selectivity when biological targets or matrices are concerned.

In addition, the analytical range of the assay was too high for the practical purposes of measuring estrogen micropollutants. Many *in vitro* biodegradation studies were performed using >1 mg/L E2 (see Tables 2.4 and 2.6) – i.e., several orders of magnitude above environmentally relevant concentrations (0.001–30 ng/L). However, few studies were conducted above the solubility limit of estradiol [97, 99]. Therefore, the analytical sensitivity and limit of detection need to be improved before the method is suitable for measuring estrogen biodegradation in bacteria cultures.

Chapter 7

Conclusion

The aim of this thesis was to develop fluorometric and colorimetric trace analysis methods for monitoring biodegradation of estrogens in microbial communities with the potential for high-throughput analysis. To achieve this aim, four primary objectives were set, which were addressed sequentially across Chapters 3–6. In summary, the aim of the thesis was met by development of the two spectroscopic methods (Figure 7.1). Due to the highly interdisciplinary approach undertaken, this thesis provides novel contributions towards several fields, such as analytical chemistry, environmental biotechnology, and sensor technology. The key results from this thesis and the main research contributions are summarised herein.

	Gold Standard	**Spectroscopic Assays**	
	Liquid-Liquid Extraction with HPLC-PDA	BODIPY-Estrogen Probes with Halide Quenching	AuNP Colorimetric Aptasensor
Throughput	12 Samples in 22 h (1 Sample per 2 h)	30 Samples in 6 min (300 Samples per h)	41 Samples in 32 min (76 Samples per h)
Selectivity/ Specificity	**Good** ID with retention time and wavelength	**Moderate** Possible uptake of other BODIPY molecules	**Poor** Responds to other estrogens and biological interferences
Sensitivity - Analytical Range - Slope	**Good** 0.1–1 mg/L E1: 0.0010 E2: 0.0012 BDP-E1: 0.0008 BDP-E2: 0.0011	**Good** 0.1–1 µg/L & 0.1–1 mg/L Uptake detected at 1 mg/L High Range: 1.9 Low Range: 5.0 High with KI: 0.3	**Poor** 1.4–44.6 mg/L No CDX: 0.2 With CDX: 0.2
Fit for Purpose	**Yes** Natural and fluorescent estrogens were measured in bacteria cultures, determined degradation efficiency and biological transformation product	**Yes** Fluorescent probe uptake was selectively detected by estrogen catabolising bacteria in individual and heterotrophic co-cultures	**No** Assay demonstrated lack of biological selectivity, response is affected by changes to the culture media

Figure 7.1: Comparison of the analytical methods developed in this thesis. The throughput values are indicative of processing the maximum number of samples in a single batch in the requisite incubation periods and instrument analysis times.

7.1 Summary of Objectives and Key Results

7.1.1 Objective 1

Chapter 3 presents the development and validation of an analytical workflow based on liquid-liquid extraction (LLE) and chromatographic analysis for measuring natural and BODIPY-labelled estrogens in bacteria cultures, thereby addressing the first objective:

> ***Objective 1*** – Develop an analytical method based on gold standard chromatographic methods to be used as the benchmark to compare the spectroscopic methods against for characterising estrogen biodegradation.

The developed HPLC-PDA method could detect both natural and BODIPY-estrogens, and the obtained instrument detection limits for E1 and E2 were comparable to the GC-MS method. The HPLC-PDA analytical figures of merit for BODIPY-E1 and -E2 exceeded those of the natural estrogens, due to the enhanced sensitivity of the fluorescent derivatives. In addition, this study determined that the poor hydrosolubility and aggregative properties of the BODIPY fluorophore had substantial effects on extraction recovery. These effects were overcome by incorporating hydroxypropyl-β-cyclodextrin in the culture media to maintain the BODIPY-estrogens in solution and diluting the extract with acetonitrile to fully solubilise the BODIPY-estrogens for filtration. Notably, the developed traditional analytical workflow of LLE and HPLC-PDA allows for the concurrent analysis of both natural and fluorescent estrogens with comparable recovery, accuracy, and precision.

The main research contribution of this chapter was an exploration of the affects of BODIPY conjugation on the traditional analytical workflow. When comparing the analytical performance of BODIPY-estrogens against the natural estrogens, the BODIPY fluorophore provided a greater signal-to-noise and, thus, increased sensitivity in HPLC-PDA detection. While fluorophore derivatisation has been utilised for HPLC-FLD analysis, these results support the use of BODIPY for enhanced absorbance for photodiode array detectors. In addition, this thesis developed an extraction method which could recover both natural and BODIPY-labelled estrogens concurrently. Previously, there were no available extraction methods specifically for BODIPY fluorescent probes. In particular, the poor hydrosolubility and aggregative properties of BODIPY were addressed in the extraction method design. The approach towards extraction method development in this thesis could serve as a reference for other researchers seeking to perform biochemical analysis on other BODIPY-labelled substrates.

7.1.2 Objective 2

Chapter 4 presents the degradation and fate of BODIPY-estradiol compared to natural E2 using a synthetic community of estrogen-degrading reference bacteria strains, thereby addressing the second objective:

> ***Objective 2*** – Characterise the degradation and fate of natural estrogen compared to a fluorescently-labelled estrogen by a synthetic community of estrogen-degrading bacteria.

While *C. tardaugens*, the estrogen catabolising organism, rapidly degraded natural E2, the bacteria could only partially metabolise BODIPY-E2 into BODIPY-E1. In addition, *C. tardaugens* required an abundant co-substrate (pyruvate) to transform the fluorescent estrogen, and the transformation rate was much slower than the natural E2. Conversely, *N. europaea* showed minimal degradation of both E2 and BODIPY-E2. Notably, the cometabolism rate and efficiency of E2 was less than published studies for *N. europaea*. Lastly, fluorescence microscopy showed that *C. tardaugens* actively transports both BODIPY-E2 and BODIPY-azide tag. In addition, the BODIPY-estrogen and tag appear to associate with non-degrading *E. coli*, however, we hypothesise the fluorophores are interacting with the cell membrane.

The main novel contribution of this work was in validating use of BODIPY-labelled estradiol as a potential surrogate to detect estrogen-degrading bacteria. While fluorescent probes of common biomolecules (e.g., glucose [317], glycans [202], and lipids [224]) have been utilised previously to investigate biochemical processes, fluorescent probes of xenobiotics and other exogenous chemicals have not been implemented to the same extent. Since the use of fluorescently-labelled micropollutants has not been previously explored, this thesis provides a framework with which to evaluate the biochemical fate and distribution of micropollutant fluorescent probes.

This chapter also established the culturing conditions for a synthetic microbial community to evaluate estrogen biodegradation. The synthetic community – which consisted of an estrogen cometabolising, catabolising, and a non-metabolising organism – were cultured both independently and in pairwise and trio consortia. Instead of isolating degrading bacteria *de novo*, this thesis utilised publicly available reference bacteria strains to encourage reproducibility. Estrogen biodegradation studies from the literature utilise individual strains, mixed communities from an environmental sample, or individual strains augmented into an environmental sample. The synthetic microbial community – which can be used to determine the effects of microbial interactions on biodegradation – is a compromise between controlled experiments with individual strains and uncharacterised environmental inocula. In addition, the synthetic community of estrogen degraders included chemolithoautotrophic nitrifying bacteria. The co-culture of *Nitrosomonas europaea* with specific heterotrophic bacteria has been performed very few times in the literature and never in the context of estrogen biodegradation [252, 253].

7.1.3 Objective 3

Chapter 5 presents the development and validation of a high-throughput fluorometric assay which can be used to detect the uptake of BODIPY-estradiol by estrogen-catabolising bacteria *C. tardaugens*, thereby addressing the third objective:

> ***Objective 3*** – Develop and evaluate a fluorometric method based on the fluorescently-labelled estrogen which can be used to monitor biodegradation.

Two different approaches were tested to identify uptake of BODIPY-E2. The first approach sought to detect a decrease in free BODIPY-E2 in the media by physically removing the bacteria, however, this method was unable to detect the uptake of BODIPY-E2. The second approach, based on the use of iodide quenching of extracellular BODIPY-E2, successfully detected an increase in fluorescence in *C. tardaugens* cultures compared to the non-degrading bacteria *E. coli* or the cometabolising bacteria *N. europaea*. A clear response to BODIPY-E2 uptake by *C. tardaugens* was detected in co-culture with competitive bacteria, *E. coli*. However, uptake by *C. tardaugens* was not detected in co-cultures with *N. europaea*.

In co-cultures, *N. europaea* appeared to interfere with uptake of BODIPY-E2 by *C. tardaugens*. However, the relative microbial abundance used in this work for *N. europaea* was not accurately reflective of nitrification treatment systems, which are estimated to contain 0.5–3% relative abundance of nitrifying bacteria [267, 268]. The synthetic community used in this work was selected to validate the mechanisms of the developed methods and did not accurately reflect environmental community distribution. However, the influence of *N. europaea* on the fluorometric assay highlights the value of studying estrogen biodegradation within a microbial community with realistic representation. While this is the first experiment testing biodegradation of fluorescently-labelled estrogens by individual catabolising and cometabolising organisms, further investigation is needed to understand why the competitive interaction interferes with detecting the uptake of BODIPY-labelled estrogen by *C. tardaugens*.

The main research contribution of this chapter is the development of a simple and high-throughput assay which could be used to detect the selective uptake of BODIPY-labelled estrogen. The fluorometric method is supported by knowledge of the biochemical fate and distribution of the fluorescent probe. When performed in a 96-well microplate, the method could be used to screen up to 30 test conditions in triplicate within 5 minutes (Figure 7.2). In order to process the same 30 test conditions in duplicate using the developed HPLC-PDA method (which had a 28 min run-time), analysis would require 28.5 hours on the instrument, in addition to the extraction time (2–3 hour per batch). While the autofluorescence of the cultures used in this thesis did not interfere with the method, it is recommended that non-fluorescent biological controls (i.e., samples with natural E2) be included in future work, particularly with uncharacterised microbial communities.

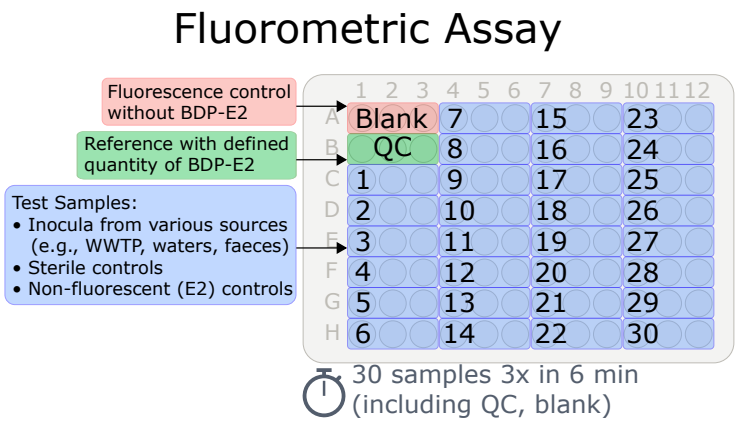

Figure 7.2: Example microplate layout for utilising the developed fluorometric assay, which highlights the increase in throughput.

7.1.4 Objective 4

Chapter 6 presents the development and validation of a simple, high-throughput colorimetric gold nanoparticles-based biosensor for the purposes of measuring estrogen in cultures with degrading bacteria, which addresses the final objective:

> ***Objective 4*** – Develop and evaluate a colorimetric method based on available colorimetric biosensors for environmental samples which has been adapted for measuring estrogen in bacteria cultures.

The method published by Liu *et al.* (2015) was adapted for measuring E2 in buffered culture media [278]. This was achieved by combining sample addition and colour development into a single step and including HPβ-CDX to solubilise E2 within the working range of the assay. The aptasensor was evaluated in accordance with industry method validation guidelines for ligand-binding assays. While the developed aptasensor demonstrated acceptable accuracy (<11% error, except at lower end of the analytical range) and precision (<6.1% RSD), the method detection limit (10 $\pm$ 10 mg/L) is several orders of magnitude above environmentally relevant concentrations. The method evaluation process revealed that the aptasensor did not have biological selectivity, as the response was impeded by changes to the bacteria culture media during growth. Interestingly, *N. europaea* and *C. tardaugens* each used a different mechanism to interfere with E2 detection. *N. europaea* altered the pH of the culture media, which impacted AuNP aggregation. Conversely, the culture media from *C. tardaugens* completely inhibited AuNP aggregation, which we hypothesise was due to the secretion of a metabolite.

The primary research contribution of this chapter was a validation of the developed colorimetric aptasensor designed to measure estrogen concentrations in microbial cultures using industry guidelines for ligand-binding assays. The nanobiosensors in the literature often evaluate

the concentration-dependent response of the sensor by sensitivity, detection limit, and chemical specificity. However, the means by which the published methods were evaluated are inconsistent and are often not done to the rigour recommended by the relevant guidelines. Since the method validation allowed us to directly compare the analytical performance with traditional analysis by HPLC, we have a more quantitative understanding of the benefits and limitations of colorimetric aptasensors for estrogen quantitation – in particular, the significant increase in throughput (Figure 7.3), as well as the increase in limit of detection.

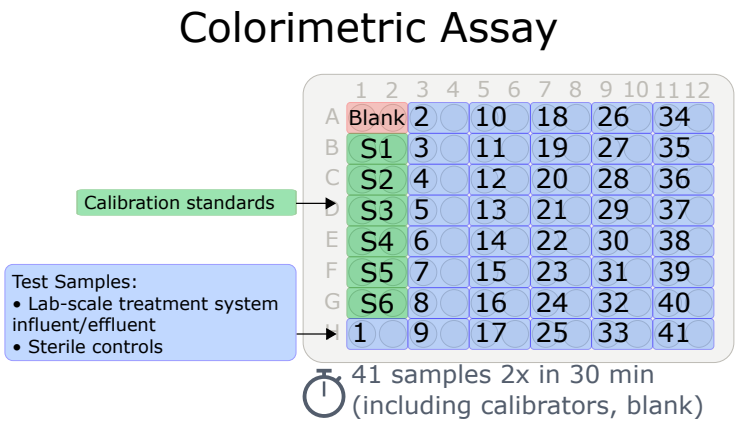

Figure 7.3: Example microplate layout for utilising the developed colorimetric assay, which highlights the increase in throughput.

In addition, this thesis reported interferences of microbial growth on AuNP colloidal stability. The interferences identified in this thesis were the changing of the media pH and the addition of a nanoparticle passivating agent, which we hypothesise is a metabolite of *C. tardaugens*. The interferences observed from the bacteria highlight the importance of conducting rigorous, systematic method validation – particularly for biological selectivity when the methods are designed for biological samples.

7.2 Recommendations for Future Work

This thesis developed two high-throughput fluorometric and colorimetric methods for monitoring biodegradation of estrogen. The fitness for purpose of the methods were evaluated against relevant industry guidelines for their respective applications and validated using a synthetic microbial community. However, there is scope for improvement and further development for both of the methods developed in this thesis.

The fluorometric method developed in this thesis was validated using a specific culture media. In theory, the method should be effective for any optically compatible matrix. However, this should be tested with different water sources – e.g., tap water, surface water, or possibly even clarified secondary treatment effluent – to determine if the dissolved organic matter interferes

with the fluorescence of the BODIPY probe. Using a sample matrix which is more analogous to the target environment for remediation would reduce the bias of selecting for estrogen-degrading bacteria which thrive better in laboratory culture media. In addition, the fluorometric method was validated with only one bacteria strain for estrogen biodegradation. This represents only one true biological replicate, as the triplicate cultures of the strain were only technical replicates. Therefore, the method should be assessed with more bacteria – for example, with an inoculum from a treatment system, compost, or sediments which is positive for estrogen biodegradation; new estrogen-degrading reference strains; or estrogen-degrading bacteria isolated *de novo*.

The fluorometric method can be further improved by eliminating the need for cyclodextrin, as we hypothesise that the inclusion complex interferes with *Nitrosomonas* estrogen cometabolism. This may be achieved by derivatising the BODIPY core with polar groups to facilitate hydrosolubility. Another aspect of the fluorometric method which could be further developed is the quenching agent. While potassium iodide was an effective quenching agent, the high concentration is most likely toxic to the cultures. A non-toxic quenching agent could allow for real-time detection in a microplate culture, eliminating the need for sampling from a batch culture.

The developed colorimetric aptasensor was ultimately not fit for the purpose of measuring estrogen removal in bacteria cultures. In hindsight, the decision to develop a method which utilised properties of the culture media to mediate the colorimetric response was not appropriate, since bacteria modify their environment during growth. However, the systematic literature review identified other approaches which do not rely on salt-induced aggregation. In colorimetric sensors, the deaggregation of cross-linked nanoparticles may be more appropriate. Another limitation of the developed aptasensor was the high analytical range, which was mostly above the solubility limit of 17β-estradiol in water. Since two of the most common E2 aptamers from the literature produced a similar dynamic range and response in this study, other recognition elements, such as molecularly imprinted polymers (MIPs) could be explored. In addition, the systematic literature review showed that colorimetric sensors had the highest detection limits. Therefore, other optical sensors based on fluorescence or surface enhanced Raman spectroscopy (SERS) could also be tested for this application.

Ultimately, the fluorometric assay could be deployed on more diverse microbial communities from the natural and built environment to screen for estrogen-degrading organisms. This technique could be used to support at least two key factors of successful bioaugmentation identified by Herrero and Stuckey (2015) [109]. The rapid method for screening samples for metabolically competent organisms will help expedite the selection of suitable bacteria for bioaugmentation. In addition, the fluorometric method could be used as a monitoring technique to supervise the survival and activity of the inoculum. While the colorimetric method requires additional development to be fit for purpose, a suitable quantitative method would be immensely advantageous. In addition to providing removal rates and efficiencies for computational models, a validated

spectroscopic method for estrogen quantitation could be used as an assay in synthetic biology approaches to bioremediation. For example, directed evolution – where microorganisms are genetically modified for enhanced micropollutant metabolism – could use the quantitative method to screen variant organisms for metabolically competent strains [318]. In conclusion, the spectroscopic methods developed and validated in this thesis represent an important step towards the design of new bioanalytical methods which address specific methodological gaps around engineering estrogen biodegradation.

Appendix A

Supplementary Data (Chapter 4)

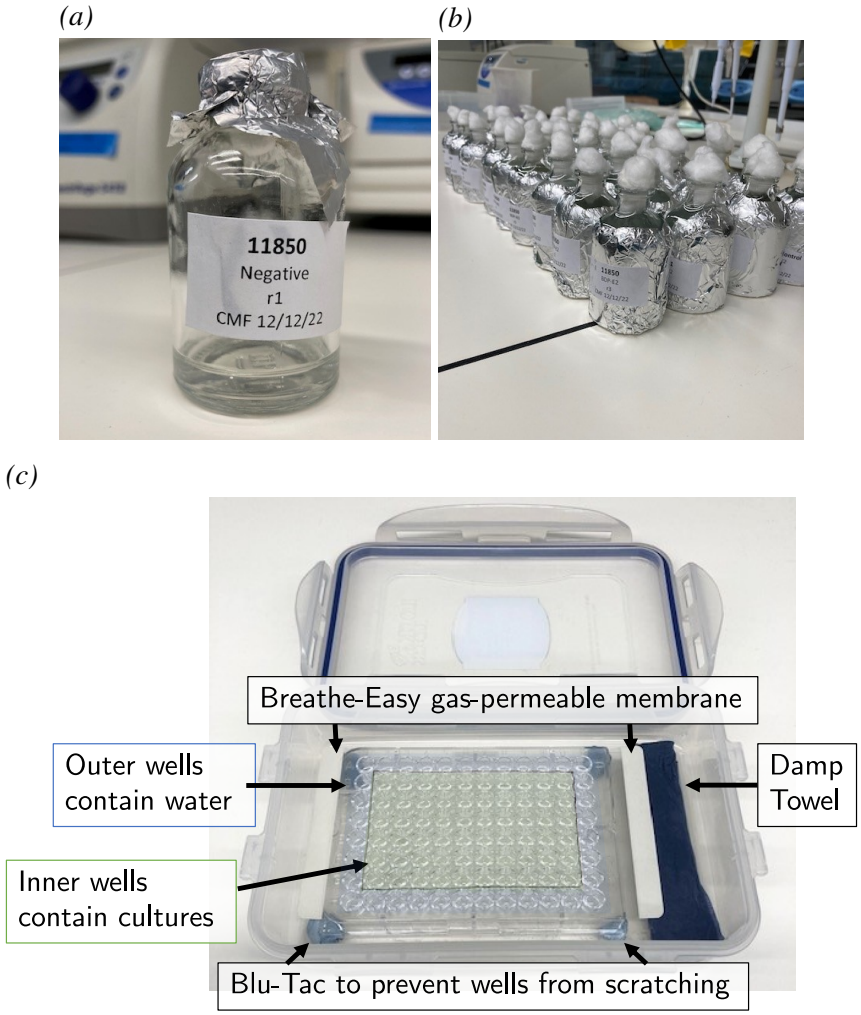

Figure A.1: Example images of (a,b) aerobic serum bottle cultures and (c) microplate in an air-tight container.

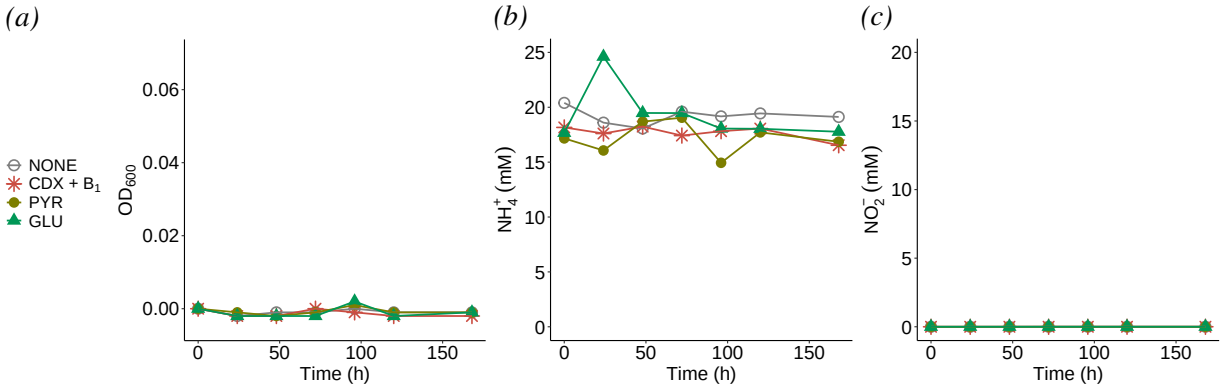

Figure A.2: Abiotic controls for N. europaea growth in the presence of different carbon sources. HPβ-CDX and thiamine (CDX + B_1), pyruvate (PYR), and glucose (GLU) or no added organic carbon (NONE). Growth was assessed by (a) OD_{600} and the metabolism of (b) NH_4^+ into (c) NO_2^-. Error bars are the standard deviation (n=3).

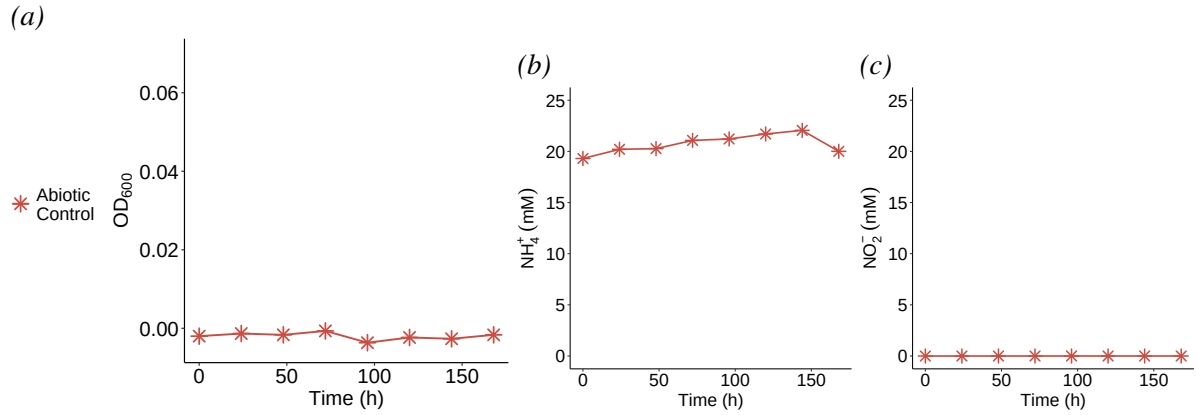

Figure A.3: Abiotic controls for growth of the three strains as pairwise and consortium co-cultures. Growth was assessed by (a) OD_{600}; the metabolism of (b) NH_4^+ into (c) NO_2^- was also evaluated. Error bars are the standard deviation (n=3).

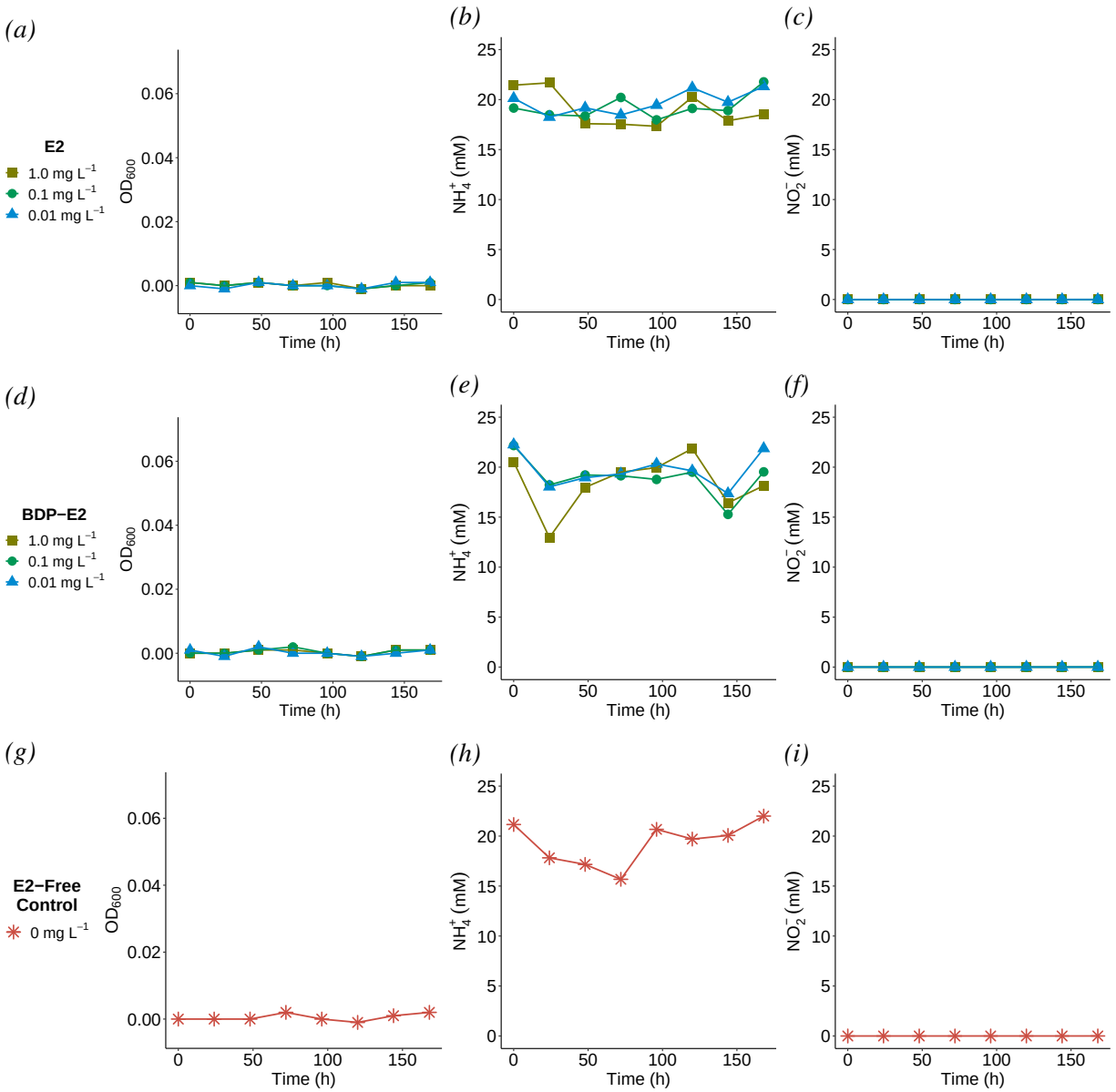

Figure A.4: Abiotic controls for N. europaea growth in the presence of different concentrations of (a,b,c) E2 and (d,e,f) BODIPY-E2. (g,h,i) Controls with no added estrogen were also assessed. Growth was assessed by (a,d,g) OD_{600} and the metabolism of (b,e,h) NH_4^+ into (c,f,i) NO_2^-. Error bars are the standard deviation (n=3).

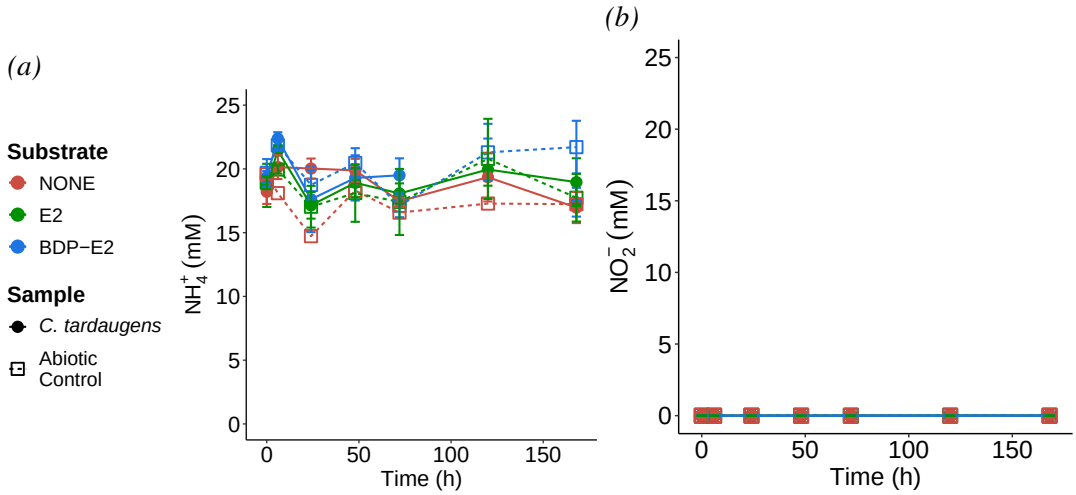

Figure A.5: (a) Ammonium and (b) nitrite levels during biodegradation of E2 (green) versus BODIPY-E2 (blue) by C. tardaugens (solid circle, solid lines) with 0.1 mg/mL Na pyruvate. E2-free controls (red) and abiotic controls (open square, dashed lines) were also evaluated. Error bars are the standard deviation (n=3).

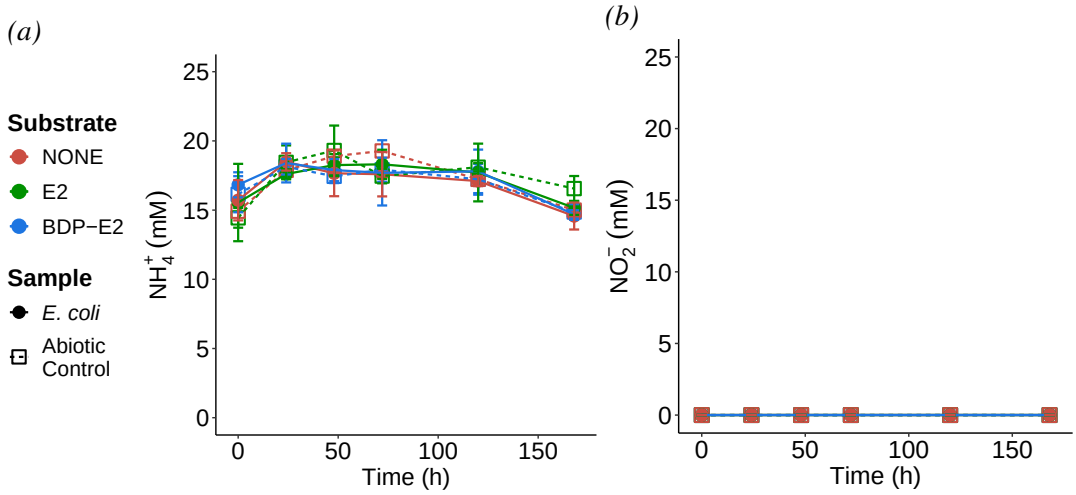

Figure A.6: (a) Ammonium and (b) nitrite levels during biodegradation of E2 (green) versus BODIPY-E2 (blue) by E. coli (solid circle, solid lines). E2-free controls (red) and abiotic controls (open square, dashed lines) were also evaluated. Error bars are the standard deviation (n=3).

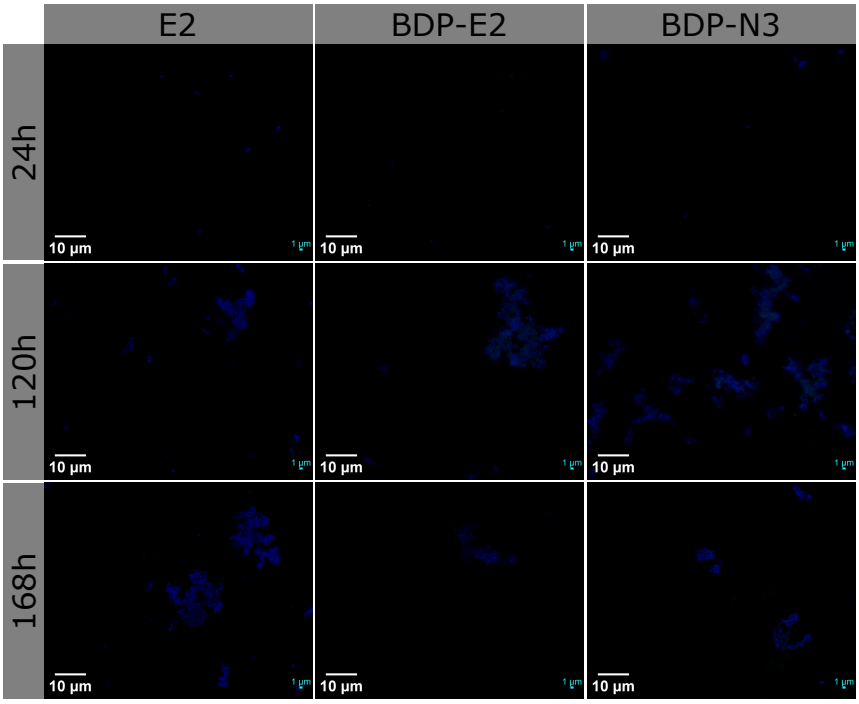

Figure A.7: Representative composite (DAPI-blue, BODIPY-green) fluorescence microscopy images of N. europaea cultured with natural and fluorescent estrogen or BODIPY-azide. Images were background subtracted for each filter separately prior to merging. Scale bars are 10 µm (lower left) and 1 µm (lower right).

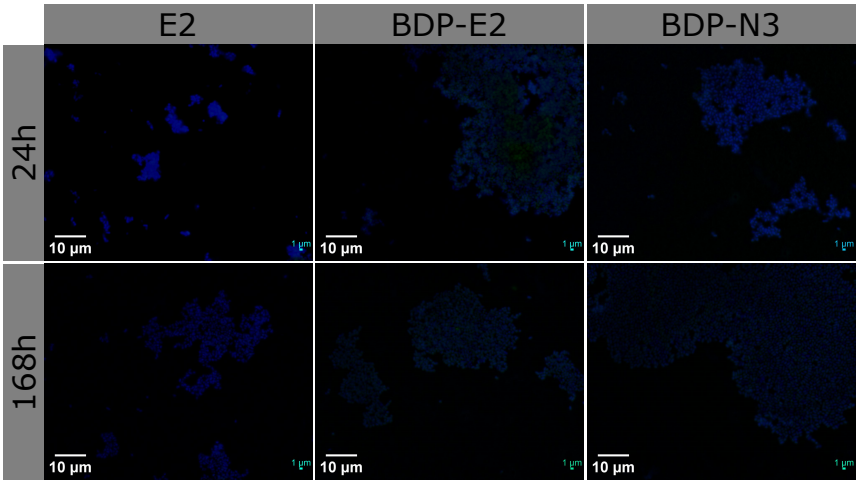

Figure A.8: Representative composite (DAPI-blue, BODIPY-green) fluorescence microscopy images of E. coli cultured with natural and fluorescent estrogen or BODIPY-azide. Images were background subtracted for each filter separately prior to merging. Scale bars are 10 µm (lower left) and 1 µm (lower right).

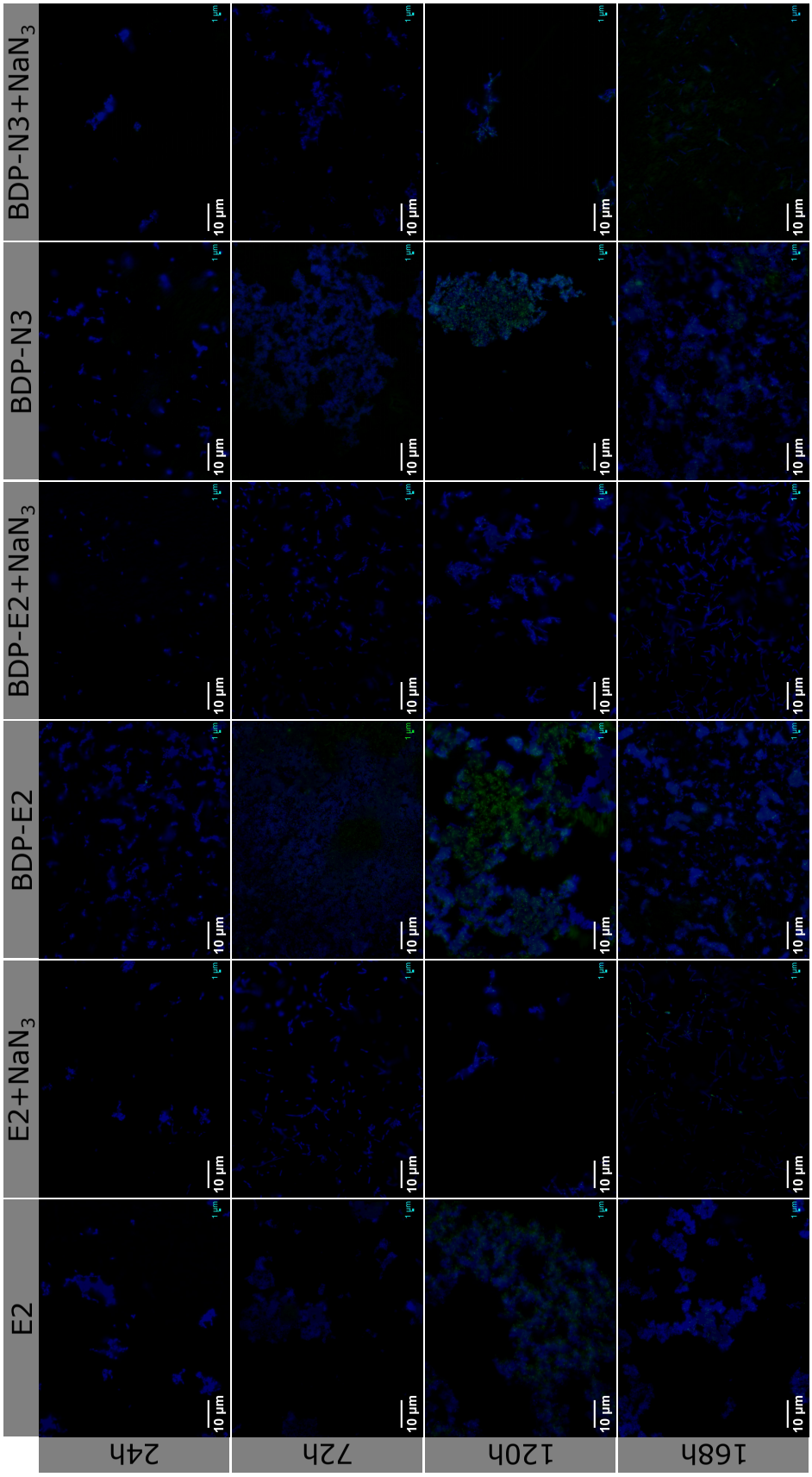

Figure A.9: Representative composite (DAPI-blue, BODIPY-green) fluorescence microscopy images of C. tardaugens cultured with natural and fluorescent estrogen or BODIPY-azide. Images were background subtracted for each filter separately prior to merging. Scale bars are 10 µm (lower left) and 1 µm (lower right).

Appendix B

Flow Cytometry Pilot Test (Chapter 4)

In Chapter 4, fluorescence microscopy was used to visualise BODIPY-E2 within estrogen-degrading bacteria. Flow cytometry (FCM) analysis – which combines optical detection with microfluidics to enumerate cell populations based on various characteristics – has been used in the literature to detect cellular uptake of fluorescent probes [201, 202, 319]. Therefore, a pilot test for using FCM to detect the selective uptake of BODIPY-E2 using the three reference strains was conducted. FCM analysis was intended to complement the results obtained by fluorescence microscopy and to explore the applicability of the technique in screening microbial populations for metabolically competent bacteria using fluorescently labelled micropollutant.

This work was done with the assistance of Laura Cossu and Dr Marta Vignola. Laura assisted in operating the FCM instrument and running the samples. The experiment design, culturing of the bacteria, and data analysis (reviewed by Dr Vignola) was performed by Celeste Felion.

Methods

The bacteria samples used in this pilot test were from the experiment in Section 5.2.5.1, in which the bacteria cultured with 1 µg/L of E2 or BODIPY-E2. Refer to the Materials & Methods of Chapter 5 for the detailed methods for culturing the bacteria used in this pilot test.

After the conclusion of the experiment described in Section 5.2.5.1, the cultures were sampled for FCM analysis. Briefly, 1 mL from each of the replicate cultures were combined together in 15-mL tubes. The pooled cultures were centrifuged at 2000*xg* for 5 m to pellet the bacteria. The supernatant was discarded, and the pellets were resuspended in 3 mL of sterile phosphate buffered saline. The washed cells were fixed by adding a 1:1 volume of 1% (v/v) glutaraldehyde in deionised water. In order to test for background, a pooled control sample was prepared by combining 1 mL of each fixed bacteria culture together in a 15-mL tube. An aliquot (1 mL) of

each fixed culture and the pooled control was added to individual microcentrifuge tubes. The remaining volume of the pooled control was filtered using a sterile 0.22-µm syringe filter, and an aliquot of the filtrate (1 mL) was added to a microcentrifuge tube. Thus, the filtered sample would show the non-cellular background fluorescence. Sample aliquots were maintained in the dark at 4°C and analysed within 2 h.

The bacteria were stained by adding 5 µL of Nile red solution (10 mg/mL in DMSO, Sigma Aldrich UK) to the 1-mL aliquots and incubating in the dark for 15 m at room temperature. FCM measurements were performed using BD Accuri C6 Plus flow cytometer (BD Biosciences) using 488 nm laser. A 50-µL aliquot of sample was injected and analysed at 60 µL/min. Density and dot plots using forward scatter (FSC) versus FITC filter (533 $\pm$ 30 nm) for green fluorescence of BODIPY-E2 and PerCP filter (670 nm, long pass) for orange-red fluorescence of Nile red were used to characterise uptake of the fluorescent estrogen.

Results

The FSC/PerCP density plots of the pooled control (Figures B.1B and E) and individual strains (Figures B.3B and E; B.4B and E; B.5B and E) suggest that the bacteria were stained with Nile red, based on the fluorescence intensity and size relative to the filtered pooled control (Figures B.2B and E) and abiotic control (Figures B.6B and E). The red boundary in the FSC/PerCP plot contains the population of putative bacteria stained with Nile red; the boundary was selected based on the *C. tardaugens* distribution (Figures B.4B and E).

A distinct population of green fluorescent bacteria was not detected in any FSC/FITC density plots with BODIPY-E2 (Figures B.1A, B.3A, B.4A, B.5A). The green fluorescence intensity of the counts were relatively low compared to that of the Nile red. While this could be due to the low working concentration of the fluorescent estrogen, interactions between fluorophores (e.g., energy transfer) could be interfering with detection of BODIPY. The blue boundary of the FSC/FITC plots contains the population of putative bacteria with BODIPY-E2, and the yellow boundary contains intense green fluorescence of smaller particles. The boundary was selected based on the *C. tardaugens* distribution (Figure B.4A) Although this pilot experiment did not detect the uptake of BODIPY-E2 by estrogen-degrading bacteria, a more thorough investigation with the following controls would give better insight into why detection did not occur:

- A separate suite of samples labelled with SYBR green DNA stain, which is the preferred fluorescent marker for bacteria numeration, should be used to validate the Nile red.
- The individual samples should be filtered to distinguish the cells from the abiotic fluorescent signals.

- A separate suite of controls which contain only BODIPY-E2 but no Nile red, as well as controls with no fluorophores at all, should be used to evaluate dual-fluorophore interactions.

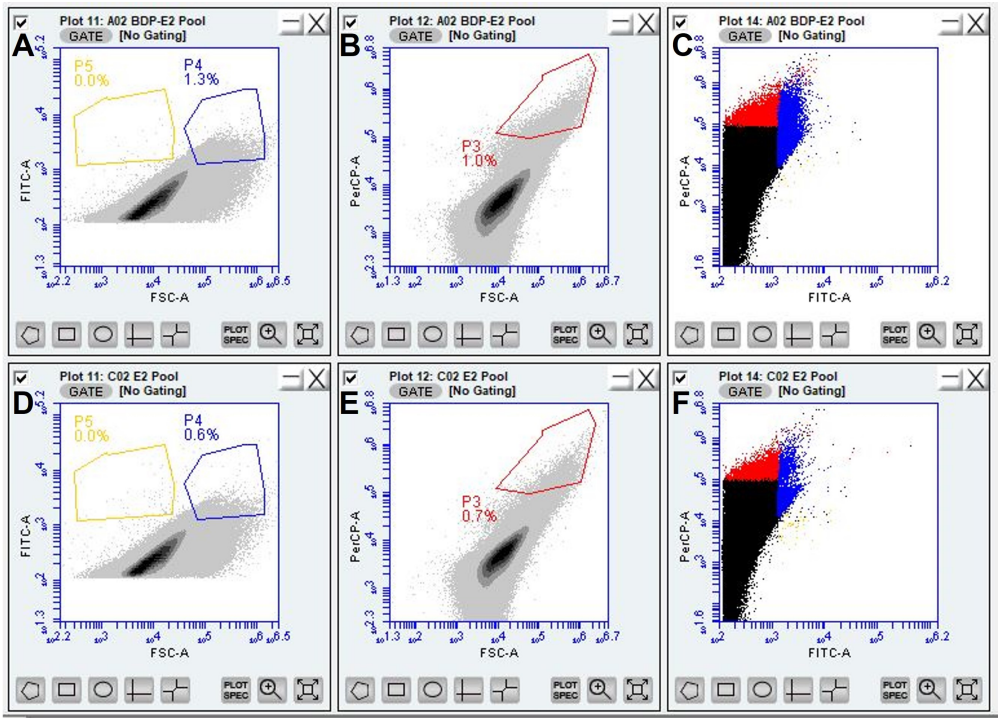

Figure B.1: Flow cytometry results for the pooled control with BODIPY-E2 cultures (A-C) and E2 cultures (D-F). Results include the gradient plots of (A,D) FITC-A (BODIPY) vs FSC-A, (B,E) PerCP-A (Nile red) vs FSC-A, and (C,F) dot plot of PerCP-A vs FITC-A.

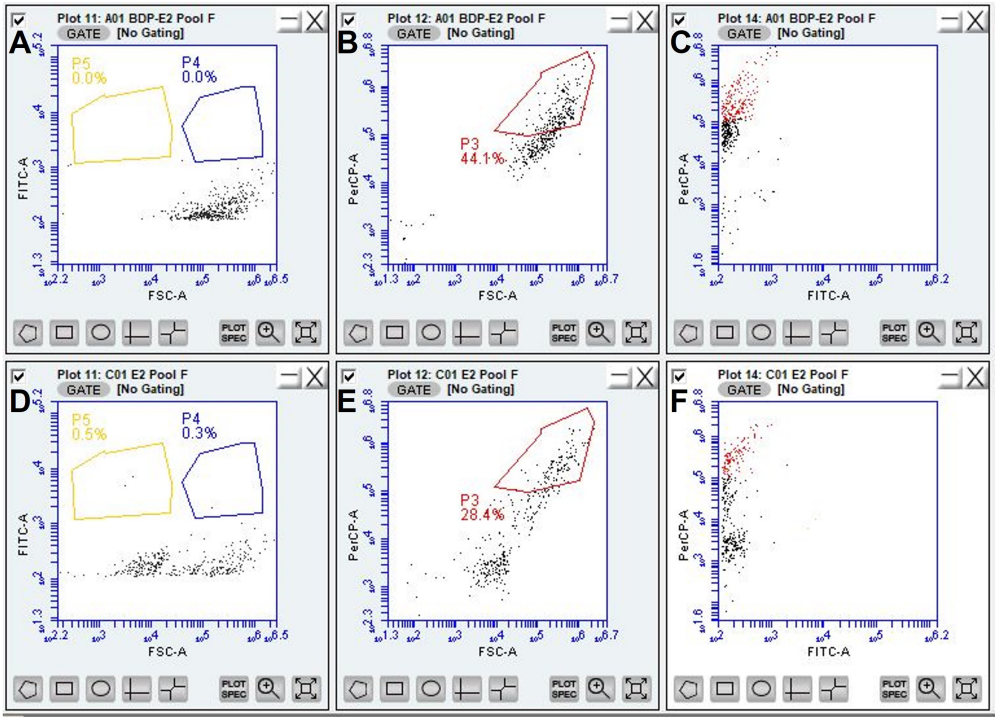

Figure B.2: Flow cytometry results for the filtered pooled control with BODIPY-E2 cultures (A-C) and E2 cultures (D-F). Results include the gradient plots of (A,D) FITC-A (BODIPY) vs FSC-A, (B,E) PerCP-A (Nile red) vs FSC-A, and (C,F) dot plot of PerCP-A vs FITC-A.

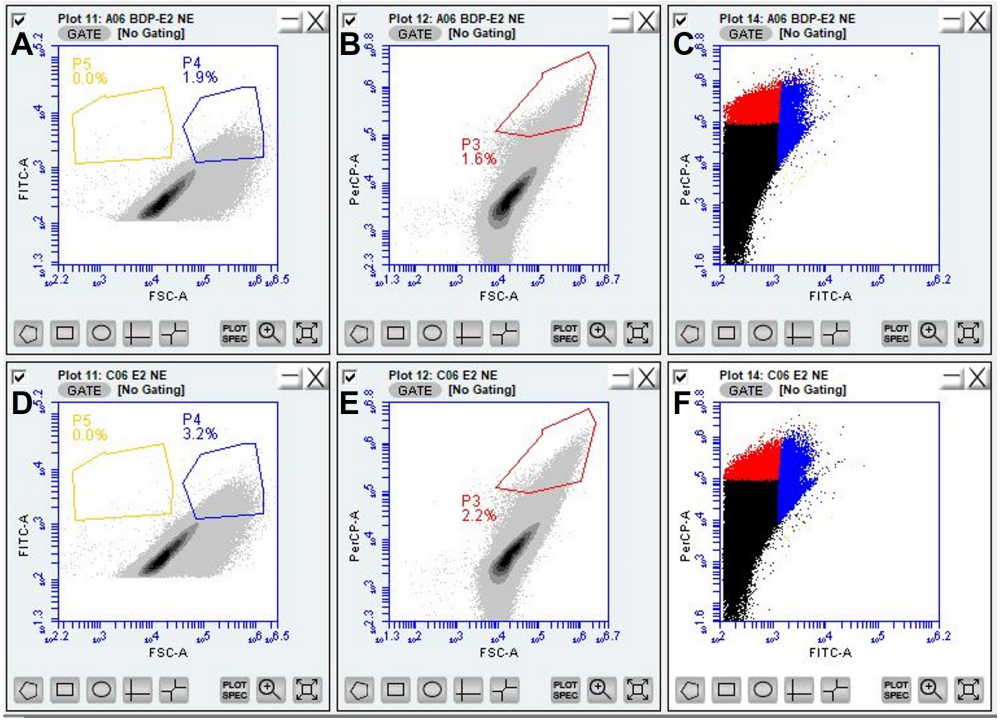

Figure B.3: Flow cytometry results for N. europaea cultured with BODIPY-E2 (A-C) and E2 (D-F). Results include the gradient plots of (A,D) FITC-A (BODIPY) vs FSC-A, (B,E) PerCP-A (Nile red) vs FSC-A, and (C,F) dot plot of PerCP-A vs FITC-A.

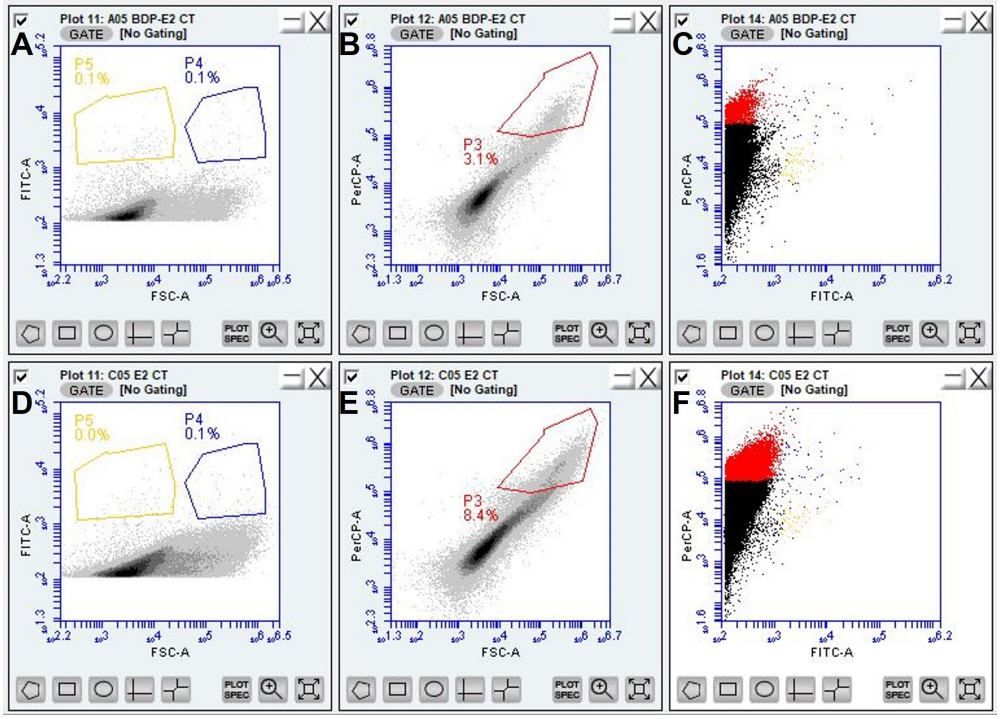

Figure B.4: Flow cytometry results for C. tardaugens cultured with BODIPY-E2 (A-C) and E2 (D-F). Results include the gradient plots of (A,D) FITC-A (BODIPY) vs FSC-A, (B,E) PerCP-A (Nile red) vs FSC-A, and (C,F) dot plot of PerCP-A vs FITC-A.

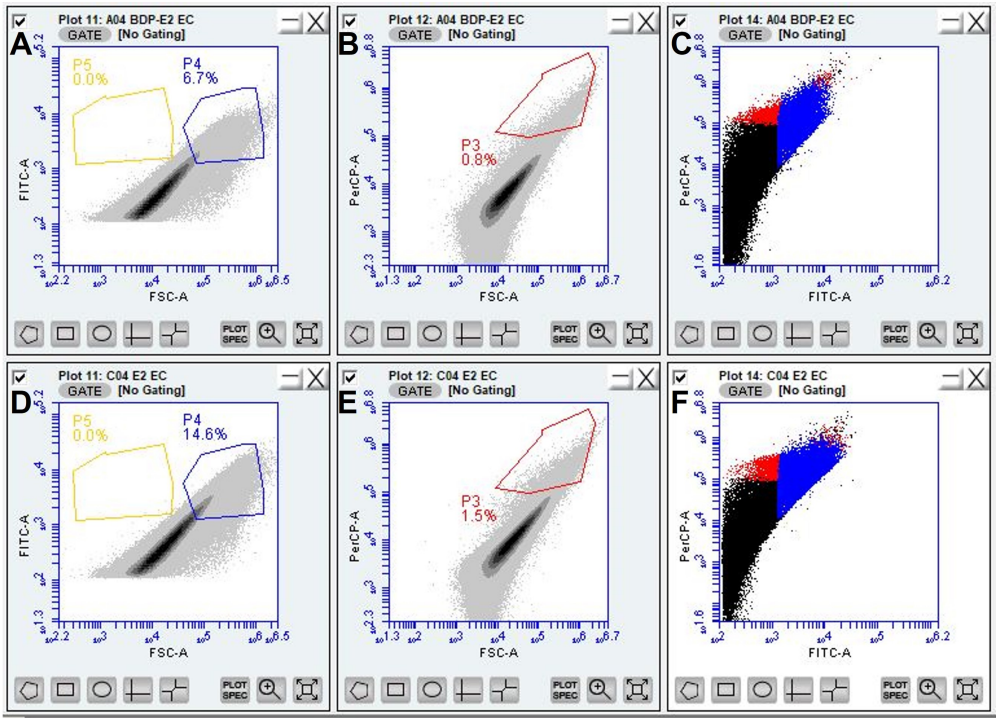

Figure B.5: Flow cytometry results for E. coli cultured with BODIPY-E2 (A-C) and E2 (D-F). Results include the gradient plots of (A,D) FITC-A (BODIPY) vs FSC-A, (B,E) PerCP-A (Nile red) vs FSC-A, and (C,F) dot plot of PerCP-A vs FITC-A..

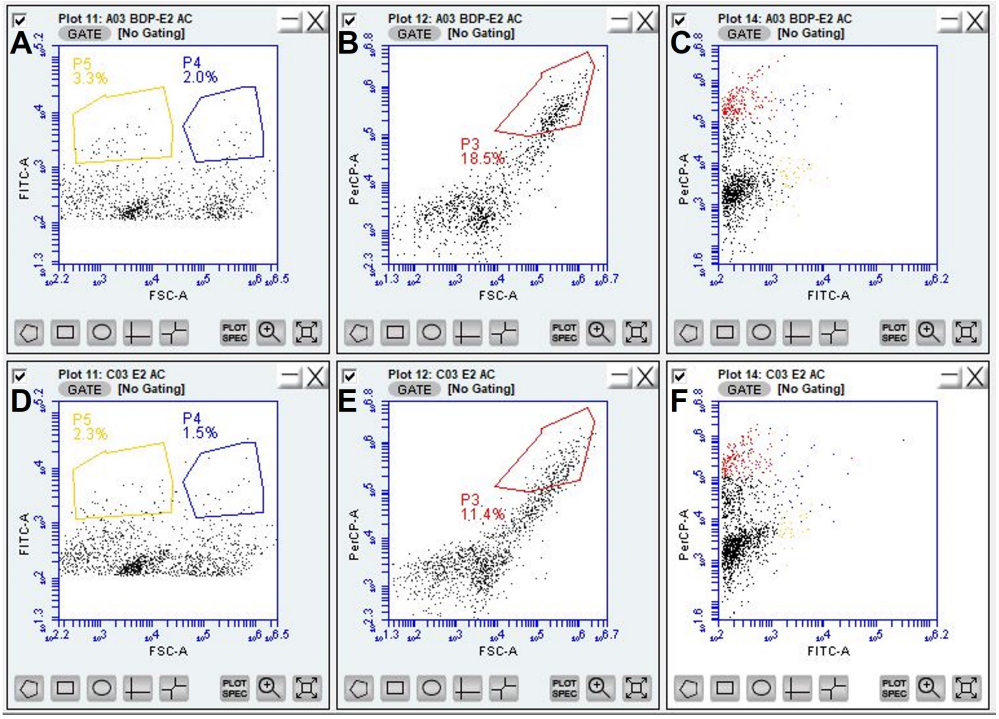

Figure B.6: Flow cytometry results for abiotic culture controls with BODIPY-E2 (A-C) and E2 (D-F). Results include the gradient plots of (A,D) FITC-A (BODIPY) vs FSC-A, (B,E) PerCP-A (Nile red) vs FSC-A, and (C,F) dot plot of PerCP-A vs FITC-A.

Appendix C

Metabolomics Pilot Test (Chapter 4)

In Chapter 4, the fate of E2 and BODIPY-E2 in *N. europaea* cultures could not be determined by HPLC-PDA analysis, since the levels of potential degradation were so low. In addition, E2 and the fluorescent surrogate showed similar toxicity and metabolic inhibition of the *Nitrosomonas*. In order to determine the degradation products the fluorescent estrogen and the impact of estrogens on the bacteria, we elected to try non-targeted analysis of the excreted metabolites. The work presented here is the pilot test to determine if we could recover metabolites for LC-MS analysis.

This work was done with the assistance of Dr Clement Regnault and Prof Phil Whitfield at the University of Glasgow Polyomics Facility for Lipidomics and Metabolomics. The experiment design, culturing of the bacteria, sample extraction, and data analysis was performed by Celeste Felion. Dr Regnault analysed the samples by LC-MS using a method developed by Polyomics and processed the instrument data using the IDEOM application [320]. The IDEOM file and an experiment report was then provided to Celeste for analysis.

Methods

The bacteria samples used in this pilot test were from the experiment in Section 4.2.5.1, in which *N. europaea* was cultured with 10, 100, and 1000 µg/L of E2 or BODIPY-E2. Refer to the Materials & Methods of Chapter 4 for the detailed methods for culturing the bacteria used in this pilot test. The specific cultures used for this pilot test are listed in Table C.1; the samples were collected from only one replicate flask.

Sample Preparation

Samples were extracted according to the "Sample Preparation for Liquids (August 2013)" protocol from Polyomics. Briefly, 10 µL of culture sample was added to a microcentrifuge tube on

Table C.1: List of samples used for LC-MS analysis.

ID	Sample	Substrate
AC000200	Abiotic Control	None
AC010200	Abiotic Control	100 µg L^{-1} E2
AC020200	Abiotic Control	100 µg L^{-1}L BDP-E2
NE000200	*N. europaea*	None
NE010200	*N. europaea*	100 µg L^{-1} E2
NE020200	*N. europaea*	100 µg L^{-1} BDP-E2
Pooled QC	Samples Pooled	E2 and BDP-E2
Matrix Blank	Extraction Solvent	–

ice with 400 µL of extraction solvent (chloroform/methanol/water in 1:3:1 ratio). For the pooled QC, 5 µL of each culture sample was added to a microcentrifuge tube with 1.2 mL of extraction solvent. The matrix blank contained 1.2 mL of extraction solvent and was processed alongside the test samples. The extraction tubes were vortexed in a cold room (4°C) for 5 min, then centrifuged for 3 min at 13,000*xg* and 4°C. An aliquot of supernatant (360 µL for the samples and 1080 µL for the pooled QC and matrix blank) was added to a cryovial and stored at -80°C until analysis.

Instrument Analysis and Data Processing by Polyomics

Chromatography was carried out on a Dionex UltiMate 3000 RSLC system (Thermo Fisher Scientific, UK) using a ZIC-pHILIC column (150 mm × 4.6 mm, 5 µm column, Merck Sequant). The column was maintained at 25°C and samples were eluted with a linear gradient between (A) 20 mM ammonium carbonate in water and (B) acetonitrile over 26 min at a flow rate of 0.3 mL/min (Table C.2). The injection volume was 10 µl and samples were maintained at 5°C prior to injection.

For the MS analysis, a Thermo Orbitrap QExactive (Thermo Fisher Scientific) was operated in polarity switching mode; the MS settings are given in Table C.3. For positive mode ionisation: source voltage +3.8 kV, S-Lens RF Level 30.00, S-Lens Voltage -25.00 (V), Skimmer Voltage -15.00 (V), Inject Flatopole Offset -8.00 (V), Bent Flatapole DC -6.00 (V). For negative mode ionisation: source voltage -3.8 kV. In addition, lock-mass correction was applied: three m/z for positive mode, 83.0604, 149.0233, 445.1200; and one m/z for negative mode, 89.0244.

Table C.2: Gradient elution profile used for LC-MS analysis.

Time (min)	%A	%B
0	20	80
15	80	20
15	95	5
17	95	5
17	20	80
24	20	80

Table C.3: Mass spectrometer settings.

Setting	Value
Resolution	70,000
AGC	1e6
m/z Range	70–1050
Sheath gas	40
Auxiliary gas	5
Sweep gas	1
Probe temperature	150°C
Capillary temperature	320°C

Results

The total ion chromatograms (Figure C.1) did not reveal a significant difference between the matrix blank, abiotic controls, and the biotic test samples. There were two distinctly large peaks detected in negative ionisation which were not observed in the matrix blank (Figure C.1b). The large peak observed at 770 s contained $[M\text{-}H]^-$, $[2M\text{-}H]^-$, and $[3M\text{-}H]^-$ ions from orthophosphate (H_3PO_4) and $[M\text{-}H]^-$ ion from pyrophosphate ($H_4P_2O_7$). The large peak at 864 s contained the $[M\text{-}H]^-$, $[M+Na\text{-}2H]^-$, and $[2M\text{-}H]^-$ ions from sulphate (H_2SO_4). Since MMB media contains phosphate and sulphate salts, these peaks were attributed to the sample matrix.

According to the analysis report provided by Polyomics, "IDEOM performs metabolite annotation by matching the exact mass and retention time (RT) of a metabolic feature to the exact mass and predicted RT of compounds in the [IDEOM] database." In order to enable analysis

by the IDEOM application, the LC-MS data for each sample was artificially triplicated. The IDEOM analysis revealed up to 118 putative metabolites across the six test conditions. However, the ion abundance values ($\sim 10^4$) of the metabolites were lower than expected; for example, an ion abundance 10^5–10^6 is expected for amino acids. The abiotic control with BODIPY-E2 (AC020200) contained very high quantities of multiple metabolites compared to the other test samples; this sample may have become contaminated during sample preparation. Comparing the biotic samples with the other two abiotic controls, eight unique m/z-retention time combinations were identified and are shown in Table C.4. The metabolites have not been confirmed with a standard, however, the putative identification determined from the molecular formula indicates they are primarily associated with amino acid metabolism. Further work is required to improve the extraction recovery and increase the number and abundance of metabolites before the metabolic footprint of *N. europaea* can be investigated thoroughly.

(a)

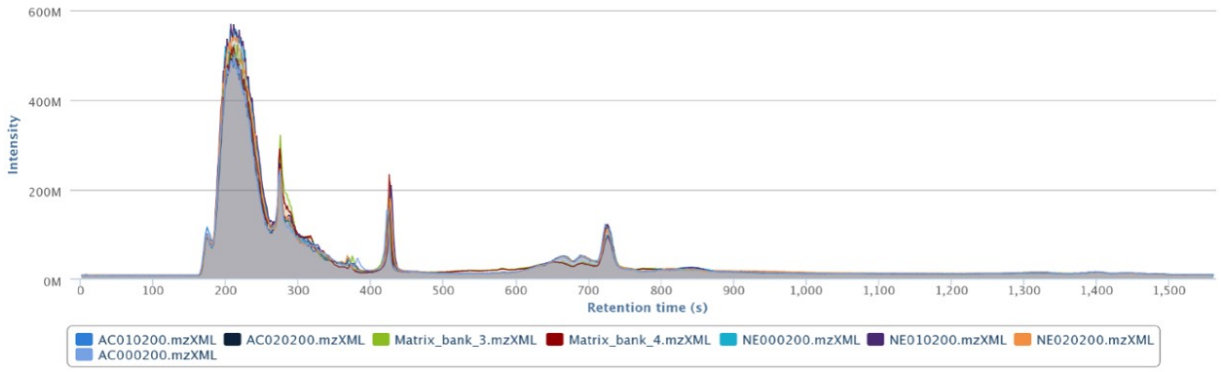

(b)

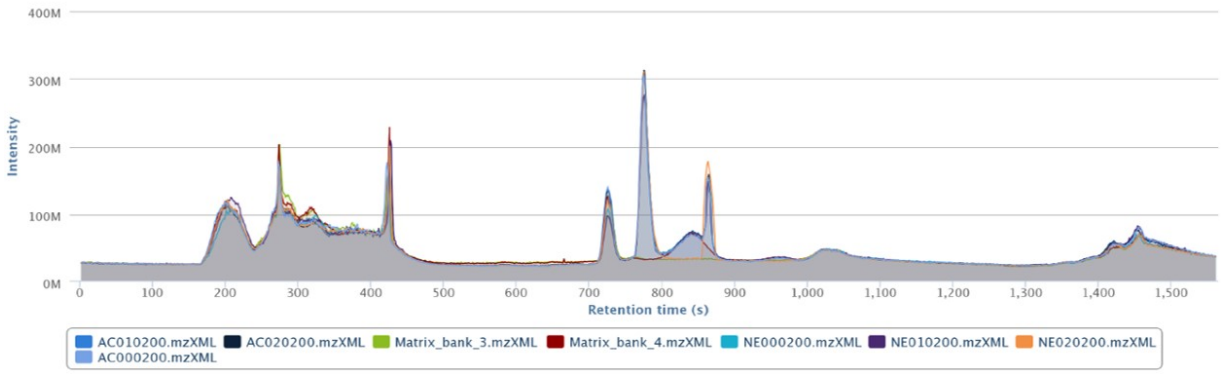

Figure C.1: (a) Positive and (b) negative total ion chromatograms for the abiotic controls (AC) and bacteria (NE) samples with E2 (010200), BODIPY-E2 (020200), or no substrate (000200).

Table C.4: Detected m/z values which were selectively present in the biotic samples.

m/z	Ret. Time (min)	Formula	Putative Metabolite	Pathway	Max Intensity
142.0379	7.818872	$C_5H_6N_2O_3$	4-Imidazolone-5-acetate	His metabolism	33920
720.4948	2.815961	$C_{38}H_{73}O_{10}P$	1-16:0-2-trans-16:1-phosphatidylglycerol	–	26081
146.1055	17.00576	$C_6H_{14}N_2O_2$	D-Lysine	Lys degradation	67483
162.1005	16.90647	$C_6H_{14}N_2O_3$	N6-Hydroxy-L-lysine	Lys degradation	63958
175.0482	9.671172	$C_6H_9NO_5$	N-Acetyl-L-aspartate	Ala and Asp metabolism	25967
236.1272	7.127528	$C_{11}H_{16}N_4O_2$	CPX	–	266296
173.0689	7.234117	$C_7H_{11}NO_4$	N-Acetyl-L-glutamate 5-semialdehyde	Arg and Pro metabolism	103575
166.0849	7.279616	$C_{13}H_{24}N_4O_6$	Leu-Asn-Ser	Hydrophobic peptide	1584574

Appendix D

Supplementary Data (Chapter 5)

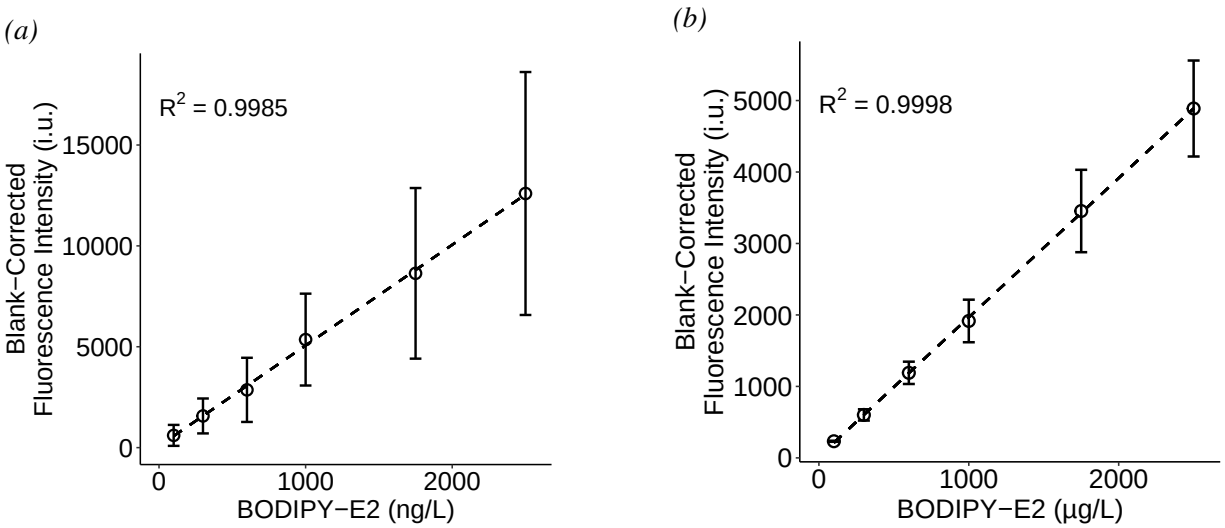

Figure D.1: Calibration curve of the spectrofluorometer for measuring BODIPY-E2 in MMB media with 2% HPβ-CDX for the (a) low analytical range and (b) high analytical range. Points are the mean of calibration standards measured in three batches and error bars are standard deviation.

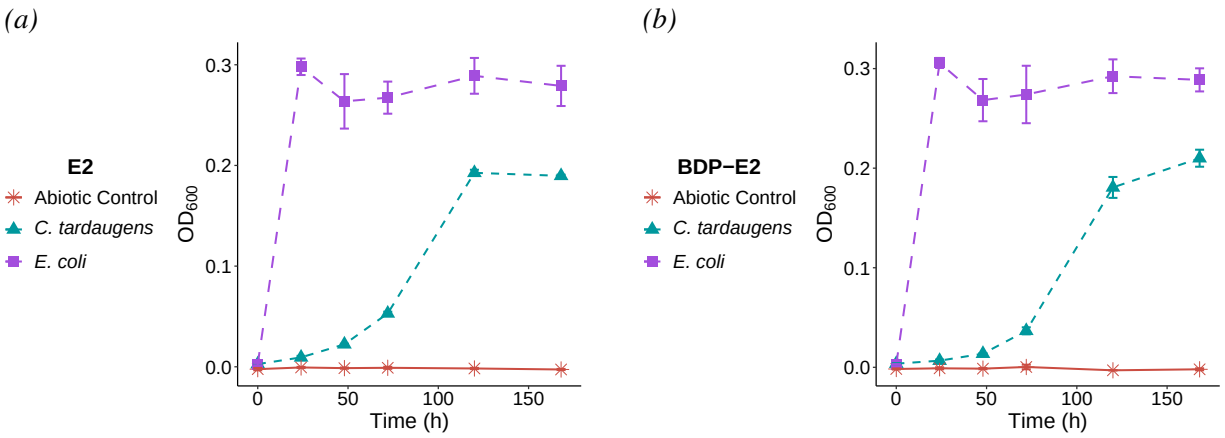

Figure D.2: Growth results (OD_{600}) for testing 1 mg/L E2 (a) and BODIPY-E2 (b) with physical separation.

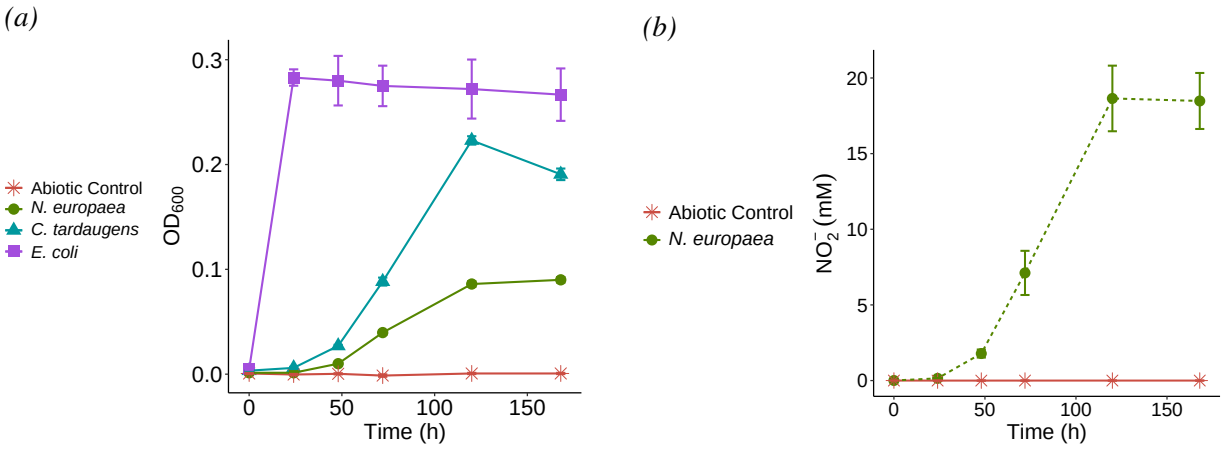

Figure D.3: (a) Growth results (OD_{600}) for testing 1 mg/L BODIPY-E2 with 1 M KI quencher. (b) The production of NO_2^- by N europaea was also measured. Results are the mean and standard deviation (n=3).

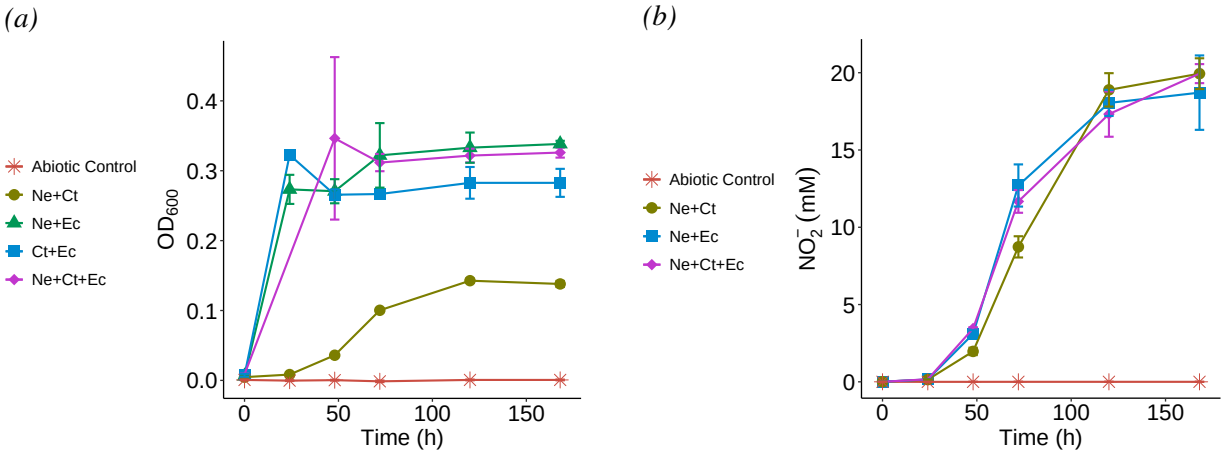

Figure D.4: (a) Growth results (OD_{600}) for testing mixed cultures containing 1 mg/L BODIPY-E2 with 1 M KI quencher. (b) The production of NO_2^- by N europaea was also measured. Results are the mean and standard deviation (n=3).

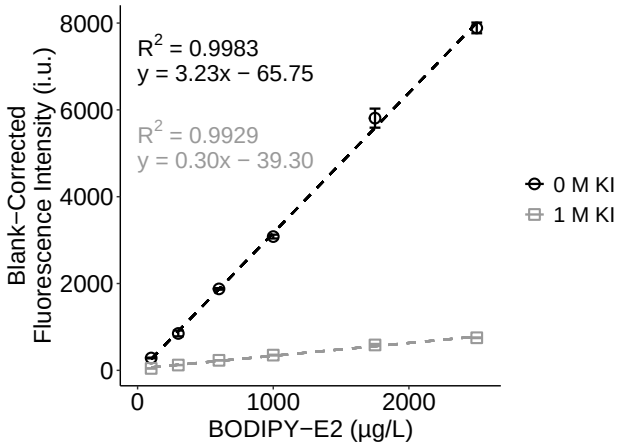

Figure D.5: Calibration standard curve for the high analytical range of BODIPY-E2 in in MMB media with 2% HPβ-CDX, with (grey) or without (black) 1 M KI. Points are the mean of calibration standards measured in triplicate (one batch) and error bars are standard deviation.

Appendix E

Publications for Systematic Literature Review (Chapter 6)

Table E.1: Master key for systematic literature review results.

Field	Type	Description
ArticleID	Text	Unique number for each article
1stAuthor	Text	First author in author list
PubYear	Date	Publication year
DOI	Text	Article DOI
Design	Y/N	"Y"= method development; "N"= no method development
Application	Y/N	"Y"= spectroscopic technique was used for an experiment related to measuring or characterizing the contaminant, recovery experiments not included; "N"= not used in an experiment
MP	Text	Micropollutant; "EE2"= 17alpha-ethinylestradiol; "E2"= 17beta-estradiol; "E1"= estrone; "ERY"= erythromycin; "CLA"= clarithromycin; "AZI"= azithromycin; "AMO"= amoxicillin; "CIP"= ciprofloxacin
Quant/Qual	QT/QL	"QT"= quantitative analysis; "QL"= qualitative analysis
SensorType	Text	Type of biosensors; "A"= absorbance; "E"=electrochemical; "F"= fluorescence; "IR"= infrared; "L"=luminescence; "P"= piezoelectric; "R"= Raman or Rayleigh scattering; "RI"=refractive index; "O"=other
SensorSubtype	Text	Subtypes of the biosensors; more specific descriptors
NanoType	Text	Type of nanomaterials used in the method
Recognition	Text	Biological recognition element; Aptamer or Antibody
RangeLow	Numerical	The lowest concentration (in ug/L, AKA ppb) in the method's analytical range
RangeHigh	Numerical	The highest concentration (in ug/L, AKA ppb) in the method's analytical range
LowLimit	Numerical	The low limit concentration (in ug/L AKA ppb); if bot LOQ and LOD are reported, the lowest of these (LOD) is reported
LimitType	Text	The type of the reported low limit; "LOD"= limit of detection; "LOQ"= limit of quantitation
LODdetermination	Text	The calculation or method used to estimate LOD
Matrix	Text	The type of sample matrices tested

Table E.2: List of publications from systematic literature review, continued to next page.

ArticleID	1stAuthor	PubYear	DOI	Design	Application	MP	Quant/Qual	SensorType	SensorSubtype	NanoType	Recognition	RangeLow	RangeHigh	LowLimit	LimitType	LODdetermination	Matrix
1	Suo	2020	10.1016/j.snb.2020.128586	Y	N	E2	QT	F	FRET	NCB/AgNC	Aptamer	5.45E-03	4.09E+02	4.09E-03	LOD	S/N = 3	Buffer
2	Yao	2020	10.1016/j.snb.2020.128308	Y	N	E2	QT	R	SERS	AuCOF	Aptamer	3.54E-02	7.27E-01	2.18E-03	LOD	Not stated	Water
2	Yao	2020	10.1016/j.snb.2020.128308	Y	N	E2	QT	R	RRS	AuCOF	Aptamer	8.17E-03	8.99E-02	5.45E-03	LOD	Not stated	Water
2	Yao	2020	10.1016/j.snb.2020.128308	Y	N	E2	QT	R	SERS,RRS	AuCOF	Aptamer	8.17E-03	9.07E-01	1.63E-03	LOD	Not stated	Water
3	Song	2020	10.1016/j.ihazmat.2020.122024	Y	N	AMO	QT	E	EIS	TiO2gC3N4@AuNP	Aptamer	1.83E-01	1.10E+00	7.31E-02	LOD		Buffer, Wastewater
4	Zhang	2020	10.1039/d0nr01901a	Y	N	E2	QT	E	DPV	AuDODA	Aptamer	2.72E-02	2.72E+02	9.75E-05	LOD	3 Blank_Sd/Slope	Water, Serum
5	Minopoli	2020	10.1016/j.snb.2020.127699	Y	N	E2	QT	A	LSPR	AuNP	Antibody	3.00E-03	2.72E+01	3.00E-03	LOD	Not stated	Water, Tap Water
6	Feng	2020	10.1016/j.snb.2019.127443	Y	N	E2	QT	E	PEC	BiVO4/Bi2S3 NA	Aptamer	2.72E-07	1.36E-01	8.72E-08	LOD	Not stated	Water, Urine
7	Brognara	2020	10.3762/bjnano.11.87	Y	N	E2	QT	R	SERS	TiO2/AuNP	Aptamer	2.72E-01	2.72E+03	NA	NA		Water
8	Zaid	2020	10.3390/nano10071346	Y	N	E2	QT	E	EIS	CD	Aptamer	2.72E-04	2.72E+01	1.36E-04	LOD	3 Blank_Sd/Slope	Buffer, River Water
9	Yao	2019	10.1016/j.snb.2019.03.078	Y	N	E2	QT	A	ICA	MNP	Antibody	2.00E-01	5.00E+00	2.00E-01	LOD	Visual	Buffer,Milk, Prawn, Fish, Chicken
10	Pu	2019	10.1007/s11270-019-4171-4	Y	N	E2	QT	A	LSPR	AuNP	Aptamer	5.45E-02	1.36E+00	2.72E-02	LOD	Not stated	Water, Fishpond Water, Lake Water, Tap Water
11	Pu	2019	10.1016/j.talanta.2018.10.021	Y	N	E2	QT	R	SERS	Au@AgNP	Aptamer	2.72E-05	2.72E-01	7.49E-07	LOD	Not stated	Water, Aquaculture Water, Lake Water, Tap Water
12	Singh	2019	10.1016/j.bios.2018.10.004	Y	N	E2	QT	E	EIS	ZnONR	Antibody	1.00E-04	2.00E-01	1.00E-05	LOD	S/N = 3	Water, Tap Water, Packaged Water
13	Kumbhat	2019	10.1016/j.jpba.2018.10.015	Y	N	E2	QT	RI	SPR	Au Film	Antibody	1.00E-02	1.00E+03	1.00E-03	LOD	S/N = 3	Buffer
14	Wang	2018	10.1016/j.bios.2018.02.012	Y	N	E2	QT	E	DPV	MWCNT/THI/AuNP	Antibody	1.00E-02	1.00E+02	1.00E-02	LOD	S/N = 3	Buffer, Serum
15	Li	2018	10.1016/S1872-2040(17)61079-X	Y	N	E2	QT	A	LSPR	AuNP-AuNP-UCNP	Aptamer	1.00E+01	1.50E+02	5.00E-01	LOD	Not stated	Water, River Water
16	Scala-Benuzzi	2018	10.1021/acs.analchem.8b00028	Y	Y	EE2	QT	E	SWV	SNP	Antibody	5.00E-04	1.20E-01	1.00E-04	LOD		Water, River Water, Tap Water
17	Du	2018	10.1021/acs.analchem.8b00162	Y	N	E2	QT	L	ECL	Eu2O3/gC3N4	Aptamer	2.72E-06	2.72E+00	9.07E-07	LOD	S/N = 3	Buffer, Ethanol, Milk Powder
18	Jia	2018	10.1016/j.snb.2017.07.061	Y	N	E2	QT	A	LSPR	spioMNP	Antibody	3.91E+00	1.00E+03	3.24E+00	LOD	S/N = 3	Water, Milk
19	Liu	2017	10.1021/acsami.7b07047	Y	N	E2	QT	E	PEC	TiO2/BiVO4	Aptamer	2.72E-05	6.81E-02	6.81E-06	LOD	S/N = 3	Buffer, Urine
20	Lee	2017	10.1016/j.bios.2017.03.061	Y	N	E2	QT	F	MEF	Ag/Al Film	Aptamer	1.00E-03	1.00E+02	1.00E-03	LOD	Not stated	Water, Wastewater
21	Tan	2017	10.1002/chem.201702220	Y	N	E2	QT	L	UCL	UCNPs	Aptamer	2.72E-02	2.72E-01	2.72E-02	LOQ		Buffer, Serum
22	Alsager	2017	10.1021/acs.analchem.7b00906	Y	N	E2	QT	A	LFA	AuNP	Aptamer	1.36E+01	2.72E+02	1.36E+01	LOD	S/N = 3	Water, River Water
23	Du	2017	10.1016/j.bios.2017.01.034	Y	N	E2	QT	E	PEC	Fe2O3/NG/AuNR	Aptamer	2.72E-07	2.72E-01	8.99E-08	LOD	S/N = 3	Buffer, Ethanol, Milk Powder
24	Boltovets	2017	10.1016/j.bios.2016.11.017	Y	N	E2	QT	RI	SPR	Au Film	Antibody	1.00E-01	1.00E+03	1.00E-03	LOD	Not stated	Buffer
25	Peng	2016	10.1007/s12274-016-1270-z	Y	N	CIP	QT	A	LSPR	AuNP	Antibody	1.00E-01	2.50E+00	2.50E-01	LOD		Buffer, Milk
26	Huang	2016	10.1016/j.bios.2015.12.024	Y	N	E2	QT	F	QD	CdTe QC/Ru	Aptamer	2.18E+01	1.09E+02	1.01E+01	LOD	3Sd	Buffer, Serum
27	Zhang	2016	10.1038/srep23391	Y	N	E2	QT	E	CV	Au@PDNr/CoFe2O6/rGO	Antibody	1.00E-02	1.80E+01	3.30E-03	LOD	Not stated	Buffer, River Water
28	Duo	2016	10.1039/c5cc09066k	Y	N	E2	QT	F	FRET	GO	Aptamer	2.72E-05	2.72E-01	1.91E-05	LOD	3Sd	Ethyl Acetate
29	Na	2016	10.1039/c6tb00897f	Y	N	E2	QT	E	FET	UCPPyNT	Aptamer	2.72E-07	2.72E-01	2.72E-07	LOD	Not stated? S/N=3?	Buffer
30	Zhang	2016	10.1071/CH14735	Y	N	E2	QT	A	LSPR	AuNP	Aptamer	4.28E-01	9.53E+01	4.28E-01	LOD	3 Blank_Sd/Slope	Water, Environmental Water
31	Zhang	2016	10.1016/j.microc.2015.08.024	Y	N	CIP	QT	F	FRET	AuNP/UCP	Antibody	1.00E+00	8.00E+01	2.00E-01	LOD		Water, Tap Water, Pond Water, River Water
32	Li	2015	10.1016/j.matlet.2015.06.079	Y	N	E2	QT	A	LSPR	AuNP	Aptamer	1.00E+01	9.00E+01	3.00E+00	LOD	Not stated	Water, Tap Water
33	Chen	2015	10.1039/c5nr04987c	Y	N	AMO	QT	A	ICA	AuNP	Antibody	2.50E-01	5.00E+00	2.50E-01	LOD		Buffer, Milk
34	Zhu	2015	10.1016/j.bios.2015.03.050	Y	N	E2	QT	E	EIS	NPore Polymer	Aptamer	2.72E-07	2.72E+02	2.72E-07	LOD	S/N = 3	Buffer, Urine, Tap Water
35	Alsager	2015	10.1021/acs.analchem.5b00335	Y	N	E2	QT	A	LSPR	AuNP	Aptamer	5.45E-02	2.18E-01	5.45E-02	LOD	Not stated	Water
35	Alsager	2015	10.1021/acs.analchem.5b00335	Y	N	E2	QT	A	LSPR	AuNP	Aptamer	1.36E+01	2.18E+02	1.36E+01	LOD	Not stated	Urine
36	Monerris	2015	10.1016/j.snb.2014.11.048	Y	N	E2	QT	E	SWV	AuNP-cys-Au Disk	Antibody	5.40E-04	1.36E+01	8.40E-04	LOD	3Blank_Sd	Buffer, Bovine Serum
37	Chavez	2014	10.1039/c4an01376j	Y	N	E2	QT	A	LSPR	AuNP	Aptamer	2.72E+02	1.36E+03	NA	NA		Buffer
38	Huang	2014	10.1016/j.snb.2014.05.055	Y	N	E2	QT	E	DPV	AuNP/VS2NF	Aptamer	2.72E-03	2.72E+00	2.72E-04	LOD	3 Blank_Sd/Slope	Buffer, Urine
39	Alsager	2014	10.1016/j.bios.2014.02.004	Y	N	E2	QT	E	TRPS	PsNP	Aptamer	1.36E+00	2.72E+01	1.36E+00	LOD	Not stated	Buffer
39	Alsager	2014	10.1016/j.bios.2014.02.004	Y	N	E2	QT	R	DLS	PsNP	Aptamer	1.36E+00	2.72E+01	1.36E+00	LOD	Not stated	Buffer
40	Fan	2014	10.1021/es405685y	Y	Y	E2	QT	E	PEC	CdSeNP/TiO2NT	Aptamer	1.36E-05	4.09E-03	8.99E-06	LOD	3Blank_Sd	Buffer, Hospital Wastewater, Lake Water
41	Huang	2014	10.1039/c4ay01478b	Y	N	E2	QT	E	DPV	WS2NS/AuNP	Aptamer	2.72E-03	2.72E+00	2.72E-04	LOD	3 Blank_Sd/Slope	Buffer, Serum, River Water
42	Long	2014	10.1039/c3ra45554h	Y	N	E2	QT	F	FRET	QD	Aptamer	2.23E-01	5.58E+00	5.99E-02	LOD	S/N = 3	Buffer, Tap Water, Bottled Water, Wastewater
43	Ricciardi	2013	10.1016/j.bios.2012.08.043	Y	N	E2	QT	P	MC	MC	Antibody	1.00E-05	4.00E-03	2.00E-05	LOD	S/N = 3	Buffer, Serum
44	Karabchevsky	2013	10.3390/bios3010157	Y	N	E1	QL	RI	SPR	AgNL	Antibody	NA	NA	NA	NA		Water
45	Liu	2009	10.1016/j.talanta.2008.09.027	Y	N	E2	QT	E	SWV	AuNP	Antibody	2.50E-02	4.00E+00	6.00E-03	LOD	Blank_mean - 3Blank_Sd	Buffer, Serum
46	Adrian	2009	10.1016/j.trac.2009.04.011	Y	N	CIP	QT	RI	EV	WGCh	Antibody	4.40E+00	7.03E+01	1.00E+00	LOD		Buffer, Milk
47	Sun	2008	10.1021/ac7024893	Y	N	E1	QT	E	DPV	MOSI NW	Antibody	2.00E-03	2.00E-02	1.40E-03	LOD		Buffer
48	Dutta	2007	10.1039/b704723a	Y	N	E2	QT	P	MC	MC	Antibody	2.72E-03	2.72E-01	2.72E-03	LOD	Visual?	Buffer
49	Zhang	2020	10.1016/j.procbio.2020.08.012	Y	N	E2	QT	A	LSPR	AuNP	Antibody	2.72E-02	1.09E+01	2.72E-02	LOD	Visual	Water, Serum
50	Cezaro	2020	10.1109/JSEN.2020.3000582	Y	N	E1	QT	P	MC	MC	Antibody	1.00E-02	5.00E+01	2.60E-02	LOD		Water, Tap Water
50	Cezaro	2020	10.1109/JSEN.2020.3000582	Y	N	E2	QT	P	MC	MC	Antibody	1.00E-02	5.00E+01	9.00E-03	LOD	Blank_mean + 3Blank_Sd	Water, Tap Water
51	Huang	2020	10.1002/bab.2008	Y	N	E2	QT	A	ELISA	AuNP	Antibody+Aptamer	4.09E-01	1.36E+01	4.00E-01	LOD	S/N = 3	Buffer, Serum
52	Li	2020	10.1016/j.bios.2020.112089	Y	N	E2	QT	E	PEC	FeOOH/CuInS2	Aptamer	1.00E-05	1.00E+03	3.65E-06	LOD	S/N = 3	Water, Tap Water, Lake Water
53	Yan	2020	10.1016/j.bios.2019.111739	Y	N	E2	QT	E	PEC	NzIn2S4@NH2MIL125(Ti)	Antibody	5.00E-04	2.00E+01	3.00E-04	LOD	S/N = 3	Water, Lake Water
54	Ming	2019	10.1021/acssensors.9b01633	Y	Y	E2	QT	E	DPV	NH2SWCNT/NMB/AuNP	Aptamer	1.00E-02	5.00E+02	5.00E-03	LOD	S/N = 3	Buffer, Serum
55	Chen	2019	10.1021/acssensors.9b00963	Y	N	E2	QT	F	DNA dye	AuNP@Fe3O4	Aptamer	1.07E-04	9.53E-01	3.21E-05	LOD	S/N = 3	Buffer, Milk, Fish, Pork
56	Hu	2019	10.1007/s00604-019-3629-9	Y	N	CIP	QT	F	FRET	CNT/MoSe2	Aptamer	6.30E-01	8.00E+01	6.30E-01	LOD		Buffer, Milk
57	Hendrickson	2019	10.1002/jsfa.9605	Y	N	CIP	QT	A	LSPR	AuNP/ICA	Antibody	4.00E-02	2.20E+00	5.00E+00	LOD		Buffer, Milk
58	Liu	2019	10.1007/s00604-019-3465-y	Y	N	E2	QT	E	DPV	AuNP-Thi-CNT	Aptamer	3.27E-03	1.63E+01	4.09E-04	LOD	Not stated	Buffer, Serum
59	Li	2019	10.1016/j.bios.2018.10.047	Y	N	E2	QT	E	FET	GFET	Aptamer	1.36E-01	1.36E+02	1.01E-02	LOD	3Blank_Sd	Buffer, Tap Water
60	Yao	2019	10.1007/s00604-018-3114-x	Y	N	E2	QT	R	SERS	Au@AgNP	Aptamer	2.72E-04	2.72E+00	2.72E-05	LOD	Not stated	Buffer, Urine
61	Cao	2018	10.1016/j.ab.2018.06.027	Y	N	E2	QT	RI	SPR	Cr/Au Film	Antibody	2.72E-03	5.45E-01	8.17E-05	LOD	Blank_mean - 3Blank_Sd	Buffer
62	Hu	2018	10.1016/j.snb.2018.03.155	Y	N	CIP	QT	E	EIS	MWCNT/N2O5	Aptamer	5.00E-01	8.00E+00	5.00E-01	LOD		Buffer, Milk
63	Jiang	2018	10.1007/s00216-018-1095-6	Y	N	E2	QT	RI	Etalon	pNIPAm/Au	Aptamer	5.00E-03	2.00E-01	1.20E-03	LOD	3Blank_Sd	Water, Milk
64	Rather	2018	10.1039/c7an02092a	Y	N	E2	QT	E	SWV	ERGO/GCE	Aptamer	2.72E-07	2.72E-01	1.36E-06	LOD	3 Blank_Sd/Slope	Buffer, Wastewater
65	Li	2018	10.1166/jnn.2018.14235	Y	N	E2	QT	F	FRET	QD/AuNP	Aptamer	5.00E-01	1.50E+02	5.70E-02	LOD		Water, Tap Water, Swine Feed Water
66	Liu	2018	10.1016/j.snb.2017.08.003	Y	N	E2	QT	R	SERS	Au@AgCSNP	Aptamer	2.72E-05	2.72E+00	1.36E-05	LOD	Not stated	Buffer, Sewer Water, River Water
67	Lavaee	2017	10.1007/s00604-017-2213-4	Y	N	CIP	QT	A	LSPR	AuNP	Aptamer	1.09E+00	1.36E+02	3.27E-01	LOD		Water, Serum, Milk
68	Ni	2017	10.1016/j.ab.2017.01.021	Y	N	E2	QT	F	FRET	AuNP	Aptamer	1.31E-01	5.45E+01	1.31E-01	LOD	3 Blank_Sd/Slope	Water, Environmental Water
69	Monerris	2016	10.1016/j.microc.2016.06.001	Y	N	E1	QT	E	SWV	pNAP/AuNP	Antibody	8.00E-05	2.00E+02	6.10E-05	LOD		Buffer, Tap Water
70	Chen	2016	10.1080/03067319.2016.1264582	Y	N	E2	QT	P	MC	MC	Antibody	1.00E+02	1.00E+04	4.00E+01	LOD	3 Blank_Sd/Slope?	Buffer, Facial Cleanser, Skin Milk
71	Zheng	2015	10.1116/1.4935246	Y	N	E2	QT	E	FET	CNT	Aptamer	1.36E+01	4.36E+02	1.36E+01	LOD	Not stated	Water
72	Fan	2015	10.1016/j.bios.2015.01.015	Y	N	E2	QT	E	DPV	NiHCFNP/AuNP	Aptamer	2.72E-04	2.72E-01	2.18E-05	LOD	3Blank_Sd	Buffer, Wastewater
73	Zhang	2014	10.1039/c4ra13066a	Y	N	E2	QT	E	SWV	CuS2	Antibody	2.50E-02	7.50E+00	7.50E-03	LOD	Not stated	Buffer, River Water, Lake Water

List of publications from systematic literature review, continued from previous page.

ArticleID	1stAuthor	PubYear	DOI	Design	Application	MP	Quant/Qual	SensorType	SensorSubtype	NanoType	Recognition	RangeLow	RangeHigh	LowLimit	LimitType	LODdetermination	Matrix
74	Zhang	2014	10.1016/j.bios.2013.08.042	Y	N	E2	QT	E	SWASV	FeO4-NH2NP/GS	Antibody	5.00E-05	1.00E+02	1.50E-05	LOD	S/N = 3	Buffer, Tap Water, River Water
75	Dharuman	2013	10.1016/j.electacta.2013.10.128	Y	N	E2	QT	E	CV	ErG/AuNP	Antibody	2.72E-04	2.72E+05	2.72E-07	LOD	Not stated	Buffer
76	Ma	2013	10.1039/c3tb20932f	Y	N	E2	QT	E	CV	Pt@SBA-15	Antibody	5.00E-03	8.00E+00	1.20E-03	LOD	S/N = 3	Buffer, River Water
77	Schirlagl	2012	10.1016/j.snb.2012.07.036	Y	N	E2	QT	P	MC	MC/MIP	Antibody	5.00E+02	5.00E+03	5.00E+02	LOD	Not stated	Water
78	Olowu	2010	10.3390/s101109872	Y	N	E2	QT	E	SWV	PEDOT/AuNP	Aptamer	2.72E-02	2.72E+01	5.45E-03	LOD	Not stated	Buffer
79	Martinez	2010	10.1016/j.bios.2009.10.031	Y	N	EE2	QT	E	Amp	MNP	Antibody	1.00E-04	1.50E+00	6.00E-06	LOD		Buffer, Tap Water, Water, River Water
80	Liu	2010	10.1016/j.bios.2009.10.047	Y	N	E2	QT	E	SWV	AuNP	Antibody	1.80E-02	1.20E+00	1.80E-02	LOD	Blank_mean - 3Blank_Sd	Buffer
80	Liu	2010	10.1016/j.bios.2009.10.047	Y	N	E2	QT	E	EIS	AuNP	Antibody	5.00E-02	1.00E+00	2.60E-02	LOD	Blank_mean - 3Blank_Sd	Buffer
81	Soh	2015	10.1021/acs.analchem.5b00875	Y	N	E2	QT	A	LSPR	AuNP	Aptamer	2.72E-02	2.72E+03	2.72E-02	LOD	3Blank_Sd	Methanol, Synthetic Saliva
82	Huang	2015	10.1016/j.bios.2014.08.010	Y	N	E2	QT	E	DPV	CoS/AuNP	Aptamer	2.72E-04	2.72E-01	1.91E-04	LOD	3Blank_Sd	Water, Urine
83	Huang	2015	10.1007/s00604-014-1352-0	Y	N	E2	QT	E	DPV	GOx/AuNP/CuS	Aptamer	1.36E-04	1.36E+00	1.63E-05	LOD	3 Blank_Sd/Slope	Buffer, Urine
84	Zhu	2020	10.1039/d0tc04202a	Y	N	CIP	QT	E	EIS	AuCOF	Aptamer	1.00E-05	5.00E-01	2.34E-06	LOD		Buffer, Milk
85	Zhang	2020	10.1016/j.snb.2020.128458	Y	N	AMO	QL	A	LFIA	ACN	Antibody	2.00E+00	2.00E+00	2.00E+00	LOD		Milk
85	Zhang	2020	10.1016/j.snb.2020.128458	Y	N	AMO	QL	A	LFIA	AuNP	Antibody	5.00E+00	5.00E+00	5.00E+00	LOD		Milk
86	Zeng	2019	10.1039/c9qm00429g	Y	N	ERY	QT	A	ICA	AuNP	Antibody	1.00E-01	5.00E+00	8.50E-02	LOD		Milk
86	Zeng	2019	10.1039/c9qm00429g	Y	N	CLA	QT	A	ICA	AuNP	Antibody	1.00E-01	2.50E+00	9.50E-02	LOD		Milk
86	Zeng	2019	10.1039/c9qm00429g	Y	N	AZI	QT	A	ICA	AuNP	Antibody	2.50E-01	1.00E+01	1.75E-01	LOD		Milk
87	Yu	2019	10.1039/c9ay00657e	Y	N	CIP	QT	A	ICA	AuNP	Antibody	7.80E-01	2.50E+01	7.50E-01	LOD		Buffer, Fish, Shrimp, Beef
88	Liu	2019	10.1021/acs.analchem.9b00534	Y	N	E1	QT	R	SERS	AuNP	Aptamer	2.72E-03	1.36E+01	1.36E-03	LOD		Water, Farm Wastewater, Mat. Hospital Wastewater, Tap Water, Surface Water near Farm, Surface Water near Mat. Hospital
88	Liu	2019	10.1021/acs.analchem.9b00534	Y	N	E2	QT	R	SERS	AuNP	Aptamer	2.72E-03	1.36E+01	1.36E-03	LOD	3 Blank_Sd/Slope	Water, Farm Wastewater, Mat. Hospital Wastewater, Tap Water, Surface Water near Farm, Surface Water near Mat. Hospital
88	Liu	2019	10.1021/acs.analchem.9b00534	Y	N	EE2	QT	R	SERS	AuNP	Aptamer	2.72E-03	1.36E+01	1.36E-03	LOD		Water, Farm Wastewater, Mat. Hospital Wastewater, Tap Water, Surface Water near Farm, Surface Water near Mat. Hospital
89	Yao	2019	10.1016/j.snb.2019.03.078	Y	N	E2	QT	A	ICA	MNP	Antibody	2.00E-01	5.00E+00	2.00E-01	LOD	Visual	Buffer, Milk, Fish, Chicken, Prawn
90	Ren	2019	10.1007/s00604-019-3266-3	Y	N	E2	QT	F	UCF	BP-Au@T-cDNA/UCNP	Aptamer	1.00E-01	1.00E+02	9.20E-02	LOD	Not stated	Buffer, Milk, Serum, Urine, River Water
91	Liu	2019	10.1016/j.talanta.2018.10.035	Y	N	E2	QT	E	DPV	Graphene	Aptamer	1.90E-05	2.70E-03	1.40E-05	LOD	3Blank_Sd	Water, Tap Water
92	Suaebah	2019	10.18494/SAM.2019.2231	Y	N	E2	QT	F	FQ	NCD	Aptamer	2.72E+01	2.72E+04	2.72E+01	LOD	Visual	Buffer
93	Li	2019	10.1039/c9nj05435a	Y	N	E2	QT	E	PEC	In2S3/CeTiO2/CdS	Aptamer	1.00E-05	1.00E+02	4.00E-06	LOD	S/N = 3	Buffer, Tap Water, Lake Water
94	Hendrickson	2018	10.1134/S000368381806008X	Y	N	CIP	QT	A	ICA	AuNP	Antibody	2.00E-01	8.00E-01	1.00E-02	LOD		Buffer, Milk
95	Wang	2018	10.1039/c8qm00336j	Y	N	E2	QT	A	ICA	AuNP	Antibody	1.00E+00	1.00E+01	1.10E+00	LOD	0.1Blank ?	Buffer, Milk
95	Wang	2018	10.1039/c8qm00336j	Y	N	EE2	QT	A	ICA	AuNP	Antibody	5.00E+00	5.00E+01	4.85E+00	LOD		Buffer, Milk
96	Qi	2018	10.1039/c8an00591e	Y	N	E2	QT	F	FQ	GNP	Aptamer	1.02E+00	2.00E+01	1.02E+00	LOD	Not stated	Buffer, Groundwater
97	Scala-Benuzzi	2018	10.1016/j.microc.2018.05.038	Y	N	EE2	QT	F	FPAD	SBA-15	Antibody	1.00E-04	1.00E-01	5.00E-05	LOD		Water, River Water, Tap Water, Bottled Water
98	*Svobodová*	*2017*	*10.1016/j.jsbmb.2016.09.018*	*N*	*Y*	*E2*	*QL*	*RI*	*SPR*	*Au Film*	*Aptamer*	*NA*	*NA*	*NA*	*NA*		*Water*
99	Du	2015	10.1039/c4an01952k	Y	N	E2	QT	F	FQ	DC-AuNP/MMP	Antibody	1.00E-05	1.00E+00	6.37E-06	LOD	Not stated	Buffer, Urine
100	Ke	2014	10.1016/j.electacta.2014.06.014	Y	N	E2	QT	E	EIS	dAu/BDD	Aptamer	2.72E-06	2.72E-01	1.36E-06	LOD	3Blank_Sd	Buffer, Surface Water
101	Chaisuwan	2013	10.1016/j.bios.2013.02.041	Y	N	E2	QT	E	DPASV	QD	Antibody	5.00E-02	1.00E+00	5.00E-02	LOD	Not stated	Water, Tap Water, Wastewater
102	Kanso	2013	10.1021/ac303406c	Y	N	E2	QT	E	SWV	MMB	Antibody	1.00E-04	1.00E-01	1.00E-03	LOD	0.15Blank ?	Buffer, Bottled Water, Lake Water, Raw Wastewater, Treated Wastewater
102	Kanso	2013	10.1021/ac303406c	Y	N	EE2	QT	E	SWV	MMB	Antibody	1.00E-02	1.00E+00	1.00E-02	LOD		Buffer, Bottled Water, Lake Water, Raw Wastewater, Treated Wastewater
102	Kanso	2013	10.1021/ac303406c	Y	N	E2	QT	A	ELISA	MMB	Antibody	1.00E-01	1.00E+02	3.60E-02	LOD	0.15Blank ?	Buffer, Bottled Water, Lake Water, Raw Wastewater, Treated Wastewater
102	Kanso	2013	10.1021/ac303406c	Y	N	EE2	QT	A	ELISA	MMB	Antibody	1.00E-01	1.00E+02	5.00E-02	LOD		Buffer, Bottled Water, Lake Water, Raw Wastewater, Treated Wastewater
103	He	2020	10.1007/s00604-020-4155-5	Y	N	E2	QT	F	RCA/MCE	AuNP/Fe3O4NC	Aptamer	2.00E-01	2.00E+00	6.80E-03	LOD	S/N = 3	Buffer, Milk
104	Cincotto	2016	10.1016/j.talanta.2015.09.061	Y	N	EE2	QT	E	Amp	AgNP/SiO2/GO	Antibody	1.00E-01	1.00E+01	6.50E-02	LOD		Urine
105	Yang	2015	10.1016/j.lwt.2015.04.022	Y	N	E2	QT	A	ICA	AuNP	Antibody	6.25E-02	2.00E+00	3.71E-02	LOD	Visual	Buffer, Milk
106	Liu	2014	10.1038/srep07571	Y	N	E2	QT	A	LSPR	AuNP	Aptamer	1.00E-01	1.00E+05	1.00E-01	LOD	Visual	Water
107	Kim	2011	10.1016/j.bios.2011.03.030	Y	N	E2	QT	A	LSPR	AuNP	Aptamer	1.36E+04	2.72E+04	1.36E+04	LOD	Blank_mean + 3Blank_Sd	Water

Appendix F

Design of Experiments for Aptasensor Optimisation (Chapter 6)

Since the 35-base aptamer was expected to have a lower limit of detection than the 76-base aptamer according to the literature, a face-centered central composite design of experiments (DoE) was used to confirm the ratio of AuNPs, aptamer, and sample volume used in this work were optimal [192, 279]. The central composite design (CCD) tests the low and high levels of each factors' working ranges, as well as axial points which allow for estimating quadratic effects [321]. In a face-centered CCD, the tested axial points are in the center of the face of each factorial space, so that three levels are tested for each factor. By using CCD, we can employ response surface methodology (RSM) to optimise the three selected parameters.

Other parameters, such as reaction times and temperatures, do not vary between published methods. However, the AuNPs are often independently synthesised in each study, with varying sizes and concentrations [192, 199, 200]. In addition, the concentration of aptamer and NaCl are also independently validated. However, as noted in Chapter 6, NaCl has been replaced here with the sample media which contains buffering salts; therefore, since the ionic strength of the sample is fixed, we can only vary the volume of sample added to the reaction.

Three levels were used for each factor: 15, 25, or 35 µL of AuNPs (x1); 50, 100, or 150 nM of 35-mer aptamer (x2); 15, 25; 35 µL of MMB media (x3). Fifteen permutations were analysed in random order in two experimental blocks, with three replications of the centre point in each block (Table F.1). In order to determine the best combination of reagents, we specifically evaluated the analytical sensitivity and limit of detection. These metrics were determined by measuring the response of six concentrations of E2 (0.032, 0.32, 3.2, 32, 320, and 360 µM) analysed in duplicate.

Since the data points available for each permutation were limited, a four-parameter logistic curve was fit to the data in lieu of a linear regression:

$$y = d + \frac{a-d}{1+(\frac{x}{c})^b}, \tag{F.1}$$

where y is the measured response, x is the concentration of E2, a is the parameter for the lower bound response, d is the parameter for the upper bound response, b is the slope, and c is the concentration at the midpoint between a and d. Four-parameter logistic models are commonly used for describing bioreceptor-ligand binding [222]. The goodness-of-fit for each concentration-response curve ($n = 20$) was evaluated using Pearson's correlation coefficient (R), with a mean correlation value of 0.956 and median of 0.996, indicating that the model is acceptable. Only two experimental tests – runs 6 and 7 from block 1 – were poorly fit by the model, with an R of 0.495 and 0.748, respectively. From this equation, the slope b and the x value at 10% greater than a ($x_{10\%}$) are used to estimate sensitivity and detection limit, respectively. The parameter results from the non-linear regression as well as the goodness-of-fit and LOD estimates are shown in Table F.2 and Figure F.1.

Response surface methodology was then used to determine the optimum combination of AuNP volume, aptamer concentration, and sample volumes [280, 321]. Interaction plots showed clear interactions by each of the three parameters for both the LOD and slope (Figures F.2 and F.3). A first-order RSM was performed for both the LOD and slope (Figures F.4a and F.4b). Both first-order models obtained very poor R^2 values and non-significant p-values (Figures F.5 and F.6). However, the lack of fit p-value for both models were both > 0.05, indicating the first-order models did not have lack of fit. After performing a second-order RSM ((Figures F.7a, F.7b, F.8, F.9)), the R^2 for both responses improved from the first-order RSM, but were still poor. While the second-order RSM model's p-value for LOD remained insignificant, the second-order RSM model's $p = 0.027$ for the slope. The lack of fit p-values for both second-order models further increased.

In using RSM, the objective was to find the minimum LOD and maximum slope. This is given as the stationary point of response surface by the second-order RSM. The stationary point of response surface for the LOD values were 1.06 for x1, 0.17 for x2, and -1.55 for x3 – two of which are outside the coded limits of -1 to $+1$. Given the poor correlation of the model and the calculated inflection points being outside the experimental range, RSM was not useful in identifying the optimum combination of reagents for LOD. Furthermore, the calculated minimum, median, and maximum $x_{10\%}$ were 2.76, 3.45, and 4.30 log_{10} nM E2 (or 582, 2800, and 19500 nM E2), respectively. Each of these is substantially greater than the reported LOD of 0.2 nM obtained by Alsager et al. (2015) [192]. Therefore, other parameters may be influencing the lower limits of the method, such as nanoparticle size, shape, or uniformity.

The stationary point of response surface for the slope values were all within the experimental range. The optimum combination of reagents for the greatest slope were: 25 µL AuNPs, 100 nM

of 35-base aptamer, and 25 µL of sample in MMB media. These observations are supported by the results in Chapter 6 Figure 6.10b, which showed a slightly steeper slope when a higher sample volume was used. Interestingly, the optimum slope combination was the centre-point of the face-centered CCD. Of the six centre-point experiment replicates, one slope value of 70 was calculated by the regression; this is a statistical outlier. However, the other five b values had a mean of 12 ± 4. The overall median slope from the DoE was 14, or 9 when the five experiments which calculated slopes of 70 were excluded. Here, the optimum combination of AuNPs, aptamer, and sample volumes is not a remarkable improvement of the slope obtained for each combination.

In Chapter 6, a smaller sample volume (which was selected as the minimum volume required to induce particle aggregation) was used, as was a smaller aptamer concentration (which was deemed sufficient to stabilise the particles against salt-induced aggregation). However, the final aptasensor in the main text used a different aptamer, which may perform differently. Nonetheless, the aptasensor appears to be fairly robust against modifications to the concentrations of reagents used. It is unclear why the limit of detection of the 35-base aptamer from the literature could not be reproduced. However, we can be confident that the combinations of AuNP volume, sample volume, and aptamer concentration are practical, and any further refinement and development of the chosen parameters would be ineffectual, particularly to the main aims of the thesis.

Table F.1: Face-centered central composite design of experiments for testing the volumes of AuNPs and samples in MMB media (μL) and aptamer concentration (nM).

Block	Run	AuNP (x1)	Aptamer (x2)	Sample (x3)	x1	x2	x3
1	1	35	50	15	1	-1	-1
	2	25	100	25	0	0	0
	3	15	50	15	-1	-1	-1
	4	25	100	25	0	0	0
	5	35	50	35	1	-1	1
	6	15	150	15	-1	1	-1
	7	15	50	35	-1	-1	1
	8	35	150	35	1	1	1
	9	15	150	35	-1	1	1
	10	35	150	15	1	1	-1
	11	25	100	25	0	0	0
2	1	25	150	25	0	1	0
	2	35	100	25	1	0	0
	3	25	100	35	0	0	1
	4	25	100	25	0	0	0
	5	25	50	25	0	-1	0
	6	15	100	25	-1	0	0
	7	25	100	25	0	0	0
	8	25	100	25	0	0	0
	9	25	100	15	0	0	-1

Table F.2: Results of the four-parameter logistic regression fit for the E2 dilutions tested by the design of experiments.

Run Set	a	b	c	d	R	$x_{10\%}$
B1S1	0.61	8.47	4.29	0.99	0.9999	3.31
B1S2	0.58	17.53	4.13	0.97	1.0000	3.64
B1S3	0.50	3.61	7.20	1.55	0.9981	3.92
B1S4	0.43	9.09	4.68	0.78	0.9986	3.68
B1S5	0.89	70.00	3.53	1.08	0.9619	3.42
B1S6	0.89	70.00	4.44	0.96	0.4950	4.30
B1S7	0.94	70.00	3.50	1.07	0.7484	3.39
B1S8	0.80	13.30	3.89	1.06	0.9963	3.30
B1S9	0.73	70.00	4.43	1.06	0.9868	4.29
B1S10	0.75	18.00	3.97	1.05	0.9987	3.51
B1S11	0.73	15.18	4.06	1.07	0.9998	3.51
B2S1	0.74	5.02	4.28	1.15	0.9964	2.76
B2S2	0.74	16.39	4.17	1.06	0.9985	3.65
B2S3	0.87	70.00	3.60	1.07	0.9904	3.49
B2S4	0.68	9.21	4.22	1.07	0.9994	3.32
B2S5	0.56	8.22	4.37	0.82	0.9957	3.34
B2S6	0.87	22.36	4.01	1.06	0.9805	3.63
B2S7	0.74	7.55	4.11	1.11	0.9900	3.08
B2S8	0.76	6.62	4.66	1.14	0.9988	3.34
B2S9	0.74	9.70	4.11	1.08	0.9940	3.28

The run set refers to the block (B#) and run (S#). Parameters *a-d* refer to Equation F.1, where b is the slope and $x_{10\%}$ is used to represent the limit of detection in log_{10} of nanomolar E2. R is the correlation coefficient of the model.

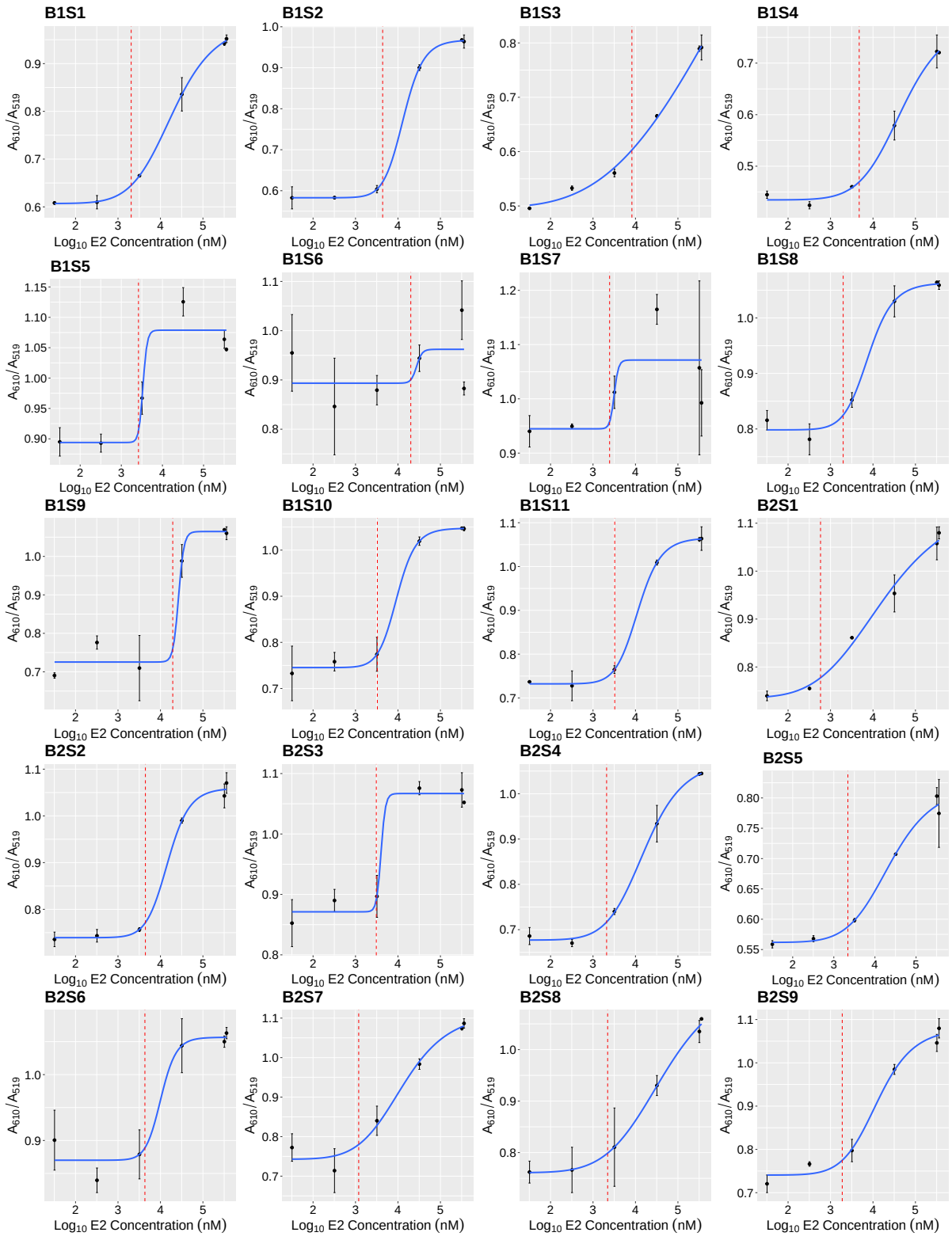

Figure F.1: Results from the DoE showing the aptasensor response for the different conditions given in Table F.1. The data is labelled for each run set by block (B#) and run (S#). Points are the mean of duplicates and error bars are standard deviation. The 4-parameter curve fit is shown with the blue curve, and the $x_{10\%}$ is indicated with the dashed red line.

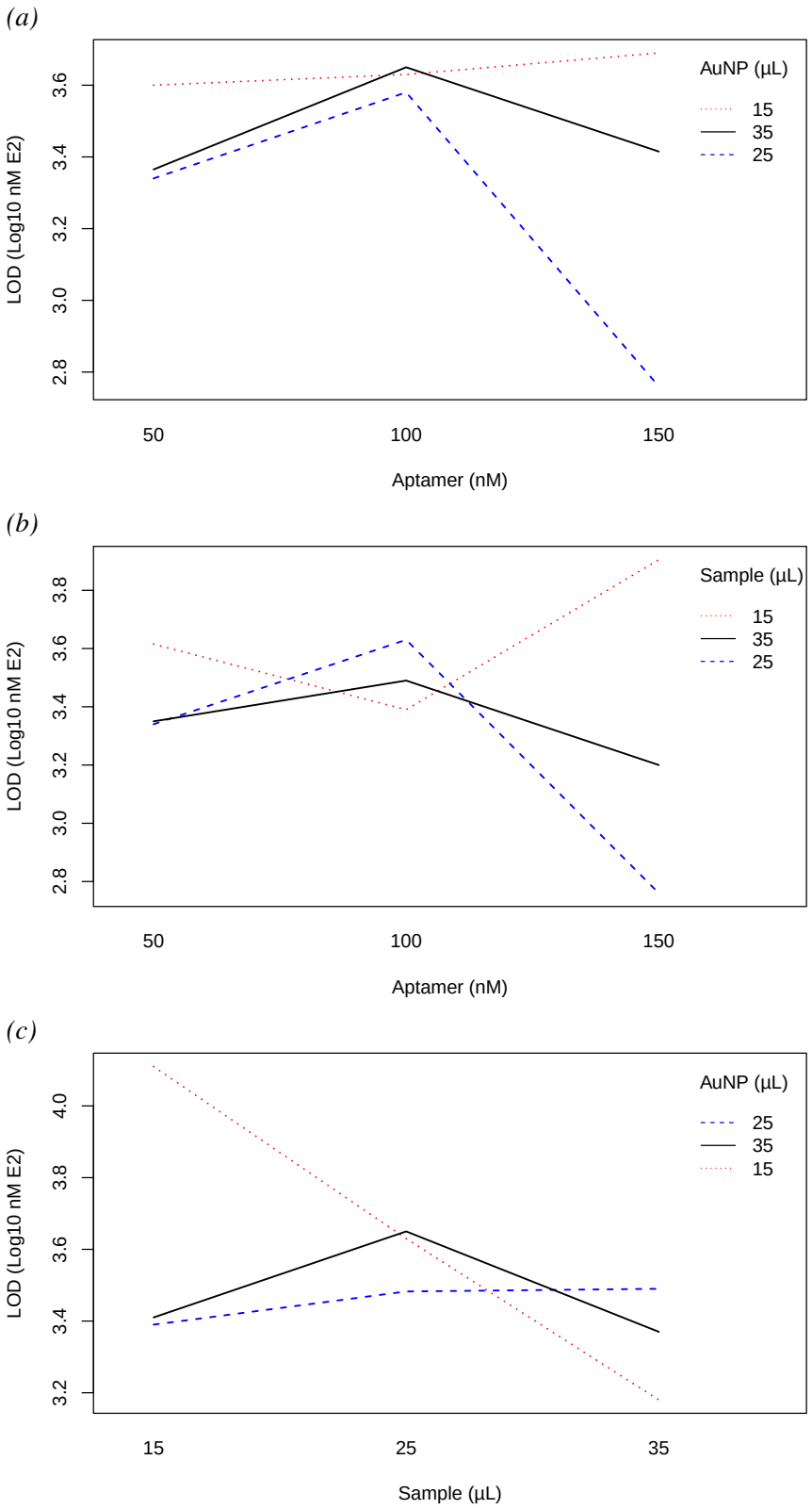

Figure F.2: Interaction plots for limit of detection comparing (a) aptamer concentration versus AuNP volume, (b) aptamer concentration versus sample volume, and (c) sample volume versus AuNP volume.

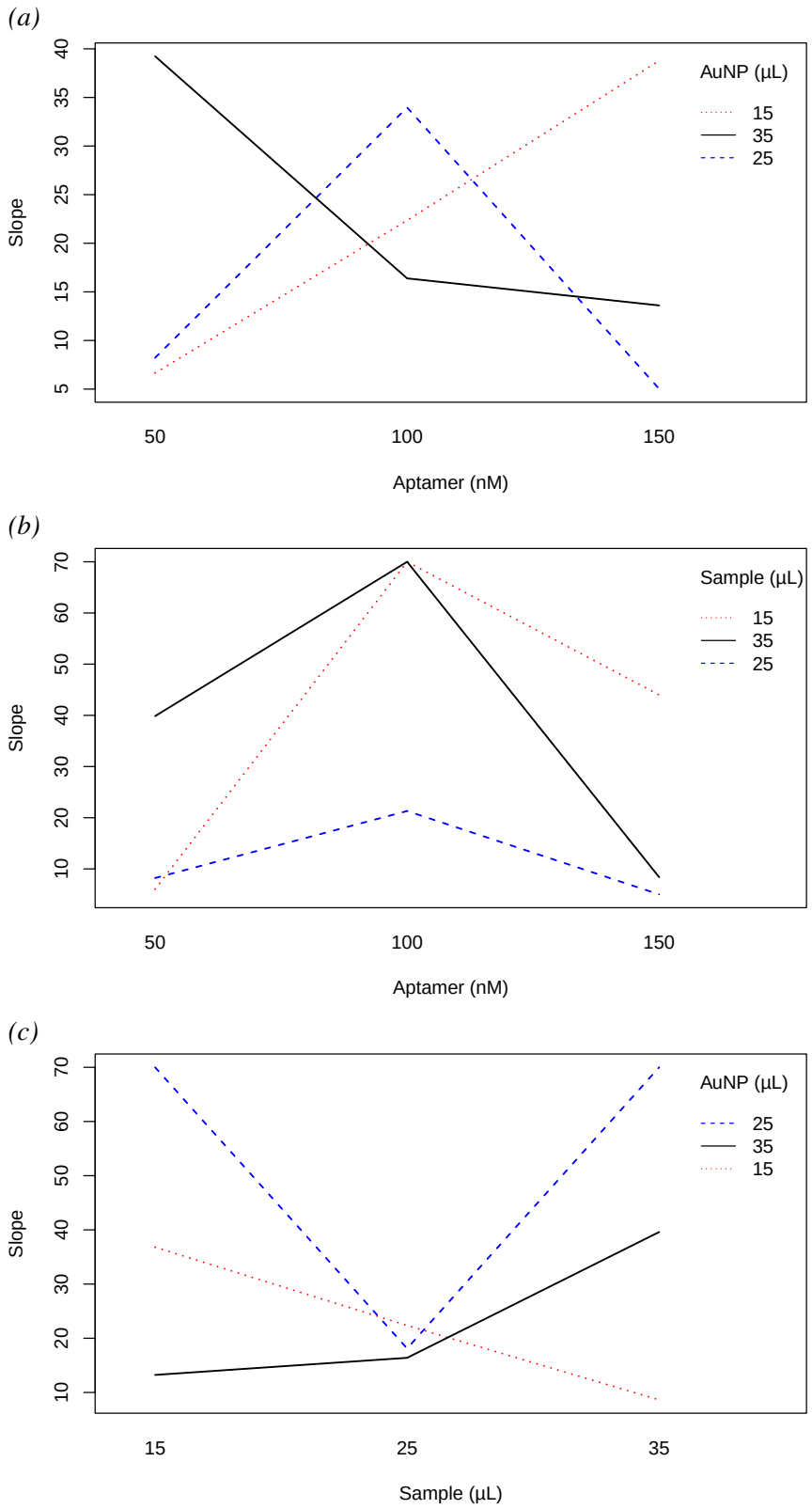

Figure F.3: Interaction plots for slope comparing (a) aptamer concentration versus AuNP volume, (b) aptamer concentration versus sample volume, and (c) sample volume versus AuNP volume.

(a)

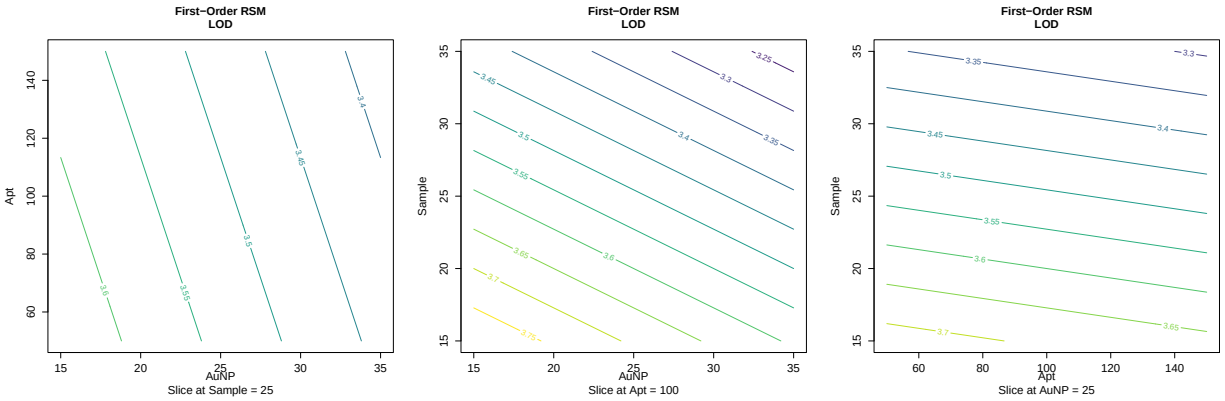

(b)

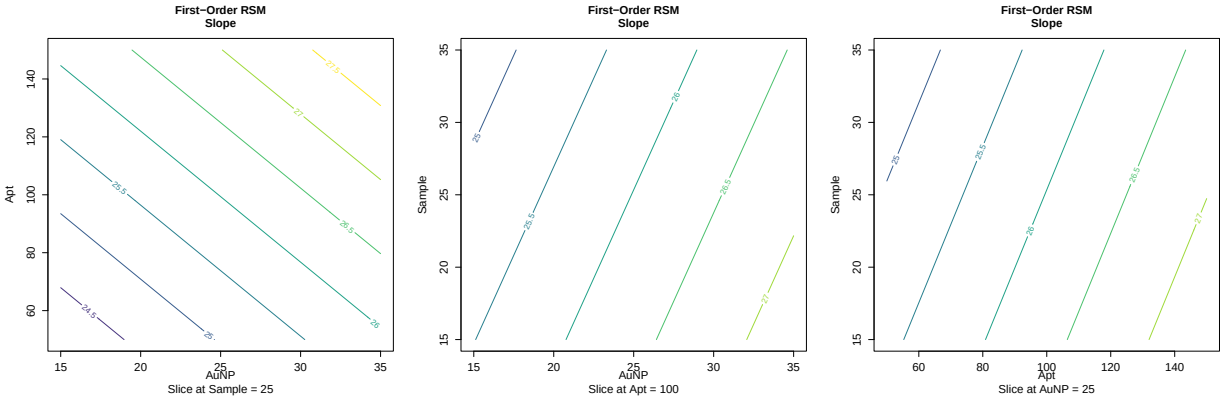

Figure F.4: First-order response surface method contour plots of AuNP volume, aptamer concentration, and sample volume on (a) limit of detection and (b) slope.

```
Call:
rsm(formula = EC10x ~ FO(x1, x2, x3), data = CCD1)

             Estimate Std. Error t value Pr(>|t|)
(Intercept)  3.508000   0.079725 44.0011   <2e-16 ***
x1          -0.100000   0.112749 -0.8869   0.3883
x2          -0.030000   0.112749 -0.2661   0.7936
x3          -0.184000   0.112749 -1.6319   0.1222
---
Signif. codes:  0 ‘***’ 0.001 ‘**’ 0.01 ‘*’ 0.05 ‘.’ 0.1 ‘ ’ 1

Multiple R-squared:  0.1804,Adjusted R-squared:  0.02667
F-statistic: 1.174 on 3 and 16 DF,  p-value: 0.3508

Analysis of Variance Table

Response: EC10x
               Df  Sum Sq Mean Sq F value Pr(>F)
FO(x1, x2, x3)  3 0.44756 0.14919  1.1736 0.3508
Residuals      16 2.03396 0.12712
Lack of fit    11 1.38843 0.12622  0.9776 0.5500
Pure error      5 0.64553 0.12911

Direction of steepest ascent (at radius 1):
        x1         x2         x3
-0.4726878 -0.1418063 -0.8697455

Corresponding increment in original units:
     AuNP       Apt    Sample
-4.726878 -7.090317 -8.697455
```

Figure F.5: First-order response surface method output for limit of detection. In the code, LOD is referred to as "EC10x".

```
Call:
rsm(formula = Slope ~ FO(x1, x2, x3), data = CCD1)

            Estimate Std. Error t value  Pr(>|t|)
(Intercept)  26.0125     6.4458  4.0356 0.0009577 ***
x1            0.8850     9.1157  0.0971 0.9238646
x2            0.9780     9.1157  0.1073 0.9158950
x3           -0.3620     9.1157 -0.0397 0.9688144
---
Signif. codes:  0 ‘***’ 0.001 ‘**’ 0.01 ‘*’ 0.05 ‘.’ 0.1 ‘ ’ 1

Multiple R-squared:  0.001405,Adjusted R-squared:  -0.1858
F-statistic: 0.007504 on 3 and 16 DF,  p-value: 0.9991

Analysis of Variance Table

Response: Slope
               Df  Sum Sq Mean Sq F value Pr(>F)
FO(x1, x2, x3)  3    18.7    6.24  0.0075 0.9991
Residuals      16 13295.4  830.96
Lack of fit    11 10446.0  949.64  1.6664 0.2986
Pure error      5  2849.4  569.88

Direction of steepest ascent (at radius 1):
        x1         x2         x3
 0.6470458  0.7150405 -0.2646673

Corresponding increment in original units:
     AuNP       Apt    Sample
 6.470458 35.752024 -2.646673
```

Figure F.6: First-order response surface method output for slope.

(a)

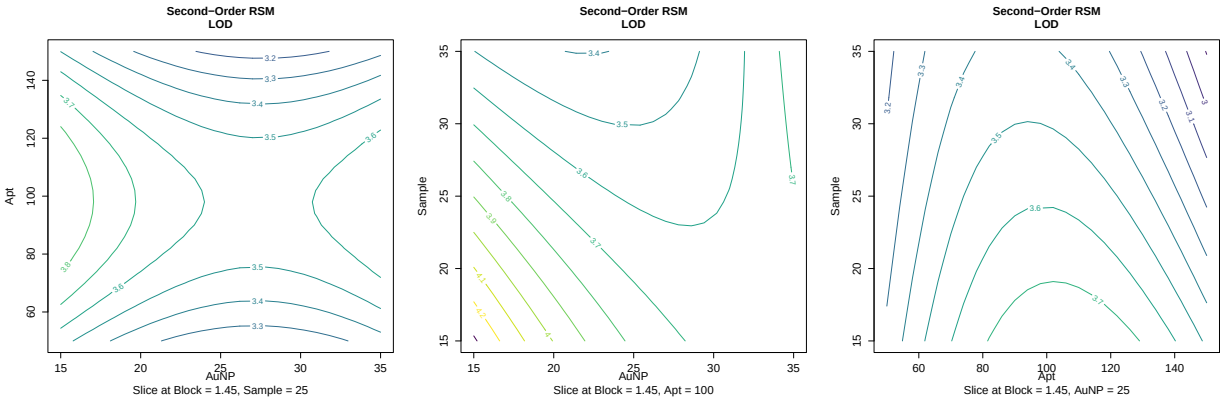

(b)

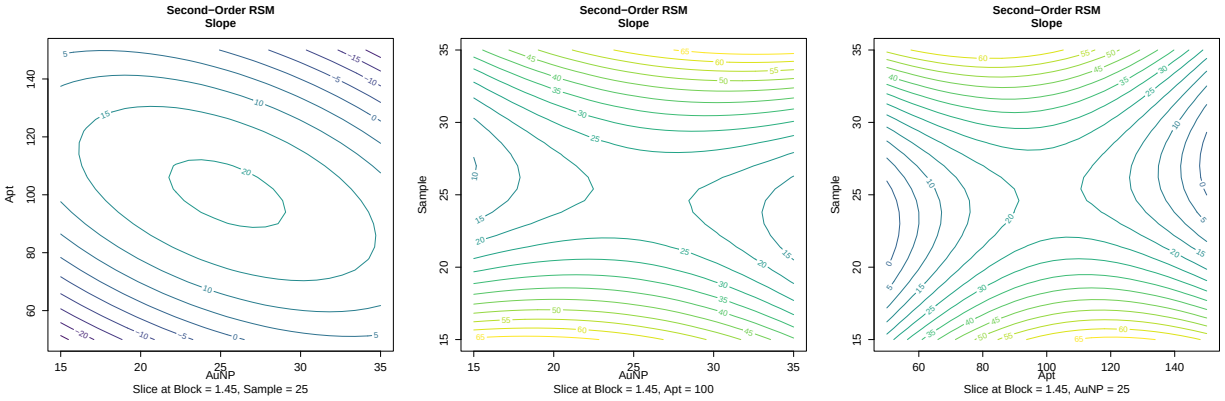

Figure F.7: Second-order response surface method contour plots of AuNP volume, aptamer concentration, and sample volume on (a) limit of detection and (b) slope.

```
Call:
rsm(formula = EC10x ~ Block + SO(x1, x2, x3), data = CCD1)

            Estimate Std. Error t value  Pr(>|t|)
(Intercept)  3.81448    0.36619 10.4166 2.545e-06 ***
Block       -0.15692    0.19324 -0.8120    0.4377
x1          -0.10000    0.11009 -0.9084    0.3874
x2          -0.03000    0.11009 -0.2725    0.7914
x3          -0.18400    0.11009 -1.6714    0.1290
x1:x2       -0.01000    0.12308 -0.0812    0.9370
x1:x3        0.22250    0.12308  1.8077    0.1041
x2:x3       -0.11000    0.12308 -0.8937    0.3947
x1^2         0.21070    0.21448  0.9824    0.3516
x2^2        -0.37930    0.21448 -1.7685    0.1108
x3^2         0.01070    0.21448  0.0499    0.9613
---
Signif. codes:  0 ‘***’ 0.001 ‘**’ 0.01 ‘*’ 0.05 ‘.’ 0.1 ‘ ’ 1

Multiple R-squared:  0.5604,Adjusted R-squared:  0.07206
F-statistic: 1.148 on 10 and 9 DF,  p-value: 0.4229

Analysis of Variance Table

Response: EC10x
                Df  Sum Sq  Mean Sq F value Pr(>F)
Block            1 0.02948 0.029480  0.2432 0.6337
FO(x1, x2, x3)   3 0.44756 0.149187  1.2310 0.3541
TWI(x1, x2, x3)  3 0.49365 0.164550  1.3577 0.3165
PQ(x1, x2, x3)   3 0.42007 0.140024  1.1554 0.3789
Residuals        9 1.09076 0.121195
Lack of fit      5 0.44689 0.089379  0.5553 0.7340
Pure error       4 0.64387 0.160967

Stationary point of response surface:
        x1         x2         x3
 1.0611267  0.1715922 -1.5525549

Stationary point in original units:
      AuNP        Apt     Sample
 35.611267 108.579612   9.474451

Eigenanalysis:
eigen() decomposition
$values
[1]  0.2614364 -0.0322412 -0.3870943

$vectors
          [,1]       [,2]        [,3]
x1  0.90974502 -0.4147713 -0.01813168
x2 -0.04254903 -0.1365908  0.98971337
x3  0.41298133  0.8996153  0.14191088
```

Figure F.8: Second-order response surface method output for limit of detection. In the code, LOD is referred to as "EC10x".

```
Call:
rsm(formula = Slope ~ Block + SO(x1, x2, x3), data = CCD1)

             Estimate Std. Error t value Pr(>|t|)
(Intercept)  -0.57417   17.60974 -0.0326 0.974701
Block        14.81401    9.29289  1.5941 0.145373
x1            0.88500    5.29406  0.1672 0.870933
x2            0.97800    5.29406  0.1847 0.857532
x3           -0.36200    5.29406 -0.0684 0.946979
x1:x2       -14.43750    5.91894 -2.4392 0.037413 *
x1:x3        13.63750    5.91894  2.3040 0.046689 *
x2:x3       -17.35750    5.91894 -2.9325 0.016688 *
x1^2         -9.21909   10.31393 -0.8938 0.394677
x2^2        -21.97409   10.31393 -2.1305 0.061969 .
x3^2         41.40591   10.31393  4.0146 0.003043 **
---
Signif. codes:  0 ‘***’ 0.001 ‘**’ 0.01 ‘*’ 0.05 ‘.’ 0.1 ‘ ’ 1

Multiple R-squared:  0.8105,Adjusted R-squared:    0.6
F-statistic:  3.85 on 10 and 9 DF,  p-value: 0.02734

Analysis of Variance Table

Response: Slope
                Df Sum Sq Mean Sq F value  Pr(>F)
Block            1  461.5  461.54  1.6468 0.23146
FO(x1, x2, x3)   3   18.7    6.24  0.0222 0.99517
TWI(x1, x2, x3)  3 5565.6 1855.21  6.6194 0.01179
PQ(x1, x2, x3)   3 4745.8 1581.94  5.6443 0.01870
Residuals        9 2522.4  280.27
Lack of fit      5   59.0   11.79  0.0192 0.99971
Pure error       4 2463.5  615.87

Stationary point of response surface:
           x1            x2            x3
 0.0405844743  0.0090823174 -0.0004084495

Stationary point in original units:
     AuNP       Apt    Sample
 25.40584 100.45412  24.99592

Eigenanalysis:
eigen() decomposition
$values
[1]  43.711319  -7.849931 -25.648657

$vectors
         [,1]       [,2]        [,3]
x1  0.1458840  0.9165920 -0.37225916
x2 -0.1453269 -0.3523476 -0.92451678
x3  0.9785693 -0.1889715 -0.08180364
```

Figure F.9: Second-order response surface method output for slope.

References

[1] United States Environmental Protection Agency, "The History of Drinking Water Treatment," Feb. 2000.

[2] "Transforming Our World: The 2030 Agenda for Sustainable Development," in *A New Era in Global Health* (W. Rosa, ed.), New York, NY: Springer Publishing Company, June 2017.

[3] M. Adeel, X. Song, Y. Wang, D. Francis, and Y. Yang, "Environmental impact of estrogens on human, animal and plant life: A critical review," *Environment International*, vol. 99, pp. 107–119, Feb. 2017.

[4] Y. Luo, W. Guo, H. H. Ngo, L. D. Nghiem, F. I. Hai, J. Zhang, S. Liang, and X. C. Wang, "A review on the occurrence of micropollutants in the aquatic environment and their fate and removal during wastewater treatment," *Science of The Total Environment*, vol. 473-474, pp. 619–641, Mar. 2014.

[5] V. de Lorenzo, "Biodegradation and Bioremediation: An Introduction," in *Consequences of Microbial Interactions with Hydrocarbons, Oils, and Lipids: Biodegradation and Bioremediation* (R. Steffan, ed.), pp. 1–21, Cham: Springer International Publishing, 2018.

[6] B. Du, G. Fan, W. Yu, S. Yang, J. Zhou, and J. Luo, "Occurrence and risk assessment of steroid estrogens in environmental water samples: A five-year worldwide perspective," *Environmental Pollution*, vol. 267, pp. 1–13, Dec. 2020.

[7] A. W. Norman and H. L. Henry, "13 Estrogens and Progestins," in *Hormones* (G. Litwack, ed.), pp. 275–320, Elsevier Science & Technology Books, 3rd ed., 2014.

[8] A. W. Norman and H. L. Henry, "2 Steroid Hormones: Chemistry, Biosynthesis, and Metabolism," in *Hormones* (G. Litwack, ed.), pp. 27–54, Elsevier Science & Technology Books, 3rd ed., 2014.

[9] M. P. Thomas and B. V. Potter, "The structural biology of oestrogen metabolism," *The Journal of Steroid Biochemistry and Molecular Biology*, vol. 137, pp. 27–49, Sept. 2013.

[10] J. W. Mueller, L. C. Gilligan, J. Idkowiak, W. Arlt, and P. A. Foster, "The Regulation of Steroid Action by Sulfation and Desulfation," *Endocrine Reviews*, vol. 36, pp. 526–563, Oct. 2015.

[11] B. Fretwell, Liz Nicol, Rob Whiting, Alice Baynes, Olwenn Martin, Virginie Keller, and Clarissa Rizzo, "Likelihood of three endocrine disrupting substances reaching drinking water DWI 70/2/328 (25853) - Final Report," Jan. 2021.

[12] The European Commission, "Commission Implementing Decision (EU) 2018/840 of 5 June 2018 establishing a watch list of substances for Union-wide monitoring in the field of water policy pursuant to Directive 2008/105/EC of the European Parliament and of the Council and repealing Commission Implementing Decision (EU) 2015/495- (notified under document C(2018)3362)," 2018.

[13] United States Environmental Protection Agency, "Drinking Water Contaminant Candidate List 4—Final," Nov. 2016.

[14] K. Kümmerer, "Emerging Contaminants versus Micro-pollutants," *CLEAN - Soil, Air, Water*, vol. 39, pp. 889–890, Oct. 2011.

[15] M. Ciślak, I. Kruszelnicka, J. Zembrzuska, and D. Ginter-Kramarczyk, "Estrogen pollution of the European aquatic environment: A critical review," *Water Research*, vol. 229, p. 119413, Feb. 2023.

[16] Q.-Q. Zhang, C. Xing, Y.-Y. Cai, X.-T. Yan, and G.-G. Ying, "How much do human and livestock actually contribute to steroids emission and surface water pollution from past to the future: A global research," *Science of The Total Environment*, vol. 772, pp. 1–10, June 2021.

[17] A. Johnson, R. Williams, and P. Matthiessen, "The potential steroid hormone contribution of farm animals to freshwaters, the United Kingdom as a case study," *Science of The Total Environment*, vol. 362, pp. 166–178, June 2006.

[18] K. Wojnarowski, P. Podobiński, P. Cholewińska, J. Smoliński, and K. Dorobisz, "Impact of Estrogens Present in Environment on Health and Welfare of Animals," *Animals*, vol. 11, p. 2152, July 2021.

[19] A. M. Vajda, L. B. Barber, J. L. Gray, E. M. Lopez, J. D. Woodling, and D. O. Norris, "Reproductive Disruption in Fish Downstream from an Estrogenic Wastewater Effluent," *Environmental Science & Technology*, vol. 42, pp. 3407–3414, May 2008.

[20] L. B. Barber, A. M. Vajda, C. Douville, D. O. Norris, and J. H. Writer, "Fish Endocrine Disruption Responses to a Major Wastewater Treatment Facility Upgrade," *Environmental Science & Technology*, vol. 46, pp. 2121–2131, Feb. 2012.

[21] K. A. Kidd, P. J. Blanchfield, K. H. Mills, V. P. Palace, R. E. Evans, J. M. Lazorchak, and R. W. Flick, "Collapse of a fish population after exposure to a synthetic estrogen," *Proceedings of the National Academy of Sciences*, vol. 104, pp. 8897–8901, May 2007.

[22] M. Muller, F. Rabenoelina, P. Balaguer, D. Patureau, K. Lemenach, H. Budzinski, D. Barceló, M. L. de Alda, M. Kuster, J.-P. Delgenès, and G. Hernandez-Raquet, "Chemical and biological analysis of endocrine-disrupting hormones and estrogenic activity in an advanced sewage treatment plant," *Environmental Toxicology and Chemistry*, vol. 27, no. 8, p. 1649, 2008.

[23] K. A. Hicks, M. L. M. Fuzzen, E. K. McCann, M. J. Arlos, L. M. Bragg, S. Kleywegt, G. R. Tetreault, M. E. McMaster, and M. R. Servos, "Reduction of Intersex in a Wild Fish Population in Response to Major Municipal Wastewater Treatment Plant Upgrades," *Environmental Science & Technology*, vol. 51, pp. 1811–1819, Feb. 2017.

[24] B. J. Park and K. Kidd, "Effects of the synthetic estrogen ethinylestradiol on early life stages of mink frogs and green frogs in the wild and in situ," *Environmental Toxicology and Chemistry*, vol. 24, no. 8, pp. 2027–2036, 2005.

[25] M. R. Lambert, G. S. J. Giller, L. B. Barber, K. C. Fitzgerald, and D. K. Skelly, "Suburbanization, estrogen contamination, and sex ratio in wild amphibian populations," *Proceedings of the National Academy of Sciences of the United States of America*, vol. 112, pp. 11881–11886, Sept. 2015.

[26] S. Jobling, R. Williams, A. Johnson, A. Taylor, M. Gross-Sorokin, M. Nolan, C. R. Tyler, R. van Aerle, E. Santos, and G. Brighty, "Predicted Exposures to Steroid Estrogens in U.K. Rivers Correlate with Widespread Sexual Disruption in Wild Fish Populations," *Environmental Health Perspectives*, vol. 114, pp. 32–39, Apr. 2006.

[27] S. Wang, Z. Zhu, J. He, X. Yue, J. Pan, and Z. Wang, "Steroidal and phenolic endocrine disrupting chemicals (EDCs) in surface water of Bahe River, China: Distribution, bioaccumulation, risk assessment and estrogenic effect on Hemiculter leucisculus," *Environmental Pollution*, vol. 243, pp. 103–114, Dec. 2018.

[28] J. Song, M. Nagae, Y. Takao, and K. Soyano, "Field survey of environmental estrogen pollution in the coastal area of Tokyo Bay and Nagasaki City using the Japanese common goby Acanthogobius flavimanus," *Environmental Pollution*, vol. 258, pp. 1–8, Mar. 2020.

[29] L. J. Guillette, T. S. Gross, G. R. Masson, J. M. Matter, H. F. Percival, and A. R. Woodward, "Developmental abnormalities of the gonad and abnormal sex hormone concentrations in juvenile alligators from contaminated and control lakes in Florida.," *Environmental Health Perspectives*, vol. 102, pp. 680–688, Aug. 1994.

[30] United States Environmental Protection Agency, "Basic Information about Nonpoint Source (NPS) Pollution," Sept. 2015.

[31] F. B. R. Gomes, P. A. A. Fernandes, S. E. C. Bottrel, E. M. F. Brandt, and R. D. O. Pereira, "Fate, occurrence, and removal of estrogens in livestock wastewaters," *Water Science and Technology*, vol. 86, pp. 814–833, Aug. 2022.

[32] R. Stuetz and T. Stephenson, "Water Quality," in *Principles of water and wastewater treatment processes*, pp. 1–22, London: IWA Pub., 2009. OCLC: 870994921.

[33] R. Stuetz and T. Stephenson, "Flowsheeting," in *Principles of water and wastewater treatment processes*, pp. 23–44, London: IWA Pub., 2009. OCLC: 870994921.

[34] D. Hendricks, "Water Treatment," in *Fundamentals of Water Treatment Unit Processes : Physical, Chemical, and Biological*, pp. 3–20, Taylor & Francis Group, 1st ed., 2010.

[35] Z.-h. Liu, G.-n. Lu, H. Yin, Z. Dang, and B. Rittmann, "Removal of Natural Estrogens and Their Conjugates in Municipal Wastewater Treatment Plants: A Critical Review," *Environmental Science & Technology*, vol. 49, pp. 5288–5300, May 2015.

[36] O. Braga, G. A. Smythe, A. I. Schäfer, and A. J. Feitz, "Fate of Steroid Estrogens in Australian Inland and Coastal Wastewater Treatment Plants," *Environmental Science & Technology*, vol. 39, pp. 3351–3358, May 2005.

[37] H. Andersen, H. Siegrist, B. Halling-Sørensen, and T. A. Ternes, "Fate of Estrogens in a Municipal Sewage Treatment Plant," *Environmental Science & Technology*, vol. 37, pp. 4021–4026, Sept. 2003.

[38] V. Gabet-Giraud, C. Miège, J. Choubert, S. M. Ruel, and M. Coquery, "Occurrence and removal of estrogens and beta blockers by various processes in wastewater treatment plants," *Science of The Total Environment*, vol. 408, pp. 4257–4269, Sept. 2010.

[39] C. Baronti, R. Curini, G. D'Ascenzo, A. Di Corcia, A. Gentili, and R. Samperi, "Monitoring Natural and Synthetic Estrogens at Activated Sludge Sewage Treatment Plants and in a Receiving River Water," *Environmental Science & Technology*, vol. 34, pp. 5059–5066, Dec. 2000.

[40] C. Desbrow, E. J. Routledge, G. C. Brighty, J. P. Sumpter, and M. Waldock, "Identification of Estrogenic Chemicals in STW Effluent. 1. Chemical Fractionation and in Vitro Biological Screening," *Environmental Science & Technology*, vol. 32, pp. 1549–1558, June 1998.

[41] S. K. Behera, H. W. Kim, J.-E. Oh, and H.-S. Park, "Occurrence and removal of antibiotics, hormones and several other pharmaceuticals in wastewater treatment plants of the largest industrial city of Korea," *Science of The Total Environment*, vol. 409, pp. 4351–4360, Sept. 2011.

[42] M. E. Valdés, D. J. Marino, D. A. Wunderlin, G. M. Somoza, A. E. Ronco, and P. Carriquiriborde, "Screening Concentration of E1, E2 and EE2 in Sewage Effluents and Surface Waters of the "Pampas" Region and the "Río de la Plata" Estuary (Argentina)," *Bulletin of Environmental Contamination and Toxicology*, vol. 94, pp. 29–33, Jan. 2015.

[43] A. K. Sarmah, G. L. Northcott, F. D. L. Leusch, and L. A. Tremblay, "A survey of endocrine disrupting chemicals (EDCs) in municipal sewage and animal waste effluents in the Waikato region of New Zealand," *Science of The Total Environment*, vol. 355, pp. 135–144, Feb. 2006.

[44] N. W. Shappell, L. O. Billey, D. Forbes, T. A. Matheny, M. E. Poach, G. B. Reddy, and P. G. Hunt, "Estrogenic Activity and Steroid Hormones in Swine Wastewater through a Lagoon Constructed-Wetland System," *Environmental Science & Technology*, vol. 41, pp. 444–450, Jan. 2007.

[45] D. R. Raman, E. L. Williams, A. C. Layton, R. T. Burns, J. P. Easter, A. S. Daugherty, M. D. Mullen, and G. S. Sayler, "Estrogen Content of Dairy and Swine Wastes," *Environmental Science & Technology*, vol. 38, pp. 3567–3573, July 2004.

[46] W. Zheng, S. R. Yates, and S. A. Bradford, "Analysis of Steroid Hormones in a Typical Dairy Waste Disposal System," *Environmental Science & Technology*, vol. 42, pp. 530–535, Jan. 2008.

[47] Scientific Committee on Health, Environmental and Emerging Risks, "Scientific Opinion on "Draft Environmental Quality Standards for Priority Substances under the Water

Framework Directive" 17-Alpha-Ethinylestradiol (EE2), Beta-Estradiol (E2) and Estrone (E1)," tech. rep., European Commission, Mar. 2022.

[48] M. Cargouet, D. Perdiz, A. Mouatassimsouali, S. Tamisierkarolak, and Y. Levi, "Assessment of river contamination by estrogenic compounds in Paris area (France)," *Science of The Total Environment*, vol. 324, pp. 55–66, May 2004.

[49] P. Labadie and E. M. Hill, "Analysis of estrogens in river sediments by liquid chromatography–electrospray ionisation mass spectrometry: Comparison of tandem mass spectrometry and time-of-flight mass spectrometry," *Journal of Chromatography A*, vol. 1141, pp. 174–181, Feb. 2007.

[50] D. Rechsteiner, S. Schrade, M. Zähner, M. Müller, J. Hollender, and T. D. Bucheli, "Occurrence and Fate of Natural Estrogens in Swiss Cattle and Pig Slurry," *Journal of Agricultural and Food Chemistry*, vol. 68, pp. 5545–5554, May 2020.

[51] S. Arnon, O. Dahan, S. Elhanany, K. Cohen, I. Pankratov, A. Gross, Z. Ronen, S. Baram, and L. S. Shore, "Transport of Testosterone and Estrogen from Dairy-Farm Waste Lagoons to Groundwater," *Environmental Science & Technology*, vol. 42, pp. 5521–5526, Aug. 2008.

[52] C. Deich, M. Kanwischer, R. Zhang, and J. J. Waniek, "Natural and synthetic estrogenic compounds in the Pearl River Estuary and northern shelf of the South China Sea," *Oceanologia*, vol. 65, pp. 30–43, Jan. 2023.

[53] Y. Koh, T. Chiu, A. Boobis, E. Cartmell, M. Scrimshaw, and J. Lester, "Treatment and Removal Strategies for Estrogens from Wastewater," *Environmental Technology*, vol. 29, pp. 245–267, Mar. 2008. Publisher: Taylor & Francis _eprint: https://doi.org/10.1080/09593330802099122.

[54] M. Clara, N. Kreuzinger, B. Strenn, O. Gans, and H. Kroiss, "The solids retention time—a suitable design parameter to evaluate the capacity of wastewater treatment plants to remove micropollutants," *Water Research*, vol. 39, pp. 97–106, Jan. 2005.

[55] E. Fernandez-Fontaina, F. Omil, J. M. Lema, and M. Carballa, "Influence of nitrifying conditions on the biodegradation and sorption of emerging micropollutants," *Water Research*, vol. 46, pp. 5434–5444, Oct. 2012.

[56] M. Gardner, V. Jones, S. Comber, M. D. Scrimshaw, T. Coello - Garcia, E. Cartmell, J. Lester, and B. Ellor, "Performance of UK wastewater treatment works with respect to trace contaminants," *Science of The Total Environment*, vol. 456-457, pp. 359–369, July 2013.

[57] F. D. L. Leusch, H. F. Chapman, W. Körner, S. R. Gooneratne, and L. A. Tremblay, "Efficacy of an Advanced Sewage Treatment Plant in Southeast Queensland, Australia, to Remove Estrogenic Chemicals," *Environmental Science & Technology*, vol. 39, pp. 5781–5786, Aug. 2005.

[58] M. Servos, D. Bennie, B. Burnison, A. Jurkovic, R. McInnis, T. Neheli, A. Schnell, P. Seto, S. Smyth, and T. Ternes, "Distribution of estrogens, 17β-estradiol and estrone, in Canadian municipal wastewater treatment plants," *Science of The Total Environment*, vol. 336, pp. 155–170, Jan. 2005.

[59] T. A. Ternes, M. Stumpf, J. Mueller, K. Haberer, and M. Servos, "Behavior and occurrence of estrogens in municipal sewage treatment plants – I. Investigations in Germany, Canada and Brazil," *The Science of The Total Environment*, vol. 225, p. 10, Jan. 1999.

[60] J. Margot, C. Kienle, A. Magnet, M. Weil, L. Rossi, L. F. de Alencastro, C. Abegglen, D. Thonney, N. Chèvre, M. Schärer, and D. Barry, "Treatment of micropollutants in municipal wastewater: Ozone or powdered activated carbon?," *Science of The Total Environment*, vol. 461-462, pp. 480–498, Sept. 2013.

[61] M.-L. Janex-Habibi, A. Huyard, M. Esperanza, and A. Bruchet, "Reduction of endocrine disruptor emissions in the environment: The benefit of wastewater treatment," *Water Research*, vol. 43, pp. 1565–1576, Apr. 2009.

[62] S. K. Khanal, B. Xie, M. L. Thompson, S. Sung, S.-K. Ong, and J. H. van Leeuwen, "Fate, Transport, and Biodegradation of Natural Estrogens in the Environment and Engineered Systems," *Environmental Science & Technology*, vol. 40, pp. 6537–6546, Nov. 2006.

[63] C.-P. Yu, R. A. Deeb, and K.-H. Chu, "Microbial degradation of steroidal estrogens," *Chemosphere*, vol. 91, pp. 1225–1235, May 2013.

[64] K. Anderson, P. Sallis, and S. Uyanik, "24 - Anaerobic treatment processes," in *Handbook of Water and Wastewater Microbiology* (D. Mara and N. Horan, eds.), pp. 391–426, London: Academic Press, Jan. 2003.

[65] Q. Zhang, C. Xue, G. Owens, and Z. Chen, "Isolation and identification of 17β-estradiol degrading bacteria and its degradation pathway," *Journal of Hazardous Materials*, vol. 423, p. 127185, Feb. 2022.

[66] Y. Wang, X. Zhao, K. Tian, F. Meng, D. Zhou, X. Xu, H. Zhang, and H. Huo, "Identification and genome analysis of a novel 17β-estradiol degradation bacterium, Lysinibacillus sphaericus DH-B01," *3 Biotech*, vol. 10, p. 166, Apr. 2020.

[67] W. Xiong, C. Yin, Y. Wang, S. Lin, Z. Deng, and R. Liang, "Characterization of an efficient estrogen-degrading bacterium Stenotrophomonas maltophilia SJTH1 in saline-, alkaline-, heavy metal-contained environments or solid soil and identification of four 17β-estradiol-oxidizing dehydrogenases," *Journal of Hazardous Materials*, vol. 385, p. 121616, Mar. 2020.

[68] H. Roh, N. Subramanya, F. Zhao, C.-P. Yu, J. Sandt, and K.-H. Chu, "Biodegradation potential of wastewater micropollutants by ammonia-oxidizing bacteria," *Chemosphere*, vol. 77, pp. 1084–1089, Nov. 2009.

[69] Y.-X. Ren, K. Nakano, M. Nomura, N. Chiba, and O. Nishimura, "Effects of bacterial activity on estrogen removal in nitrifying activated sludge," *Water Research*, vol. 41, pp. 3089–3096, July 2007.

[70] N. H. Tran, T. Urase, and O. Kusakabe, "The characteristics of enriched nitrifier culture in the degradation of selected pharmaceutically active compounds," *Journal of Hazardous Materials*, vol. 171, pp. 1051–1057, Nov. 2009.

[71] J. Vader, C. van Ginkel, F. Sperling, J. de Jong, W. de Boer, J. de Graaf, M. van der Most, and P. Stokman, "Degradation of ethinyl estradiol by nitrifying activated sludge," *Chemosphere*, vol. 41, pp. 1239–1243, Oct. 2000.

[72] J. Shi, S. Fujisawa, S. Nakai, and M. Hosomi, "Biodegradation of natural and synthetic estrogens by nitrifying activated sludge and ammonia-oxidizing bacterium Nitrosomonas europaea," *Water Research*, vol. 38, pp. 2323–2330, May 2004.

[73] T. Yi and W. F. Harper, "The Link between Nitrification and Biotransformation of 17α-Ethinylestradiol," *Environmental Science & Technology*, vol. 41, pp. 4311–4316, June 2007.

[74] A. Alfreider, V. Grimus, M. Luger, A. Ekblad, M. M. Salcher, and M. Summerer, "Autotrophic carbon fixation strategies used by nitrifying prokaryotes in freshwater lakes," *FEMS Microbiology Ecology*, vol. 94, p. fiy163, Aug. 2018.

[75] B. Pauwels, K. Wille, H. Noppe, H. De Brabander, T. Van de Wiele, W. Verstraete, and N. Boon, "17α-ethinylestradiol cometabolism by bacteria degrading estrone, 17β-estradiol and estriol," *Biodegradation*, vol. 19, pp. 683–693, Sept. 2008.

[76] A. Bodor, N. Bounedjoum, G. E. Vincze, Erdeiné Kis, K. Laczi, G. Bende, Szilágyi, T. Kovács, K. Perei, and G. Rákhely, "Challenges of unculturable bacteria: environmental perspectives," *Reviews in Environmental Science and Bio/Technology*, vol. 19, pp. 1–22, Mar. 2020.

[77] H. Zhang, Y. Lu, Y. Li, L. Wang, W. Zhang, L. Wang, L. Niu, and Z. Jia, "Bacterial contribution to 17β-estradiol mineralization in lake sediment as revealed by 13C-DNA stable isotope probing," *Environmental Pollution*, vol. 286, pp. 1–8, Oct. 2021.

[78] C.-P. Yu, H. Roh, and K.-H. Chu, "17β-Estradiol-Degrading Bacteria Isolated from Activated Sludge," *Environmental Science & Technology*, vol. 41, pp. 486–492, Jan. 2007.

[79] T. Hashimoto, K. Onda, T. Morita, B. S. Luxmy, K. Tada, A. Miya, and T. Murakami, "Contribution of the Estrogen-Degrading Bacterium *Novosphingobium* sp. Strain JEM-1 to Estrogen Removal in Wastewater Treatment," *Journal of Environmental Engineering*, vol. 136, pp. 890–896, Sept. 2010.

[80] K. Fujii, S. Kikuchi, M. Satomi, N. Ushio-Sata, and N. Morita, "Degradation of 17 -Estradiol by a Gram-Negative Bacterium Isolated from Activated Sludge in a Sewage Treatment Plant in Tokyo, Japan," *Applied and Environmental Microbiology*, vol. 68, pp. 2057–2060, Apr. 2002.

[81] J. Ke, W. Zhuang, K. Y.-H. Gin, M. Reinhard, L. T. Hoon, and J.-H. Tay, "Characterization of estrogen-degrading bacteria isolated from an artificial sandy aquifer with ultrafiltered secondary effluent as the medium," *Applied Microbiology and Biotechnology*, vol. 75, pp. 1163–1171, July 2007.

[82] F. Kurisu, M. Ogura, S. Saitoh, A. Yamazoe, and O. Yagi, "Degradation of natural estrogen and identification of the metabolites produced by soil isolates of Rhodococcus sp. and Sphingomonas sp.," *Journal of Bioscience and Bioengineering*, vol. 109, pp. 576–582, June 2010.

[83] S. Weber, P. Leuschner, P. Kampfer, W. Dott, and J. Hollender, "Degradation of estradiol and ethinyl estradiol by activated sludge and by a defined mixed culture," *Applied Microbiology and Biotechnology*, vol. 67, pp. 106–112, Apr. 2005.

[84] D. W. Payne and P. Talalay, "Isolation of novel microbial 3 alpha-, 3 beta-, and 17 beta-hydroxysteroid dehydrogenases. Purification, characterization, and analytical applications of a 17 beta-hydroxysteroid dehydrogenase from an Alcaligenes sp.," *Journal of Biological Chemistry*, vol. 260, pp. 13648–13655, Nov. 1985.

[85] C. Li, L. Lan, M. A. Tadda, S. Zhu, Z. Ye, and D. Liu, "Interaction between 17β-estradiol degradation and nitrification in mariculture wastewater by Nitrosomonas europaea and MBBR," *Science of The Total Environment*, vol. 705, p. 135846, Feb. 2020.

[86] T. Zhang, G. Xiong, and E. Maser, "Characterization of the steroid degrading bacterium S19-1 from the Baltic Sea at Kiel, Germany," *Chemico-Biological Interactions*, vol. 191, pp. 83–88, May 2011.

[87] Q. Zeng, Y. Li, G. Gu, J. Zhao, C. Zhang, and J. Luan, "Sorption and Biodegradation of 17β-Estradiol by Acclimated Aerobic Activated Sludge and Isolation of the Bacterial Strain," *Environmental Engineering Science*, vol. 26, pp. 783–790, Apr. 2009.

[88] J. S. Sabirova, L. F. F. Cloetens, L. Vanhaecke, I. Forrez, W. Verstraete, and N. Boon, "Manganese-oxidizing bacteria mediate the degradation of 17α-ethinylestradiol," *Microbial Biotechnology*, vol. 1, no. 6, pp. 507–512, 2008.

[89] G. Xiong, E. Draus, Y. Luo, and E. Maser, "3α-Hydroxysteroid dehydrogenase/carbonyl reductase as a tool for isolation and characterization of a new marine steroid degrading bacterial strain," *Chemico-Biological Interactions*, vol. 178, pp. 206–210, Mar. 2009.

[90] T. Yoshimoto, F. Nagai, J. Fujimoto, K. Watanabe, H. Mizukoshi, T. Makino, K. Kimura, H. Saino, H. Sawada, and H. Omura, "Degradation of Estrogens by Rhodococcus zopfii and Rhodococcus equi Isolates from Activated Sludge in Wastewater Treatment Plants," *Applied and Environmental Microbiology*, vol. 70, pp. 5283–5289, Sept. 2004.

[91] D. O'Grady, S. Evangelista, and V. Yargeau, "Removal of Aqueous 17α-Ethinylestradiol by Rhodococcus Species," *Environmental Engineering Science*, vol. 26, pp. 1393–1400, Sept. 2009.

[92] R. Haiyan, J. Shulan, N. ud din Ahmad, W. Dao, and C. Chengwu, "Degradation characteristics and metabolic pathway of 17α-ethynylestradiol by Sphingobacterium sp. JCR5," *Chemosphere*, vol. 66, pp. 340–346, Jan. 2007.

[93] L. Jiang, J. Yang, and J. Chen, "Isolation and characteristics of 17β-estradiol-degrading Bacillus spp. strains from activated sludge," *Biodegradation*, vol. 21, pp. 729–736, Sept. 2010.

[94] Q. Qiu, P. Wang, H. Kang, Y. Wang, K. Tian, and H. Huo, "Genomic Analysis of a New Estrogen-Degrading Bacterial Strain, *Acinetobacter* sp. DSSKY-A-001," *International Journal of Genomics*, vol. 2019, p. e2804134, June 2019. Publisher: Hindawi.

[95] H. Zhao, K. Tian, Q. Qiu, Y. Wang, H. Zhang, S. Ma, S. Jin, and H. Huo, "Genome Analysis of Rhodococcus Sp. DSSKP-R-001: A Highly Effective β-Estradiol-Degrading Bacterium," *International Journal of Genomics*, vol. 2018, p. e3505428, Oct. 2018. Publisher: Hindawi.

[96] P. Wang, D. Zheng, and R. Liang, "Isolation and characterization of an estrogen-degrading Pseudomonas putida strain SJTE-1," *3 Biotech*, vol. 9, p. 61, Jan. 2019.

[97] Y.-L. Chen, H.-Y. Fu, T.-H. Lee, C.-J. Shih, L. Huang, Y.-S. Wang, W. Ismail, and Y.-R. Chiang, "Estrogen Degraders and Estrogen Degradation Pathway Identified in an Activated Sludge," *Applied and Environmental Microbiology*, vol. 84, Mar. 2018.

[98] Y.-L. Chen, C.-P. Yu, T.-H. Lee, K.-S. Goh, K.-H. Chu, P.-H. Wang, W. Ismail, C.-J. Shih, and Y.-R. Chiang, "Biochemical Mechanisms and Catabolic Enzymes Involved in Bacterial Estrogen Degradation Pathways," *Cell Chemical Biology*, vol. 24, pp. 712–724.e7, June 2017.

[99] J. Ibero, B. Galán, V. Rivero-Buceta, and J. L. García, "Unraveling the 17β-Estradiol Degradation Pathway in Novosphingobium tardaugens NBRC 16725," *Frontiers in Microbiology*, vol. 11, pp. 1–21, Dec. 2020.

[100] E. R. Olivera and J. M. Luengo, "Steroids as Environmental Compounds Recalcitrant to Degradation: Genetic Mechanisms of Bacterial Biodegradation Pathways," *Genes*, vol. 10, July 2019.

[101] R. G. Coombe, Y. Y. Tsong, P. B. Hamilton, and C. J. Sih, "Mechanisms of Steroid Oxidation by Microorganisms," *The Journal of Biological Chemistry*, vol. 241, pp. 1587–1595, Apr. 1966.

[102] H. B. Lee and D. Liu, "Degradation of 17β-Estradiol and its Metabolites by Sewage Bacteria," *Water, Air, and Soil Pollution*, vol. 134, pp. 351–366, Feb. 2002.

[103] S. Nakai, A. Yamamura, S. Tanaka, J. Shi, M. Nishikawa, Y. Nakashimada, and M. Hosomi, "Pathway of 17β-estradiol degradation by Nitrosomonas europaea and reduction in 17b-estradiol-derived estrogenic activity," *Environmental Chemistry Letters*, vol. 9, pp. 1–6, Mar. 2011.

[104] L. Iasur-Kruh, Y. Hadar, and D. Minz, "Isolation and Bioaugmentation of an Estradiol-Degrading Bacterium and Its Integration into a Mature Biofilm," *Applied and Environmental Microbiology*, vol. 77, pp. 3734–3740, June 2011.

[105] W. Peng, S. Lin, Z. Deng, and R. Liang, "Bioaugmentation removal and microbiome analysis of the synthetic estrogen 17α-ethynylestradiol from hostile conditions and environmental samples by Pseudomonas citronellolis SJTE-3," *Chemosphere*, vol. 317, p. 137893, Mar. 2023.

[106] F. P. J. Vandecasteele, T. F. Hess, and R. L. Crawford, "Using Genetic Algorithms To Optimize Functions of Microbial Ecosystems," in *Manual of Environmental Microbiology*, pp. 1072–1078, John Wiley & Sons, Ltd, 2007.

[107] E. Butler and Y.-T. Hung, "Bioaugmentation for Water Resources Protection," in *Advances in Water Resources Management* (L. K. Wang, C. T. Yang, and M.-H. S. Wang, eds.), Handbook of Environmental Engineering, pp. 339–401, Cham: Springer International Publishing, 2016.

[108] M. L. B. da Silva and P. J. J. Alvarez, "Bioaugmentation," in *Handbook of Hydrocarbon and Lipid Microbiology* (K. N. Timmis, ed.), pp. 4531–4544, Berlin, Heidelberg: Springer, 2010.

[109] M. Herrero and D. Stuckey, "Bioaugmentation and its application in wastewater treatment: A review," *Chemosphere*, vol. 140, pp. 119–128, Dec. 2015.

[110] W. Dejonghe, N. Boon, D. Seghers, E. M. Top, and W. Verstraete, "Bioaugmentation of soils by increasing microbial richness: missing links," *Environmental Microbiology*, vol. 3, no. 10, pp. 649–657, 2001.

[111] A. C. Singer, C. J. van der Gast, and I. P. Thompson, "Perspectives and vision for strain selection in bioaugmentation," *Trends in Biotechnology*, vol. 23, pp. 74–77, Feb. 2005.

[112] O. Muter, "Current Trends in Bioaugmentation Tools for Bioremediation: A Critical Review of Advances and Knowledge Gaps," *Microorganisms*, vol. 11, p. 710, Mar. 2023.

[113] S. El Fantroussi and S. N. Agathos, "Is bioaugmentation a feasible strategy for pollutant removal and site remediation?," *Current Opinion in Microbiology*, vol. 8, pp. 268–275, June 2005.

[114] E. Schwartz and K. M. Scow, "Repeated inoculation as a strategy for the remediation of low concentrations of phenanthrene in soil," *Biodegradation*, vol. 12, pp. 201–207, May 2001.

[115] R. Jittawattanarat, K. Kostarelos, and E. Khan, "Immobilized-Cell-Augmented Activated Sludge Process for Treating Wastewater Containing Hazardous Compounds," *Water Environment Research*, vol. 79, no. 5, pp. 461–471, 2007.

[116] C. E. Schaefer, D. R. Lippincott, and R. J. Steffan, "Field-Scale Evaluation of Bioaugmentation Dosage for Treating Chlorinated Ethenes," *Groundwater Monitoring & Remediation*, vol. 30, no. 3, pp. 113–124, 2010.

[117] A. E. Smith, K. Hristova, I. Wood, D. M. Mackay, E. Lory, D. Lorenzana, and K. M. Scow, "Comparison of Biostimulation versus Bioaugmentation with Bacterial Strain PM1 for Treatment of Groundwater Contaminated with Methyl Tertiary Butyl Ether (MTBE)," *Environmental Health Perspectives*, vol. 113, pp. 317–322, Mar. 2005.

[118] F. Suja, F. Rahim, M. R. Taha, N. Hambali, M. Rizal Razali, A. Khalid, and A. Hamzah, "Effects of local microbial bioaugmentation and biostimulation on the bioremediation of total petroleum hydrocarbons (TPH) in crude oil contaminated soil based on laboratory and field observations," *International Biodeterioration & Biodegradation*, vol. 90, pp. 115–122, May 2014.

[119] N. Singhal and O. Perez-Garcia, "Degrading Organic Micropollutants: The Next Challenge in the Evolution of Biological Wastewater Treatment Processes," *Frontiers in Environmental Science*, vol. 4, pp. 1–5, May 2016.

[120] S.-J. Haig, C. Gauchotte-Lindsay, G. Collins, and C. Quince, "Bioaugmentation Mitigates the Impact of Estrogen on Coliform-Grazing Protozoa in Slow Sand Filters," *Environmental Science & Technology*, vol. 50, pp. 3101–3110, Mar. 2016.

[121] H. Roh and K.-H. Chu, "Effects of solids retention time on the performance of bioreactors bioaugmented with a 17β-estradiol-utilizing bacterium, Sphingomonas strain KC8," *Chemosphere*, vol. 84, pp. 227–233, June 2011.

[122] J. Shi, Y. Suzuki, B.-D. Lee, S. Nakai, and M. Hosomi, "Isolation and characterization of the ethynylestradiol-biodegrading microorganism Fusarium proliferatum strain HNS-1," *Water Science and Technology*, vol. 45, pp. 175–179, June 2002.

[123] K. Sys, N. Boon, and W. Verstraete, "Development and validation of evolutionary algorithm software as an optimization tool for biological and environmental applications," *Journal of Microbiological Methods*, vol. 57, pp. 309–322, June 2004.

[124] M. M. Nourouzi, T. G. Chuah, T. S. Choong, and F. Rabiei, "Modeling biodegradation and kinetics of glyphosate by artificial neural network," *Journal of Environmental Science and Health, Part B*, vol. 47, pp. 455–465, May 2012.

[125] U. Roy, S. Sengupta, P. Das, A. Bhowal, and S. Datta, "Integral approach of sorption coupled with biodegradation for treatment of azo dye using Pseudomonas sp.: batch, toxicity, and artificial neural network," *3 Biotech*, vol. 8, p. 192, Mar. 2018.

[126] Y. A. Mustafa, S. J. Mohammed, and M. J. M. Ridha, "Polyaromatic hydrocarbons biodegradation using mix culture of microorganisms from sewage waste sludge: appli-

cation of artificial neural network modelling," *Journal of Environmental Health Science and Engineering*, vol. 20, pp. 405–418, June 2022.

[127] S. Aouaouda, M. T. Khadir, G. Mourot, and J. Ragot, "Systematic simplification methodology applied to an activated sludge reactor model," in *International Workshop on Systems, Signal Processing and their Applications, WOSSPA*, pp. 143–146, May 2011.

[128] M. Knarr, M. Goltz, G. Lamont, and J. Huang, "In situ bioremediation of perchlorate-contaminated groundwater using a multi-objective parallel evolutionary algorithm," in *The 2003 Congress on Evolutionary Computation, 2003. CEC '03.*, vol. 3, pp. 1604–1611 Vol.3, Dec. 2003.

[129] M. Zafar, S. Kumar, and S. Kumar, "Optimization of napthalene biodegradation by a genetic algorithm based response surface methodology," *Brazilian Journal of Chemical Engineering*, vol. 27, pp. 89–99, Mar. 2010.

[130] S. C. Béranger, B. E. Sleep, B. S. Lollar, and F. P. Monteagudo, "Transport, biodegradation and isotopic fractionation of chlorinated ethenes: modeling and parameter estimation methods," *Advances in Water Resources*, vol. 28, pp. 87–98, Jan. 2005.

[131] F. Mohammadi, Z. Yavari, M. R. Nikoo, A. Al-Nuaimi, and H. Karimi, "Machine learning model optimization for removal of steroid hormones from wastewater," *Chemosphere*, vol. 343, p. 140209, Dec. 2023.

[132] H. A. Laitinen, "History of Trace Analysis," *Journal of Research of the National Bureau of Standards*, vol. 93, pp. 175–185, May 1988.

[133] C. Miège, P. Bados, C. Brosse, and M. Coquery, "Method validation for the analysis of estrogens (including conjugated compounds) in aqueous matrices," *TrAC Trends in Analytical Chemistry*, vol. 28, pp. 237–244, Feb. 2009.

[134] S. Wang, Z. Xu, G. Fang, Y. Zhang, and J. He, "Separation and determination of estrone in environmental and drinking water using molecularly imprinted solid phase extraction coupled with HPLC," *Journal of Separation Science*, vol. 31, pp. 1181–1188, Apr. 2008.

[135] C. Ripollés, M. Ibáñez, J. V. Sancho, F. J. López, and F. Hernández, "Determination of 17β-estradiol and 17α-ethinylestradiol in water at sub-ppt levels by liquid chromatography coupled to tandem mass spectrometry," *Analytical Methods*, vol. 6, pp. 5028–2037, June 2014.

[136] J. Quintana, J. Carpinteiro, I. Rodrıguez, R. Lorenzo, A. Carro, and R. Cela, "Determination of natural and synthetic estrogens in water by gas chromatography with mass

spectrometric detection," *Journal of Chromatography A*, vol. 1024, pp. 177–185, Jan. 2004.

[137] V. Pérez-Fernández, L. Mainero Rocca, P. Tomai, S. Fanali, and A. Gentili, "Recent advancements and future trends in environmental analysis: Sample preparation, liquid chromatography and mass spectrometry," *Analytica Chimica Acta*, vol. 983, pp. 9–41, Aug. 2017.

[138] P. He and D. S. Aga, "Comparison of GC-MS/MS and LC-MS/MS for the analysis of hormones and pesticides in surface waters: advantages and pitfalls," *Analytical Methods*, vol. 11, no. 11, pp. 1436–1448, 2019.

[139] R. D. Boyd, C. Basic, and R. A. Bentham, "Method Development and Fitness for Purpose," in *Trace Quantitative Analysis by Mass Spectrometry*, pp. 461–438, John Wiley & Sons, Ltd, 2008.

[140] International Council for Harmonisation of Technical Requirements for Registration of Pharmaceuticals for Human Use, "ICH guideline M10 on bioanalytical method validation and study sample analysis," vol. M10, July 2022.

[141] K. Danzer, "Selectivity and specificity in analytical chemistry. General considerations and attempt of a definition and quantification," *Fresenius' Journal of Analytical Chemistry*, vol. 369, pp. 397–402, Mar. 2001.

[142] J. M. Miller and J. C. Miller, "Calibration methods in instrumental analysis: regression and correlation," in *Statistics and Chemometrics for Analytical Chemistry*, pp. 110–151, Pearson Education Limited, 6th ed., 2010.

[143] H.-Y. Chen and C. Chen, "Evaluation of Calibration Equations by Using Regression Analysis: An Example of Chemical Analysis," *Sensors (Basel, Switzerland)*, vol. 22, p. 447, Jan. 2022.

[144] B. Magnusson and U. Örnemark, eds., *Eurachem Guide: The Fitness for Purpose of Analytical Methods – A Laboratory Guide to Method Validation and Related Topics*. 2nd ed., 2014. OCLC: 1039221699.

[145] U.S. Department of Health and Human Services, Food and Drug Administration, Center for Drug Evaluation and Research (CDER), and Center for Veterinary Medicine (CVM), "Bioanalytical Method Validation Guidance for Industry," 2018.

[146] R. D. Boyd, C. Basic, and R. A. Bentham, "Tools of the Trade II. Theory of Chromatography," in *Trace Quantitative Analysis by Mass Spectrometry*, pp. 51–107, John Wiley & Sons, Ltd, 2008.

[147] D. C. Harris, "Introduction to Analytical Separations," in *Quantitative Chemical Analysis*, pp. 501–527, W. H. Freeman and Company, 7th ed., 2007.

[148] D. C. Harris, "Gas Chromatography," in *Quantitative Chemical Analysis*, pp. 528–555, W. H. Freeman and Company, 7th ed., 2007.

[149] S. C. Moldoveanu, V. David, S. C. Moldoveanu, and V. David, "Derivatization Methods in GC and GC/MS," in *Gas Chromatography - Derivatization, Sample Preparation, Application*, IntechOpen, Dec. 2018.

[150] D. C. Harris, "High-Performance Liquid Chromatography," in *Quantitative Chemical Analysis*, pp. 556–587, W. H. Freeman and Company, 7th ed., 2007.

[151] R. D. Boyd, C. Basic, and R. A. Bentham, "Tools of the Trade III. Separation Practicalities," in *Trace Quantitative Analysis by Mass Spectrometry*, pp. 109–171, John Wiley & Sons, Ltd, 2008.

[152] D. C. Harris, "Spectrophotometers," in *Quantitative Chemical Analysis*, pp. 424–452, W. H. Freeman and Company, 7th ed., 2007.

[153] D. C. Harris, "Mass Spectrometry," in *Quantitative Chemical Analysis*, pp. 474–500, W. H. Freeman and Company, 7th ed., 2007.

[154] R. D. Boyd, C. Basic, and R. A. Bentham, "Tools of the Trade VI. Ion Detection and Data Processing," in *Trace Quantitative Analysis by Mass Spectrometry*, pp. 345–371, John Wiley & Sons, Ltd, 2008.

[155] R. D. Boyd, C. Basic, and R. A. Bentham, "Tools of the Trade V. Mass Analyzers for Quantitation: Separation of Ions by m/z Values," in *Trace Quantitative Analysis by Mass Spectrometry*, pp. 245–343, John Wiley & Sons, Ltd, 2008.

[156] R. D. Boyd, C. Basic, and R. A. Bentham, "Tools of the Trade IV. Interfaces and Ion Sources for Chromatography–Mass Spectrometry," in *Trace Quantitative Analysis by Mass Spectrometry*, pp. 173–244, John Wiley & Sons, Ltd, 2008.

[157] B. K. Matuszewski, M. L. Constanzer, and C. M. Chavez-Eng, "Strategies for the Assessment of Matrix Effect in Quantitative Bioanalytical Methods Based on HPLC-MS/MS," *Analytical Chemistry*, vol. 75, pp. 3019–3030, July 2003.

[158] D. C. Harris, "Fundamentals of Spectrophotometery," in *Quantitative Chemical Analysis*, pp. 378–401, W. H. Freeman and Company, 7th ed., 2007.

[159] B. P. Kafle, "Chapter 1 - Spectrophotometry and its application in chemical analysis," in *Chemical Analysis and Material Characterization by Spectrophotometry* (B. P. Kafle, ed.), pp. 1–16, Elsevier, Jan. 2020.

[160] B. Valeur and M. N. Berberan-Santos, "Structural Effects on Fluorescence Emission," in *Molecular Fluorescence*, pp. 75–107, John Wiley & Sons, Ltd, 2nd ed., 2012.

[161] M. Taniguchi and J. S. Lindsey, "Absorption and Fluorescence Spectral Database of Chlorophylls and Analogues," *Photochemistry and Photobiology*, vol. 97, no. 1, pp. 136–165, 2021.

[162] K. Y. Chan, B. M. Gavaghan, A. W. Stoeckel, K. Irizarry, and P. M. Hare, "Solvent Effects on the Steady State Photophysics of Estrone and 17β-Estradiol," *Photochemistry and Photobiology*, vol. 88, pp. 295–303, Mar. 2012.

[163] F. Huang, F. Gao, C. Li, and L. C. Campos, "Photodegradation of free estrogens driven by UV light: Effects of operation mode and water matrix," *Science of The Total Environment*, vol. 835, p. 155515, Aug. 2022.

[164] European Chemicals Agency, "Assessment Report: Imidacloprid Product-type 18 (Insecticides, Acaricides and Products to control other Arthropods)," Feb. 2011.

[165] European Chemicals Agency, "Assessment Report: Clothianidin Product-type 18 (Insecticides, Acaricides and Products to control other Arthropods)," Oct. 2014.

[166] National Center for Biotechnology Information, "PubChem Compound Summary for CID 2519, Caffeine," June 2023.

[167] National Center for Biotechnology Information, "PubChem Compound Summary for CID 1983, Acetaminophen," June 2023.

[168] B. Valeur and M. N. Berberan-Santos, "Autofluorescence and Fluorescence Labeling in Biology and Medicine," in *Molecular Fluorescence: Principles and Applications*, pp. 479–505, John Wiley & Sons, Ltd, 2nd ed., 2012.

[169] B. Valeur and M. N. Berberan-Santos, "Chemical Sensing via Fluorescence," in *Molecular Fluorescence: Principles and Applications*, pp. 409–478, John Wiley & Sons, Ltd, 2nd ed., 2012.

[170] B. Valeur and M. N. Berberan-Santos, "Introduction," in *Molecular Fluorescence*, pp. 1–30, John Wiley & Sons, Ltd, 2nd ed., 2012.

[171] L. D. Lavis and R. T. Raines, "Bright Ideas for Chemical Biology," *ACS Chemical Biology*, vol. 3, pp. 142–155, Mar. 2008.

[172] G. U. Nienhaus and K. Nienhaus, "Fluorescence Labeling," in *Fluorescence Microscopy* (U. Kubitscheck, ed.), pp. 143–173, Weinheim, Germany: Wiley-VCH Verlag GmbH & Co. KGaA, Apr. 2013.

[173] A. Pernthaler, J. Pernthaler, and R. Amann, "Fluorescence In Situ Hybridization and Catalyzed Reporter Deposition for the Identification of Marine Bacteria," *Applied and Environmental Microbiology*, vol. 68, pp. 3094–3101, June 2002.

[174] F. Leira, M. C. Louzao, J. M. Vieites, L. M. Botana, and M. R. Vieytes, "Fluorescent microplate cell assay to measure uptake and metabolism of glucose in normal human lung fibroblasts," *Toxicology in Vitro*, vol. 16, pp. 267–273, June 2002.

[175] B. Quinn, "Preparation and Maintenance of Live Tissues and Primary Cultures for Toxicity Studies," in *Biochemical Ecotoxicology*, pp. 33–47, Elsevier, 2014.

[176] T. M. Edwards, H. E. Morgan, C. Balasca, N. K. Chalasani, L. Yam, and A. M. Roark, "Detecting Estrogenic Ligands in Personal Care Products using a Yeast Estrogen Screen Optimized for the Undergraduate Teaching Laboratory," *Journal of Visualized Experiments : JoVE*, p. 55754, Jan. 2018.

[177] B. Valeur and M. N. Berberan-Santos, "Excitation Energy Transfer," in *Molecular Fluorescence*, pp. 213–261, John Wiley & Sons, Ltd, 2nd ed., 2012.

[178] H. Aldewachi, T. Chalati, M. N. Woodroofe, N. Bricklebank, B. Sharrack, and P. Gardiner, "Gold nanoparticle-based colorimetric biosensors," *Nanoscale*, vol. 10, no. 1, pp. 18–33, 2018.

[179] B. Kuswandi, "Nanobiosensor approaches for pollutant monitoring," *Environmental Chemistry Letters*, vol. 17, pp. 975–990, June 2019.

[180] C. Chen and J. Wang, "Optical biosensors: an exhaustive and comprehensive review," *The Analyst*, vol. 145, pp. 1605–1628, Jan. 2020.

[181] B. D. Malhotra and M. A. Ali, "Nanomaterials in Biosensors: Fundamentals and Applications," in *Micro and Nano Technologies*, pp. 1–74, William Andrew Publishing, 2018.

[182] J. W. Trzciński, L. Panariello, M. O. Besenhard, Y. Yang, A. Gavriilidis, and S. Guldin, "Synthetic guidelines for the precision engineering of gold nanoparticles," *Current Opinion in Chemical Engineering*, vol. 29, pp. 59–66, Sept. 2020.

[183] J. Turkevich, P. C. Stevenson, and J. Hillier, "A study of the nucleation and growth processes in the synthesis of colloidal gold," *Discussions of the Faraday Society*, vol. 11, p. 55, May 1951.

[184] G. Frens, "Controlled Nucleation for the Regulation of the Particle Size in Monodisperse Gold Suspensions," *Nature Physical Science*, vol. 241, pp. 20–22, Jan. 1973.

[185] T. Kim, C.-H. Lee, S.-W. Joo, and K. Lee, "Kinetics of gold nanoparticle aggregation: Experiments and modeling," *Journal of Colloid and Interface Science*, vol. 318, pp. 238–243, Feb. 2008.

[186] R. Pamies, J. G. H. Cifre, V. F. Espín, M. Collado-González, F. G. D. Baños, and J. G. de la Torre, "Aggregation behaviour of gold nanoparticles in saline aqueous media," *Journal of Nanoparticle Research*, vol. 16, p. 2376, Apr. 2014.

[187] E. Petryayeva and U. J. Krull, "Localized surface plasmon resonance: Nanostructures, bioassays and biosensing—A review," *Analytica Chimica Acta*, vol. 706, pp. 8–24, Nov. 2011.

[188] V. I. Chegel and A. M. Lopatynskyi, "Physics of the Phenomenon and Theoretical Background of Surface Plasmon Resonance Method," in *Molecular Plasmonics* (V. I. Chegel and A. M. Lopatynskyi, eds.), pp. 23–79, Jenny Stanford Publishing, 1 ed., Nov. 2020.

[189] N. Harris, M. G. Blaber, and G. C. Schatz, "Optical Properties of Metal Nanoparticles," in *Encyclopedia of Nanotechnology* (B. Bhushan, ed.), pp. 1950–1969, Dordrecht: Springer Netherlands, 2012.

[190] A. Ruscito and M. C. DeRosa, "Small-Molecule Binding Aptamers: Selection Strategies, Characterization, and Applications," *Frontiers in Chemistry*, vol. 4, May 2016.

[191] Y. S. Kim, H. S. Jung, T. Matsuura, H. Y. Lee, T. Kawai, and M. B. Gu, "Electrochemical detection of 17β-estradiol using DNA aptamer immobilized gold electrode chip," *Biosensors and Bioelectronics*, vol. 22, pp. 2525–2531, May 2007.

[192] O. A. Alsager, S. Kumar, B. Zhu, J. Travas-Sejdic, K. P. McNatty, and J. M. Hodgkiss, "Ultrasensitive Colorimetric Detection of 17β-Estradiol: The Effect of Shortening DNA Aptamer Sequences," *Analytical Chemistry*, vol. 87, pp. 4201–4209, Apr. 2015.

[193] M. McKeague, A. De Girolamo, S. Valenzano, M. Pascale, A. Ruscito, R. Velu, N. R. Frost, K. Hill, M. Smith, E. M. McConnell, and M. C. DeRosa, "Comprehensive Analytical Comparison of Strategies Used for Small Molecule Aptamer Evaluation," *Analytical Chemistry*, vol. 87, pp. 8608–8612, Sept. 2015.

[194] P. Sandström, M. Boncheva, and B. Åkerman, "Nonspecific and Thiol-Specific Binding of DNA to Gold Nanoparticles," *Langmuir*, vol. 19, pp. 7537–7543, Sept. 2003.

[195] H. Li and L. Rothberg, "Colorimetric detection of DNA sequences based on electrostatic interactions with unmodified gold nanoparticles," *Proceedings of the National Academy of Sciences*, vol. 101, pp. 14036–14039, Sept. 2004.

[196] J. Liu, "Adsorption of DNA onto gold nanoparticles and graphene oxide: surface science and applications," *Physical Chemistry Chemical Physics*, vol. 14, pp. 10485–10496, June 2012.

[197] Y. S. Kim, J. H. Kim, I. A. Kim, S. J. Lee, and M. B. Gu, "The affinity ratio—Its pivotal role in gold nanoparticle-based competitive colorimetric aptasensor," *Biosensors and Bioelectronics*, vol. 26, pp. 4058–4063, June 2011.

[198] O. H. Shayesteh and R. Ghavami, "Two colorimetric ampicillin sensing schemes based on the interaction of aptamers with gold nanoparticles," *Microchimica Acta*, vol. 186, p. 485, July 2019.

[199] Y. Li, J. Xu, M. Jia, Z. Yang, Z. Liang, J. Guo, Y. Luo, F. Shen, and C. Sun, "Colorimetric determination of 17β-estradiol based on the specific recognition of aptamer and the salt-induced aggregation of gold nanoparticles," *Materials Letters*, vol. 159, pp. 221–224, Nov. 2015.

[200] H. Pu, Z. Huang, D.-W. Sun, X. Xie, and W. Zhou, "Development of a Highly Sensitive Colorimetric Method for Detecting 17β-Estradiol Based on Combination of Gold Nanoparticles and Shortening DNA Aptamers," *Water, Air, & Soil Pollution*, vol. 230, p. 124, June 2019.

[201] A. Natarajan and F. Srienc, "Dynamics of Glucose Uptake by Single Escherichia coli Cells," *Metabolic Engineering*, vol. 1, pp. 320–333, Oct. 1999.

[202] S. Leivers, L. Lagos, P. Garbers, S. L. La Rosa, and B. Westereng, "Technical pipeline for screening microbial communities as a function of substrate specificity through fluorescent labelling," *Communications Biology*, vol. 5, p. 444, Dec. 2022.

[203] L. Hao, J. Li, A. Kappler, and M. Obst, "Mapping of Heavy Metal Ion Sorption to Cell-Extracellular Polymeric Substance-Mineral Aggregates by Using Metal-Selective Fluorescent Probes and Confocal Laser Scanning Microscopy," *Applied and Environmental Microbiology*, vol. 79, pp. 6524–6534, Nov. 2013.

[204] M. J. Gauthier, V. M. Torregrossa, M. C. Babelona, R. Cornax, and J. J. Borrego, "An Intercalibration Study of the Use of 4-Methylumbelliferyl-β-D-Glucuronide for the Specific Enumeration of Escherichia coli in Seawater and Marine Sediments," *Systematic and Applied Microbiology*, vol. 14, pp. 183–189, Mar. 1991.

[205] J. D. Berg and L. Fiksdal, "Rapid Detection of Total and Fecal Coliforms in Water by Enzymatic Hydrolysis of 4-Methylumbelliferone-r-D-Galactoside," *Applied and Environmental Microbiology*, vol. 54, Aug. 1988.

[206] S.-J. Haig, *Characterising the functional ecology of slow sand filters through environmental genomics*. PhD thesis, Sept. 2014.

[207] J. Bañuelos, "BODIPY Dye, the Most Versatile Fluorophore Ever?," *The Chemical Record*, vol. 16, pp. 335–348, Feb. 2016.

[208] J. Rao, A. Dragulescu-Andrasi, and H. Yao, "Fluorescence imaging in vivo: recent advances," *Current Opinion in Biotechnology*, vol. 18, pp. 17–25, Feb. 2007.

[209] F. Sozmen, S. Kolemen, H.-O. Kumada, M. Ono, H. Saji, and E. U. Akkaya, "Designing BODIPY-based probes for fluorescence imaging of β-amyloid plaques," *RSC Adv.*, vol. 4, pp. 51032–51037, Sept. 2014.

[210] R. Connally, D. Veal, and J. Piper, "High resolution detection of fluorescently labeled microorganisms in environmental samples using time-resolved fluorescence microscopy," *FEMS Microbiology Ecology*, vol. 41, pp. 239–245, Sept. 2002.

[211] M. S. T. Gonçalves, "Fluorescent Labeling of Biomolecules with Organic Probes," *Chemical Reviews*, vol. 109, pp. 190–212, Jan. 2009.

[212] G. Ulrich, R. Ziessel, and A. Harriman, "The Chemistry of Fluorescent Bodipy Dyes: Versatility Unsurpassed," *Angewandte Chemie International Edition*, vol. 47, pp. 1184–1201, Feb. 2008.

[213] E. Antina, N. Bumagina, Y. Marfin, G. Guseva, L. Nikitina, D. Sbytov, and F. Telegin, "BODIPY Conjugates as Functional Compounds for Medical Diagnostics and Treatment," *Molecules*, vol. 27, p. 1396, Feb. 2022.

[214] A. M. Hansen, A. L. Sewell, R. H. Pedersen, D.-L. Long, N. Gadegaard, and R. Marquez, "Tunable BODIPY derivatives amenable to 'click' and peptide chemistry," *Tetrahedron*, vol. 69, pp. 8527–8533, Sept. 2013.

[215] D. Marushchak, S. Kalinin, I. Mikhalyov, N. Gretskaya, and L. B. Å. Johansson, "Pyrromethene dyes (BODIPY) can form ground state homo and hetero dimers: Photophysics and spectral properties," *Spectrochimica Acta Part A: Molecular and Biomolecular Spectroscopy*, vol. 65, pp. 113–122, Sept. 2006.

[216] Y. Tokoro, A. Nagai, and Y. Chujo, "Nanoparticles via H-aggregation of amphiphilic BODIPY dyes," *Tetrahedron Letters*, vol. 51, pp. 3451–3454, June 2010.

[217] X. Dai, X. Chen, Y. Zhao, Y. Yu, X. Wei, X. Zhang, and C. Li, "A Water-Soluble Galactose-Decorated Cationic Photodynamic Therapy Agent Based on BODIPY to Selectively Eliminate Biofilm," *Biomacromolecules*, vol. 19, pp. 141–149, Jan. 2018.

[218] S. L. Niu, G. Ulrich, R. Ziessel, A. Kiss, P.-Y. Renard, and A. Romieu, "Water-Soluble BODIPY Derivatives," *Organic Letters*, vol. 11, pp. 2049–2052, May 2009.

[219] Y. Hayashi, K. Zama, E. Abe, N. Okino, T. Inoue, K. Ohno, and M. Ito, "A sensitive and reproducible fluorescent-based HPLC assay to measure the activity of acid as well as neutral β-glucocerebrosidases," *Analytical Biochemistry*, vol. 383, pp. 122–129, Dec. 2008.

[220] C. Felion, R. Lopez-Gonzalez, A. L. Sewell, R. Marquez, and C. Gauchotte-Lindsay, "BODIPY-Labeled Estrogens for Fluorescence Analysis of Environmental Microbial Degradation," *ACS Omega*, vol. 7, pp. 41284–41295, Nov. 2022.

[221] H. Wickham, *ggplot2: Elegant Graphics for Data Analysis*. Springer-Verlag New York, 2016.

[222] J. Abraham, "International Conference On Harmonisation Of Technical Requirements For Registration Of Pharmaceuticals For Human Use," in *Handbook of Transnational Economic Governance Regimes* (A. Brouder and C. Tietje, eds.), pp. 1041–1054, Brill, Oct. 2009.

[223] K.-J. Huang, Q.-S. Jing, C.-Y. Wei, and Y.-Y. Wu, "Spectrofluorimetric determination of glutathione in human plasma by solid-phase extraction using graphene as adsorbent," *Spectrochimica Acta Part A: Molecular and Biomolecular Spectroscopy*, vol. 79, pp. 1860–1865, Sept. 2011.

[224] V. H. Quinlivan, M. H. Wilson, J. Ruzicka, and S. A. Farber, "An HPLC-CAD/fluorescence lipidomics platform using fluorescent fatty acids as metabolic tracers," *Journal of Lipid Research*, vol. 58, pp. 1008–1020, May 2017.

[225] X.-J. Xiong, H. Wang, W.-B. Rao, X.-F. Guo, and H.-S. Zhang, "1,3,5,7-Tetramethyl-8-aminozide-difluoroboradiaza-s-indacene as a new fluorescent labeling reagent for the determination of aliphatic aldehydes in serum with high performance liquid chromatography," *Journal of Chromatography A*, vol. 1217, pp. 49–56, Jan. 2010.

[226] K. Yuan, X. Wang, S. K. Mellerup, I. Kozin, and S. Wang, "Spiro-BODIPYs with a Diaryl Chelate: Impact on Aggregation and Luminescence," *The Journal of Organic Chemistry*, vol. 82, pp. 13481–13487, Dec. 2017.

[227] Q. Yan, L. Yang, and S. Li, "Solid-Phase Extraction Combined with High Performance Liquid Chromatography-Diode Array Detector for Rapid Determination of Estrogens in Milk," *Tropical Journal of Pharmaceutical Research*, vol. 14, p. 2077, Dec. 2015.

[228] R. L. Pérez and G. M. Escandar, "Liquid chromatography with diode array detection and multivariate curve resolution for the selective and sensitive quantification of estrogens in natural waters," *Analytica Chimica Acta*, vol. 835, pp. 19–28, July 2014.

[229] Y. Kanie, M. Taniuchi, and O. Kanie, "Evaluation of reversed-phase nano liquid chromatography conditions by using reversed-phase thin layer chromatography based on Hansen solubility parameters for the analysis of amphiphilic glycosylsphingolipid transformations," *Journal of Chromatography A*, vol. 1534, pp. 123–129, Jan. 2018.

[230] S. T. Furlong, K. S. Thibault, L. M. Morbelli, J. J. Quinn, and R. A. Rogers, "Uptake and compartmentalization of fluorescent lipid analogs in larval Schistosoma mansoni.," *Journal of Lipid Research*, vol. 36, p. 12, Jan. 1995.

[231] M. Thompson, "The estimation and use of recovery factors," Sept. 2008.

[232] C.-P. Yu, R. Ahuja, G. Sayler, and K.-H. Chu, "Quantitative Molecular Assay for Fingerprinting Microbial Communities of Wastewater and Estrogen-Degrading Consortia," *Applied and Environmental Microbiology*, vol. 71, pp. 1433–1444, Mar. 2005.

[233] W. Zheng, X. Li, S. R. Yates, and S. A. Bradford, "Anaerobic Transformation Kinetics and Mechanism of Steroid Estrogenic Hormones in Dairy Lagoon Water," *Environmental Science & Technology*, vol. 46, pp. 5471–5478, May 2012.

[234] W. Zheng, Y. Zou, X. Li, and M. L. Machesky, "Fate of estrogen conjugate 17α-estradiol-3-sulfate in dairy wastewater: Comparison of aerobic and anaerobic degradation and

metabolite formation," *Journal of Hazardous Materials*, vol. 258-259, pp. 109–115, Aug. 2013.

[235] J. Skotnicka-Pitak, W. O. Khunjar, N. G. Love, and D. S. Aga, "Characterization of Metabolites Formed During the Biotransformation of 17α-Ethinylestradiol by *Nitrosomonas europaea* in Batch and Continuous Flow Bioreactors," *Environmental Science & Technology*, vol. 43, pp. 3549–3555, May 2009.

[236] K. Yoshioka, H. Takahashi, T. Homma, M. Saito, K.-B. Oh, Y. Nemoto, and H. Matsuoka, "A novel fluorescent derivative of glucose applicable to the assessment of glucose uptake activity of Escherichia coli," *Biochimica et Biophysica Acta (BBA) - General Subjects*, vol. 1289, pp. 5–9, Feb. 1996.

[237] M. Benincasa, S. Pacor, R. Gennaro, and M. Scocchi, "Rapid and Reliable Detection of Antimicrobial Peptide Penetration into Gram-Negative Bacteria Based on Fluorescence Quenching," *Antimicrobial Agents and Chemotherapy*, vol. 53, pp. 3501–3504, Aug. 2009.

[238] W. Phetsang, R. Pelingon, M. S. Butler, S. Kc, M. E. Pitt, G. Kaeslin, M. A. Cooper, and M. A. T. Blaskovich, "Fluorescent Trimethoprim Conjugate Probes To Assess Drug Accumulation in Wild Type and Mutant Escherichia coli," *ACS Infectious Diseases*, vol. 2, pp. 688–701, Oct. 2016.

[239] J. Tao, R. K. Diaz, C. R. V. Teixeira, and T. J. Hackmann, "Transport of a Fluorescent Analogue of Glucose (2-NBDG) versus Radiolabeled Sugars by Rumen Bacteria and *Escherichia coli*," *Biochemistry*, vol. 55, pp. 2578–2589, May 2016.

[240] H. H. Kazan, E. Özcan, E. T. Eçik, and B. Çoşut, "Novel 17α-Etinylestradiol-Substituted BODIPY Dyes: Synthesis, Photophysical Properties and Fluorescence Imaging Studies in Breast Cancer Cell Lines," *ChemistrySelect*, vol. 3, pp. 2962–2967, Mar. 2018.

[241] J. Liao, R. Sportsman, J. Harris, and A. Stahl, "Real-time quantification of fatty acid uptake using a novel fluorescence assay," *Journal of Lipid Research*, vol. 46, pp. 597–602, Mar. 2005.

[242] K. Chilvers, J. Perry, A. James, and R. Reed, "Synthesis and evaluation of novel fluorogenic substrates for the detection of bacterial beta-galactosidase," *Journal of Applied Microbiology*, vol. 91, pp. 1118–1130, Dec. 2001.

[243] K. Koyama, T. Hirao, A. Toriba, and K. Hayakawa, "An analytical method for measuring α -amylase activity in starch-containing foods: An assay for amylase activity in starch-containing foods," *Biomedical Chromatography*, vol. 27, pp. 583–588, May 2013.

[244] P. Bandhuvula, Z. Li, R. Bittman, and J. D. Saba, "Sphingosine 1-phosphate lyase enzyme assay using a BODIPY-labeled substrate," *Biochemical and Biophysical Research Communications*, vol. 380, pp. 366–370, Mar. 2009.

[245] A. Bollmann, E. French, and H. J. Laanbroek, "Isolation, Cultivation, and Characterization of Ammonia-Oxidizing Bacteria and Archaea Adapted to Low Ammonium Concentrations," in *Methods in Enzymology*, vol. 486, pp. 55–88, Elsevier, 2011.

[246] ATCC, "Escherichia coli (Migula) Castellani and Chalmers Product Sheet (700926)," 2023.

[247] Leibniz Institute, "Caenibius tardaugens DSM 16702."

[248] N. G. Hommes, L. A. Sayavedra-Soto, and D. J. Arp, "Chemolithoorganotrophic Growth of Nitrosomonas europaea on Fructose," *Journal of Bacteriology*, vol. 185, p. 6, Dec. 2003.

[249] A. Krummel and H. Harms, "Effect of organic matter on growth and cell yield of ammonia-oxidizing bacteria," *Archives of Microbiology*, vol. 133, pp. 50–54, Nov. 1982.

[250] R. Hermsen, H. Okano, C. You, N. Werner, and T. Hwa, "A growth-rate composition formula for the growth of *E. coli* on co-utilized carbon substrates," *Molecular Systems Biology*, vol. 11, p. 801, Apr. 2015.

[251] S. Park and R. L. Ely, "Candidate Stress Genes of Nitrosomonas europaea for Monitoring Inhibition of Nitrification by Heavy Metals," *Applied and Environmental Microbiology*, vol. 74, pp. 5475–5482, Sept. 2008.

[252] Y. Yu, P. Han, L.-J. Zhou, Z. Li, M. Wagner, and Y. Men, "Ammonia Monooxygenase-Mediated Cometabolic Biotransformation and Hydroxylamine-Mediated Abiotic Transformation of Micropollutants in an AOB/NOB Coculture," *Environmental Science & Technology*, vol. 52, pp. 9196–9205, July 2018.

[253] M. Petrovich, C.-Y. Wu, A. Rosenthal, K.-F. Chen, A. I. Packman, and G. F. Wells, "Nitrosomonas europaea biofilm formation is enhanced by Pseudomonas aeruginosa," *FEMS Microbiology Ecology*, vol. 93, May 2017.

[254] L. Casali, L. Mazzei, R. Sun, M. R. Chierotti, R. Gobetto, D. Braga, F. Grepioni, and S. Ciurli, "Thiocarbamoyl Disulfides as Inhibitors of Urease and Ammonia Monooxygenase: Crystal Engineering for Novel Materials," *Crystal Growth & Design*, vol. 22, pp. 4528–4537, July 2022.

[255] E. B. Estrada-Arriaga and P. N. Mijaylova, "Influence of operational parameters (sludge retention time and hydraulic residence time) on the removal of estrogens by membrane bioreactor," *Environmental Science and Pollution Research*, vol. 18, pp. 1121–1128, Aug. 2011.

[256] M. M. Amin, B. Bina, K. Ebrahim, Z. Yavari, and F. Mohammadi, "Biodegradation of natural and synthetic estrogens in moving bed bioreactor," *Chinese Journal of Chemical Engineering*, vol. 26, pp. 393–399, Feb. 2018.

[257] H. Huang, L. Jin, J. Hu, Y. Wang, and H. Ren, "Removal of Steroid Estrogens and Total Nitrogen by Denitrification Biofilter with UV/Peracetic Acid Pretreatment: Performance, Microbial Characteristics, and Mechanism," *ACS ES&T Water*, vol. 3, pp. 1093–1104, Apr. 2023.

[258] Z. Gao, A. Ali, J. Su, Q. Chang, Y. Bai, Y. Wang, and Y. Liu, "Bioaugmented removal of 17β-estradiol, nitrate and Mn(II) by polypyrrole@corn cob immobilized bioreactor: Performance optimization, mechanism, and microbial community response," *Environmental Pollution*, vol. 299, p. 118896, Apr. 2022.

[259] G. Hu, A. Henke, R. J. Karpowicz, M. S. Sonders, F. Farrimond, R. Edwards, D. Sulzer, and D. Sames, "New Fluorescent Substrate Enables Quantitative and High-throughput Examination of Vesicular Monoamine Transporter 2 (VMAT2)," *ACS chemical biology*, vol. 8, pp. 1947–1954, Sept. 2013.

[260] S. Jørgensen, E. Nielsen, D. Peters, and T. Dyhring, "Validation of a fluorescence-based high-throughput assay for the measurement of neurotransmitter transporter uptake activity," *Journal of Neuroscience Methods*, vol. 169, pp. 168–176, Mar. 2008.

[261] S. Fery-Forgues, J.-P. Fayet, and A. Lopez, "Drastic changes in the fluorescence properties of NBD probes with the polarity of the medium: involvement of a TICT state?," *Journal of Photochemistry and Photobiology A: Chemistry*, vol. 70, pp. 229–243, Mar. 1993.

[262] AAT Bioquest, "C1-Bodi Fluor 500/510-C12 [equivalent to BODIPY® 500/510 C1, C12]."

[263] B. Kamel, M. Sayem El-Daher, W. Bachir, A. Ibrahim, and S. Aljalali, "Effect of Solvents on the Fluorescent Spectroscopy of BODIPY-520 Derivative," *Journal of Spectroscopy*, vol. 2022, p. e1172183, June 2022.

[264] X. Wang, Q. Wang, and Q. Qi, "Identification of riboflavin: revealing different metabolic characteristics between Escherichia coli BL21(DE3) and MG1655," *FEMS Microbiology Letters*, vol. 362, pp. 1–7, June 2015.

[265] C. D. Geddes, "Optical halide sensing using fluorescence quenching: theory, simulations and applications - a review," *Measurement Science and Technology*, vol. 12, p. R53, Aug. 2001.

[266] A. Chmyrov, T. Sandén, and J. Widengren, "Iodide as a Fluorescence Quencher and Promoter—Mechanisms and Possible Implications," *The Journal of Physical Chemistry B*, vol. 114, pp. 11282–11291, Sept. 2010.

[267] J. Johnston, T. LaPara, and S. Behrens, "Composition and Dynamics of the Activated Sludge Microbiome during Seasonal Nitrification Failure," *Scientific Reports*, vol. 9, p. 4565, Mar. 2019.

[268] S. Begmatov, A. G. Dorofeev, V. V. Kadnikov, A. V. Beletsky, N. V. Pimenov, N. V. Ravin, and A. V. Mardanov, "The structure of microbial communities of activated sludge of large-scale wastewater treatment plants in the city of Moscow," *Scientific Reports*, vol. 12, p. 3458, Mar. 2022.

[269] K. Guo and H. Gao, "Physiological Roles of Nitrite and Nitric Oxide in Bacteria: Similar Consequences from Distinct Cell Targets, Protection, and Sensing Systems," *Advanced Biology*, vol. 5, p. 2100773, July 2021.

[270] P. Jiang, Y. Wang, L. Zhao, C. Ji, D. Chen, and L. Nie, "Applications of Gold Nanoparticles in Non-Optical Biosensors," p. 23, Nov. 2018.

[271] H. Malekzad, P. Sahandi Zangabad, H. Mirshekari, M. Karimi, and M. R. Hamblin, "Noble metal nanoparticles in biosensors: recent studies and applications," *Nanotechnology Reviews*, vol. 6, pp. 301–329, June 2017.

[272] J. M. Carnerero, A. Jimenez-Ruiz, E. M. Grueso, and R. Prado-Gotor, "Understanding and improving aggregated gold nanoparticle/dsDNA interactions by molecular spectroscopy and deconvolution methods," *Physical Chemistry Chemical Physics*, vol. 19, pp. 16113–16123, May 2017.

[273] A. Minopoli, N. Sakač, B. Lenyk, R. Campanile, D. Mayer, A. Offenhäusser, R. Velotta, and B. Della Ventura, "LSPR-based colorimetric immunosensor for rapid and sensitive 17β-estradiol detection in tap water," *Sensors and Actuators B: Chemical*, vol. 308, p. 127699, Apr. 2020.

[274] S. Liu, Y. Chen, Y. Wang, and G. Zhao, "Group-Targeting Detection of Total Steroid Estrogen Using Surface-Enhanced Raman Spectroscopy," *Analytical Chemistry*, vol. 91, pp. 7639–7647, June 2019.

[275] X. Liu, K. Deng, H. Wang, C. Li, S. Zhang, and H. Huang, "Aptamer based ratiometric electrochemical sensing of 17β-estradiol using an electrode modified with gold nanoparticles, thionine, and multiwalled carbon nanotubes," *Microchimica Acta*, vol. 186, p. 347, June 2019.

[276] J. Liu and Y. Lu, "Preparation of aptamer-linked gold nanoparticle purple aggregates for colorimetric sensing of analytes," *Nature Protocols*, vol. 1, pp. 246–252, June 2006.

[277] W. Haiss, N. T. K. Thanh, J. Aveyard, and D. G. Fernig, "Determination of Size and Concentration of Gold Nanoparticles from UV-Vis Spectra," *Analytical Chemistry*, vol. 79, pp. 4215–4221, June 2007.

[278] J. Liu, W. Bai, S. Niu, C. Zhu, S. Yang, and A. Chen, "Highly sensitive colorimetric detection of 17β-estradiol using split DNA aptamers immobilized on unmodified gold nanoparticles," *Scientific Reports*, vol. 4, p. 7571, May 2015.

[279] M. Svobodová, V. Skouridou, M. L. Botero, M. Jauset-Rubio, T. Schubert, A. S. Bashammakh, M. S. El-Shahawi, A. O. Alyoubi, and C. K. O'Sullivan, "The characterization and validation of 17β-estradiol binding aptamers," *The Journal of Steroid Biochemistry and Molecular Biology*, vol. 167, pp. 14–22, Mar. 2017.

[280] R. V. Lenth, "Response-Surface Methods in *R* , Using **rsm**," *Journal of Statistical Software*, no. 2.10.2, 2020.

[281] F. Commo, "N-Parameter Logistic Regression," Dec. 2016.

[282] F. Pfeiffer and G. Mayer, "Selection and Biosensor Application of Aptamers for Small Molecules," *Frontiers in Chemistry*, vol. 4, June 2016.

[283] The European Commission, "Proposal for a Directive of the European Parliament and of the Council amending Directives 2000/60/EC and 2008/105/EC as regards priority substances in the field of water policy," Tech. Rep. COM(2011) 876, European Commission, Jan. 2012.

[284] The European Parliament and the Council of the European Union, "Directive 2013/39/EU of the European Parliament and of the Council of 12 August 2013 amending Directives 2000/60/EC and 2008/105/EC as regards priority substances in the field of water policy-Text with EEA relevance," 2013.

[285] The European Commission, "Commission Implementing Decision (EU) 2015/495 of 20 March 2015 establishing a watch list of substances for Union-wide monitoring in the field of water policy pursuant to Directive 2008/105/EC of the European Parliament and of the Council," 2015.

[286] M. Dou, J. M. García, S. Zhan, and X. Li, "Interfacial nano-biosensing in microfluidic droplets for high-sensitivity detection of low-solubility molecules," *Chemical Communications*, vol. 52, pp. 3470–3473, Feb. 2016.

[287] F. Long, H. Shi, and H. Wang, "Fluorescence resonance energy transfer based aptasensor for the sensitive and selective detection of 17β-estradiol using a quantum dot-bioconjugate as a nano-bioprobe," *RSC Adv.*, vol. 4, pp. 2875–2881, Oct. 2014.

[288] X. Ni, B. Xia, L. Wang, J. Ye, G. Du, H. Feng, X. Zhou, T. Zhang, and W. Wang, "Fluorescent aptasensor for 17β-estradiol determination based on gold nanoparticles quenching the fluorescence of Rhodamine B," *Analytical Biochemistry*, vol. 523, pp. 17–23, Apr. 2017.

[289] X. Chen, J. Wang, H.-Y. Shen, X. Su, Y. Cao, T. Li, and N. Gan, "Microfluidic Chip for Multiplex Detection of Trace Chemical Contaminants Based on Magnetic Encoded Aptamer Probes and Multibranched DNA Nanostructures as Signal Tags," *ACS Sensors*, vol. 4, pp. 2131–2139, Aug. 2019.

[290] L. He, Z. Shen, J. Wang, J. Zeng, W. Wang, H. Wu, Q. Wang, and N. Gan, "Simultaneously responsive microfluidic chip aptasensor for determination of kanamycin, aflatoxin M1, and 17β-estradiol based on magnetic tripartite DNA assembly nanostructure probes," *Microchimica Acta*, vol. 187, p. 176, Mar. 2020.

[291] T. Suo, M. Sohail, Y. Ma, B. Li, Y. Chen, X. Zhang, and X. Zhou, "A versatile turn-on fluorometric biosensing profile based on split aptamers-involved assembly of nanocluster beacon sandwich," *Sensors and Actuators B: Chemical*, vol. 324, p. 128586, Dec. 2020.

[292] O. A. Alsager, S. Kumar, and J. M. Hodgkiss, "Lateral Flow Aptasensor for Small Molecule Targets Exploiting Adsorption and Desorption Interactions on Gold Nanoparticles," *Analytical Chemistry*, vol. 89, pp. 7416–7424, July 2017.

[293] J. L. Chávez, J. K. Leny, S. Witt, G. M. Slusher, J. A. Hagen, and N. Kelley-Loughnane, "Plasmonic aptamer–gold nanoparticle sensors for small molecule fingerprint identification," *The Analyst*, vol. 139, pp. 6214–6222, Oct. 2014.

[294] D. Zhang, W. Zhang, J. Ye, S. Zhan, B. Xia, J. Lv, H. Xu, G. Du, and L. Wang, "A Label-Free Colorimetric Biosensor for 17β-Estradiol Detection Using Nanoparticles Assembled by Aptamer and Cationic Polymer," *Australian Journal of Chemistry*, vol. 69, no. 1, p. 12, 2016.

[295] Q.-F. Li, S.-Y. Ren, Y. Wang, J.-L. Bai, Y. Peng, B.-A. Ning, Q.-J. Lyu, and Z.-X. Gao, "Efficient Detection of Environmental Estrogens Bisphenol A and Estradiol By Sensing System Based on AuNP-AuNP-UCNP Triple Structure," *Chinese Journal of Analytical Chemistry*, vol. 46, pp. 486–492, Apr. 2018.

[296] Y. Peng, L. Li, X. Mu, and L. Guo, "Aptamer-gold nanoparticle-based colorimetric assay for the sensitive detection of thrombin," *Sensors and Actuators B: Chemical*, vol. 177, pp. 818–825, Feb. 2013.

[297] U. Nobbman, "Polydispersity - What does it mean for DLS and Chromatography?," Oct. 2017.

[298] C. L. Nehl and J. H. Hafner, "Shape-dependent plasmon resonances of gold nanoparticles," *Journal of Materials Chemistry*, vol. 18, p. 2415, Feb. 2008.

[299] G. Trefalt, I. Szilagyi, and M. Borkovec, "Poisson–Boltzmann description of interaction forces and aggregation rates involving charged colloidal particles in asymmetric electrolytes," *Journal of Colloid and Interface Science*, p. 10, June 2013.

[300] National Center for Biotechnology Information, "PubChem Compound Summary for CID 5757, Estradiol," May 2023.

[301] B. Aswathy, G. S. Avadhani, S. Suji, and G. Sony, "Synthesis of β-cyclodextrin functionalized gold nanoparticles for the selective detection of Pb2+ ions from aqueous solution," *Frontiers of Materials Science*, vol. 6, pp. 168–175, June 2012.

[302] R. Rajamanikandan, A. D. Lakshmi, and M. Ilanchelian, "Smart phone assisted, rapid, simplistic, straightforward and sensitive biosensing of cysteine over other essential amino acids by β-cyclodextrin functionalized gold nanoparticles as a colorimetric probe," *New Journal of Chemistry*, vol. 44, pp. 12169–12177, June 2020.

[303] K. Saito, K. McGehee, and Y. Norikane, "Size-controlled synthesis of cyclodextrin-capped gold nanoparticles for molecular recognition using surface-enhanced Raman scattering," *Nanoscale Advances*, vol. 3, pp. 3272–3278, Apr. 2021.

[304] S. Liu, "A simple one-step pretreatment, highly sensitive and selective sensing of 17β-estradiol in environmental water samples using surface-enhanced Raman spectroscopy," *Sensors and Actuators B: Chemical*, p. 8, Aug. 2018.

[305] I. F. M. A. Nasri, *Optical Sensors Based on Asymmetric Plasmonic Nanostructures for Environmental Monitoring*. PhD thesis, University of Glasgow, Oct. 2019.

[306] M. Molina-Delgado, M. P. Aguilar-Caballos, and A. Gómez-Hens, "Simultaneous photometric microplate assay for free and total thiamine using gold nanoparticles and alkaline phosphatase," *Microchimica Acta*, vol. 183, pp. 1385–1390, Apr. 2016.

[307] D. Arp, L. Sayavedra-Soto, and N. Hommes, "Molecular biology and biochemistry of ammonia oxidation by Nitrosomonas europaea," *Archives of Microbiology*, vol. 178, pp. 250–255, Oct. 2002.

[308] K. Afshinnia and M. Baalousha, "Effect of phosphate buffer on aggregation kinetics of citrate-coated silver nanoparticles induced by monovalent and divalent electrolytes," *Science of The Total Environment*, vol. 581-582, pp. 268–276, Mar. 2017.

[309] S. Wagner, A. Gondikas, E. Neubauer, T. Hofmann, and F. Von Der Kammer, "Spot the Difference: Engineered and Natural Nanoparticles in the Environment-Release, Behavior, and Fate," *Angewandte Chemie International Edition*, pp. n/a–n/a, Oct. 2014.

[310] C. Ratzke and J. Gore, "Modifying and reacting to the environmental pH can drive bacterial interactions," *PLOS Biology*, vol. 16, p. e2004248, Mar. 2018.

[311] G. S. Geleta, "A colorimetric aptasensor based on gold nanoparticles for detection of microbial toxins: an alternative approach to conventional methods," *Analytical and Bioanalytical Chemistry*, vol. 414, pp. 7103–7122, Oct. 2022.

[312] A. Kasoju, D. Shahdeo, A. A. Khan, N. S. Shrikrishna, S. Mahari, A. M. Alanazi, M. A. Bhat, J. Giri, and S. Gandhi, "Fabrication of microfluidic device for Aflatoxin M1 detection in milk samples with specific aptamers," *Scientific Reports*, vol. 10, p. 4627, Mar. 2020.

[313] J. Halliwell and C. Gwenin, "A Label Free Colorimetric Assay for the Detection of Active Botulinum Neurotoxin Type A by SNAP-25 Conjugated Colloidal Gold," *Toxins*, vol. 5, pp. 1381–1391, Aug. 2013.

[314] A. Liu, Y. Zhang, W. Chen, X. Wang, and F. Chen, "Gold nanoparticle-based colorimetric detection of staphylococcal enterotoxin B using ssDNA aptamers," *European Food Research and Technology*, vol. 237, pp. 323–329, Sept. 2013.

[315] Y. Luan, J. Chen, G. Xie, C. Li, H. Ping, Z. Ma, and A. Lu, "Visual and microplate detection of aflatoxin B2 based on NaCl-induced aggregation of aptamer-modified gold nanoparticles," *Microchimica Acta*, vol. 182, pp. 995–1001, Apr. 2015.

[316] B. Mondal, S. Ramlal, P. S. Lavu, B. N, and J. Kingston, "Highly Sensitive Colorimetric Biosensor for Staphylococcal Enterotoxin B by a Label-Free Aptamer and Gold Nanoparticles," *Frontiers in Microbiology*, vol. 9, p. 179, Feb. 2018.

[317] K. Yoshioka, M. Saito, K.-B. Oh, Y. Nemoto, H. Matsuoka, M. Natsume, and H. Abe, "Intracellular Fate of 2-NBDG, a Fluorescent Probe for Glucose Uptake Activity, in *Escherichia coli* Cells," *Bioscience, Biotechnology, and Biochemistry*, vol. 60, pp. 1899–1901, Jan. 1996.

[318] P. R. Yaashikaa, M. K. Devi, and P. S. Kumar, "Engineering microbes for enhancing the degradation of environmental pollutants: A detailed review on synthetic biology," *Environmental Research*, vol. 214, p. 113868, Nov. 2022.

[319] R. Rezgui, K. Blumer, G. Yeoh-Tan, A. J. Trexler, and M. Magzoub, "Precise quantification of cellular uptake of cell-penetrating peptides using fluorescence-activated cell sorting and fluorescence correlation spectroscopy," *Biochimica et Biophysica Acta (BBA) - Biomembranes*, vol. 1858, pp. 1499–1506, July 2016.

[320] D. J. Creek, A. Jankevics, K. E. V. Burgess, R. Breitling, and M. P. Barrett, "IDEOM: an Excel interface for analysis of LC–MS-based metabolomics data," *Bioinformatics*, vol. 28, pp. 1048–1049, Apr. 2012.

[321] P. Tobias and L. Trutna, "Chapter 5. Process Improvement," in *NIST/SEMATECH e-Handbook of Statistical Methods*, 2012.